Doctoral Dissertation

Nonequilibrium quantum many-body physics in ultracold atoms subject to dissipation

---

Kazuki Yamamoto

Condensed Matter Theory Group, Department of Physics

Kyoto University

January, 2023

Abstract

Recent progress in ultracold atoms has enabled control of dissipation and single-atom measurement at ultimate resolution as well as flexible tuning of physical parameters. When extracting information of quantum systems by measurement of the system, observers play a role as an environment, and their backaction induces a change in the quantum states of the system. In particular, when we deal with physics at ultimate resolution in ultracold atoms, backaction caused by measurement of the system becomes significant. Motivated by such backgrounds, a lot of studies have been done in recent years by using dissipation such as particle loss, dephasing, and measurement backaction, and it is reported both theoretically and experimentally that dissipation can realize unique nonequilibrium phenomena in *open quantum systems*. On the other hand, many-body effects, which are known to bring about rich phenomena induced by correlation, have not been fully understood yet in nonequilibrium quantum systems subject to dissipation.

In this thesis, we investigate several representative quantum many-body phenomena in ultracold atoms with dissipation. First, motivated by recent experimental advances in ultracold atoms, we analyze a non-Hermitian (NH) BCS Hamiltonian with a complex-valued interaction arising from inelastic scattering between fermions. We develop a mean-field theory to obtain a NH gap equation for order parameters, which are different from the standard BCS ones due to the inequivalence of left and right eigenstates in the NH physics. We find unconventional phase transitions unique to NH systems: Superfluidity shows reentrant behavior with increasing dissipation as a consequence of non-diagonalizable exceptional points, lines, and surfaces in the quasiparticle Hamiltonian for weak attractive interactions. For strong attractive interactions, the superfluid gap never collapses but is enhanced by dissipation due to an interplay between the BCS-BEC crossover and the continuous quantum Zeno effect. Our results lay the groundwork for studies of fermionic superfluidity subject to inelastic collisions.

Next, going beyond the NH framework, we predict a new mechanism to induce collective excitations and a nonequilibrium phase transition of fermionic superfluids via a sudden switch-on of two-body loss, for which we extend the BCS theory to fully incorporate a change in particle number. We find that a sudden switch-on of dissipation induces an amplitude oscillation of the superfluid order parameter accompanied by a chirped phase rotation as a consequence of particle loss. We demonstrate that when dissipation is introduced to one of the two superfluids coupled via a Josephson junction, it gives rise to a nonequilibrium dynamical phase transition characterized by the vanishing dc Josephson current. The dissipation-induced collective modes and nonequilibrium phase transition can be realized with ultracold fermionic atoms subject to inelastic collisions.

Furthermore, we study how translationally invariant couplings of many-particle systems and nonequilibrium baths can be used to rectify particle currents, for which we consider minimal setups to realize bath-induced currents in nonequilibrium steady states of one-dimensional (1D) open fermionic systems. We first analyze dissipative dynamics associated with a nonreciprocal Lindblad operator and identify a class of Lindblad operators that are sufficient to acquire a unidirectional current. We show that unidirectional particle transport can in general occur when a Lindblad operator is reciprocal provided that the inversion symmetry and the time-reversal symmetry of the microscopic Hamiltonian are broken. We demonstrate this mechanism on the basis of both analytical and numerical approaches including the Rashba spin-orbit coupling and the Zeeman magnetic field.

Finally, we demonstrate the universal properties of dissipative Tomonaga-Luttinger (TL) liquids by calculating correlation functions and performing finite-size scaling analysis of a NH XXZ spin chain as a prototypical model in 1D open quantum many-body systems. Our analytic calculation is based on effective field theory with bosonization, finite-size scaling approach in CFT, and the

Bethe-ansatz (BA) solution. Our numerical analysis is based on the density-matrix renormalization group generalized to NH systems (NH-DMRG). We uncover that the model in the massless regime with weak dissipation belongs to the universality class characterized by the complex-valued TL parameter, which is related to the complex generalization of the $c = 1$ CFT. As the dissipation strength increases, the values of the TL parameter obtained by the NH-DMRG begin to deviate from those obtained by the BA analysis, indicating that the model becomes massive for strong dissipation. Our results can be tested with the two-component Bose-Hubbard system of ultracold atoms subject to two-body loss.

Contents

List of publications

Papers related to the thesis

1. **Kazuki Yamamoto**, Masaya Nakagawa, Kyosuke Adachi, Kazuaki Takasan, Masahito Ueda, and Norio Kawakami
Theory of Non-Hermitian Fermionic Superfluidity with a Complex-Valued Interaction
Physical Review Letters **123**, 123601 (2019)
Highly Cited Paper in Web of Science Core Collection (Mar. 2021 – Oct. 2022)

2. **Kazuki Yamamoto**, Masaya Nakagawa, Naoto Tsuji, Masahito Ueda, and Norio Kawakami
Collective Excitations and Nonequilibrium Phase Transition in Dissipative Fermionic Superfluids
Physical Review Letters **127**, 055301 (2021)

3. **Kazuki Yamamoto**, Yuto Ashida, and Norio Kawakami
Rectification in nonequilibrium steady states of open many-body systems
Physical Review Research **2**, 043343 (2020)

4. **Kazuki Yamamoto**, Masaya Nakagawa, Masaki Tezuka, Masahito Ueda, and Norio Kawakami
Universal properties of dissipative Tomonaga-Luttinger liquids: Case study of a non-Hermitian XXZ spin chain
Physical Review B **105**, 205125 (2022)

Papers not included in the thesis

5. **Kazuki Yamamoto** and Norio Kawakami
Universal description of dissipative Tomonaga-Luttinger liquids with SU(N) spin symmetry: Exact spectrum and critical exponents
Physical Review B **107**, 045110 (2023)

Abbreviations used in this thesis

AF	Anti-Ferromagnetic
AMO	Atomic, Molecular, and Optical
BCS	Bardeen-Cooper-Schrieffer
BEC	Bose-Einstein Condensate, or Bose-Einstein Condensation
BA	Bethe Ansatz
CFT	Conformal Field Theory
CTC	Closed-Time-Contour
DMRG	Density-Matrix Renormalization Group
GL	Ginzburg-Landau
NESSs	Non-Equilibrium Steady States
NH	Non-Hermitian
tGGE	time-Dependent Generalized Gibbs Ensemble
TL	Tomonaga-Luttinger
QZE	Quantum Zeno Effect
1D	One-Dimensional

Chapter 1

Introduction and background

1.1 Overview of this thesis

First of all, we explain the organization of this theses. This thesis consists of six chapters, including our results in Chaps. 2, 3, 4, and 5. In this chapter, we give an introduction to understand quantum many-body physics in ultracold atoms subject to dissipation. In Sec. 1.2, we give an introduction about open quantum systems and non-Hermitian (NH) quantum systems, which naturally appear in atomic, molecular, and optical (AMO) systems coupled to Markovian environments. Sec. 1.3 is devoted to the explanation of analytical and numerical methods which are beneficial to analyze open quantum systems. In Sec. 1.4, we review the basics of quantum many-body phenomena, which is helpful to understand our results in the subsequent chapters.

In Chap. 2, we demonstrate how fermionic superfluidity in ultracold atoms is affected by inelastic collisions. This chapter gives a generalized property of fermionic superfluids without dissipation discussed in Sec. 1.4.1. Our approach is based on the generalization of the standard Bardeen-Cooper-Schrieffer (BCS) theory to a situation in which fermions interact with each other via a complex-valued attraction. As a result, we find that non-Hermiticity leads to unique reentrant quantum phase transitions in superfluids.

In Chap. 3, we theoretically investigate nonequilibrium dynamics followed by a sudden switch-on of two-particle loss due to inelastic collisions between atoms. Based on closed-time-contour (CTC) path integrals discussed in Sec. 1.3.1, we formulate a dissipative BCS theory that fully incorporates a change in particle number, which is included via quantum jump terms in the Lindblad equation. As an experimentally relevant model, we propose introducing a particle loss in one of two coupled superfluids, and find a nonequilibrium phase transition characterized by the vanishing dc Josephson current.

In Chap. 4, we study a unidirectional particle transport in nonequilibrium steady states (NESSs) of one-dimensional (1D) open fermionic systems subject to homogeneous dissipation, based on the time-dependent generalized Gibbs ensemble (tGGE) approach discussed in Sec. 1.3.2. We demonstrate both reciprocal and nonreciprocal dissipation can be used to induce nonreciprocal transport in NESSs.

In Chap. 5, we study the NH XXZ spin chain by starting from an experimentally relevant two-component Bose-Hubbard model with two-body loss and applying a quantum trajectory method to the Lindblad master equation. We derive correlation functions by using the effective field theory, and obtain the energy spectrum in a finite system consistent with the finite-size scaling formula generalized to NH Tomonaga-Luttinger (TL) liquids. Based on the NH density-matrix renormalization group (DMRG) algorithm discussed in Sec. 1.3.3, we also report the numerical demonstration of the analytically obtained results for the NH XXZ spin chain.

Finally, in Chap. 6, we conclude this thesis.

1.2 Ultracold atoms with dissipation

In this section, we review the basics of ultracold atoms subject to dissipation. First, we introduce open quantum systems, and then explain NH quantum systems, which are effective description of

open quantum systems.

1.2.1 Open quantum systems

In recent years, open quantum systems have been actively studied both experimentally and theoretically [1–3]. In many cases, coupling to the environment causes decoherence of quantum states and it is often detrimental to their control. Remarkably, dissipation can also be instrumental in the preparation of novel states in open quantum systems. To date, a number of theoretical studies have shown that dissipation drastically alters various aspects of quantum many-body physics [4–15]. In particular, the interplay between unitary many-body dynamics and nonunitary state evolution due to dissipation leads to various unconventional phenomena such as dissipative quantum phase transitions [16–18], and measurement-induced entanglement transitions [19–30]. It is worth noting that high controllability of ultracold atoms has enabled studies and observations of novel quantum phases unique to open quantum systems [31–39], e.g., continuous quantum Zeno effect (QZE) [40–42], loss-induced Dicke state [43], and fermionic superfluidity in ultracold atoms undergoing inelastic collisions [44–52]. In this subsection, we first derive the Lindblad master equation that describes the Markovian dynamics in open quantum systems, and explain QZE, which is a prototypical dissipation-induced phenomenon.

Lindblad master equation

In dissipative open quantum systems, the dynamics, after environmental degrees of freedom are traced out, is nonunitary and described by a completely positive and trace-preserving map [2, 53]. Such nonunitary dynamics is described by the Lindblad master equation, and is relevant for AMO systems. We here derive the Lindblad equation by taking an ensemble average of quantum trajectories, which are the stochastic process followed by dissipative dynamics. At $t = 0$, we assume that the system is in the initial state given by the density operator

$$\rho(t=0) = |\phi(t=0)\rangle\langle\phi(t=0)|. \tag{1.1}$$

The dynamics of the density operator gives the quantum master equation. Here, we consider the following two types of stochastic process:

- The system follows the nonunitary dynamics described by the NH Hamiltonian H_{eff}. This dynamics does not change the particle number of the system
- The particle number of the system changes as a result of dissipation. This dynamics is described by the jump operator (Lindblad operator).

The resulting Lindblad master equation is calculated as follows.

First, we consider that the system evolves according to the NH Hamiltonian H_{eff}. By approximating the dynamics up to the first order with respect to δt, the quantum state after time δt is given by

$$|\phi'(t+\delta t)\rangle = (1 - iH_{\text{eff}}\delta t)\,|\phi(t)\rangle \tag{1.2}$$

Here, we have to pay careful atttention to the fact that the dynamics of the system does not follow the unitary evolution as a result of the non-Hermiticity in H_{eff}. Then, this quantum state is realized with the probability that is smaller than 1, and should be normalized by the norm. The square of this norm gives the probability where the normalized state is realized after time δt. This probability is given by

$$\begin{aligned}
\langle\phi'(t+\delta t)|\phi'(t+\delta t)\rangle =& \langle\phi(t)|(1 + iH_{\text{eff}}^{\dagger}\delta t)(1 - iH_{\text{eff}}\delta t)|\phi(t)\rangle \\
\simeq& 1 - i\langle\phi(t)|(H_{\text{eff}} - H_{\text{eff}}^{\dagger})|\phi(t)\rangle\delta t \\
=& 1 - \delta p \\
=& 1 - \sum_i \delta p_i.
\end{aligned} \tag{1.3}$$

Here, the subscript i stands for the label such as coordinates or wave numbers. We obtain the normalized state $|\phi_1(t+\delta t)\rangle$ as

$$|\phi_1(t+\delta t)\rangle = \frac{|\phi'(t+\delta t)\rangle}{\sqrt{1-\delta p}} = \frac{(1-iH_{\rm eff}\delta t)\,|\phi(t)\rangle}{\sqrt{1-\delta p}}. \tag{1.4}$$

As in the same way, we can treat the jump process which changes the particle number of the system. Due to the conservation of the probability, the total probability of the non-unitary dynamics described by $H_{\rm eff}$ and the jump process should be 1. Then, from Eq. (1.3), we see that the probability δp gives the jump process, and we can introduce the jump operator (Lindblad operator) L_i, which is defined by

$$L_i^\dagger L_i \equiv i(H_{\rm eff} - H_{\rm eff}^\dagger). \tag{1.5}$$

As δp_i is given by

$$\sum_i \delta p_i = \langle\phi(t)|i(H_{\rm eff} - H_{\rm eff}^\dagger)|\phi(t)\rangle\delta t \tag{1.6}$$

$$= \sum_i \langle\phi(t)|L_i^\dagger L_i|\phi(t)\rangle\delta t, \tag{1.7}$$

the quantum state after time δt corresponding to the jump process is given by (the state is normalized)

$$|\phi_{2i}(t+\delta t)\rangle = \frac{L_i|\phi(t)\rangle\sqrt{\delta t}}{\sqrt{\delta p_i}} = \frac{L_i|\phi(t)\rangle}{\sqrt{\delta p_i/\delta t}}. \tag{1.8}$$

As a result, by introducing the density operator at time t as

$$\rho(t) = |\phi(t)\rangle\langle\phi(t)|, \tag{1.9}$$

we obtain the ensemble average of the trajectory dynamics at time $t+\delta t$ as

$$\begin{aligned}\overline{\rho(t+\delta t)} &= (1-\delta p)|\phi_1(t+\delta t)\rangle\langle\phi_1(t+\delta t)| + \sum_i \delta p_i|\phi_{2i}(t+\delta t)\rangle\langle\phi_{2i}(t+\delta t)| \\ &= \rho(t) - i\delta t(H_{\rm eff}\rho(t) - \rho(t)H_{\rm eff}^\dagger) + \delta t\sum_i L_i\rho(t)L_i^\dagger.\end{aligned} \tag{1.10}$$

Equation (1.10) holds regardless of whether $\rho(t)$ is a pure state or not. Finally, by dividing Eq. (1.10) by δt, we obtain the Lindblad master equation:

$$\begin{aligned}\dot\rho &= \mathcal{L}\rho \\ &= -i(H_{\rm eff}\rho - \rho H_{\rm eff}^\dagger) + \sum_i L_i\rho L_i^\dagger \\ &= -i[H,\rho] - \frac{1}{2}\sum_i \left(L_i^\dagger L_i\rho + \rho L_i^\dagger L_i - 2L_i\rho L_i^\dagger\right).\end{aligned} \tag{1.11}$$

Here, we note that H is the Hermitian Hamiltonian of the system, and

$$H_{\rm eff} = H - \frac{i}{2}\sum_i L_i^\dagger L_i. \tag{1.12}$$

Thus, we see that the nonunitary dynamics described by the NH Hamiltonian $H_{\rm eff}$ corresponds to the one between quantum jumps in a single quantum trajectory, and thus the NH dynamics does not change the particle number of the system though it feels the effect of dissipation. It depends on the system how long such NH dynamics is realized in real experiments.

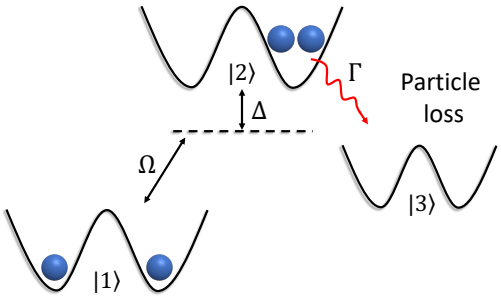

Figure 1.1: Schematic figure of Rabi oscillations in two-level systems

Continuous quantum Zeno effect

One of the prototypical loss-induced phenomena in open quantum systems is QZE, which arises for strong dissipation (two-body loss) regime. Intuitively, when dissipation rate is large, particles seem to be lost into the surrounding environment as a result of inelastic collisions, and it seems that the observed loss increases too. However, in real experiments, observed loss decreases for strong dissipation, and such counterintuitive phenomena are called QZE.

We explain the detailed mechanism in the following. We consider the Rabi oscillation in two-level systems shown in Fig. 1.1 [2]. In Fig. 1.1, the state $|1\rangle$ has one particle in each site, the state $|2\rangle$ has two particles in one site, and the state $|3\rangle$ has no particles. Here, Ω is the Rabi frequency, Δ is the detuning, and Γ is the decay rate from the state $|2\rangle$ to the state $|3\rangle$. Then, the effective Hamiltonian of the systems is given by

$$H_{\text{eff}} = -\frac{\Omega}{2}\sigma_x - \Delta\sigma_+\sigma_- - \mathrm{i}\frac{\Gamma}{2}\sigma_+\sigma_-, \tag{1.13}$$

where σ_i is the Pauli matrix defined by

$$\sigma_x = \begin{pmatrix} 0 & 1 \\ 1 & 0 \end{pmatrix}, \quad \sigma_y = \begin{pmatrix} 0 & -i \\ i & 0 \end{pmatrix}, \quad \sigma_z = \begin{pmatrix} 1 & 0 \\ 0 & -1 \end{pmatrix}, \tag{1.14}$$

and we have introduced

$$\sigma_+ = \begin{pmatrix} 0 & 1 \\ 0 & 0 \end{pmatrix}, \quad \sigma_- = \sigma_+^\dagger. \tag{1.15}$$

We set the basis of the matrix representation to be $(|1\rangle, |2\rangle)$. We see that the last term in the effective Hamiltonian (1.13) denotes the effect of dissipation.

Then, we calculate the observed decay rate of the state $|1\rangle$, which we define as Γ_{eff}. That is, we want to know how the initial state $|1\rangle$ is affected by dissipation when the decay rate Γ is increased. We consider the second-order perturbative process with H_{eff} between the states $|1\rangle$ and $|2\rangle$, and study how particles are affected by dissipation as a result of the NH Hamiltonian H_{eff}. Here, we assume that the Rabi frequency Ω is sufficiently smaller than the detuning Δ or the decay rate Γ. Then, by using the perturbative approach with respect to

$$H_1 = -\frac{\Omega}{2}\sigma_x, \tag{1.16}$$

the energy shift for the state $|1\rangle$ is calculated up to the second order as follows:

$$E_1 = \frac{\langle 1|\, H_1\, |2\rangle \langle 2|\, H_1\, |1\rangle}{\Delta + i\Gamma/2} = \frac{\Omega^2}{4\Delta^2 + \Gamma^2}(\Delta - i\Gamma/2). \tag{1.17}$$

As E_1 denotes the energy shift including the effect of dissipation, the time evolution of the state $|1\rangle$ described by the energy E_1 is given by

$$\exp\left(-iE_1 t\right)|1\rangle = \exp\left[-i\frac{\Omega^2}{4\Delta^2 + \Gamma^2}\left(\Delta - i\frac{\Gamma}{2}\right)t\right]|1\rangle\,. \tag{1.18}$$

The decay of the state $|1\rangle$ is obtained by the squared norm of Eq. (1.18) as

$$P_{\rm loss} = \exp\left[-\frac{\Omega^2}{4\Delta^2+\Gamma^2}\Gamma t\right]. \tag{1.19}$$

Thus, the effective decay rate of the state $|1\rangle$, that is, $\Gamma_{\rm eff}$, is calculated as

$$\Gamma_{\rm eff} = \frac{\Omega^2}{4\Delta^2+\Gamma^2}\Gamma. \tag{1.20}$$

In Eq. (1.20), for small Γ, we see that $\Gamma_{\rm eff}$ increases as we increase the dissipation rate Γ. This is an intuitive result. However, for large Γ, we see from (1.20) that the observed loss rate $\Gamma_{\rm eff}$ decreases as we increase Γ. This is QZE, which shows that the system tends to freeze in its initial state for large dissipation rate Γ, and thereby observed loss decreases. Though QZE was first suggested in mathematics [54], it is observed in many experiments, and the first observation in ultracold atoms was in 2008 [40], in which spinless bosons of 1D ^{87}Rb Bose-Einstein condensate (BEC) were used.

At the end of this subsection, we explain how to calculate dissipative dynamics of the particle number in the system. For simplicity, we consider the Lieb-Liniger model [12, 55] given by

$$H = -\frac{1}{2m}\sum_i \frac{\partial^2}{\partial x_i^2} + g\sum_{i<j}\delta(x_i - x_j) \tag{1.21}$$

$$= -\frac{1}{2m}\int dx \Psi^\dagger(x)\frac{d^2}{dx^2}\Psi(x) + \frac{{\rm Re}(g)}{2}\int dx \Psi^{\dagger 2}(x)\Psi^2(x). \tag{1.22}$$

When the system is subject to two-body losses of bosons, the system dynamics is given by the Lindblad master equation $d\rho/dt = -i[H,\rho] + \mathcal{D}(\rho)$, where $\mathcal{D}(\rho)$ describes the coupling to the environments, and is given by

$$\mathcal{D}(\rho) = \frac{{\rm Im}(g)}{2}\int dx \left(2\Psi^2(x)\rho\Psi^{\dagger 2}(x) - \Psi^{\dagger 2}(x)\Psi^2(x)\rho - \rho\Psi^{\dagger 2}(x)\Psi^2(x)\right). \tag{1.23}$$

In experiments, the loss coefficient is determined by the time-evolution of the particle number in the system, which is easily obtained as follows. We use the fact that expectation values are given by

$${\rm Tr}(\rho A) = {\rm Tr}(\rho A^\dagger) = [{\rm Tr}(\rho A)]^* \in \mathbb{R} \quad (A\text{: Hermitian}). \tag{1.24}$$

By multiplying the particle number operator n to the Lindblad master equation (1.11) and taking the trace, we obtain

$$\begin{aligned}
\frac{d\langle n\rangle}{dt} &= -i{\rm Tr}\left[n\left[H,\rho\right]\right] + {\rm Tr}\left[n\mathcal{D}(\rho)\right] \\
&= {\rm Tr}\left[n\mathcal{D}(\rho)\right] \\
&= \frac{{\rm Im}(g)}{2}\int dx {\rm Tr}[2\Psi^{\dagger 3}(x)\Psi^3(x)\rho - \Psi^\dagger(x)\Psi(x)\Psi^{\dagger 2}(x)\Psi^2(x)\rho \\
&\qquad\qquad - \Psi^{\dagger 2}(x)\Psi^2(x)\Psi^\dagger(x)\Psi(x)\rho] \\
&= \frac{{\rm Im}(g)}{2}\int dx {\rm Tr}[2\Psi^{\dagger 3}(x)\Psi^3(x)\rho - \Psi^\dagger(x)(1+\Psi^\dagger(x)\Psi(x))\Psi^\dagger(x)\Psi^2(x)\rho \\
&\qquad\qquad - \Psi^{\dagger 2}(x)\Psi(x)(1+\Psi^\dagger(x)\Psi(x))\Psi(x)\rho] \\
&= \frac{{\rm Im}(g)}{2}\int dx {\rm Tr}\left[2\Psi^{\dagger 3}(x)\Psi^3(x)\rho - 2\Psi^{\dagger 2}(x)\Psi^2(x)\rho - 2\Psi^{\dagger 2}(x)\Psi(x)\Psi^\dagger(x)\Psi^2(x)\rho\right] \\
&= -2{\rm Im}(g)\int dx {\rm Tr}\left[\Psi^{\dagger 2}(x)\Psi^2(x)\rho\right] \\
&= -2{\rm Im}(g)g^{(2)}\langle n\rangle^2,
\end{aligned} \tag{1.25}$$

where $g^{(2)}$ is given by

$$g^{(2)} = \frac{\langle\Psi^{\dagger 2}\Psi^2\rangle}{\langle n\rangle^2}. \tag{1.26}$$

We note that $g^{(2)}$ becomes 1 in the limit of no correlation.

1.2.2 Non-Hermitian quantum systems

In recent years, NH quantum systems, which are effective descriptions of open quantum systems, have been actively studied both experimentally and theoretically [56]. NH quantum systems arise when the system undergoes dissipation to an environment [2, 57]. It has been revealed that non-Hermiticity drastically alters the properties of a number of quantum phenomena that have been established in the Hermitian physics, such as quantum phase transitions [58–62], quantum critical behavior [63–68], topological phases [69–80], and magnetism [81, 82]. Such theoretical predictions have been confirmed experimentally by using optical systems and ultracold atoms [83–92]. However, since most of the previous studies dealt with single-particle physics, exploration of many-body physics in NH systems is still in its infancy [63, 64, 66, 67].

In general, for the realization of NH quantum many-body systems, postselection of measurement outcomes by means of quantum-gas microscopy can be utilized [56, 63, 64, 82, 93], and such experimental progress has facilitated investigations of NH quantum systems. NH quantum systems have a lot of unique properties that have not been obtained in conventional Hermitian systems. For example, the energy spectrum in a closed system is always real as a result of Hermiticity of the system Hamiltonian. However, NH Hamiltonian gives complex-valued energy spectra as a result of dissipation, and the imaginary part of the energy gives decay rates of the eigenstates. This is easily understood as the time evolution of the system is described by the Schrödinger equation $i\partial_t|\psi\rangle = H_{\rm eff}|\psi\rangle$, where $H_{\rm eff}$ is the NH Hamiltonian of the system. Thus, eigenstates differ from right ones to left ones (ket vectors to bra vectors), and the definition of expectation values in general becomes nontrivial.

To understand the property of NH Hamiltonian in detail, we give an example of the NH XY model [81]. We consider a 1D XY Hamiltonian described by

$$H = \sum_n (J_x \sigma_n^x \sigma_{n+1}^x + J_y \sigma_n^y \sigma_{n+1}^y), \tag{1.27}$$

where σ_n^i is the Pauli matrix. By considering a decay event of up spins, the effective NH Hamiltonian of the system is given by

$$H_{\rm eff} = H - \frac{i\gamma}{4}\sum_n (\sigma_n^z + 1) \tag{1.28}$$

$$= \sum_n \Big[2J(\sigma_n^+\sigma_{n+1}^- + \sigma_n^-\sigma_{n+1}^+) + 2J'(\sigma_n^+\sigma_{n+1}^+ + \sigma_n^-\sigma_{n+1}^-) - \frac{i\gamma}{4}(\sigma_n^z + 1)\Big], \tag{1.29}$$

where we have introduced $J = \frac{J_x+J_y}{2}$ and $J' = \frac{J_x-J_y}{2}$.

In the case of two atoms, the eigenvalues and eigenstates of the effective Hamiltonian are simply written down as

$$\lambda_1^\pm = -i\frac{\gamma}{2} \pm \frac{1}{2}\sqrt{64J'^2 - \gamma^2}, \quad \lambda_2^\pm = -i\frac{\gamma}{2} \pm 4J \tag{1.30}$$

$$|u_1^\pm\rangle = \frac{1}{\mathcal{N}} \begin{pmatrix} \frac{-i\gamma \pm \sqrt{64J'^2-\gamma^2}}{8J'} \\ 0 \\ 0 \\ 1 \end{pmatrix}, \quad |u_2^\pm\rangle = \begin{pmatrix} 0 \\ \frac{\pm 1}{\sqrt{2}} \\ \frac{1}{\sqrt{2}} \\ 0 \end{pmatrix}. \tag{1.31}$$

We see that the eigenvalues $\lambda_1^\pm$ have a unique property in NH quantum systems. First, $\lambda_1^\pm$ are complex conjugate to each other, and this property only arises in NH quantum mechanics. Moreover, the eigenvalues $\lambda_1^\pm$ become degenerate when $J' = \gamma/8$, and this point is called the exceptional point, which has obtained tremendous interest in NH quantum systems.

1.3 Analytical and numerical methods in open quantum systems

Open quantum systems offer a new opportunity to investigate nonequilibrium phenomena, where couplings to the environment play a central role. However, dissipation makes the system complicated, and in general, it becomes more difficult to deal with quantum states in dissipative systems

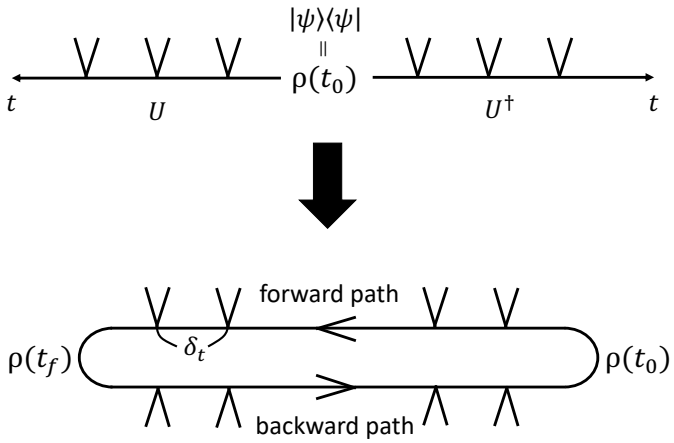

Figure 1.2: Schematic figure of CTC for pure states

than those in closed systems. In this section, we introduce several useful techniques to approach dissipative phenomena both analytically and numerically.

1.3.1 Closed-time-contour path integrals for Lindblad equations

We here explain the philosophy of CTC path integrals (so-called Keldysh path integrals) for the Lindblad master equation (1.11) [3]. Figure 1.2 shows the idea of CTC path integrals for pure states. As the Lindblad operator is a superoperator, it acts both on the bra vector and the ket vector of the density matrix. By denoting the time evolution of the ket side $U|\psi\rangle$ as a forward path, and that of the bra side $\langle\psi|U^\dagger$ as a backward path, respectively, we obtain CTC as shown in Fig. 1.2. We note that, in a closed system, we only have to deal with the forward path as we assume adiabatic process in equilibrium. However, in open quantum systems, we have to consider both forward and backward paths as adiabatic approximation generally breaks down.

We then go on to the details of how to construct CTC path integral. For simplicity, we consider bosonic cases. We start with a generating functional given by

$$Z_{t_f,t_0} = \mathrm{Tr}\rho(t_f) = \mathrm{Tr}e^{(t_f-t_0)\mathcal{L}}\rho(t_0), \tag{1.32}$$

where we note that time evolution of the density matrix is given by

$$\rho(t) = e^{(t-t_0)\mathcal{L}}\rho(t_0) \equiv \lim_{N\to\infty}(1+\delta_t\mathcal{L})^N\rho(t_0). \tag{1.33}$$

As in the case of conventional path integrals in a closed system, we follow a procedure to decompose the time evolution into small time steps.

It is then useful to introduce a bosonic coherent state, which is defined as

$$|\psi\rangle = \exp(\psi b^\dagger)|0\rangle, \tag{1.34}$$
$$b|\psi\rangle = \psi|\psi\rangle, \tag{1.35}$$

where $|0\rangle$ is the vacuum in Fock space. Then, we obtain several useful equations of coherent states such as

$$\langle\psi|b^\dagger = \langle\psi|\psi^*, \tag{1.36}$$
$$\langle\psi|\phi\rangle = e^{\psi^*\phi}. \tag{1.37}$$

We note that the completeness condition is given by

$$\mathbf{1} = \int\frac{d\psi d\psi^*}{\pi}e^{-\psi^*\psi}|\psi\rangle\langle\psi|. \tag{1.38}$$

By using the time step $t_n \equiv t_0 + \delta_t n$ and the completeness condition, we can write down the density matrix ρ_n at time t_n as

$$\rho_{n+1} = e^{\delta_t \mathcal{L}} \rho_n \simeq (1 + \delta_t \mathcal{L}) \rho_n, \tag{1.39}$$

$$\rho_n = \int \frac{d\psi_{+,n} d\psi^*_{+,n}}{\pi} \frac{d\psi_{-,n} d\psi^*_{-,n}}{\pi} e^{-\psi^*_{+,n}\psi_{+,n} - \psi^*_{-,n}\psi_{-,n}} \langle \psi_{+,n}|\rho_n|\psi_{-,n}\rangle |\psi_{+,n}\rangle\langle\psi_{-,n}|. \tag{1.40}$$

Then, we easily obtain

$$\langle \psi_{+,n+1}|\rho_{n+1}|\psi_{-,n+1}\rangle = \int \frac{d\psi_{+,n} d\psi^*_{+,n}}{\pi} \frac{d\psi_{-,n} d\psi^*_{-,n}}{\pi} e^{i\delta_t(-\psi_{+,n} i\partial_t \psi^*_{+,n} - \psi^*_{-,n} i\partial_t \psi_{-,n} - i\mathcal{L})} \langle \psi_{+,n}|\rho_n|\psi_{-,n}\rangle, \tag{1.41}$$

where we have assumed normal ordering of the Hamiltonian, introduced the eigenvalue of the Liouvillian $\mathcal{L}$ as

$$\mathcal{L} = \frac{\langle \psi_{+,n+1}|\mathcal{L}(|\psi_{+,n}\rangle\langle\psi_{-,n}|)|\psi_{-,n+1}\rangle}{\langle \psi_{+,n+1}|\psi_{+,n}\rangle\langle\psi_{-,n}|\psi_{-,n+1}\rangle}, \tag{1.42}$$

and used the following equations

$$\langle \psi_{+,n+1}|\psi_{+,n}\rangle = e^{\psi^*_{+,n+1}\psi_{+,n}}, \tag{1.43}$$

$$(\psi^*_{+,n+1} - \psi^*_{+,n})\psi_{+,n} = \delta_t \psi_{+,n} \partial_t \psi^*_{+,n}. \tag{1.44}$$

Finally, by taking the limit $\delta_t \to 0$ ($N \to \infty$), $t_0 \to -\infty$, $t_f \to \infty$, and ignoring the boundary term $\langle \psi_+(t_0)|\rho(t_0)|\psi_-(t_0)\rangle$, we arrive at the final form of CTC path integrals as

$$Z = \int \mathcal{D}[\psi_+, \psi^*_+, \psi_-, \psi^*_-] e^{iS} = 1, \tag{1.45}$$

$$\mathcal{D} = [\psi_+, \psi^*_+, \psi_-, \psi^*_-] \lim_{N\to\infty} \prod_{n=0}^{N} \frac{d\psi_{+,n} d\psi^*_{+,n}}{\pi} \frac{d\psi_{-,n} d\psi^*_{-,n}}{\pi}, \tag{1.46}$$

$$S = \int_{-\infty}^{\infty} dt (\psi^*_+ i\partial_t \psi_+ - \psi^*_- i\partial_t \psi_- - i\mathcal{L}(\psi^*_+, \psi_+, \psi^*_- \psi_-)), \tag{1.47}$$

$$\mathcal{L}(\psi^*_+, \psi_+, \psi^*_- \psi_-) = -i(H_+ - H_-) + \sum_\alpha \gamma_\alpha [L_{\alpha,+} L^*_{\alpha,-} - \frac{1}{2}(L^*_{\alpha,+} L_{\alpha,+} + L^*_{\alpha,-} L_{\alpha,-})], \tag{1.48}$$

which we frequently employ by generalizing the formalism to fermionic systems in Sec. 3.

1.3.2 Time-dependent generalized Gibbs ensemble

NESSs are unique quantum phases, which are obtained as a result of couplings to environments. Though several studies have been done to approach many-body phenomena in NESSs [2, 5, 94, 95], there still lacks of general description to describe many-body physics in NESSs of open quantum systems. In this subsection, we explain how the dynamics of the system that is weakly driven by Markovian baths is determined based on the methods considered in Refs. [96–98], which make an approach to NESSs from the perspective of noneqilibrium statistical mechanics.

We consider a situation that the integrable system described by a Hamiltonian H_0 with conservation laws I_i ($i = 0, 1, \ldots, N$) is weakly perturbed by Markovian baths, thus breaking the integrability. Such a system is described by the Lindblad master equation by using a small dimensionless parameter ϵ as $\partial_t \rho = \mathcal{L}_0 \rho + \mathcal{L}_1 \rho$, $\mathcal{L}_0 \rho = -i[H_0, \rho]$, $\mathcal{L}_1 \rho = \epsilon \mathcal{D}(\rho)$, where the dissipator $\mathcal{D}(\rho)$ is given by $\mathcal{D}(\rho) = \sum_m \left(L_m \rho L^\dagger_m - \frac{1}{2} \left\{ L^\dagger_m L_m, \rho \right\} \right)$. Below, we take a perturbative approach to NESSs. If there is no perturbation by the environments, it is extensively shown that steady states of the integrable models approach to that described by a generalized Gibbs ensemble

$$\rho_0 = \frac{e^{-\sum_i \lambda_i I_i}}{\mathrm{Tr}[e^{-\sum_i \lambda_i I_i}]}. \tag{1.49}$$

Then, we track the changes of the Lagrange parameters by weak driving of the baths. We split the density operator $\rho(t)$ into zeroth-order approximation $\rho_{\rm GGE}(t)$ and corrections $\delta\rho(t)$ as

$$\rho(t) = \rho_{\rm GGE}(t) + \delta\rho(t), \tag{1.50}$$

where $\rho_{\rm GGE}(t)$ is the tGGE

$$\rho_{\rm GGE}(t) = \frac{e^{-\sum_i \lambda_i(t) I_i}}{{\rm Tr}[e^{-\sum_i \lambda_i(t) I_i}]}. \tag{1.51}$$

and $\delta\rho$ should be small in the limit $\epsilon \to 0$. As $\mathcal{L}_0\rho_{\rm GGE}(t) = 0$ by definition, the condition of NESSs $\mathcal{L}\rho = 0$ ensures that the correction $\delta\rho$ of order of ϵ (and larger) is given by

$$\delta\rho = -\mathcal{L}^{-1}\mathcal{L}_1\rho_{\rm GGE}. \tag{1.52}$$

To obtain the dynamics of Lagrange parameters $\lambda_i(t)$ that determines $\rho_{\rm GGE}$ of order of ϵ^0, it is convenient to introduce the superoperator $\mathcal{P}$

$$\mathcal{P}X \equiv -\sum_{ij} \frac{\partial\rho_{\rm GGE}}{\partial\lambda_i}(\chi^{-1})_{ij}{\rm tr}[I_j X], \tag{1.53}$$

$$\chi_{ij}(t) = \langle I_i I_j\rangle_{\rm GGE} - \langle I_i\rangle_{\rm GGE}\langle I_j\rangle_{\rm GGE}, \tag{1.54}$$

which projects the density matrix onto the space tangential to the GGE manifold spanned by $\partial\rho_{\rm GGE}(t)/\partial\lambda_i$. Here, we note that $\mathcal{P}\rho_{\rm GGE} \neq \rho_{\rm GGE}$ because $\mathcal{P}$ is not a projector onto the space of GGE matrix. By using

$$\mathcal{P}\dot{\rho} = \dot{\rho}_{\rm GGE} + \mathcal{P}\delta\dot{\rho} \tag{1.55}$$

and demanding that $\mathcal{P}\delta\dot{\rho} \sim O(\epsilon^2)$, we obtain

$$\mathcal{P}\dot{\rho} \simeq \dot{\rho}_{\rm GGE} = \sum_i \frac{\partial\rho_{\rm GGE}}{\partial\lambda_i}\frac{\partial\lambda_i}{\partial t} \tag{1.56}$$

Since $\langle I_i\rangle$ is calculated as

$$\begin{aligned}\langle\dot{I}_i\rangle &= {\rm tr}[I_i\mathcal{L}\rho] \\ &= {\rm tr}[I_i\mathcal{L}_1\rho_{\rm GGE}] + {\rm tr}[I_i\mathcal{L}_1\delta\rho] \\ &\simeq {\rm tr}[I_i\mathcal{L}_1\rho_{\rm GGE}]\end{aligned} \tag{1.57}$$

(we have used ${\rm tr}[I_i\mathcal{L}_0\delta\rho] = 0$ because $\mathcal{L}_0^\dagger I_i = i[H_0, I_i] = 0$, where the adjoint of the Liouvillian is defined by ${\rm tr}[A\mathcal{L}\rho] = {\rm tr}[(\mathcal{L}^\dagger A)\rho]$), we finally obtain the dynamics of the Lagrange parameters up to the order of ϵ from Eqs. (1.53) and (1.56) as

$$\dot{\lambda}_i = -\sum_j (\chi(t)^{-1})_{ij}{\rm tr}\left[I_j\mathcal{L}_1\rho_{\rm GGE}(t)\right]. \tag{1.58}$$

Equation (1.58) is used to determine the steady-state properties of NESSs in approximately integrable open quantum systems instead of fully calculating the Lindblad equation. For higher order corrections of the perturbation theory and numerical evidence of the validity of tGGE, see Refs. [97, 98]. We will use tGGE in Sec. 4 to study dissipation-induced transport of fermions in NESSs.

1.3.3 Non-Hermitian density-matrix renormalization group

The DMRG analysis is one of the most powerful tools to analyze 1D systems [100–105]. The principle of DMRG is the variational ansatz, in which the state is optimized by truncating the eigenstates of the density matrix according to the magnitude of the corresponding eigenvalues. However, in NH systems, the variational principle usually breaks down and an important question arises concerning the choice of the density matrix. This is because the right and left eigenvectors of

Table 1.1: Algorithm for NH-DMRG

1.	Compute the matrix representation of the spin operators and make the Hamiltonian matrix for four initial blocks (the superblock consists of a block, two sites, and another block).
2.	Calculate the right and left ground states of the superblock Hamiltonian by using the Lanzcos method. The ground state is defined by the lowest real part of the eigenspectrum.
3.	Use the right and left ground states $\psi^{R(L)}$ to create the reduced density matrix of the system block as $\rho_{i_1 i_2, i'_1 i'_2} = \frac{1}{2}\sum_{i_3 i_4}(\psi^{R}_{i_1 i_2 i_3 i_4}\psi^{R*}_{i'_1 i'_2 i_3 i_4} + \psi^{L}_{i_1 i_2 i_3 i_4}\psi^{L*}_{i'_1 i'_2 i_3 i_4})$. We emphasize that the validity of this density matrix was confirmed numerically in Ref. [99], and we do not use the traditional variational ansatz to minimize the energy. The density matrix $\rho_{i_1 i_2, i'_1 i'_2}$ is Hermitian and has real eigenvalues.
4.	Diagonalize the density matrix $\rho_{i_1 i_2, i'_1 i'_2}$ to find a set of eigenvalues and eigenvectors. Discard all but the largest m eigenvalues and associated eigenvectors.
5.	Form a new block by changing the bases to the new m states.
6.	Repeat the processes 2-5 to enlarge the system by following the standard infinite-system algorithm.
7.	Sweep the superblock by following the standard finite-system algorithm. Eigenstate prediction is conducted for the right and left eigenstates by the same transformation.

the Hamiltonian are different due to the non-Hermiticity [106] and complex eigenvalues can appear in the density matrix. In the previous studies, this problem was tackled by comparing the usage of various types of the density matrix and successful numerical results have been obtained in, e.g., quantum Hall effects [107], reaction-diffusion processes [99], NH TL liquids [108, 109], and out-of-equilibrium classical systems [110, 111]. We note that these situations are essentially different from those of equilibrium quantum systems at a nonzero temperature, where a non-symmetric transfer matrix is generated by applying a Trotter decomposition along the imaginary-time axis [112]. In the latter situations, a similar problem occurs and the non-symmetric density matrix has been used for the truncation of DMRG. However, to the best of our knowledge, no complex eigenvalues stemming from the non-Hermiticity of the transfer matrix have appeared numerically. In this sense, DMRG in NH systems offers intrinsically different situations from those in the equilibrium systems. We apply the NH-DMRG algorithm, in which complex eigenvalues occur as a result of the non-Hermiticity of the Hamiltonian, to NH quantum many-body systems. Such DMRG in NH quantum many-body systems has yet to be fully explored [108, 109, 113]. We use the algorithm detailed in Ref. [99], and we give a brief summary of the NH-DMRG algorithm in Table 1.1. We will use NH-DMRG in Sec. 5 to study ground state properties of NH XXZ spin chain.

1.4 Basics of quantum many-body phenomena

In this section, we review several prototypical quantum many-body phenomena in condensed matter physics (with no dissipation).

1.4.1 Fermionic superfluids in ultracold atoms

In this subsection, we briefly review the progress of fermionic superfluids in ultracold atoms. As is well known, fermionic superfluidity of ^{3}He is a famous example which was predicted about 50 years ago, but that in ultracold atoms has been realized in the early 2000s. This discovery has started by the observations of molecular BEC in 2003 [114–116]. These experiments have treated lower-magnetic field regions compared to the unitary regimes of BCS-BEC crossovers, and higher-magnetic field regions than the unitary regimes, that is, BCS regimes have not been realized at this point. BCS-BEC crossover has been observed in 2004, and celebrated BCS fermionic superfluidity has been realized in ultracold atoms [117–119].

There has been great advancement in experimental techniques of fermionic superfluidity in these 20 years. For example, Refs [117, 118] directly observed the condensation rate of molecular pairs, and observations of superfluid gaps and excitation spectra have been reported in Refs. [119, 120] by using radio-frequency spectroscopy. We note that s-wave fermionic superfluidity is also observed in lattice systems [121], and p-wave fermionic superfluidity has not been experimentally reported so far, mainly because of the significant problem of particle losses.

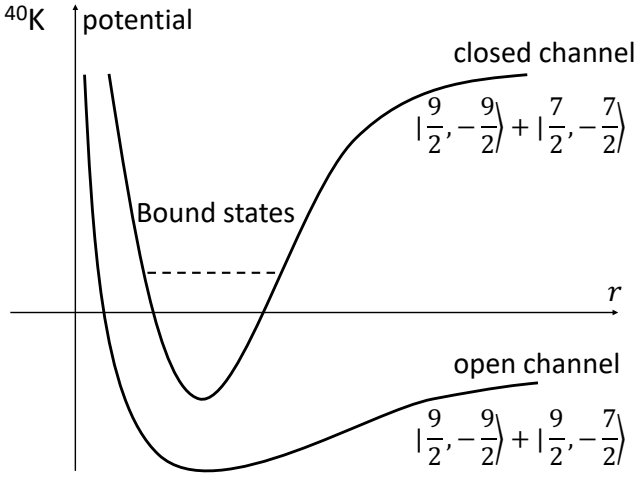

Figure 1.3: Schematic figure of the Feshbach resonance in ^{40}K

We then summarize the Feshbach resonance, which is an important experimental protocol in ultracold atoms. Feshbach resonance is the experimental technique to control interactions between atoms by using external magnetic fields. Figure 1.3 shows the schematic figure of the Feshbach resonance, and two potentials are shown with respect to two kinds of spin states, where we have used ^{40}K as an example. One is called the open channel that cannot make a bound state, and the other is called the closed channel which can make a bound state, but becomes unstable as the distance r is increased. Then, atomic interactions in the open channel are controlled via the resonance with the closed channel. As these two channels have different magnetic moments in general, atomic interactions in the open channel is controlled by using the Zeeman splitting with external magnetic fields.

Recently, another experiment to tune interactions called orbital Feshbach resonance has been actively studied in ultracold alkaline-earth-like atoms such as Yb and Sr [45]. The philosophy of the Feshbach resonance is to control interactions by using magnetic moments in the ground state ^{1}S$_0$. However, in ultracold alkaline-earth-like atoms, the ground state ^{1}S$_0$ has no magnetic moment, and it is difficult to use the conventional Feshbach resonance. Then, it is suggested in Ref. [45] that another way to realize the Feshbach resonance with the use of the metastable state ^{3}P$_0$ and the ground state ^{1}S$_0$ focusing on the difference of the magnetic moment of nuclear spin states. Orbital Feshbach resonance has been experimentally realized [49, 50] soon after the theoretical suggestion, and observations of molecular bosons have been reported [51]. Though fermionic superfluidity by using the orbital Feshbach resonance has not been reported so far, it is expected that ultracold alkaline-earth fermions are to be used for realizing novel quantum many-body phenomena by using the orbital Feshbach resonance.

1.4.2 One-dimensional spin systems

One dimensional quantum systems have been widely studied in condensed matter physics, and one of the most important understanding is the TL liquid, which gives universal properties of 1D quantum critical phenomena. In this subsection, we treat the (Hermitian) XXZ model as a prototypical example of 1D strongly correlated many-body systems. The Hamiltonian is given by

$$\begin{aligned} H &= J\sum_j (S^x_{j+1}S^x_j + S^y_{j+1}S^y_j) + J\Delta\sum_j S^z_{j+1}S^z_j \\ &= \frac{J}{2}\sum_j (S^+_{j+1}S^-_j + S^-_{j+1}S^+_j) + J\Delta\sum_j S^z_{j+1}S^z_j, \end{aligned} \tag{1.59}$$

which we generalize to dissipative systems in Sec. 5. In the following, we summarize the well-known property of this model, by deriving the sine-Gordon model with the use of bosonization and Hermitian DMRG.

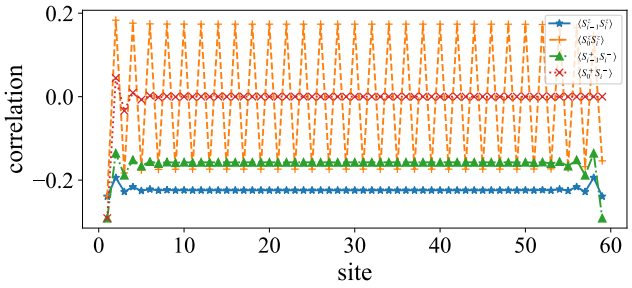

Figure 1.4: Local bond strength and correlation functions obtained by DMRG with respect to xy and z directions. The parameters are set to $L = 60$, $m = 64$, $J = 1$, and $J_z = 3$.

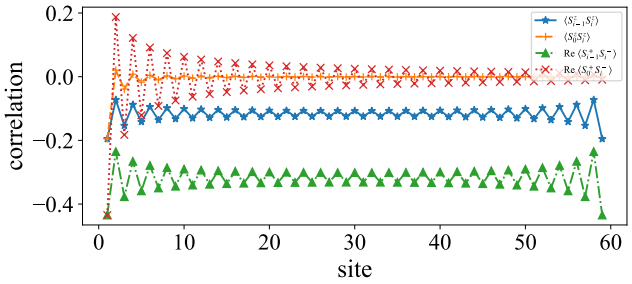

Figure 1.5: Local bond strength and correlation functions obtained by DMRG with $L = 60$, $m = 90$, $J = 1$, and $J_z = 0.3$

We first explain the details of the bosonization procedure for the XXZ model (1.59) [122]. Bosonization is conducted in terms of the fields

$$\begin{aligned}\phi(x) =& -(N_R + N_L)\frac{\pi x}{L} \\ & - \frac{i\pi}{L}\sum_{k\neq 0}\left(\frac{L|k|}{2\pi}\right)^{\frac{1}{2}}\frac{1}{k}e^{-\alpha|k|/2-ikx}(b_k^\dagger + b_{-k}),\end{aligned} \tag{1.60}$$

and

$$\begin{aligned}\theta(x) =& (N_R - N_L)\frac{\pi x}{L} \\ & + \frac{i\pi}{L}\sum_{k\neq 0}\left(\frac{L|k|}{2\pi}\right)^{\frac{1}{2}}\frac{1}{|k|}e^{-\alpha|k|/2-ikx}(b_k^\dagger - b_{-k}).\end{aligned} \tag{1.61}$$

These fields obey the commutation relations

$$\begin{aligned}[\phi(x_1), \theta(x_2)] &= \sum_{k\neq 0}\frac{\pi}{Lk}\exp[ik(x_2 - x_1) - \alpha|k|] \\ &= i\frac{\pi}{2}\mathrm{sgn}(x_2 - x_1),\end{aligned} \tag{1.62}$$

and

$$[\phi(x_1), \nabla\theta(x_2)] = i\pi\delta(x_2 - x_1). \tag{1.63}$$

Here, b_k ($b_k^\dagger$) is the annihilation (creation) operator of bosons, the subscript $r = R$ (L) denotes the right- (left-) going particles, N_r is the number of fermions above the Dirac sea in the r branch,

Table 1.2: Ground state property of the XXZ spin chain

Δ	Energy gap	Ground state	Correlation functions
$\Delta > 1$	Ising, gapped	AF, double degeneracy	AF long-range order in z direction exponential decay in xy plane
$\Delta = 1$	Heisenberg, gapless	no magnetic order, no degeneracy	power law $\times$ log correction
$\Delta < 1$	TL liquid, gapless	no magnetic order, no degeneracy	power law

L is the system size, and α is a short-distance cutoff. The fields $\phi(x)$ and $\theta(x)$ are related to the fermion operator as

$$\psi_r(x) = U_r \lim_{\alpha\to 0} \frac{1}{\sqrt{2\pi\alpha}} e^{i(\epsilon_r k_F - \frac{\pi}{L})x} e^{-i(\epsilon_r\phi(x)-\theta(x))}, \tag{1.64}$$

where U_r is the Klein factor [122], $\epsilon_R = +1$, and $\epsilon_L = -1$.

By using these bosonization dictionaries, we rewrite the XXZ Hamiltonian (1.59) and obtain the sine-Gordon Hamiltonian

$$H = H_{\rm TL} - \frac{2g_3}{(2\pi\alpha)^2}\int dx \cos(4\phi(x)), \tag{1.65}$$

where $g_3 = aJ\Delta$, and

$$H_{\rm TL} = \frac{1}{2\pi}\int dx \Big[uK(\nabla\theta(x))^2 + \frac{u}{K}(\nabla\phi(x))^2\Big], \tag{1.66}$$

with

$$uK = v_F = Ja\sin(k_F a), \tag{1.67}$$

$$\frac{u}{K} = v_F\left(1 + \frac{2J\Delta a}{\pi v_F}(1-\cos(2k_F a))\right). \tag{1.68}$$

Here, we have assumed the half-filling condition $k_F = \pi/2a$ which corresponds to the zero-magnetization sector of the XXZ model. We note that the above derivation is valid only up to the first order of Δ. If the cosine term in the sine-Gordon Hamiltonian (1.59) is irrelevant, the model reduces to the TL Hamiltonian in Eq. (1.66). This is realized for the anisotropy parameter $\Delta < 1$.

In 1D systems, DMRG is one of the most powerful numerical methods [100, 101]. We plot local bond strength and correlation functions for $\Delta > 1$ with open boundary conditions in Fig. 1.4. We see that the system shows antiferromagnetic long-range order in z direction as a result of the gapped ground state, and the correlation in xy direction shows exponential decay. On the other hand, Fig. 1.5 shows the DMRG results for $\Delta < 1$. We see that the correlation function shows power-law decay as a result of the gapless ground state in the thermodynamics limit. Finally, we summarize the ground-state property of the XXZ model (1.59) as shown in Table 1.2.

Chapter 2

Non-Hermitian fermionic superfluidity

2.1 Introduction

Fermionic superfuidity is one of the most striking quantum many-body phenomena, which has been a subject of intensive investigation in condensed matter physics [123]. More recently, ultracold atomic systems have opened a new arena to study fermionic superfluidity [117, 118, 124], where they are subject to losses due to inelastic collisions. For example, if we consider a superfluid mediated by the orbital Feshbach resonance [45–48], which controls an interaction between the ground state and an excited state of an atom [49–52], loss inevitably occurs due to inelastic processes between different orbitals. Such inelastic two-body losses cause the decay of eigenstates of the Hamiltonian and may be described by complex-valued interactions, thus providing an ideal platform to study NH fermionic superfluids. Despite its growing importance, however, theory for NH fermionic superfluidity has not been established yet [125–127].

In this chapter, we demonstrate how fermionic superfluidity in ultracold atoms is modified under inelastic collisions, by generalizing the standard BCS theory to a situation in which fermions interact with each other via a complex-valued attraction [128]. We elucidate that the non-Hermiticity alters several fundamental properties of superfluidity; for example, the order parameters of particles and holes are not necessarily complex conjugate to each other in the NH physics, and the Bogoliubov quasiparticles obey neither Fermi nor Bose statistics since eigenstates are, in general, not orthogonal to each other.

Furthermore, we find that the non-Hermiticity leads to unique quantum phase transitions in superfluids. For a weak interaction, the real part of the superfluid gap is first suppressed and then quenched with increasing dissipation. Remarkably, superfluidity is restored beyond a certain strength of dissipation and the superfluid gap is even enhanced afterwards with increasing dissipation. We show that these phase transitions emerge from exceptional points, lines and surfaces that are unique to the NH physics, where the Hamiltonian cannot be diagonalized [129, 130]. For a strong interaction, superfluidity is not suppressed and never breaks down because fermions are paired to form molecules on each site, thereby avoiding intersite decoherence. Our finding can experimentally be tested in various ultracold atomic species under inelastic collisions such as ^{173}Yb, ^{40}K, and ^{6}Li [51, 52, 119–121, 131, 132].

2.2 Setup

We consider ultracold fermionic atoms with an attractive interaction in a three-dimensional optical lattice. When atoms undergo inelastic collisions, the scattered atoms are lost from the system since a large internal energy is converted to the kinetic energy. An atomic gas undergoing two-body losses due to inelastic collisions is described by a quantum master equation

$$\dot{\rho} = -i(H_{\rm eff}\rho - \rho H_{\rm eff}^{\dagger}) + \gamma \sum_i L_i \rho L_i^{\dagger}, \tag{2.1}$$

where L_i is a Lindblad operator that describes a loss at site i with rate γ, and ρ is the density matrix of the atomic gas. When the quantum-jump term, which is the last term in the Lindblad equation, is negligible, the system is described by an effective NH Hamiltonian $H_{\rm eff} = H - \frac{i}{2}\gamma\sum_i L_i^\dagger L_i$. Such a situation is realized when we consider the dynamics over a sufficiently short time compared with the inverse loss rate $1/\gamma$ [12], which characterizes the timescale where the effect of quantum jumps becomes significant. In this case, the lowest real part of the eigenspectrum gives the effective ground state, and the imaginary part of energy corresponds to a decay rate of each eigenstate. The two-body loss is described by $L_i = c_{i\downarrow}c_{i\uparrow}$, giving a NH BCS Hamiltonian [128]

$$H_{\rm eff} = \sum_{\boldsymbol{k}\sigma}\xi_{\boldsymbol{k}}c^\dagger_{\boldsymbol{k}\sigma}c_{\boldsymbol{k}\sigma} - U\sum_i c^\dagger_{i\uparrow}c^\dagger_{i\downarrow}c_{i\downarrow}c_{i\uparrow}, \tag{2.2}$$

with a *complex-valued* interaction $U = U_1 + i\gamma/2$, where $U_1, \gamma > 0$. Here, $\xi_{\boldsymbol{k}} \equiv \epsilon_{\boldsymbol{k}} - \mu$, $\epsilon_{\boldsymbol{k}}$ is the energy dispersion, μ is the chemical potential, and $c_{\boldsymbol{k}\sigma}$ and $c_{i\sigma}$ denote annihilation operators of a spin-σ fermion with momentum $\boldsymbol{k}$ and at site i, respectively. In this chapter, we formulate a mean-field theory from $H_{\rm eff}$ and elucidate how unconventional properties of superfluidity emerge in NH BCS systems.

2.3 Non-Hermitian BCS theory

In this section, we formulate a NH mean-field theory from two perspectives: a path-integral formalism and an operator formalism.

2.3.1 Path-integral formalism

We first clarify how the standard BCS mean-field theory is changed due to non-Hermiticity by formulating it with a path-integral approach. We start with a partition function defined as

$$Z = \sum_n e^{-\beta E_n} = \sum_n {}_L\langle E_n|e^{-\beta H_{\rm eff}}|E_n\rangle_R. \tag{2.3}$$

Here, ${}_L\langle E_n|$ and $|E_n\rangle_R$ are left and right eigenstates of $H_{\rm eff}$ with eigenenergy E_n, and they satisfy an orthonormal relation ${}_L\langle E_n|E_m\rangle_R = \delta_{nm}$ [133]. We note that, as temperature is not well defined in generic open quantum systems, we only consider the infinite limit of β to elucidate the physics of the ground state and calculate the excitation spectrum. Thus, β is a parameter used to formulate a path integral and should not be regarded as the temperature of the system. We use a path-integral representation of the partition function (2.3) to perform the Hubbard-Stratonovich transformation with auxiliary fields Δ, $\bar\Delta$ and then integrate out the fermionic degrees of freedom to obtain $Z = \int \mathcal{D}\bar\Delta\mathcal{D}\Delta e^{-S_{\rm eff}(\Delta,\bar\Delta)}$. The partition function is written in the path-integral representation as

$$\begin{aligned} Z &= \int \mathcal{D}\bar c\mathcal{D}c\exp\{-S(\bar c, c)\}, \\ S(\bar c, c) &= \int_0^\beta d\tau\left(\sum_{\boldsymbol{k}\sigma}\bar c_{\boldsymbol{k}\sigma}(\tau)(\partial_\tau + \xi_{\boldsymbol{k}})c_{\boldsymbol{k}\sigma}(\tau) - U\sum_i \bar c_{i\uparrow}(\tau)\bar c_{i\downarrow}(\tau)c_{i\downarrow}(\tau)c_{i\uparrow}(\tau)\right), \end{aligned} \tag{2.4}$$

where c and $\bar c$ are Grassmann variables, and τ is the imaginary time. After performing the Hubbard-Stratonovich transformation, the partition function is rewritten as

$$Z = \int \mathcal{D}\bar c\mathcal{D}c\mathcal{D}\bar\Delta\mathcal{D}\Delta e^{-S(\bar\Delta,\Delta,\bar c,c)}, \tag{2.5}$$

$$\begin{aligned} S(\bar\Delta,\Delta,\bar c,c) = \int_0^\beta d\tau\Bigg[&\sum_{\boldsymbol{k}\sigma}\bar c_{\boldsymbol{k}\sigma}(\tau)(\partial_\tau + \xi_{\boldsymbol{k}})c_{\boldsymbol{k}\sigma}(\tau) \\ &+ \sum_i\left(\frac{\bar\Delta_i(\tau)\Delta_i(\tau)}{U} + \bar\Delta_i(\tau)c_{i\downarrow}(\tau)c_{i\uparrow}(\tau) + \Delta_i(\tau)\bar c_{i\uparrow}(\tau)\bar c_{i\downarrow}(\tau)\right)\Bigg], \end{aligned} \tag{2.6}$$

where $\bar{\Delta}_i(\tau)$ and $\Delta_i(\tau)$ are auxiliary bosonic fields, which are not necessarily complex conjugate to each other in the saddle-point approximation. Substituting $c_{i\sigma}(\tau) = \frac{1}{\sqrt{\beta N}} \sum_{\boldsymbol{k},\omega_n} e^{i(\boldsymbol{r}_i\cdot\boldsymbol{k}-\omega_n\tau)} c_{\boldsymbol{k}\sigma}(\omega_n)$, $\bar{c}_{i\sigma}(\tau) = \frac{1}{\sqrt{\beta N}} \sum_{\boldsymbol{k},\omega_n} e^{-i(\boldsymbol{r}_i\cdot\boldsymbol{k}-\omega_n\tau)} \bar{c}_{\boldsymbol{k}\sigma}(\omega_n)$, $\Delta_i(\tau) = \frac{1}{\sqrt{\beta N}} \sum_{\boldsymbol{k},\Omega_l} e^{i(\boldsymbol{r}_i\cdot\boldsymbol{k}-\Omega_l\tau)} \Delta_{\boldsymbol{k}}(\Omega_l)$ and $\bar{\Delta}_i(\tau) = \frac{1}{\sqrt{\beta N}} \sum_{\boldsymbol{k},\Omega_l} e^{-i(\boldsymbol{r}_i\cdot\boldsymbol{k}-\Omega_l\tau)} \bar{\Delta}_{\boldsymbol{k}}(\Omega_l)$ into Eq. (2.6), we have

$$\begin{aligned} S(\bar{\Delta},\Delta,\bar{c},c) =& \frac{1}{U}\sum_{\boldsymbol{k},\Omega_l} \bar{\Delta}_{\boldsymbol{k}}(\Omega_l)\Delta_{\boldsymbol{k}}(\Omega_l) + \sum_{\boldsymbol{k},\omega_n,\sigma} \bar{c}_{\boldsymbol{k}\sigma}(\omega_n)(-i\omega_n+\xi_{\boldsymbol{k}})c_{\boldsymbol{k}\sigma}(\omega_n) \\ &+ \sum_{\boldsymbol{k},\boldsymbol{k}'',\omega_n,\Omega_l} \frac{1}{\sqrt{\beta N}} \bar{\Delta}_{\boldsymbol{k}''}(\Omega_l) c_{\boldsymbol{k}''-\boldsymbol{k}\downarrow}(\Omega_l-\omega_n) c_{\boldsymbol{k}\uparrow}(\omega_n) \\ &+ \sum_{\boldsymbol{k},\boldsymbol{k}'',\omega_n,\Omega_l} \frac{1}{\sqrt{\beta N}} \Delta_{\boldsymbol{k}''}(\Omega_l) \bar{c}_{\boldsymbol{k}\uparrow}(\omega_n) \bar{c}_{\boldsymbol{k}''-\boldsymbol{k}\downarrow}(\Omega_l-\omega_n), \end{aligned} \tag{2.7}$$

where N denotes the number of lattice sites, ω_n and Ω_l are the Matsubara frequencies for fermions and bosons, respectively. In the mean-field theory, we ignore the spatial and temporal fluctuations of $\Delta_{\boldsymbol{k}''}(\Omega_l)$ and $\bar{\Delta}_{\boldsymbol{k}''}(\Omega_l)$ and thus set $\boldsymbol{k}''=0$ and $\Omega_l=0$. Then the action is described as

$$S(\bar{c},c,\bar{\Delta},\Delta) = \frac{\beta N}{U}\bar{\Delta}\Delta + \sum_{\boldsymbol{k},\omega_n} \begin{pmatrix} \bar{c}_{\boldsymbol{k}\uparrow}(\omega_n) & c_{-\boldsymbol{k}\downarrow}(-\omega_n) \end{pmatrix} \begin{pmatrix} -i\omega_n+\xi_{\boldsymbol{k}} & \Delta \\ \bar{\Delta} & -i\omega_n-\xi_{\boldsymbol{k}} \end{pmatrix} \begin{pmatrix} c_{\boldsymbol{k}\uparrow}(\omega_n) \\ \bar{c}_{-\boldsymbol{k}\downarrow}(-\omega_n) \end{pmatrix}, \tag{2.8}$$

where $\Delta = \frac{1}{\sqrt{\beta N}}\Delta_{\boldsymbol{k}=0}(0)$ and $\bar{\Delta} = \frac{1}{\sqrt{\beta N}}\bar{\Delta}_{\boldsymbol{k}=0}(0)$. Integrating out the fermionic degrees of freedom by using the formula $\int \exp\left[-\sum_{i,j}\bar{c}_i A_{ij} c_j\right] \prod_{i=1}^n \mathcal{D}\bar{c}_i \mathcal{D}c_i = \det A$, we obtain

$$Z = \int \mathcal{D}\bar{\Delta}\mathcal{D}\Delta e^{-S_{\rm eff}(\Delta,\bar{\Delta})}, \tag{2.9}$$

where

$$\begin{aligned} S_{\rm eff}(\bar{\Delta},\Delta) &= \frac{\beta N}{U}\bar{\Delta}\Delta - \sum_{\omega_n,\boldsymbol{k}} \ln\left\{-\det\begin{pmatrix} -i\omega_n+\xi_{\boldsymbol{k}} & \Delta \\ \bar{\Delta} & -i\omega_n-\xi_{\boldsymbol{k}} \end{pmatrix}\right\} \\ &= -\sum_{\omega_n,\boldsymbol{k}} \ln(\omega_n^2+\xi_{\boldsymbol{k}}^2+\bar{\Delta}\Delta) + \frac{\beta N}{U}\bar{\Delta}\Delta, \end{aligned} \tag{2.10}$$

is the effective action. Finally, the saddle point condition for the partition function, $\partial S_{\rm eff}/\partial\Delta = \partial S_{\rm eff}/\partial\bar{\Delta} = 0$, yields the NH gap equation

$$\frac{N}{U} = \sum_{\boldsymbol{k}} \frac{1}{2\sqrt{\xi_{\boldsymbol{k}}^2+\bar{\Delta}\Delta}} \tanh\frac{\beta\sqrt{\xi_{\boldsymbol{k}}^2+\bar{\Delta}\Delta}}{2}, \tag{2.11}$$

if there exists a nontrivial solution other than $\Delta=\bar{\Delta}=0$, where we set β to infinity to obtain an effective ground state. The chemical potential μ is determined so that the mean particle number in the NH ensemble (2.3) is equal to the particle number of the density-matrix sector of interest (see Appendix for this chapter).

In NH physics, four distinct types of order parameters can be defined according to whether left and right eigenstates are assigned to the bra or ket vectors in the expectation value. Importantly, the expectation value of an operator A calculated from the NH ensemble (2.3) should correspond to ${}_L\langle A\rangle_R \equiv \sum_n {}_L\langle E_n|A|E_n\rangle_R e^{-\beta E_n}/Z$. Thus, the order parameters corresponding to the superfluid gap are given by differentiating

$$e^{-S_{\rm eff}(\Delta,\bar{\Delta})} = \int \mathcal{D}\bar{c}\mathcal{D}c e^{-S(\bar{\Delta},\Delta,\bar{c},c)} \tag{2.12}$$

with respect to Δ and $\bar{\Delta}$ and using the saddle point condition $\partial S_{\rm eff}/\partial\Delta = \partial S_{\rm eff}/\partial\bar{\Delta} = 0$ as

$$\Delta = -\frac{U}{N}\sum_{\boldsymbol{k}} {}_L\langle c_{-\boldsymbol{k}\downarrow}c_{\boldsymbol{k}\uparrow}\rangle_R, \tag{2.13}$$

$$\bar{\Delta} = -\frac{U}{N}\sum_{\boldsymbol{k}} {}_L\langle c^\dagger_{\boldsymbol{k}\uparrow}c^\dagger_{-\boldsymbol{k}\downarrow}\rangle_R, \tag{2.14}$$

indicating that $\bar{\Delta} \neq \Delta^*$ since $|E_n\rangle_L \neq |E_n\rangle_R$. Here, we have used the expectation values defined as

$$\sum_{\boldsymbol{k}} {}_L\langle c_{-\boldsymbol{k}\downarrow} c_{\boldsymbol{k}\uparrow}\rangle_R = \frac{\int \mathcal{D}\bar{c}\mathcal{D}c \sum_{\boldsymbol{k},\omega_n} c_{-\boldsymbol{k}\downarrow}(-\omega_n) c_{\boldsymbol{k}\uparrow}(\omega_n) e^{-S}}{\int \mathcal{D}\bar{c}\mathcal{D}c e^{-S}},$$
$$\sum_{\boldsymbol{k}} {}_L\langle c^\dagger_{\boldsymbol{k}\uparrow} c^\dagger_{-\boldsymbol{k}\downarrow}\rangle_R = \frac{\int \mathcal{D}\bar{c}\mathcal{D}c \sum_{\boldsymbol{k},\omega_n} \bar{c}_{\boldsymbol{k}\uparrow}(\omega_n) \bar{c}_{-\boldsymbol{k}\downarrow}(-\omega_n) e^{-S}}{\int \mathcal{D}\bar{c}\mathcal{D}c e^{-S}}. \tag{2.15}$$

As discussed Sec. 2.4, this leads to various intriguing consequences on the properties of a NH superfluid.

2.3.2 Operator formalism

To elucidate the effect of non-Hermiticity, let us apply the mean-field decoupling to the NH BCS Hamiltonian with the simplest s-wave pairing interaction

$$H_{\rm eff} = \sum_{\boldsymbol{k}\sigma} \xi_{\boldsymbol{k}} c^\dagger_{\boldsymbol{k}\sigma} c_{\boldsymbol{k}\sigma} - \frac{U}{N} \sum_{\boldsymbol{k}\boldsymbol{k}'} c^\dagger_{\boldsymbol{k}\uparrow} c^\dagger_{-\boldsymbol{k}\downarrow} c_{-\boldsymbol{k}'\downarrow} c_{\boldsymbol{k}'\uparrow}. \tag{2.16}$$

Substituting $c^\dagger_{\boldsymbol{k}\uparrow} c^\dagger_{-\boldsymbol{k}\downarrow} = {}_L\langle c^\dagger_{\boldsymbol{k}\uparrow} c^\dagger_{-\boldsymbol{k}\downarrow}\rangle_R + \delta(c^\dagger_{\boldsymbol{k}\uparrow} c^\dagger_{-\boldsymbol{k}\downarrow})$ and $c_{-\boldsymbol{k}\downarrow} c_{\boldsymbol{k}\uparrow} = {}_L\langle c_{-\boldsymbol{k}\downarrow} c_{\boldsymbol{k}\uparrow}\rangle_R + \delta(c_{-\boldsymbol{k}\downarrow} c_{\boldsymbol{k}\uparrow})$ into Eq. (2.16) and neglecting the second-order terms in δ, we obtain the mean-field Hamiltonian as

$$H_{\rm MF} = \sum_{\boldsymbol{k}} \begin{pmatrix} c^\dagger_{\boldsymbol{k}\uparrow} & c_{-\boldsymbol{k}\downarrow} \end{pmatrix} \begin{pmatrix} \xi_{\boldsymbol{k}} & \Delta \\ \bar{\Delta} & -\xi_{\boldsymbol{k}} \end{pmatrix} \begin{pmatrix} c_{\boldsymbol{k}\uparrow} \\ c^\dagger_{-\boldsymbol{k}\downarrow} \end{pmatrix} = \sum_{\boldsymbol{k}} \begin{pmatrix} \bar{\gamma}_{\boldsymbol{k}\uparrow} & \gamma_{-\boldsymbol{k}\downarrow} \end{pmatrix} \begin{pmatrix} E_{\boldsymbol{k}} & 0 \\ 0 & -E_{\boldsymbol{k}} \end{pmatrix} \begin{pmatrix} \gamma_{\boldsymbol{k}\uparrow} \\ \bar{\gamma}_{-\boldsymbol{k}\downarrow} \end{pmatrix}, \tag{2.17}$$

where the quasiparticle operators are given by

$$\begin{aligned} \bar{\gamma}_{\boldsymbol{k}\uparrow} &= u_{\boldsymbol{k}} c^\dagger_{\boldsymbol{k}\uparrow} - \bar{v}_{\boldsymbol{k}} c_{-\boldsymbol{k}\downarrow}, \\ \bar{\gamma}_{-\boldsymbol{k}\downarrow} &= \bar{v}_{\boldsymbol{k}} c_{\boldsymbol{k}\uparrow} + u_{\boldsymbol{k}} c^\dagger_{-\boldsymbol{k}\downarrow}, \\ \gamma_{\boldsymbol{k}\uparrow} &= u_{\boldsymbol{k}} c_{\boldsymbol{k}\uparrow} - v_{\boldsymbol{k}} c^\dagger_{-\boldsymbol{k}\downarrow}, \\ \gamma_{-\boldsymbol{k}\downarrow} &= v_{\boldsymbol{k}} c^\dagger_{\boldsymbol{k}\uparrow} + u_{\boldsymbol{k}} c_{-\boldsymbol{k}\downarrow}, \end{aligned} \tag{2.18}$$

and the coefficients are given by

$$u_{\boldsymbol{k}} = \sqrt{\frac{E_{\boldsymbol{k}} + \xi_{\boldsymbol{k}}}{2E_{\boldsymbol{k}}}}, \quad v_{\boldsymbol{k}} = -\sqrt{\frac{(E_{\boldsymbol{k}} - \xi_{\boldsymbol{k}})}{2E_{\boldsymbol{k}}}} \frac{\sqrt{\Delta}}{\sqrt{\bar{\Delta}}}, \quad \bar{v}_{\boldsymbol{k}} = -\sqrt{\frac{(E_{\boldsymbol{k}} - \xi_{\boldsymbol{k}})}{2E_{\boldsymbol{k}}}} \frac{\sqrt{\bar{\Delta}}}{\sqrt{\Delta}}. \tag{2.19}$$

We note that the quasiparticle energy $E_{\boldsymbol{k}}$ is given by $E_{\boldsymbol{k}} = \sqrt{\xi^2_{\boldsymbol{k}} + \bar{\Delta}\Delta}$, and the coefficients satisfy $u^2_{\boldsymbol{k}} + v_{\boldsymbol{k}}\bar{v}_{\boldsymbol{k}} = 1$. In the Hermitian limit, $\bar{\gamma}_{\boldsymbol{k}\sigma}$ and $\bar{v}_{\boldsymbol{k}}$ respectively reduce to $\gamma^\dagger_{\boldsymbol{k}\sigma}$ and $v^*_{\boldsymbol{k}}$ which describe the Bogoliubov quaiparticles. Here, we note that the mean-field Hamiltonian is NH since $\Delta^* \neq \bar{\Delta}$, and the quasiparticle operators $\gamma_{\boldsymbol{k}\sigma}$ and $\bar{\gamma}_{\boldsymbol{k}\sigma}$ are not Hermitian conjugate to each other. Therefore, the Hamiltonian cannot be diagonalized via a unitary transformation.

As a result, the right and left ground states are defined by $\gamma_{\boldsymbol{k}\sigma}|{\rm BCS}\rangle_R = 0$ and $\bar{\gamma}^\dagger_{\boldsymbol{k}\sigma}|{\rm BCS}\rangle_L = 0$, respectively, where

$$|{\rm BCS}\rangle_R = \prod_{\boldsymbol{k}} \left(u_{\boldsymbol{k}} + v_{\boldsymbol{k}} c^\dagger_{\boldsymbol{k}\uparrow} c^\dagger_{-\boldsymbol{k}\downarrow} \right) |0\rangle, \tag{2.20}$$

$$|{\rm BCS}\rangle_L = \prod_{\boldsymbol{k}} \left(u^*_{\boldsymbol{k}} + \bar{v}^*_{\boldsymbol{k}} c^\dagger_{\boldsymbol{k}\uparrow} c^\dagger_{-\boldsymbol{k}\downarrow} \right) |0\rangle, \tag{2.21}$$

and $|0\rangle$ is the vacuum for fermions. They satisfy ${}_L\langle{\rm BCS}|{\rm BCS}\rangle_R = 1$ and reproduce the ordinary BCS ground state in the Hermitian limit. We thus obtain $H\bar{\gamma}_{\boldsymbol{k}\sigma}|{\rm BCS}\rangle_R = E_{\boldsymbol{k}}\bar{\gamma}_{\boldsymbol{k}\sigma}|{\rm BCS}\rangle_R$ and $H^\dagger\gamma^\dagger_{\boldsymbol{k}\sigma}|{\rm BCS}\rangle_L = E^*_{\boldsymbol{k}}\gamma^\dagger_{\boldsymbol{k}\sigma}|{\rm BCS}\rangle_L$, which imply that $\bar{\gamma}_{\boldsymbol{k}\sigma}$ and $\gamma^\dagger_{\boldsymbol{k}\sigma}$ create the right and left eigenstates, respectively, when acted on the ground state. Here, we have shifted the ground state energy to zero. Using Eqs. (2.13), (2.14), (2.20), and (2.21), we obtain the $\beta \to \infty$ limit of the NH gap equation

as $N/U = \sum_{\boldsymbol{k}} 1/2E_{\boldsymbol{k}}$, which is solved self-consistently. We note that the quasiparticle operators satisfy an anticommutation relation $\{\gamma_{\boldsymbol{k}\sigma}, \bar{\gamma}_{\boldsymbol{k}'\sigma'}\} = \delta_{\boldsymbol{k}\boldsymbol{k}'}\delta_{\sigma\sigma'}$, although these quasiparticles obey neither Fermi nor Bose statistics due to $\gamma^\dagger_{\boldsymbol{k}\sigma} \neq \bar{\gamma}_{\boldsymbol{k}\sigma}$, reflecting non-Hermiticity of the mean-field Hamiltonian.

Here, we point out an important relation between the order parameters Δ and $\bar{\Delta}$. In the Hermitian case, they are complex conjugate to each other and we can choose a gauge where Δ is real without loss of generality. This is equivalent to requiring $H^\dagger_{\rm MF} = H^*_{\rm MF}$ in the matrix representation in the Fock-state basis in the Hilbert space. Now we consider the NH case. As in the Hermitian case, the NH BCS Hamiltonian (2.16) satisfies a symmetry relation $H^\dagger = H^*$ under the matrix representation in terms of Fock states, indicating that the left eigenstates are obtained through complex conjugation of the right ones. The NH BCS Hamiltonian has the U(1) symmetry as in the Hermitian case and this is not affected by the complex nature of the interaction. Then, when a superfluid is formed, its ground states become degenerate due to spontaneous U(1) symmetry breaking. The BCS ground states (2.20) and (2.21) are consistent with these properties if

$$\begin{aligned} \Delta(\theta) &= \Delta_0 e^{i\theta}, \\ \bar{\Delta}(\theta) &= \Delta_0 e^{-i\theta}, \end{aligned} \tag{2.22}$$

where $\Delta_0 \in \mathbb{C}$ and θ is the U(1) phase. By choosing a special gauge for which $H^\dagger_{\rm MF} = H^*_{\rm MF}$ is satisfied, we have $\Delta = \bar{\Delta}$. Here, we note that the relation (2.22) is specific to the NH BCS Hamiltonian (2.16) and may be changed depending on symmetry of a NH Hamiltonian.

2.4 Quantum phase transition of Non-Hermitian superfluids

In this section, we elucidate how unconventional phase transitions emerge by solving the gap equation (2.11).

2.4.1 Reentrant superfluidity

We solve the gap equation at $\beta \to \infty$ numerically. Figure 2.1 shows the superfluid order parameter Δ_0. Here, for simplicity, we consider a system with particle-hole symmetry, and set the chemical potential measured from the Fermi energy to zero (see Appendix for this chapter). For small U_1, ${\rm Re}\Delta_0$ is suppressed by dissipation γ and then vanishes, indicating a breakdown of superfluidity. Remarkably, as γ increases, the superfluid solution reappears, and the gap size ${\rm Re}\Delta_0$ is enhanced due to dissipation, eventually exceeding the value in the Hermitian limit. On the other hand, for strong attractive interaction, ${\rm Re}\Delta_0$ is not suppressed, but rather enhanced due to dissipation.

The qualitative difference between the cases of weak and strong attractions is explained by an interplay between the BCS-BEC crossover [134–137] and dissipation. In the strong-dissipation limit, the behavior of the system is governed by QZE [40–42, 138–140], which suppresses tunneling to neighboring sites, leading to localization of particles. In the case of weak attraction, the inter-site coherence of Cooper pairs is suppressed by dissipation and the superfluidity is destroyed. However, localization due to the QZE facilitates formation of on-site molecules of fermions for strong dissipation and consequently superfluidity reappears. In fact, the solution of the gap equation approaches $\Delta_0 = U/2$ in the strong-dissipation limit, as shown by the dashed lines in Fig. 2.1. This is consistent with the fact that the physics is dominated by the on-site interaction under the QZE, supporting our mean-field analysis. On the other hand, under strong attraction, fermions form bosonic molecules almost at single sites and thus the molecules can survive under dissipation. In this case, the effect of dissipation is to give rise to an effective one-body loss of molecules and the remaining molecules can undergo BEC.

We have also conducted numerical calculations for an intermediate strength of the interaction $U_1/t = 2.5$ as shown in Fig. 2.2. We see from Fig. 2.2 that the real part of the superfluid gap is suppressed by dissipation but does not vanish. Moreover, it is even enhanced and eventually exceeds the value of the Hermitian limit as the dissipation increases, which is attributed to the confinement of Cooper pairs to individual sites due to the QZE. While the superfluid does not

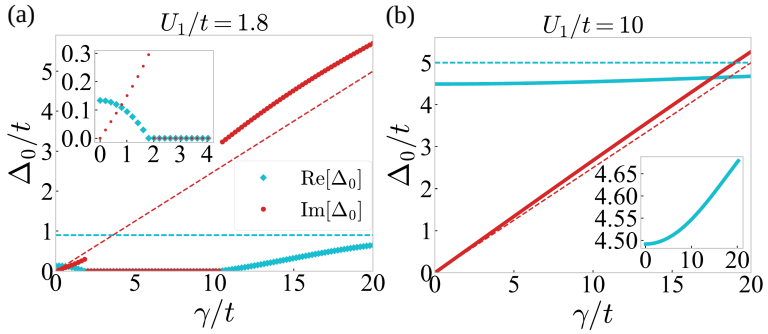

Figure 2.1: Numerical solution of Δ_0 as a function of γ/t obtained from the NH gap equation (2.11) at $\beta \to \infty$ and $\mu = 0$ for (a) $U_1/t = 1.8$ and (b) $U_1/t = 10$. We assume a cubic lattice with energy dispersion $\epsilon_{\boldsymbol{k}} = -2t(\cos k_x + \cos k_y + \cos k_z)$, where t is the hopping amplitude. The dashed lines denote the asymptotic behavior in the strong-dissipation limit. The insets show (a) an enlarged view near the origin (weak dissipation) and (b) that of the real part.

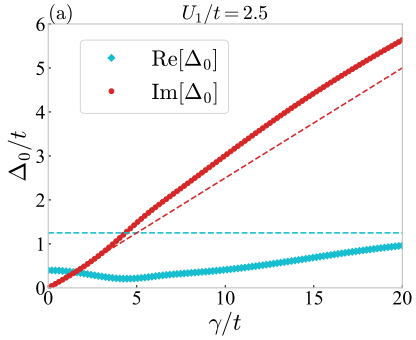

Figure 2.2: Superfluid gap obtained from the NH gap equation at $\beta \to \infty$ for $U_1 = 2.5$. The chemical potential measured from the Fermi energy is set to zero and a cubic lattice is assumed as in Fig. 2.1. The dashed lines show the asymptotic behavior in the strong-dissipation limit.

exhibit an unconventional phase transition with exceptional points in this case, a remnant of the phase transition in a weak attraction can be seen as the minimum of $\mathrm{Re}\Delta_0$ in Fig. 2.2.

2.4.2 Emergence of exceptional manifolds

We here point out that the breakdown and restoration of superfluidity present clear signatures of the emergence of exceptional points, where the Hamiltonian cannot be diagonalized [129, 130]. In fact, when $\mathrm{Re}\Delta_0 = 0$, the mean-field Hamiltonian H_{MF} cannot be diagonalized for $\xi_{\boldsymbol{k}} = \pm \mathrm{Im}\Delta_0$. Figure 2.3(a) shows the real part of the energy spectrum of quasiparticles in two dimensions. The regions where the orange and blue surfaces merge form exceptional points, lines (Fig. 2.3(c)), and surfaces (Fig. 2.3(d)) in one-, two-, and three-dimensional systems, respectively. Such characteristic behavior has its origin in a parity-particle-hole (CP) symmetry of the mean-field Hamiltonian $H_{\mathrm{MF}}(\boldsymbol{k}) = \epsilon_{\boldsymbol{k}}\sigma_z + i\mathrm{Im}\Delta_0\sigma_x$. In fact, as a function of the momentum, $H_{\mathrm{MF}}(\boldsymbol{k})$ exhibits spontaneous breaking of the CP symmetry at the exceptional points, whose dimensionality is indeed protected by the symmetry constraint.

We here explain the details. At the breakdown and restoration points of the superfluid gap, the gap is pure imaginary and the mean-field Hamiltonian $H_{\mathrm{MF}}(\boldsymbol{k})$ satisfies the following CP symmetry [141]

$$CPH_{\mathrm{MF}}(\boldsymbol{k})(CP)^{-1} = -H_{\mathrm{MF}}(\boldsymbol{k}), \tag{2.23}$$

where $CP = \sigma_x K$, $\sigma_{x,z}$ are the Pauli matrices, and K is complex conjugation [141–144]. This is similar to parity-time ($\mathcal{PT}$) symmetry [58, 59], which is expressed for a general Hamiltonian $H(\boldsymbol{k})$

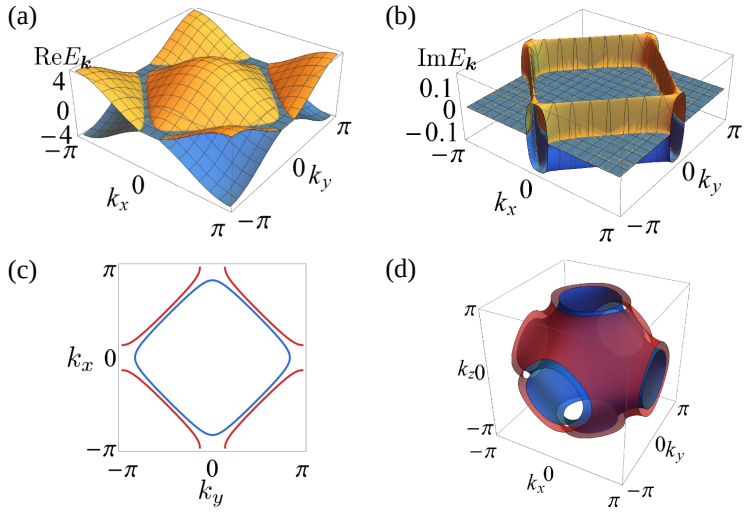

Figure 2.3: (a) Real and (b) imaginary parts of the quasiparticle energy spectrum $E_{\boldsymbol{k}} = \pm\sqrt{\epsilon_{\boldsymbol{k}}^2 + \Delta_0^2}$ (orange for positive sign, blue for negative sign) at critical points. (c) Exceptional lines in two dimensions. (d) Exceptional surfaces in three dimensions. The energy dispersion is for a square lattice $\epsilon_{\boldsymbol{k}} = -2(\cos k_x + \cos k_y)$ in (a), (b) and (c), and for a cubic lattice $\epsilon_{\boldsymbol{k}} = -2(\cos k_x + \cos k_y + \cos k_z)$ in (d). The gap is set to $\Delta_0 = 0.19i$ for (a), (b) and (c), and $\Delta_0 = 0.4i$ for (d).

as

$$\mathcal{PT}H(\boldsymbol{k})(\mathcal{PT})^{-1} = H(\boldsymbol{k}), \tag{2.24}$$

and they are indeed equivalent to each other as can be seen if we multiply the Hamiltonian by i [77]. Consequently, as the $\mathcal{PT}$ symmetry dictates that the eigenspectrum of the Hamiltonian appears as real or complex-conjugate pairs [59], the CP symmetry dictates that the eigenspectrum appears as pure imaginary or anti-complex-conjugate pairs (Fig. 2.4). One can easily confirm that the CP symmetry is unbroken if the eigenspectrum is pure imaginary; otherwise it is spontaneously broken.

A generic two-band Hamiltonian with the CP symmetry can be written as

$$H(\boldsymbol{k}) = ia(\boldsymbol{k})\sigma_0 + b_z(\boldsymbol{k})\sigma_z + id_x(\boldsymbol{k})\sigma_x + id_y(\boldsymbol{k})\sigma_y, \tag{2.25}$$

where $a(\boldsymbol{k}), b_z(\boldsymbol{k}), d_x(\boldsymbol{k}), d_y(\boldsymbol{k}) \in \mathbb{R}$ (σ_0 is the 2×2 identity matrix). Since its eigenvalues are given by $ia(\boldsymbol{k}) \pm \sqrt{b_z(\boldsymbol{k})^2 - d_x(\boldsymbol{k})^2 - d_y(\boldsymbol{k})^2}$, the spontaneous CP-symmetry-breaking transition occurs when

$$b_z(\boldsymbol{k})^2 - d_x(\boldsymbol{k})^2 - d_y(\boldsymbol{k})^2 = 0, \tag{2.26}$$

which is accompanied by the emergence of exceptional points. We note that only a single condition (2.26) is needed for the exceptional point, while two conditions are needed for an exceptional point in a system without any symmetry [141–144]. Because of this symmetry constraint, the exceptional points form a $(d-1)$-dimensional surface in d-dimensional systems. In our case, we have $a(\boldsymbol{k}) = d_y(\boldsymbol{k}) = 0, b_z(\boldsymbol{k}) = \xi_{\boldsymbol{k}}$, and $d_x(\boldsymbol{k}) = \mathrm{Im}\Delta_0$ from the mean-field Hamiltonian $H_{\mathrm{MF}}(\boldsymbol{k})$. The quasiparticle energy spectra and exceptional points depicted in Fig. 2.3 are consistent with the above general argument.

Thus, the quantum phase transitions of the NH superfluid cannot be classified into the conventional first- or second-order phase transitions in Hermitian systems, but are attributed to the emergence of exceptional points unique to non-Hermiticity. We note here that the two exceptional points corresponding to the breakdown and restoration of superfluidity merge and disappear as the strength of attraction increases. Furthermore, the emergence of exceptional manifolds leads to some intriguing dynamics in the NH superfluid. In Fig. 2.3(b), the imaginary part of the quasiparticle energy takes a positive finite value only in between the exceptional lines or surfaces, amplifying quasiparticle distribution in the particular region of the Brillouin zone through the time

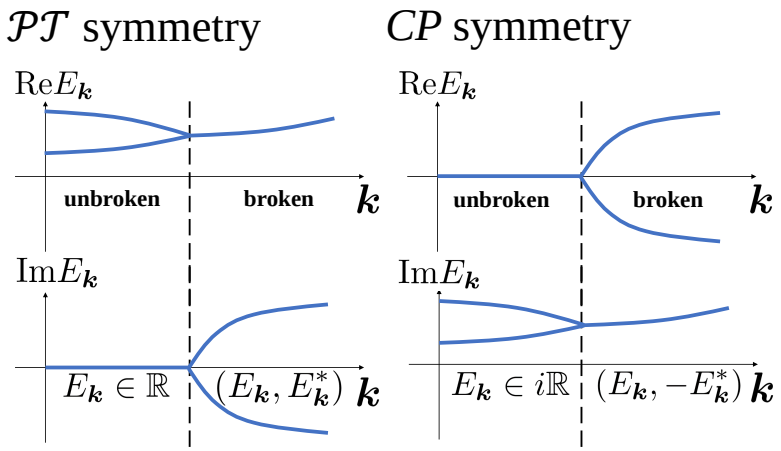

Figure 2.4: Schematic diagrams for the eigenspectrum of a Hamiltonian that has $\mathcal{PT}$ symmetry (left) or CP symmetry (right). The dashed lines indicate the points of spontaneous symmetry breaking.

evolution. The characteristic structure in Fig. 2.3(b), which can be used as a smoking gun of the non-Hermiticity, can be observed as long as $\mathrm{Im}\Delta_0 > 0$ even in a region away from the breakdown and restoration points.

2.4.3 Phase diagram

We note that the nontrivial solution of the NH gap equation may give a metastable superfluid, which corresponds to a local minimum of the real part of the energy. Whether the superfluid is metastable or not is decided from comparison of ground-state energies between the superfluid state and the normal state, as detailed in the following. Using Eq. (2.10), the condensation energy is given by the difference in energy between the superfluid and normal states as

$$\begin{aligned} E &= \frac{1}{\beta}\left(S_{\rm eff}(\Delta_0 e^{i\theta}, \Delta_0 e^{-i\theta}) - S_{\rm eff}(0,0)\right) \\ &= \frac{N}{U}\Delta_0^2 + \frac{1}{\beta}\sum_{\omega_n \boldsymbol{k}}\Bigg\{ \log(i\omega_n + |\xi_{\boldsymbol{k}}|) + \log(-i\omega_n + |\xi_{\boldsymbol{k}}|) \\ &\qquad\qquad - \log(i\omega_n + \sqrt{\xi_{\boldsymbol{k}}^2 + \Delta_0^2}) - \log(-i\omega_n + \sqrt{\xi_{\boldsymbol{k}}^2 + \Delta_0^2})\Bigg\} \\ &= \frac{N}{U}\Delta_0^2 - \frac{1}{\beta}\sum_{\omega_n, \boldsymbol{k}} \log\left(1 + \frac{\Delta_0^2}{\omega_n^2 + \xi_{\boldsymbol{k}}^2}\right). \end{aligned} \tag{2.27}$$

Using the integration contour in Fig. 2.5, we can calculate the sum over the Matsubara frequency as

$$E = \frac{N}{U}\Delta_0^2 + \frac{1}{2\pi i}\sum_{\boldsymbol{k}} \oint_{C_2} dz \log\left(1 + \frac{\Delta_0^2}{-z^2 + \xi_{\boldsymbol{k}}^2}\right) f(z), \tag{2.28}$$

where $f(z) = (e^{\beta z} + 1)^{-1}$ is the Fermi distribution function. We here note that the integrand in Eq. (2.28) has a branch cut on the lines connecting the branch points of Eq. (2.27) as shown in Fig. 2.5. We thus obtain

$$E = \frac{N}{U}\Delta_0^2 - \sum_{\boldsymbol{k}} \int_{|\xi_{\boldsymbol{k}}|}^{\sqrt{\xi_{\boldsymbol{k}}^2 + \Delta_0^2}} dz \tanh\frac{\beta z}{2}. \tag{2.29}$$

In the $\beta \to \infty$ limit, the condensation energy is given by

$$E = \frac{N}{U}\Delta_0^2 - \sum_{\boldsymbol{k}} (\sqrt{\xi_{\boldsymbol{k}}^2 + \Delta_0^2} - |\xi_{\boldsymbol{k}}|). \tag{2.30}$$

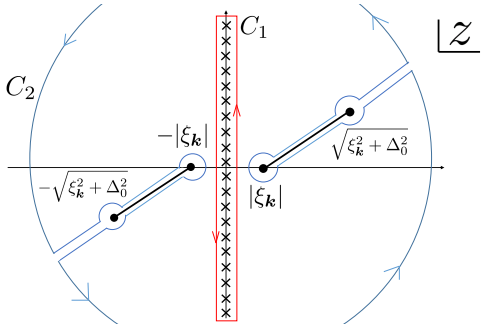

Figure 2.5: Integration contour in the calculation of the condensation energy.

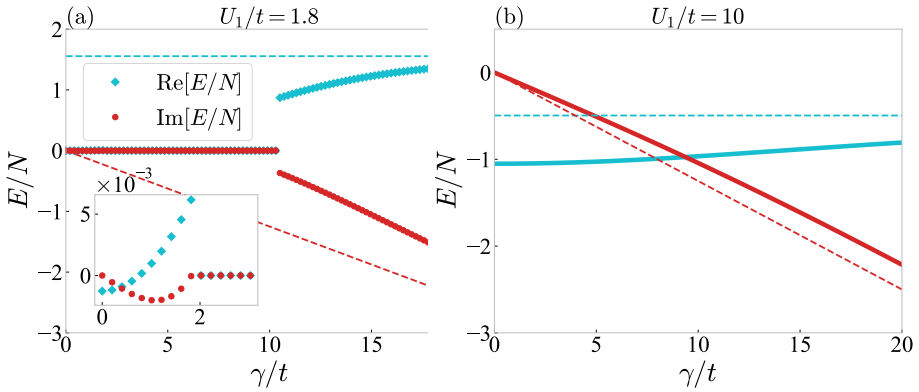

Figure 2.6: Condensation energy (2.30) as a function of γ/t. We here assume the cubic lattice, and the interaction and the chemical potential are set to the same values as in Fig. 2.1, respectively. The dashed lines show the asymptotic behavior in the strong-dissipation limit. The inset in (a) shows an enlarged view of the weak-dissipation regime.

Figure 2.6 shows the condensation energy for the parameters corresponding to those in Fig. 2.1. For $U_1/t = 1.8$, we find that the superfluid state is energetically stable only in the weak-dissipation region. For a region where the real part of the condensation energy is positive, the nontrivial solution of the NH gap equation gives a local minimum of the real part of energy, leading to a metastable superfluid solution. We also find that the nontrivial solution of the gap equation in the strong-dissipation regime gives a metastable state because the energy is higher than that of the trivial solution. On the other hand, for $U_1/t = 10$, the superfluid is always energetically stable, and we can observe the steady enhancement of the superfluid gap.

We have also calculated the condensation energy for the intermediate regime. From Fig. 2.7, the superfluid state under sufficiently strong dissipation becomes metastable due to the positive condensation energy.

From these results, we obtain a phase diagram of the NH BCS model as shown in Fig. 2.8. In the blue region, the superfluid state is an effective ground state of the NH BCS Hamiltonian. When the dissipation is increased, the superfluid state remains stable if the attraction is sufficiently strong. When the system enters the red region, the superfluid state becomes metastable with respect to the real part of the energy. The metastable superfluid undergoes an unconventional quantum phase transition due to exceptional points in the case of weak attractions, leading to the disappearance of the superfluid state in the yellow region. Here we remark that a similar phase diagram is obtained from an exact solution of a 1D NH Hubbard model [15]. Although a similar formulation to obtain the gap equation can be made for a continuum system, the reentrant superfluidity is unique to the lattice system since the localization due to the QZE cannot occur without a lattice. On the other hand, the breakdown of the superfluidity and the related phase transitions can occur in the continuum system.

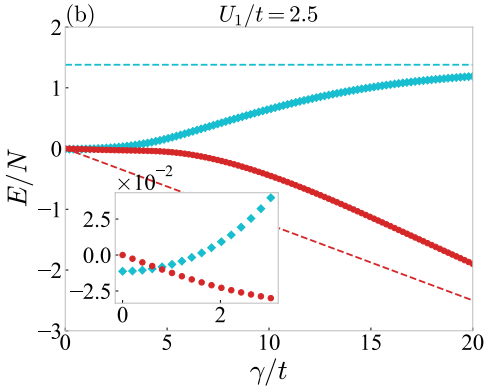

Figure 2.7: Condensation energy (2.30) for $U_1 = 2.5$. The chemical potential measured from the Fermi energy is set to zero and a cubic lattice is assumed as in Fig. 2.1. The dashed lines show the asymptotic behavior in the strong-dissipation limit. The inset shows an enlarged view in the weak-dissipation regime.

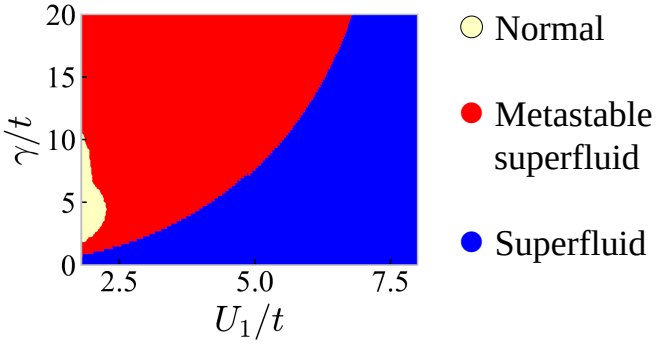

Figure 2.8: Phase diagram of the NH BCS model at $\beta \to \infty$ and $\mu = 0$. The yellow region corresponds to the normal state. The red region shows the metastable superfluid state for which a nontrivial solution of the gap equation gives a local energy minimum. The blue region shows the superfluid state corresponding to a nontrivial solution of the gap equation that gives an effective ground state. A region with small U_1 is not shown because of the limitation of numerical calculations.

2.4.4 Analytical calculation at a constant density of states

We here explain that a similar phase diagram is obtained by assuming a constant density of states. The gap equation (2.11) can be solved analytically if the density of states ρ_0 is constant. Under this assumption, the gap equation in the $\beta \to \infty$ limit reads

$$\log\left|\frac{\sqrt{\omega_D^2+\Delta_0^2}+\omega_D}{\Delta_0}\right| + i\mathrm{Arg}\frac{\sqrt{\omega_D^2+\Delta_0^2}+\omega_D}{\Delta_0} = \frac{1}{\rho_0}\left(\frac{U_1}{|U|^2} - i\frac{\gamma}{2|U|^2}\right), \tag{2.31}$$

where $\omega_D = 1/2\rho_0$ is the energy cutoff. Here, we set a branch cut of $\sqrt{z}$ and $\log z$ to $z \in (-\infty, 0)$ and assume that $\mathrm{Re}\Delta_0$ is positive without loss of generality. Results obtained below do not depend on the choice of the branch cut. Then, the argument is restricted to $\mathrm{Arg}\frac{\sqrt{\omega_D^2+\Delta_0^2}+\omega_D}{\Delta_0} \in (-\frac{\pi}{2}, \frac{\pi}{2})$ and the gap equation has nontrivial solutions if and only if U_1 satisfies $\rho_0 U_1 < \frac{1}{\pi}$ and γ satisfies $0 \le \gamma \le \gamma^{c_1}$ or $\gamma \ge \gamma^{c_2}$, where γ^{c_1} and γ^{c_2} are determined from $(\rho_0\pi U_1)^2 + (\rho_0\pi\gamma/2 - 1)^2 = 1$ as

$$\gamma^{c_1} = \frac{2}{\rho_0\pi}(1 - \sqrt{1-(\rho_0\pi U_1)^2}), \tag{2.32}$$

$$\gamma^{c_2} = \frac{2}{\rho_0\pi}(1 + \sqrt{1-(\rho_0\pi U_1)^2}). \tag{2.33}$$

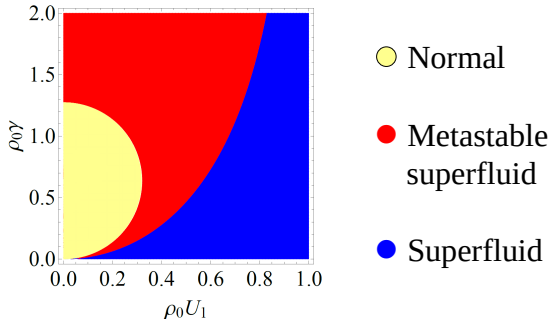

Figure 2.9: Phase diagram obtained from Eqs. (2.34) and (2.35). The yellow region corresponds to the normal state where the gap equation has only a trivial solution $\Delta_0 = 0$. The red region indicates a metastable superfluid state which corresponds to nontrivial solutions of the gap equation but is not an effective ground state. The blue region corresponds to a superfluid phase where a nontrivial solution of the gap equation gives an effective ground state.

Under the above conditions, the nontrivial solution of the gap equation at $\beta \to \infty$ is given by

$$\Delta_0 = \frac{\omega_D}{\sinh\left(\frac{1}{\rho_0 U}\right)}. \tag{2.34}$$

This gives the behavior consistent with Fig. 2.1.

Next, we calculate the condensation energy (2.30) for a constant density of states. In this case, Eq. (2.30) can be rewritten as

$$\frac{E}{N} = \frac{\Delta_0^2}{U} - \frac{1}{2}\rho_0\omega_D^2\left(-2 + 2\sqrt{1+\alpha^2} - \alpha^2\left(\mathrm{Log}\alpha^2 - 2\mathrm{Log}(1+\sqrt{1+\alpha^2})\right)\right), \tag{2.35}$$

where $\alpha = \frac{\Delta_0}{\omega_D}$. This gives the behavior consistent with Fig. 2.6.

Finally, we show a phase diagram in Fig. 2.9 obtained from the analytical solutions of the gap equation with a constant density of states. In Fig. 2.9, the yellow region corresponds to the normal state, where the gap equation has only a trivial solution $\Delta_0 = 0$. This phase is surrounded by the red region, where the gap equation has the nontrivial solution (2.34) which corresponds to the metastable superfluid state, since the nontrivial solution gives a local minimum of the real part of energy due to a positive condensation energy. When the attractive interaction U_1 is sufficiently strong, the system is in the superfluid phase (blue region in Fig. 2.9), where the nontrivial solution of the gap equation gives an effective ground state. The phase diagram is qualitatively consistent with the numerical results obtained in Fig. 2.8.

2.5 Towards experimental realization

The NH quantum phase transitions can be observed by controlling a two-body loss rate. Since the superfluid is metastable in the red region, it can be realized by slowly increasing dissipation from the blue region. For weak attraction U_1, the superfluid undergoes an unconventional phase transition to the normal state due to the exceptional points. To observe the reappearance of the superfluidity under large γ, we may first prepare a metastable superfluid at large U_1 and γ, and then decrease U_1. Finally, the metastablity of the superfluid can be confirmed through comparison of the results between fast and slow increases of the dissipation from $\gamma = 0$.

Here we discuss the detailed experimental setup for probing the NH superfluidity by taking into account the relevant timescale in cold atom experiments. As mentioned in Sec. 2.2, the NH dynamics is realized when we neglect the quantum-jump term in the master equation. To fulfill this condition, the loss rate γ should be much smaller than the energy scale that governs the timescale for relaxation towards a quasi-equilibrium state. In superfluid states, the thermalization proceeds in a timescale of hopping of atoms to neighboring sites [121]. Thus, for a BCS superfluid in which $\gamma, U_1 \ll t$ is satisfied, the NH breakdown of superfluid may be observed. We note that, as inferred

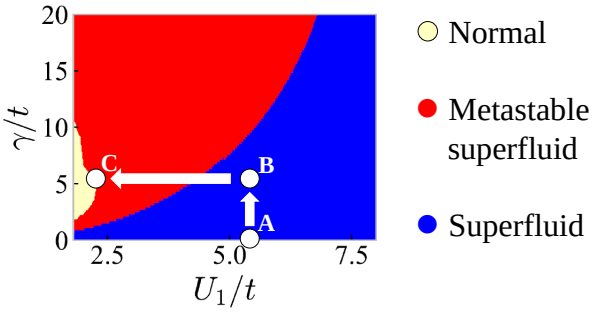

Figure 2.10: Experimental protocol for observing the reentrant superfluidity. We first prepare on-site pairing superfluidity for large attraction U_1 (A) and then introduce large dissipation γ using a sudden application of photoassocitiation (B). The system will reach the reentrant superfluid region by decreasing U_1 (C).

from Figs. 2.8 and 2.9, the breakdown of superfluid due to exceptional points can be induced by small dissipation in the BCS regime, which justifies the NH dynamics. On the other hand, for the reentrant superfluidity, which is another unique phenomenon in the NH superfluid, dissipation larger than the hopping is required (see Figs. 2.8 and 2.9). This seems to invalidate the assumption for the ignorance of the quantum-jump term. However, as mentioned in Sec. 2.4, the physics behind the reentrant superfluidity is the QZE, which suppresses the hopping and facilitates the formation of on-site molecules. The manifestation of the QZE can be observed by using the following protocol. Hence, a large dissipation is not incompatible with the ignorance of the quantum-jump term.

The experimental protocol is illustrated in Fig. 2.10. We first prepare a superfluid state for large attraction U_1, where atom pairs are confined to each lattice site. Then, we introduce large dissipation $\gamma/t \sim 5$ using photoassociation techniques [42]. Finally, we decrease the attraction U_1 by tuning the magnetic field for a Feshbach resonance, which can be operated fast on the order of few $10\mu s$ [121]. If we do not have dissipation, atoms in the on-site molecular pairs tunnel to neighboring sites at a hopping rate t, which gives a timescale of the order of 100 μs [121]. However, under a large dissipation in the quantum Zeno regime, the tunneling of atoms is suppressed by the QZE and thus the dissociation of molecules after ramping down the attraction U_1 is delayed. Consequently, even after a timescale of $1/t$, atoms surviving in the system will still form on-site molecules. Such QZE-assisted molecules can be regarded as a signature of the reentrant superfluidity. In ultracold atoms, molecules (double occupancy) can be detected by measuring binding energies. For the region of the reentrant superfluidity, the above methods can be used to determine the phase boundaries due to exceptional points.

Finally, we note that the NH dynamics is faithfully realized when we perform a quantum-gas-microscopy measurement of an atom number and then postselect the measurement outcome which does not contain any atom loss [63, 64]. Since the quantum-gas microscopy for the attractive Hubbard model was already realized [132], this method can also be used for an unambiguous observation of NH superfluidity. These NH superfluids are expected to be realized with ultracold atoms under inelastic collisions. For example, a superfluid of ^{173}Yb atoms with an orbital Feshbach resonance [45] offers one such candidate since it is inevitably accompanied by two-body losses as observed experimentally [49–51]. The effect of non-Hermiticity on the superfluid gap can be observed by spectroscopy with Raman transitions between hyperfine levels or a clock transition [51, 52]. Furthermore, concerning the control of two-body loss rates, introducing dissipation with photoassociation techniques [42] may also enable the realization of NH superfluids with ^{40}K and ^{6}Li [119–121, 131, 132]. Although the strength of dissipation is usually fixed by scattering properties of atoms, dissipation engineering using photoassociation techniques will be a feasible method for realizing the NH fermionic superfluidity.

2.6 Summary of this chapter

In this chapter, we have investigated how the BCS superfluidity is extended to NH quantum systems under inelastic interactions. We have elucidated some remarkable features unique to the NH fermionic superfluidity, such as exotic Bogoliubov quasiparticles which belong to neither fermions nor bosons and found unconventional quantum phase transitions unique to non-Hermiticity. In particular, for weak attraction, it has been revealed that the superfluidity breaks down with increasing dissipation but shows reentrant behavior as dissipation is further increased. Remarkably, these phase transitions are accompanied by distinctive features of the non-Hermiticity, i.e. the emergence of exceptional points, lines and surfaces in the quasiparticle Hamiltonian for one-, two- and three-dimensions. These characteristic features will play a decisive role in detecting NH phase transitions in experiments. On the other hand, for strong attraction, the superfluid state is not suppressed but enhanced due to the confinement of molecules to single sites via the QZE. While we have focused on a conventional s-wave superfluid, p-wave, d-wave and other exotic superfluids in NH systems will also be relevant for experiments, and merit future investigation.

2.7 Appendix for this chapter

Chemical potential in non-Hermitian systems

Here we clarify how the chemical potential is determined in NH quantum systems. A density matrix ρ of an atomic gas is decomposed into sectors, each of which has a definite particle number M as

$$\rho = \sum_M \rho^{(M)}. \tag{2.36}$$

In the short-time dynamics of the atomic gas, the time evolution of the density matrix $\rho^{(M)}$ is described by the NH Hamiltonian $H_{\rm eff}$ restricted to the M-particle Hilbert space [12]. An effective energy spectrum in the M-particle Hilbert space can be extracted by tuning the chemical potential so that the mean particle number in the NH ensemble (2.3) is

$$M = \frac{1}{Z}\sum_n {}_L\langle E_n|\hat{N}e^{-\beta H_{\rm eff}}|E_n\rangle_R, \tag{2.37}$$

where $\hat{N} = \sum_{\boldsymbol{k},\sigma} c^\dagger_{\boldsymbol{k}\sigma}c_{\boldsymbol{k}\sigma}$ is the particle-number operator. In the $\beta \to \infty$ limit, Eq. (2.37) is calculated as

$$M = {}_L\langle \mathrm{BCS}|\hat{N}|\mathrm{BCS}\rangle_R = \sum_{\boldsymbol{k}} \left(1 - \frac{\xi_{\boldsymbol{k}}}{E_{\boldsymbol{k}}}\right), \tag{2.38}$$

where the BCS ground states (2.20) and (2.21) are used. For a cubic or square lattice, a half-filling condition $M = N$ is achieved by setting $\mu = 0$ in Eq. (2.38).

We note that the expectation value of particle numbers taken by the right BCS eigenstates does not coincide with Eq. (2.38):

$$\begin{aligned}\frac{{}_R\langle \mathrm{BCS}|\hat{N}|\mathrm{BCS}\rangle_R}{{}_R\langle \mathrm{BCS}|\mathrm{BCS}\rangle_R} &= \sum_{\boldsymbol{k}} \frac{2|v_{\boldsymbol{k}}|^2}{|u_{\boldsymbol{k}}|^2 + |v_{\boldsymbol{k}}|^2} \\ &= 2\sum_{\boldsymbol{k}} \frac{\left|1 - \frac{\xi_{\boldsymbol{k}}}{E_{\boldsymbol{k}}}\right|}{\left|1 + \frac{\xi_{\boldsymbol{k}}}{E_{\boldsymbol{k}}}\right| + \left|1 - \frac{\xi_{\boldsymbol{k}}}{E_{\boldsymbol{k}}}\right|},\end{aligned} \tag{2.39}$$

since the BCS states do not conserve the particle number. However, this is not a contradiction

since in the M-particle Hilbert space, the number-conserving states

$$|\Psi_M\rangle_R \equiv \frac{1}{\mathcal{N}}\left(\sum_{\boldsymbol{k}} \alpha_{\boldsymbol{k}} c^\dagger_{\boldsymbol{k}\uparrow} c^\dagger_{-\boldsymbol{k}\downarrow}\right)^{M/2} |0\rangle$$
$$\propto \int_0^{2\pi} d\theta e^{-iM\theta/2} \prod_{\boldsymbol{k}} (u_{\boldsymbol{k}} + v_{\boldsymbol{k}}(\theta) c^\dagger_{\boldsymbol{k}\uparrow} c^\dagger_{-\boldsymbol{k}\downarrow}) |0\rangle , \tag{2.40}$$

$$|\Psi_M\rangle_L \equiv \frac{1}{\mathcal{N}}\left(\sum_{\boldsymbol{k}} \alpha^*_{\boldsymbol{k}} c^\dagger_{\boldsymbol{k}\uparrow} c^\dagger_{-\boldsymbol{k}\downarrow}\right)^{M/2} |0\rangle$$
$$\propto \int_0^{2\pi} d\theta e^{-iM\theta/2} \prod_{\boldsymbol{k}} (u^*_{\boldsymbol{k}} + \bar{v}^*_{\boldsymbol{k}}(\theta) c^\dagger_{\boldsymbol{k}\uparrow} c^\dagger_{-\boldsymbol{k}\downarrow}) |0\rangle , \tag{2.41}$$

are realized instead of the BCS states [145, 146]. Here, $\alpha_{\boldsymbol{k}} \equiv u_{\boldsymbol{k}}/v_{\boldsymbol{k}}(\theta = 0)$. For these states, the particle number does not depend on the choice of an expectation value:

$$\frac{{}_L\langle\Psi_M|\hat{N}|\Psi_M\rangle_R}{{}_L\langle\Psi_M|\Psi_M\rangle_R} = \frac{{}_R\langle\Psi_M|\hat{N}|\Psi_M\rangle_R}{{}_R\langle\Psi_M|\Psi_M\rangle_R} = M. \tag{2.42}$$

Chapter 3

Nonequilibrium dynamics of dissipative fermionic superfluids

3.1 Introduction

Collective excitations of superconductors and superfluids have been widely studied in condensed matter physics [147–166]. Recent experimental progress in ultracold atoms has enabled studies of out-of-equilibrium dynamics of superfluids [167–170]. For example, a periodic modulation of the amplitude of the order parameter excites the Higgs amplitude mode, which has been observed with ultracold fermions [169] and in solid-state systems by light illumination on BCS superconductors [171–179]. As for collective phase modes, the Nambu-Goldstone mode exists in neutral superfluids, and the relative-phase Leggett mode has been predicted for multiband superfluids [148, 179–184]. In particular, ultracold atoms allow for a dynamical control of various system parameters, offering an ideal playground to investigate collective modes. However, they suffer from atom loss due to inelastic scattering, which has received little attention in literature. The effect of particle loss in fermionic superfluids has been studied in the framework of the NH BCS theory in the previous chapter [128]; however, it ignores a significant change in particle number due to quantum jumps. It is crucially important to go beyond the NH framework to describe the long-time dynamics of a superfluid and associated collective modes of order parameters.

In this chapter, we theoretically investigate collective excitations and a nonequilibrium phase transition of fermionic superfluids driven by a sudden switch-on of two-particle loss due to inelastic collisions between atoms [185]. By formulating a dissipative BCS theory that fully incorporates a change in particle number, we find that dissipation fundamentally alters the superfluid order parameter and induces collective oscillations in its amplitude and phase. In particular, we elucidate that a coupling between the order parameter and dissipation leads to a chirped phase rotation, in sharp contrast to the case of an interaction quench in closed systems [see Fig. 3.1(a)].

To experimentally observe the collective phenomena induced by dissipation, we propose introducing a particle loss in one of two coupled superfluids to induce a relative-phase oscillation analogous to the Leggett mode [148, 179–184] [see Fig. 3.1(b)]. The phase mode causes an oscillation of a Josephson current around a nonvanishing dc component. Remarkably, when dissipation becomes strong, the coupled system undergoes a nonequilibrium phase transition characterized by the vanishing dc Josephson current, which can be regarded as a generalization of a dynamical phase transition [157, 158, 186, 187] to dissipative quantum systems. Our findings can experimentally be tested with ultracold atoms through introduction of dissipation via a photoassociation process [42, 92].

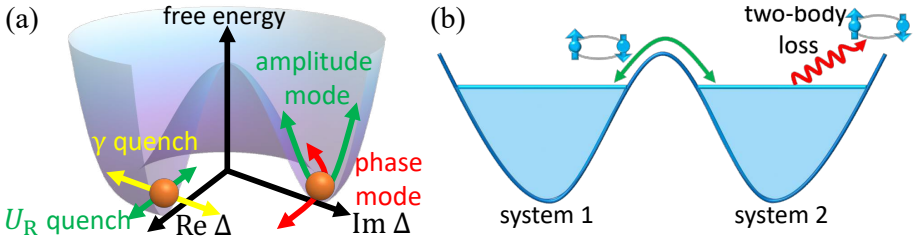

Figure 3.1: (a) Schematic illustration of the amplitude and phase modes in a Mexican-hat free-energy potential as a function of the complex order parameter Δ, when either the interaction $U_{\rm R}$ or the dissipation γ is suddenly switched on. A sudden quench of the interaction $U_{\rm R}$ and that of the dissipation γ kick Δ in a direction parallel and perpendicular to the radial direction, respectively. Note that a finite change of γ excites both the phase and amplitude modes. (b) Two superfluids coupled via a Josephson junction, where one superfluid (system 2) is subject to two-body loss.

3.2 Setup

We consider ultracold fermionic atoms described by the three-dimensional attractive Hubbard model

$$H = \sum_{\boldsymbol{k}\sigma} \epsilon_{\boldsymbol{k}} c^\dagger_{\boldsymbol{k}\sigma} c_{\boldsymbol{k}\sigma} - U_{\rm R} \sum_i c^\dagger_{i\uparrow} c^\dagger_{i\downarrow} c_{i\downarrow} c_{i\uparrow}, \tag{3.1}$$

where $U_{\rm R} > 0$, $\epsilon_{\boldsymbol{k}}$ is the single-particle energy dispersion, and $c_{\boldsymbol{k}\sigma}$ ($c_{i\sigma}$) denotes the annihilation operator of a spin-σ fermion with momentum $\boldsymbol{k}$ (at site i). When the system is subject to inelastic collisions, scattered atoms are lost to a surrounding environment, resulting in dissipative dynamics as observed experimentally [37, 42, 43, 188]. Here, we study the time evolution of the density matrix ρ which is described by the Lindblad equation [2, 53]

$$d\rho/dt = \mathcal{L}\rho = -i[H,\rho] - \frac{\gamma}{2}\sum_i (\{L_i^\dagger L_i, \rho\} - 2L_i \rho L_i^\dagger), \tag{3.2}$$

where $L_i = c_{i\downarrow} c_{i\uparrow}$ is a Lindblad operator that describes two-body loss with loss rate $\gamma > 0$. We note that the kinetic energy of lost atoms is large because of large internal energy of atoms before inelastic collisions. Under such situations, atoms after inelastic collisions are quickly lost into the surrounding environment and the Born-Markov approximation is justified [11, 12, 40].

3.3 Dissipative BCS theory

In this section, we develop a dissipative BCS theory that fully incorporates the effect of quantum jumps in the Lindblad master equation.

3.3.1 Path-integral formalism

We first study how the standard BCS theory is generalized in open dissipative systems by formulating a time-dependent mean-field theory in terms of CTC path integrals [3, 189]. We start with a generating functional defined as

$$Z = {\rm tr}\rho = \int \mathcal{D}[c_-, \bar{c}_-, c_+, \bar{c}_+] e^{iS} = 1, \tag{3.3}$$

with an action

$$\begin{aligned} S = \int_{-\infty}^{\infty} dt \Big[\sum_{\boldsymbol{k}\sigma} (\bar{c}_{\boldsymbol{k}\sigma+} i\partial_t c_{\boldsymbol{k}\sigma+} - \bar{c}_{\boldsymbol{k}\sigma-} i\partial_t c_{\boldsymbol{k}\sigma-}) - H_+ \\ + H_- + \frac{i\gamma}{2} \sum_i (\bar{L}_{i+} L_{i+} + \bar{L}_{i-} L_{i-} - 2L_{i+} \bar{L}_{i-}) \Big], \end{aligned} \tag{3.4}$$

where the subscripts + and − denote forward and backward paths, $H_\alpha = \sum_{\boldsymbol{k}\sigma} \epsilon_{\boldsymbol{k}} \bar{c}_{\boldsymbol{k}\sigma\alpha} c_{\boldsymbol{k}\sigma\alpha} - U_{\rm R} \sum_i \bar{c}_{i\uparrow\alpha}\bar{c}_{i\downarrow\alpha}c_{i\downarrow\alpha}c_{i\uparrow\alpha}$, $L_{i\alpha} = c_{i\downarrow\alpha}c_{i\uparrow\alpha}$, and $\bar{L}_{i\alpha} = \bar{c}_{i\uparrow\alpha}\bar{c}_{i\downarrow\alpha}$ ($\alpha = +, -$). Note that the action has U(1) symmetry under $c_{i\sigma\alpha} \to e^{i\theta} c_{i\sigma\alpha}$ though the particle number is not conserved [190, 191]. The action (3.4) is rewritten as

$$S = \int_{-\infty}^{\infty} dt \Big[\sum_{\boldsymbol{k}\sigma} \Big(\bar{c}_{\boldsymbol{k}\sigma+}(i\partial_t - \epsilon_{\boldsymbol{k}}) c_{\boldsymbol{k}\sigma+} - \bar{c}_{\boldsymbol{k}\sigma-}(i\partial_t - \epsilon_{\boldsymbol{k}}) c_{\boldsymbol{k}\sigma-} \Big) + \sum_{\boldsymbol{k}\boldsymbol{k}'} (U \bar{c}_{\boldsymbol{k}\uparrow+}\bar{c}_{-\boldsymbol{k}\downarrow+} c_{-\boldsymbol{k}'\downarrow+} c_{\boldsymbol{k}'\uparrow+} - U^* \bar{c}_{\boldsymbol{k}\uparrow-}\bar{c}_{-\boldsymbol{k}\downarrow-} c_{-\boldsymbol{k}'\downarrow-} c_{\boldsymbol{k}'\uparrow-} - i\gamma c_{-\boldsymbol{k}\downarrow+} c_{\boldsymbol{k}\uparrow+} \bar{c}_{\boldsymbol{k}'\uparrow-} \bar{c}_{-\boldsymbol{k}'\downarrow-}) \Big], \tag{3.5}$$

where $U = U_R + i\gamma/2$ is an effective complex coupling constant including a contribution from the atom loss [128]. Then, we can perform the Hubbard-Stratonovich transformation for each term in the second line of Eq. (3.5) with auxiliary fields Δ_α ($\alpha = +, -, \pm$) as

$$iU \bar{c}_{\boldsymbol{k}\uparrow+}\bar{c}_{-\boldsymbol{k}\downarrow+} c_{-\boldsymbol{k}'\downarrow+} c_{\boldsymbol{k}'\uparrow+} \to -i\Delta_+ \bar{c}_{\boldsymbol{k}\uparrow+}\bar{c}_{-\boldsymbol{k}\downarrow+} - i\bar{\Delta}_+ c_{-\boldsymbol{k}\downarrow+} c_{\boldsymbol{k}\uparrow+} + \frac{\bar{\Delta}_+\Delta_+}{iU}, \tag{3.6}$$

$$-iU^* \bar{c}_{\boldsymbol{k}\uparrow-}\bar{c}_{-\boldsymbol{k}\downarrow-} c_{-\boldsymbol{k}'\downarrow-} c_{\boldsymbol{k}'\uparrow-} \to i\Delta_- \bar{c}_{\boldsymbol{k}\uparrow-}\bar{c}_{-\boldsymbol{k}\downarrow-} + i\bar{\Delta}_- c_{-\boldsymbol{k}\downarrow-} c_{\boldsymbol{k}\uparrow-} - \frac{\bar{\Delta}_-\Delta_-}{iU^*}, \tag{3.7}$$

$$\gamma c_{-\boldsymbol{k}\downarrow+} c_{\boldsymbol{k}\uparrow+} \bar{c}_{\boldsymbol{k}'\uparrow-} \bar{c}_{-\boldsymbol{k}'\downarrow-} \to -\Delta_\pm \bar{c}_{\boldsymbol{k}\uparrow-}\bar{c}_{-\boldsymbol{k}\downarrow-} - \bar{\Delta}_\pm c_{-\boldsymbol{k}\downarrow+} c_{\boldsymbol{k}\uparrow+} - \frac{\bar{\Delta}_\pm\Delta_\pm}{\gamma}, \tag{3.8}$$

which yield

$$S = \int dt \Bigg\{ \sum_{\boldsymbol{k}} \Bigg[\bar{\psi}^t_{\boldsymbol{k}+} \begin{pmatrix} i\partial_t - \epsilon_{\boldsymbol{k}} & -\Delta_+ \\ -\bar{\Delta}_+ + i\bar{\Delta}_\pm & -i\partial_t + \epsilon_{\boldsymbol{k}} \end{pmatrix} \psi_{\boldsymbol{k}+} - \bar{\psi}^t_{\boldsymbol{k}-} \begin{pmatrix} i\partial_t - \epsilon_{\boldsymbol{k}} & -\Delta_- - i\Delta_\pm \\ -\bar{\Delta}_- & -i\partial_t + \epsilon_{\boldsymbol{k}} \end{pmatrix} \psi_{\boldsymbol{k}-} \Bigg] + \frac{\bar{\Delta}_+\Delta_+}{iU} - \frac{\bar{\Delta}_-\Delta_-}{iU^*} - \frac{\bar{\Delta}_\pm\Delta_\pm}{\gamma} \Bigg\}, \tag{3.9}$$

where $\bar{\psi}_{\boldsymbol{k}\alpha} = \begin{pmatrix} \bar{c}_{\boldsymbol{k}\uparrow\alpha}, & c_{-\boldsymbol{k}\downarrow\alpha} \end{pmatrix}^t$ and $\psi_{\boldsymbol{k}\alpha} = \begin{pmatrix} c_{\boldsymbol{k}\uparrow\alpha}, & \bar{c}_{-\boldsymbol{k}\downarrow\alpha} \end{pmatrix}^t$ ($\alpha = +, -$). From the saddle-point condition $\langle \partial S/\partial\Delta_\alpha \rangle = \langle \partial S/\partial\bar{\Delta}_\alpha \rangle = 0$ ($\alpha = +, -, \pm$), we obtain

$$\Delta_+ = -\frac{U}{N_0} \sum_{\boldsymbol{k}} \langle c_{-\boldsymbol{k}\downarrow+} c_{\boldsymbol{k}\uparrow+} \rangle, \quad \bar{\Delta}_+ = -\frac{U}{N_0} \sum_{\boldsymbol{k}} \langle c^\dagger_{\boldsymbol{k}\uparrow+} c^\dagger_{-\boldsymbol{k}\downarrow+} \rangle, \tag{3.10}$$

$$\Delta_- = -\frac{U^*}{N_0} \sum_{\boldsymbol{k}} \langle c_{-\boldsymbol{k}\downarrow-} c_{\boldsymbol{k}\uparrow-} \rangle, \quad \bar{\Delta}_- = -\frac{U^*}{N_0} \sum_{\boldsymbol{k}} \langle c^\dagger_{\boldsymbol{k}\uparrow-} c^\dagger_{-\boldsymbol{k}\downarrow-} \rangle, \tag{3.11}$$

$$\Delta_\pm = \frac{\gamma\Delta_+}{U}, \quad \bar{\Delta}_\pm = \frac{\gamma\bar{\Delta}_-}{U^*}, \tag{3.12}$$

where N_0 is the number of lattice sites and $\langle \cdots \rangle$ is the expectation value for fixed Δ_α and $\bar{\Delta}_\alpha$. Then, we can reduce the number of the auxiliary fields by using $\langle c_{-\boldsymbol{k}\downarrow\alpha} c_{\boldsymbol{k}\uparrow\alpha} \rangle = {\rm tr}(c_{-\boldsymbol{k}\downarrow} c_{\boldsymbol{k}\uparrow} \rho)$ ($\alpha = +, -$) and ${\rm tr}(A^\dagger\rho) = [{\rm tr}(A\rho)]^*$ [189], giving

$$\Delta_+ = \bar{\Delta}^*_-, \tag{3.13}$$

$$\Delta_- = \bar{\Delta}^*_+. \tag{3.14}$$

Finally, the action (3.9) is rewritten in a quadratic form of fermionic Grassmann fields [128] as

$$S = \int dt \sum_{\boldsymbol{k}} \Bigg\{ \bar{\psi}^t_{\boldsymbol{k}+} \begin{pmatrix} i\partial_t - \epsilon_{\boldsymbol{k}} & -\Delta \\ -\Delta^* & -i\partial_t + \epsilon_{\boldsymbol{k}} \end{pmatrix} \psi_{\boldsymbol{k}+} - \bar{\psi}^t_{\boldsymbol{k}-} \begin{pmatrix} i\partial_t - \epsilon_{\boldsymbol{k}} & -\Delta \\ -\Delta^* & -i\partial_t + \epsilon_{\boldsymbol{k}} \end{pmatrix} \psi_{\boldsymbol{k}-} \Bigg\}, \tag{3.15}$$

where the superfluid order parameter of the system is given by

$$\Delta = -\frac{U}{N_0} \sum_{\boldsymbol{k}} {\rm tr}(c_{-\boldsymbol{k}\downarrow} c_{\boldsymbol{k}\uparrow} \rho) \equiv -\frac{U}{N_0} \sum_{\boldsymbol{k}} \langle c_{-\boldsymbol{k}\downarrow} c_{\boldsymbol{k}\uparrow} \rangle. \tag{3.16}$$

Importantly, the order parameter includes the loss rate γ, which leads to dissipation-induced collective modes as discussed below.

3.3.2 Operator formalism

Here, we explain the operator formalism of the BCS theory for a dissipative superfluid. First, we note that an operator $|\psi_+\rangle\langle\psi_-|$ acting on the Hilbert space of the system can be mapped to a tensor-product state $|\psi_+\rangle \otimes |\psi_-\rangle$ in the doubled Hilbert space $\mathbb{H}_+ \otimes \mathbb{H}_-$ [192, 193]. Using this mapping, we can rewrite the Liouvillian as

$$\begin{aligned} i\mathcal{L} &= H_+ - H_- + i\sum_i \gamma_i (L_{i+}L_{i-}^\dagger - \frac{1}{2}L_{i+}^\dagger L_{i+} - \frac{1}{2}L_{i-}^\dagger L_{i-}) \\ &= \mathcal{H}_+ - \mathcal{H}_-^* + i\gamma \sum_{\boldsymbol{k}\boldsymbol{k}'} c_{-\boldsymbol{k}\downarrow+}c_{\boldsymbol{k}\uparrow+}c_{\boldsymbol{k}'\uparrow-}^\dagger c_{-\boldsymbol{k}'\downarrow-}^\dagger, \end{aligned} \tag{3.17}$$

where $L_{i\alpha} = c_{i\downarrow\alpha}c_{i\uparrow\alpha}$, and $c_{i\sigma\alpha}$ ($c_{\boldsymbol{k}\sigma\alpha}$) with $\alpha = +, -$ is the fermion annihilation operator in the real (momentum) space that acts on the Hilbert space $\mathbb{H}_\alpha$. The fermion operator with subscript $+$ ($-$) corresponds to the fermion field in the forward (backward) path in the path-integral formalism. The BCS Hamiltonian equivalent to Eq. (3.1) is given by

$$H_\alpha = \sum_{\boldsymbol{k}\sigma} \epsilon_{\boldsymbol{k}} c_{\boldsymbol{k}\sigma\alpha}^\dagger c_{\boldsymbol{k}\sigma\alpha} - U_{\rm R}\sum_{\boldsymbol{k}\boldsymbol{k}'} c_{\boldsymbol{k}\uparrow\alpha}^\dagger c_{-\boldsymbol{k}\downarrow\alpha}^\dagger c_{-\boldsymbol{k}'\downarrow\alpha} c_{\boldsymbol{k}'\uparrow\alpha}, \tag{3.18}$$

and $\mathcal{H}_\alpha$ is defined as

$$\begin{aligned} \mathcal{H}_\alpha &= H_\alpha - \frac{1}{2}i\gamma\sum_i L_{i\alpha}^\dagger L_{i\alpha} \\ &= \sum_{\boldsymbol{k}\sigma} \epsilon_{\boldsymbol{k}} c_{\boldsymbol{k}\sigma\alpha}^\dagger c_{\boldsymbol{k}\sigma\alpha} - U\sum_{\boldsymbol{k}\boldsymbol{k}'} c_{\boldsymbol{k}\uparrow\alpha}^\dagger c_{-\boldsymbol{k}\downarrow\alpha}^\dagger c_{-\boldsymbol{k}'\downarrow\alpha} c_{\boldsymbol{k}'\uparrow\alpha}. \end{aligned} \tag{3.19}$$

By applying the mean-field approximation to $\mathcal{L}$, we obtain the mean-field Liouvillian as

$$\begin{aligned} i\mathcal{L}_{\rm MF} =& \sum_{\boldsymbol{k}\sigma} \epsilon_{\boldsymbol{k}} c_{\boldsymbol{k}\sigma+}^\dagger c_{\boldsymbol{k}\sigma+} + \Delta_+ \sum_{\boldsymbol{k}} c_{\boldsymbol{k}\uparrow+}^\dagger c_{-\boldsymbol{k}\downarrow+}^\dagger + (\bar{\Delta}_+ - \frac{i\gamma}{U^*}\bar{\Delta}_-)\sum_{\boldsymbol{k}} c_{-\boldsymbol{k}\downarrow+}c_{\boldsymbol{k}\uparrow+} \\ &- \sum_{\boldsymbol{k}\sigma} \epsilon_{\boldsymbol{k}} c_{\boldsymbol{k}\sigma-}^\dagger c_{\boldsymbol{k}\sigma-} - (\Delta_- + \frac{i\gamma}{U}\Delta_+)\sum_{\boldsymbol{k}} c_{\boldsymbol{k}\uparrow-}^\dagger c_{-\boldsymbol{k}\downarrow-}^\dagger - \bar{\Delta}_- \sum_{\boldsymbol{k}} c_{-\boldsymbol{k}\downarrow-}c_{\boldsymbol{k}\uparrow-} \\ =& \sum_{\boldsymbol{k}} \Psi_{\boldsymbol{k}+}^\dagger \begin{pmatrix} \epsilon_{\boldsymbol{k}} & \Delta_+ \\ \bar{\Delta}_+ - \frac{i\gamma}{U^*}\bar{\Delta}_- & -\epsilon_{\boldsymbol{k}} \end{pmatrix} \Psi_{\boldsymbol{k}+} - \sum_{\boldsymbol{k}} \Psi_{\boldsymbol{k}-}^\dagger \begin{pmatrix} \epsilon_{\boldsymbol{k}} & \Delta_- + \frac{i\gamma}{U}\Delta_+ \\ \bar{\Delta}_- & -\epsilon_{\boldsymbol{k}} \end{pmatrix} \Psi_{\boldsymbol{k}-}, \end{aligned} \tag{3.20}$$

where $\Psi_{\boldsymbol{k}} = \begin{pmatrix} c_{\boldsymbol{k}\uparrow}, & c_{-\boldsymbol{k}\downarrow}^\dagger \end{pmatrix}^t$ is the Nambu spinor. As we see from Eq. (3.17) and Eq. (3.19), the Liouvillian is invariant under the U(1) gauge transformations $c_{\boldsymbol{k}\sigma+} \to e^{i\theta}c_{\boldsymbol{k}\sigma+}$ and $c_{\boldsymbol{k}\sigma-} \to e^{i\theta}c_{\boldsymbol{k}\sigma-}$. Moreover, under the exchange of forward and backward operators, $Pc_{\boldsymbol{k}\sigma+}P^{-1} = c_{\boldsymbol{k}\sigma-}$ and $Pc_{\boldsymbol{k}\sigma+}^\dagger P^{-1} = c_{\boldsymbol{k}\sigma-}^\dagger$ with $P^2 = 1$, the Liouvillian has the following symmetry

$$P(i\mathcal{L})^\dagger P^{-1} = -i\mathcal{L}. \tag{3.21}$$

By imposing the same symmetry on the mean-field Liouvillian as $P(i\mathcal{L}_{\rm MF})^\dagger P^{-1} = -i\mathcal{L}_{\rm MF}$, we obtain the relations for the order parameters as $\Delta_+^* = \bar{\Delta}_-$, and $\Delta_-^* = \bar{\Delta}_+$, which coincide with those obtained in the path-integral formalism [see Eqs. (3.13) and (3.14)]. Finally, by rewriting the superfluid order parameter Δ_+ as Δ, which is defined in Eq. (3.16), we obtain the equations for the density matrix as

$$\dot{\rho} = -i[H_{\rm eff}, \rho], \tag{3.22}$$

$$H_{\rm eff} = \sum_{\boldsymbol{k}} \Psi_{\boldsymbol{k}}^\dagger \begin{pmatrix} \epsilon_{\boldsymbol{k}} & \Delta \\ \Delta^* & -\epsilon_{\boldsymbol{k}} \end{pmatrix} \Psi_{\boldsymbol{k}}. \tag{3.23}$$

In subsection 3.3.4, we show that Eq. (3.22) can be also derived from the time-dependent Bogoliubov-de Gennes analysis. We will also see that, while Eq. (3.22) appears to describe unitary evolution, it is consistent with the original Lindblad equation as a consequence of the time-dependent BCS ansatz.

3.3.3 Anderson's pseudospin representation

We use Anderson's pseudospin representation [147, 153–158, 160, 178] defined by $\boldsymbol{\sigma}_{\boldsymbol{k}} = \frac{1}{2}\Psi_{\boldsymbol{k}}^{\dagger} \cdot \boldsymbol{\tau} \cdot \Psi_{\boldsymbol{k}}$ and $H_{\rm eff} = 2\sum_{\boldsymbol{k}} \boldsymbol{b}_{\boldsymbol{k}} \cdot \boldsymbol{\sigma}_{\boldsymbol{k}}$, where $\boldsymbol{\tau} = (\tau_x, \quad \tau_y, \quad \tau_z)$ is the vector of the Pauli matrices. The pseudospins satisfy the commutation relations $[\sigma_{\boldsymbol{k}}^j, \sigma_{\boldsymbol{k}}^k] = i\epsilon_{jkl}\sigma_{\boldsymbol{k}}^l$. For simplicity of notation, we omit the bracket and regard $\boldsymbol{\sigma}_{\boldsymbol{k}}$ as the expectation value of the pseudospin operator. By using the commutation relation of the pseudospins, Eq. (3.22) is mapped to the Bloch equation:

$$\frac{d\boldsymbol{\sigma}_{\boldsymbol{k}}}{dt} = 2\boldsymbol{b}_{\boldsymbol{k}} \times \boldsymbol{\sigma}_{\boldsymbol{k}}, \tag{3.24}$$

$$\boldsymbol{b}_{\boldsymbol{k}} = (\mathrm{Re}\Delta, \quad -\mathrm{Im}\Delta, \quad \epsilon_{\boldsymbol{k}}). \tag{3.25}$$

Equation (3.24) shows that the superfluid dynamics is characterized by precession of a pseudospin in an effective magnetic field $\boldsymbol{b}_k$. Here, the order parameter is determined self-consistently from the pseudospin expectation value as

$$\Delta = |\Delta| e^{i\theta} = -\frac{U}{N_0}\sum_{\boldsymbol{k}} (\sigma_{\boldsymbol{k}}^x - i\sigma_{\boldsymbol{k}}^y). \tag{3.26}$$

It is noteworthy that the norm of the pseudospin is conserved by the Bloch equation (3.24). The time evolution of the particle number due to particle loss is obtained from Eq. (3.22) as

$$\frac{1}{N_0}\frac{dN}{dt} = -\frac{2\gamma|\Delta|^2}{|U|^2}, \tag{3.27}$$

which reflects the dynamics of the order parameter.

3.3.4 Generalization of the Bogoliubov-de Gennes analysis with a time-dependent BCS state

We here explain that Eq. (3.22) (Eq. (3.24) in the psedouspin representation) is equivalent to the Bogoliubov-de Gennes equation with a time-dependent BCS state [149, 155], which describes the unitary evolution of the density matrix.

We introduce the time-dependent BCS state of the effective Hamiltonian $H_{\rm eff} = \sum_{\boldsymbol{k}} \Psi_{\boldsymbol{k}}^{\dagger} \begin{pmatrix} \epsilon_{\boldsymbol{k}} & \Delta \\ \Delta^* & -\epsilon_{\boldsymbol{k}} \end{pmatrix} \Psi_{\boldsymbol{k}}$ as follows:

$$|\Psi_{\rm BCS}(t)\rangle = \prod_{\boldsymbol{k}} (u_{\boldsymbol{k}}(t) + v_{\boldsymbol{k}}(t) c_{\boldsymbol{k}\uparrow}^{\dagger} c_{-\boldsymbol{k}\downarrow}^{\dagger})|0\rangle, \tag{3.28}$$

$$|u_{\boldsymbol{k}}|^2 + |v_{\boldsymbol{k}}|^2 = 1, \tag{3.29}$$

where $|0\rangle$ is the vacuum of fermions. Here, the superfluid order parameter Δ is rewritten as

$$\Delta = -\frac{U}{N_0}\sum_{\boldsymbol{k}} \langle c_{-\boldsymbol{k}\downarrow} c_{\boldsymbol{k}\uparrow}\rangle = -\frac{U}{N_0}\sum_{\boldsymbol{k}} u_{\boldsymbol{k}}^*(t) v_{\boldsymbol{k}}(t). \tag{3.30}$$

Suppose that the density matrix is given by

$$\rho(t) = |\Psi_{\rm BCS}(t)\rangle \langle \Psi_{\rm BCS}(t)|. \tag{3.31}$$

Then, the time-evolution equation (3.22) is equivalent to the Bogoliubov-de Gennes equation with the time-dependent BCS state

$$i\partial_t \begin{pmatrix} u_{\boldsymbol{k}} \\ v_{\boldsymbol{k}} \end{pmatrix} = \begin{pmatrix} -\epsilon_{\boldsymbol{k}} & \Delta^* \\ \Delta & \epsilon_{\boldsymbol{k}} \end{pmatrix} \begin{pmatrix} u_{\boldsymbol{k}} \\ v_{\boldsymbol{k}} \end{pmatrix}. \tag{3.32}$$

By defining $f_{\boldsymbol{k}}(t)$ and $g_{\boldsymbol{k}}(t)$ as

$$f_{\boldsymbol{k}} = u_{\boldsymbol{k}}^* v_{\boldsymbol{k}}, \tag{3.33}$$

$$g_{\boldsymbol{k}} = \frac{1}{2}(|u_{\boldsymbol{k}}|^2 - |v_{\boldsymbol{k}}|^2), \tag{3.34}$$

Eq. (3.32) is rewritten as

$$\frac{df_{\boldsymbol{k}}}{dt} = -2i\epsilon_{\boldsymbol{k}} f_{\boldsymbol{k}} - 2i\Delta g_{\boldsymbol{k}}, \tag{3.35}$$

$$\frac{dg_{\boldsymbol{k}}}{dt} = i\Delta f^*_{\boldsymbol{k}} - i\Delta^* f_{\boldsymbol{k}}. \tag{3.36}$$

These equations take the same forms as those for closed systems [149, 155]. Finally, by defining the psedouspins as

$$f_{\boldsymbol{k}} = \sigma^x_{\boldsymbol{k}} - i\sigma^y_{\boldsymbol{k}}, \tag{3.37}$$

$$g_{\boldsymbol{k}} = -\sigma^z_{\boldsymbol{k}}, \tag{3.38}$$

we obtain the same Bloch equation as discussed in the previous subsection: $d\boldsymbol{\sigma}_{\boldsymbol{k}}/dt = 2\boldsymbol{b}_{\boldsymbol{k}} \times \boldsymbol{\sigma}_{\boldsymbol{k}}$, and $\boldsymbol{b}_{\boldsymbol{k}} = \big(\mathrm{Re}\Delta, \quad -\mathrm{Im}\Delta, \quad \epsilon_{\boldsymbol{k}}\big)$. We note that the dynamics described by Eq. (3.22) conserves the purity $\mathrm{tr}[\rho^2]$ as

$$\frac{d\mathrm{tr}[\rho^2]}{dt} = 2\mathrm{tr}\left[\rho\frac{d\rho}{dt}\right] = -2i\mathrm{tr}(\rho[H_{\mathrm{eff}}, \rho]) = 0. \tag{3.39}$$

In general, the purity should decrease during the time evolution described by the quantum master equation. This fact is consistent with the time-dependent BCS ansatz (3.28) as follows. Since $|\Psi_{\mathrm{BCS}}(t)\rangle$ can be expanded in terms of N-particle states

$$|\Psi_N\rangle = \sum_{\boldsymbol{k}_1 \cdots \boldsymbol{k}_{N/2}} a_{\boldsymbol{k}_1} \cdots a_{\boldsymbol{k}_{N/2}} c^\dagger_{\boldsymbol{k}_1\uparrow} c^\dagger_{-\boldsymbol{k}_1\downarrow} \cdots c^\dagger_{\boldsymbol{k}_{N/2}\uparrow} c^\dagger_{-\boldsymbol{k}_{N/2}\downarrow} |0\rangle \tag{3.40}$$

as

$$|\Psi_{\mathrm{BCS}}(t)\rangle = \sum_N c_N |\Psi_N\rangle, \tag{3.41}$$

the density matrix is written as

$$\begin{aligned}\rho &= |\Psi_{\mathrm{BCS}}(t)\rangle\langle\Psi_{\mathrm{BCS}}(t)| \\ &= \sum_N |c_N|^2 |\Psi_N\rangle\langle\Psi_N| + \sum_{N\neq N'} c^*_{N'} c_N |\Psi_N\rangle\langle\Psi_{N'}|.\end{aligned} \tag{3.42}$$

Then, for a gauge-invariant observable $\mathcal{O}$, its expectation value is given by

$$\langle\mathcal{O}\rangle \equiv \mathrm{tr}[\mathcal{O}\rho] = \sum_N |c_N|^2 \langle\Psi_N|\mathcal{O}|\Psi_N\rangle = \mathrm{tr}[\mathcal{O}\rho'], \tag{3.43}$$

where

$$\rho' = \sum_N |c_N|^2 |\Psi_N\rangle\langle\Psi_N| \tag{3.44}$$

is a mixed state of different particle numbers. Therefore, concerning gauge-invariant observables, the time-dependent BCS state (3.31) is indistinguishable from the mixed state (3.44) with $\mathrm{tr}[\rho'^2] < 1$. Since any physically observable quantity should be gauge invariant, the time-dependent BCS ansatz (3.28) can describe the time evolution of the density matrix consistently with the quantum master equation.

3.4 Collective excitations: phase and amplitude modes

In this section, we numerically solve the Bloch equation (3.24) self-consistently under the condition (3.26). As an initial state, we prepare a BCS ground state with $\gamma = 0$, whose pseudospin representation is given by $\sigma^x_{\boldsymbol{k}}(0) = -\Delta_0/\sqrt{{\epsilon_{\boldsymbol{k}}}^2 + \Delta_0^2}$, $\sigma^y_{\boldsymbol{k}}(0) = 0$ and $\sigma^z_{\boldsymbol{k}}(0) = -\epsilon_{\boldsymbol{k}}/\sqrt{{\epsilon_{\boldsymbol{k}}}^2 + \Delta_0^2}$ with $\Delta_0 \in \mathbb{R}$. The single-particle energy $\epsilon_{\boldsymbol{k}}$ is measured from the Fermi energy of the initial state. The bandwidth W is defined by the energy difference between the upper and lower edges of the energy

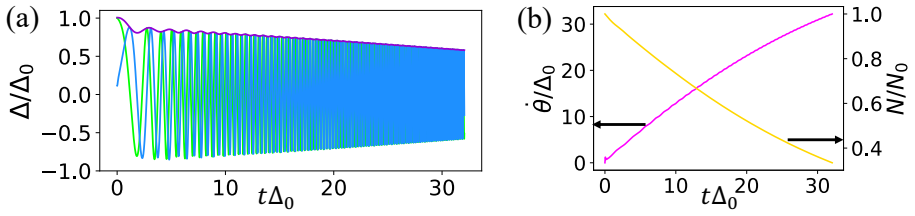

Figure 3.2: Dynamics of a superfluid after the atom loss with $\gamma = 2.81\Delta_0$ is switched on for the initial state with $U_{\rm R} = 12.2\Delta_0$ and bandwidth $W = 46.8\Delta_0$, where Δ_0 is the superfluid order parameter in the absence of the atom loss. (a) Real parts (light green), imaginary parts (blue), and the amplitude (violet) of the order parameter. (b) Angular velocity (pink) and particle number (yellow) plotted against time. The figures indicate a chirped phase rotation and an amplitude oscillation of Δ.

spectrum with a constant density of states. We then switch on the atom loss γ at $t = 0$. The results shown in Fig. 3.2 are obtained by the second-order Runge-Kutta method. In the long-time limit, the amplitude of the superfluid order parameter Δ is suppressed due to dissipation, indicating a decay of superfluidity [see Fig. 3.2(a)]. We note that the order parameter decays in the long-time limit due to a decrease of the particle number [see Fig. 3.2(b)], and such behavior has no counterpart in the quench in isolated systems [156, 157]. Remarkably, after the dissipation γ is introduced, the U(1) phase of the order parameter rotates and shows chirping, i.e., its angular velocity increases with time [see Fig. 3.2(a), (b)]. The chirping behavior is distinct from the usual dynamics in isolated systems where the U(1) phase stays constant [156–158], and is caused by the dynamical shift of the Fermi surface as detailed below.

The physical origin of the chirping of the U(1) phase can be understood from the pseudospin picture. As shown in Fig. 3.3, when the sign of $\sigma^z_{\boldsymbol{k}}$ changes from positive to negative, the magnitudes of $\sigma^x_{\boldsymbol{k}}$ and $\sigma^y_{\boldsymbol{k}}$ increase due to the norm conservation of pseudospins. This indicates that the Cooper-pair amplitude at specific momenta rapidly changes when atoms at those momenta are lost from the system. Since Cooper pairs are formed near the Fermi surface, a loss of Cooper pairs leads to a downward shift of the Fermi level.

To see the effect of the dynamics of pseudospins on the collective phase mode, we calculate the angular velocity of the order parameter. From Eq. (3.26), the real and imaginary parts of the order parameter are written as

$$|\Delta| \cos\theta = {\rm Re}\Delta = -U_1 \sum_{\boldsymbol{k}} \sigma^x_{\boldsymbol{k}} - \frac{\gamma}{2} \sum_{\boldsymbol{k}} \sigma^y_{\boldsymbol{k}}, \tag{3.45}$$

$$|\Delta| \sin\theta = {\rm Im}\Delta = -\frac{\gamma}{2} \sum_{\boldsymbol{k}} \sigma^x_{\boldsymbol{k}} + U_1 \sum_{\boldsymbol{k}} \sigma^y_{\boldsymbol{k}}. \tag{3.46}$$

By differentiating Eqs. (3.45) and (3.46) with respect to time, we obtain

$$|\Delta|^2 \frac{d\theta}{dt} = \left(U_1 {\rm Im}\Delta - \frac{\gamma}{2}{\rm Re}\Delta\right) \sum_{\boldsymbol{k}} \frac{d\sigma^x_{\boldsymbol{k}}}{dt} + \left(\frac{\gamma}{2}{\rm Im}\Delta + U_1 {\rm Re}\Delta\right) \sum_{\boldsymbol{k}} \frac{d\sigma^y_{\boldsymbol{k}}}{dt}. \tag{3.47}$$

Then, by substituting the Bloch equation (3.24) into Eq. (3.47), we arrive at

$$\frac{d\theta}{dt} = U_{\rm R}\left(1 - \frac{N}{N_0}\right) - \frac{2|U|^2}{|\Delta|^2 N_0^2} \sum_{\substack{\boldsymbol{k}\boldsymbol{k}' \\ \alpha = x,y}} \sigma^\alpha_{\boldsymbol{k}} \cdot \epsilon_{\boldsymbol{k}'} \sigma^\alpha_{\boldsymbol{k}'}, \tag{3.48}$$

in which the last term increases due to the shift of the Fermi level, leading to chirping of the U(1) phase. Here, we note that the first term on the right-hand side of Eq. (3.48) also increases as the particle number decreases; however, it is much smaller than the second term.

On the other hand, the phase rotation is understood from an initial-state free energy as a function of Δ [see Fig. 3.1(a)]. When dissipation is introduced, the sudden quench of the imaginary part of U in Eq. (3.26) pushes the order parameter towards the direction perpendicular to the radial direction irrespective of the initial choice of the gauge. Another way to understand the

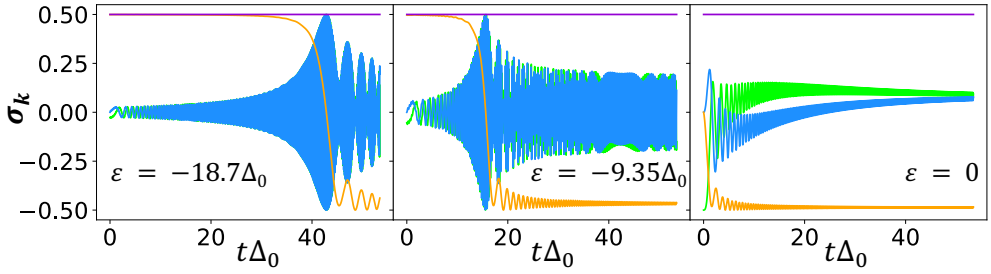

Figure 3.3: Dynamics of pseudospins [$\sigma^x_{\boldsymbol{k}}$ (light green), $\sigma^y_{\boldsymbol{k}}$ (blue), $\sigma^z_{\boldsymbol{k}}$ (orange), $|\boldsymbol{\sigma}_{\boldsymbol{k}}|$ (violet)] after the atom loss with $\gamma = 2.81\Delta_0$ is switched on for the initial state with $U_{\rm R} = 12.2\Delta_0$ and the Fermi energy $\epsilon_{\rm F} = 0$ for $\epsilon = -18.7\Delta_0$ (left), $-9.35\Delta_0$ (center), and 0 (right), where ϵ is the single-particle energy in the band $-23.4\Delta_0 \leq \epsilon \leq 23.4\Delta_0$.

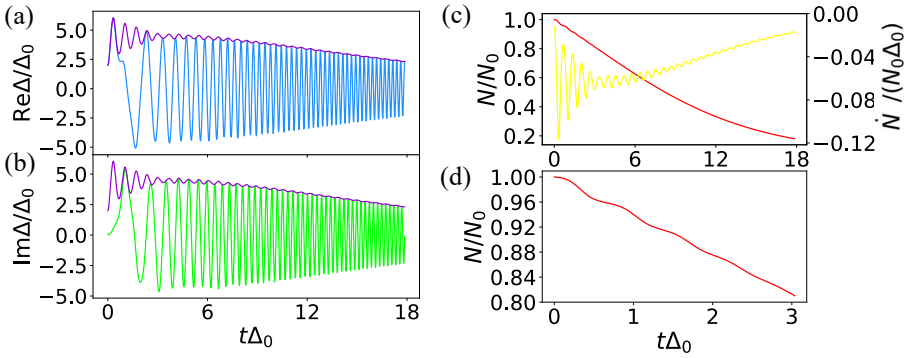

Figure 3.4: Dynamics of a superfluid after the interaction and the atom loss are suddenly changed. (a) Real parts (light green) and imaginary parts (blue) of the order parameter. The amplitudes of the order parameter are shown as violet curves in both figures. (c) The particle number of the system normalized by the initial particle number N_0 (red) and the rate of change in particle number (yellow). (d) An enlarged view of the particle number near $t = 0$. The parameters are suddenly changed from $U_{\rm R} = 8.4\Delta_0$ to $U = (16.8 + 0.45i)\Delta_0$ at $t = 0$ and the bandwidth is set to $W = 28\Delta_0$.

phase rotation is to introduce an effective chemical potential as $\Delta(t) = \exp(-2i\int_0^t \mu_{\rm eff}(t)dt)\Omega(t)$ ($\Omega \in \mathbb{R}$). By performing a global gauge transformation from Δ to Ω, the Bloch equation is written in the Larmor frame on which the energy dispersion is given by $\xi_{\boldsymbol{k}}(t) = \epsilon_{\boldsymbol{k}} - \mu_{\rm eff}(t)$. This gauge transformation indicates that the phase rotation corresponds to a decrease of the effective chemical potential, which is consistent with the behaviors of $\dot{\theta}$ and N in Fig. 3.2(b). This result can naturally be understood since the phase and the particle number are conjugate variables.

Importantly, we also find amplitude oscillations in $|\Delta|$ as shown in Fig. 3.2(a). The mechanism behind the oscillations is that the quench of the imaginary part of U changes the absolute value of Δ [see Fig. 3.1(a)]. The frequency of the amplitude oscillation is close to $2\Delta_0$ at an early stage, and increases as time evolves. This behavior is distinct from that of an isolated system, where the amplitude mode is characterized by the constant frequency. Such behavior can be observed from the measurement of the time-dependent particle number via Eq. (3.27).

We note that the amplitude oscillations are more pronounced when the interaction and the dissipation are simultaneously quenched. Figure 3.4 shows the dynamics after the dissipation γ is introduced at $t = 0$ and the interaction strength is simultaneously changed from $U_{\rm R} = 8.4\Delta_0$ to $U_{\rm R} = 16.8\Delta_0$. In Figs. 3.4(a) and (b), we see an amplitude oscillation larger than that in the loss quench dynamics shown in Figs. 3.2(a) and (b). This behavior is due to the fact that a change in the real part of U causes a large initial shift of the amplitude of the order parameter [see Fig. 3.1(a)]. As shown in Figs. 3.4(c) and (d), the amplitude of the particle-number oscillation is a few percent of the initial particle number, which can be detected with current experimental techniques [194].

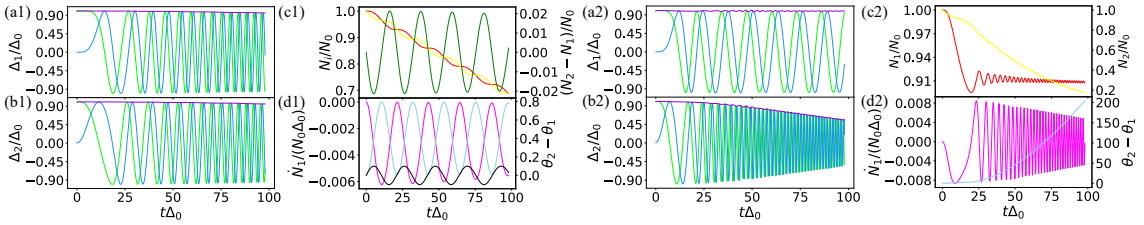

Figure 3.5: Dynamics of two fermionic superfluids after the switch-on of the atom loss γ and the tunnel coupling $V = 0.02\Delta_0$ with $U_{\rm R} = 3.06\Delta_0$ and bandwidth $W = 5.11\Delta_0$, where $\gamma = 0.03\Delta_0$ for (a1)-(d1) and $\gamma = 0.06\Delta_0$ for (a2)-(d2). (a), (b) Real parts (light green), imaginary parts (blue), and amplitudes (violet) of the order parameter for systems 1 and 2. (c) Particle numbers of system 1 (red) and system 2 (yellow), and their difference [green, in (c1)]. (d) Josephson current (pink) and phase difference (light blue) between the two systems. The black curve in (d1) shows an oscillation at frequency $\omega_{\rm L}$ for comparison.

3.5 Josephson junctions

As we have seen in the previous section, U(1) phase rotation highlights dissipative fermionic superfluids, but can be gauged out by going into the Larmor frame. To overcome this problem, in this section, we consider Josephson junctions to observe gauge-invariant physical quantities.

3.5.1 Collective excitations: Leggett mode

To observe the chirped phase rotation of the superfluid order parameter that is a unique feature of dissipative superfluids, we propose that the phase rotation induced by dissipation can be detected when two superfluids are connected via a Josephson junction, which has been realized in ultracold atoms [194–198]. As the phase difference in the two superfluid order parameters is gauge-invariant, it leads to an observable Josephson current. We introduce dissipation to one of the two superfluids as schematically illustrated in Fig. 3.1(b) and assume that they are coupled via a tunneling Hamiltonian [148, 184]

$$H_{\rm tun} = -\frac{V}{N_0}\sum_{\boldsymbol{k}\boldsymbol{k}'}(c^\dagger_{1\boldsymbol{k}\uparrow}c^\dagger_{1-\boldsymbol{k}\downarrow}c_{2-\boldsymbol{k}'\downarrow}c_{2\boldsymbol{k}'\uparrow} + \text{H.c.}), \tag{3.49}$$

where $V > 0$ is the amplitude of Cooper-pair tunneling between system 1 without dissipation and system 2 with two-particle loss. By performing a mean-field analysis, we can write the system Hamiltonian as $H_{\rm sys} = H_1 + H_2 + H_{\rm tun} = H_1' + H_2'$, where $H_i \equiv \sum_{\boldsymbol{k}\sigma}\epsilon_{\boldsymbol{k}}c^\dagger_{i\boldsymbol{k}\sigma}c_{i\boldsymbol{k}\sigma} + \sum_{\boldsymbol{k}}(\Delta_i c^\dagger_{i\boldsymbol{k}\uparrow}c^\dagger_{i-\boldsymbol{k}\downarrow} + \text{H.c.})$ $(i = 1, 2)$ is the mean-field Hamiltonian of system i and $H_i' \equiv H_i - V/N_0\sum_{\boldsymbol{k}\boldsymbol{k}'}(\langle c_{j-\boldsymbol{k}'\downarrow}c_{j\boldsymbol{k}'\uparrow}\rangle c^\dagger_{i\boldsymbol{k}\uparrow}c^\dagger_{i-\boldsymbol{k}\downarrow} + \text{H.c.})$ $[(i,j) = (1,2)$ or $(2,1)]$. In the pseudospin respresentation, the Hamiltonian is written as $H_i' = 2\sum_{\boldsymbol{k}}\boldsymbol{b}_{i\boldsymbol{k}}\cdot\boldsymbol{\sigma}_{i\boldsymbol{k}}$ with an effective magnetic field $\boldsymbol{b}_{i\boldsymbol{k}} = (\mathrm{Re}\Delta_i', \ -\mathrm{Im}\Delta_i', \ \epsilon_{i\boldsymbol{k}})$, which yields the Bloch equation $d\boldsymbol{\sigma}_{i\boldsymbol{k}}/dt = 2\boldsymbol{b}_{i\boldsymbol{k}}\times\boldsymbol{\sigma}_{i\boldsymbol{k}}$. The self-consistent conditions for the order parameters read $\Delta_1 = |\Delta_1|e^{i\theta_1} = -\frac{U_{\rm R}}{N_0}\sum_{\boldsymbol{k}}(\sigma^x_{1\boldsymbol{k}} - i\sigma^y_{1\boldsymbol{k}})$ and $\Delta_2 = |\Delta_2|e^{i\theta_2} = -\frac{U}{N_0}\sum_{\boldsymbol{k}}(\sigma^x_{2\boldsymbol{k}} - i\sigma^y_{2\boldsymbol{k}})$, where N_0 is the number of sites of each system. Here, the relations $\Delta_i' = \Delta_i - V/N_0\sum_{\boldsymbol{k}}(\sigma^x_{j\boldsymbol{k}} - i\sigma^y_{j\boldsymbol{k}})$ $[(i,j) = (1,2)$ or $(2,1)]$ are satisfied. Then, the Josephson current between the two superfluids is given by the rate of change in the particle number of system 1:

$$\frac{1}{N_0}\frac{dN_1}{dt} = -\frac{4V|\Delta_1||\Delta_2|}{U_{\rm R}|U|}\sin(\theta_2 - \theta_1 + \delta), \tag{3.50}$$

where $\delta = \tan^{-1}(-\gamma/2U_{\rm R})$ is the phase shift due to the sudden switch-on of the atom loss.

We numerically solve the coupled Bloch equations for $\boldsymbol{\sigma}_{i\boldsymbol{k}}$. We assume that dissipation γ and tunneling V are turned on at $t = 0$ for the BCS ground state. The numerical results for weak dissipation are shown in Fig. 3.5(a1)-(d1). In Figs. 3.5(a1) and (b1), the dynamics of two superfluids almost synchronize with each other because the time scale of particle loss is comparable with the inverse tunneling rate. In the pseudospin picture, the dynamics of particle numbers shown in

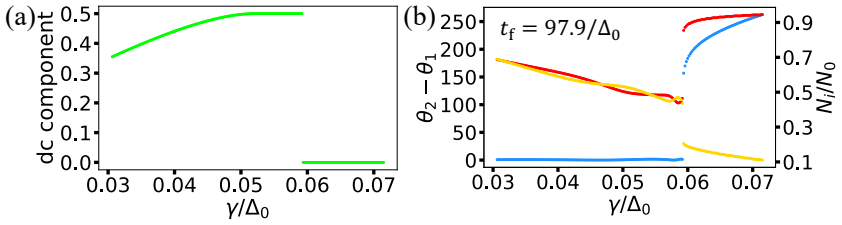

Figure 3.6: (a) DC component of the Josephson oscillation defined by $(\max_{0\le t\le t_f}\{\sin(\theta_2(t)-\theta_1(t)+\delta)\} + \min_{0\le t\le t_f}\{\sin(\theta_2(t)-\theta_1(t)+\delta)\})/2$ with $t_f = 97.9/\Delta_0$. (b) Phase difference between the two systems (blue) and particle numbers of system 1 (red) and system 2 (yellow) after a sufficiently long time ($t_f = 97.9/\Delta_0$). The parameters used are $U_R = 3.06\Delta_0$, $V = 0.02\Delta_0$, and $W = 5.11\Delta_0$.

Fig. 3.5(c1) can be interpreted as the nutation of pseudospins. Importantly, we see that, although the particle number of the system decreases in time, the corresponding amplitude of the order parameter stays almost constant. This implies that the condensate fraction against the total particle number becomes larger than that of the initial state. As inferred from Fig. 3.5(d1), the Josephson current oscillates around its dc component. Such behavior is reminiscent of Shapiro steps in a Josephson junction under irradiation of a microwave [199]; however, in the present case, the Josephson current oscillate *spontaneously without any external field*. Moreover, from Fig. 3.5(d1), the frequency of the oscillation of the phase difference between the two systems is close to that of the relative-phase mode known as the Leggett mode [148, 184] whose dispersion relation is given by $\omega_L = 2\sqrt{(\lambda_{12}+\lambda_{21})|\Delta_1||\Delta_2|/\det\lambda}$, where $\lambda_{11} = \lambda_{22} = U_R/W$, $\lambda_{12} = \lambda_{21} = V/W$ and $\det\lambda = \lambda_{11}\lambda_{22} - \lambda_{12}\lambda_{21}$. We note that ω_L includes the effect of loss through the order parameters. The Leggett mode with frequency ω_L has been discussed in the context of a collective mode in a multiband superconductor irradiated by light [184]. The agreement between the frequencies of the relative-phase modes in very different situations can be understood as follows. When dissipation is weak, the time evolution of an order parameter is given by $\Delta_i(t) = \exp(-2i\int_0^t dt\mu_{i\mathrm{eff}}(t))|\Delta_i(t)|$ with an effective chemical potentials $\mu_{i\mathrm{eff}}$. Then, by performing a global gauge transformation from $c_{i\boldsymbol{k}\sigma}$ to $c_{i\boldsymbol{k}\sigma}\exp(i\int_0^t\sum_i\mu_{i\mathrm{eff}}dt/2)$, we can linearize the Bloch equation with respect to the relative phase difference between Δ_i's by following Ref. [184].

3.5.2 Nonequilibrium dynamical phase transition

In the presence of strong dissipation, the order parameter of system 2 oscillates faster than that of system 1 [see Fig. 3.5(a2), (b2)] and the phase difference monotonically increases in time [see Fig. 3.5(d2)]. This is because the dissipation rate larger than the tunneling rate makes system 1 fail to follow the decay of system 2, resulting in the dynamics similar to that of a single superfluid shown in Fig. 3.2. In particular, the chirped phase rotation of the superfluid order parameter of system 2 can be detected from the Josephson current [Fig. 3.5(d2)]. As the superfluidity of system 2 is suppressed, the Josephson current also decays, and the particle number of system 1 settles to a constant after some transient time [see Fig. 3.5(c2)]. The latter behavior is attributed to QZE [11, 13, 40, 41, 128, 140], which states that strong dissipation prevents tunneling and inhibits loss in system 1. In fact, an effective decay rate of system 1 is given by $\gamma_{\mathrm{eff}} \equiv |V_{\mathrm{eff}}|^2/\gamma$ with an effective tunneling rate $V_{\mathrm{eff}} = V\Delta_2/U_R$ from Eq. (3.49), leading to suppression of decay $\gamma_{\mathrm{eff}} \to 0$ for $|\Delta_2|^2/\gamma \to 0$.

The two dynamically distinct regimes of superfluid behaviors suggest the existence of dynamical phases of matter [186, 187] in dissipative superfluids. The qualitative change in the superfluid behaviors with respect to the dissipation strength highlights a dynamical phase transition characterized by the vanishing dc Josephson current [Fig. 3.6(a)], where the dc component of the Josephson oscillation is defined by $(\max_{0\le t\le t_f}\{\sin(\theta_2(t)-\theta_1(t)+\delta)\} + \min_{0\le t\le t_f}\{\sin(\theta_2(t)-\theta_1(t)+\delta)\})/2$ [see Eq. (3.50)] after a sufficiently long time evolution with $t_f = 97.9/\Delta_0$. We emphasize that the dynamical phase transition in dissipative superfluids is essentially distinct from the phase transition between ground states in a NH BCS superfluid [128]. The former is caused by a change in particle number in the long-time dynamics, whereas the latter is caused by an exceptional point of a NH BCS Hamiltonian, which is relevant to the short-time dynamics during which the number

of particles does not change [200]. From Fig. 3.6(b), we see that the phase difference $\theta_2 - \theta_1$ starts to increase monotonically at the critical point and that the difference in particle number $(N_2 - N_1)/N_0$ becomes much larger. The behavior of the phase difference is reminiscent of the localization-diffusion transition of a quantum-mechanical particle moving in a washboard potential in the presence of frictional force [201–203]. However, the origin of the transition shown in Fig. 3.6 is essentially different from frictional force, since it cannot change the particle number. Moreover, as the steady state is a vacuum due to the particle loss, the dynamical phase transition is observed only in the transient dynamics, and thus distinct from steady-state transitions.

Finally, we see that the dynamical phase transition in Fig. 3.6 is triggered by the competition between the Josephson coupling and particle loss, by considering a simplified model for Josephson junctions. We consider two fermionic superfuids coupled via a Josephson junction, where two-body loss is introduced to one of them, as shown in Fig. 3.1(b). The Josephson current flowing between the two systems is given by

$$I = \frac{1}{N_0}\frac{dN_1}{dt} = -I_0 \sin(\Delta\theta), \tag{3.51}$$

where, from Eq. (3.50), $\Delta\theta = \theta_2 - \theta_1$, $I_0 = 4V|\Delta_1||\Delta_2|/U_{\mathrm{R}}|U|$, and we have neglected the phase shift δ because $\delta \ll \Delta\theta$. Taking into account the particle loss in Eq. (3.27), we obtain the rate of change in the particle number of system 1 and that of system 2 as

$$\frac{1}{N_0}\frac{dN_1}{dt} = -I_0 \sin(\Delta\theta), \tag{3.52}$$

$$\frac{1}{N_0}\frac{dN_2}{dt} = I_0 \sin(\Delta\theta) - \frac{2\gamma|\Delta_2|^2}{|U|^2}. \tag{3.53}$$

We assume that the time evolution of the phase difference $\Delta\theta$ is given by the effective chemical-potential difference $\Delta\mu_{\mathrm{eff}}$ between the two systems as

$$\frac{d\Delta\theta}{dt} = -2\Delta\mu_{\mathrm{eff}} = -\frac{W}{N_0}(N_2 - N_1), \tag{3.54}$$

where W is a bandwidth and we assume a constant density of states for simplicity (we can also understand this equation from the phenomenological time-dependent Ginzburg-Landau (GL) theory, which is explained in the appendix for this chapter). We obtain the equation of motion for $\Delta\theta$ by using Eqs. (3.52), (3.53), and (3.54) as

$$\frac{d^2\Delta\theta}{dt^2} = -2WI_0 \sin(\Delta\theta) + \frac{2\gamma W|\Delta_2|^2}{|U|^2}. \tag{3.55}$$

This system is regarded as a Josephson junction with shunt resistance $R = +\infty$, capacitance $C = 1/2W$ and an external force $F = \gamma|\Delta_2|^2/|U|^2$, which is described as

$$C\frac{d^2\Delta\theta}{dt^2} + \frac{1}{R}\frac{d\Delta\theta}{dt} + I_0 \sin(\Delta\theta) = F. \tag{3.56}$$

That is, the time evolution of $\Delta\theta$ is equivalent to that of a particle moving in a washboard potential

$$V_{\mathrm{wash}} = -2WI_0 \cos(\Delta\theta) - \frac{2\gamma W|\Delta_2|^2\Delta\theta}{|U|^2}. \tag{3.57}$$

The condition for the extremum of V_{wash} is given by $dV_{\mathrm{wash}}/d\Delta\theta = 0$, giving

$$\sin(\Delta\theta) = \frac{\gamma|\Delta_2|^2}{I_0|U|^2}. \tag{3.58}$$

The solution to this equation does not exist for $\gamma|\Delta_2|^2/I_0|U|^2 > 1$ and the time evolution of $\Delta\theta$ becomes unstable. If we assume $|\Delta_1| \simeq |\Delta_2|$ when the time evolution is sufficiently slow, we obtain the critical strength of the atom loss as

$$\gamma_c \simeq 4V, \tag{3.59}$$

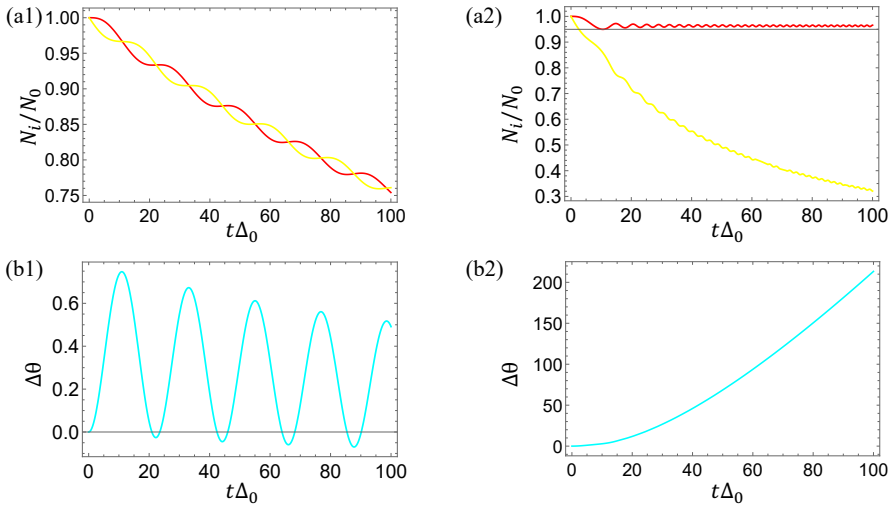

Figure 3.7: Numerical solution of N_1/N_0 (red), N_2/N_0 (yellow), and $\Delta\theta$ (light blue) in Eqs. (3.60), (3.61), and (3.62) with $W = 5.11\Delta_0$ and $I_0 = 0.009\Delta_0$. The loss rate κ_2 is set to $\kappa_2 = 0.006\Delta_0$ in (a1) and (b1), and $\kappa_2 = 0.02\Delta_0$ in (a2) and (b2).

which is of the same order of magnitude as that in Fig. 3.6 ($\gamma_c \simeq 3V$). Thus, the system exhibits a dynamical phase transition from the state in which $\Delta\theta$ oscillates around an extremum of $V_{\rm wash}$ for $\gamma < \gamma_c$ to the state in which $\Delta\theta$ slips down the washboard potential for $\gamma > \gamma_c$. Thus, the dynamical phase transition caused by the particle loss is the one between a trapped state and a running state. We note that the particle loss γ acts as an external force F rather than friction R in Eq. (3.56). The loss-induced dynamical phase transition occurs spontaneously without any external fields, and has an essentially different origin from the localization-delocalization transition induced by friction R [201–203].

These features are also obtained from a phenomenological introduction of two-body loss [11, 40], under which the rate of change in the particle number of system 1 and that of system 2 are given by

$$\frac{1}{N_0}\frac{dN_1}{dt} = -I_0 \sin(\Delta\theta), \tag{3.60}$$

$$\frac{1}{N_0}\frac{dN_2}{dt} = I_0 \sin(\Delta\theta) - \kappa_2 \left(\frac{N_2}{N_0}\right)^2, \tag{3.61}$$

where κ_2 is the two-body loss rate. By using Eqs. (3.54), (3.60), and (3.61), we obtain the equation of motion for $\Delta\theta$ as

$$\frac{d^2\Delta\theta}{dt^2} = -2WI_0 \sin(\Delta\theta) + W\kappa_2 \left(\frac{N_2}{N_0}\right)^2. \tag{3.62}$$

This system is regarded as a Josephson junction with resistance $R = +\infty$, capacitance $C = 1/2W$ and an external force $F = \frac{\kappa_2}{2}\left(\frac{N_2}{N_0}\right)^2$. As the system has the washboard potential

$$V_{\rm wash} = -2WI_0 \cos(\Delta\theta) - W\kappa_2 \left(\frac{N_2}{N_0}\right)^2 \Delta\theta, \tag{3.63}$$

the condition for the extremal of $V_{\rm wash}$ is given by

$$\sin(\Delta\theta) = \frac{\kappa_2}{2I_0}\left(\frac{N_2}{N_0}\right)^2. \tag{3.64}$$

If we assume that the variation of the parameters is sufficiently slow and approximate them as constant, the critical strength of the loss rate where the solution of $\Delta\theta$ becomes unstable is given

by

$$\kappa_{2c} \simeq 2I_0. \tag{3.65}$$

We can numerically solve Eq. (3.60), (3.61), and (3.62), and the results are shown in Fig. 3.7. We see that the results shown in Fig. 3.7(a1) and (b1) [Fig. 3.7(a2) and (b2)] are qualitatively the same as those in Fig. 3.5(c1) and (d1) [Fig. 3.5(c2) and (d2)], respectively.

3.6 Summary of this chapter

We have investigated the loss-quench dynamics of fermionic superfluids, and have demonstrated that the dynamics exhibits amplitude and phase modes with chirped oscillations, the latter of which is a salient feature of a dissipative superfluid. To observe the chirped phase rotation, we have proposed a Josephson junction comprised of dissipative and nondissipative superfluids. We have shown that the relative-phase Leggett mode can be detected from the Josephson current for weak dissipation. Remarkably, when dissipation becomes strong, the superfluids exhibit the unique nonequilibrium phase transition triggered by particle loss. Our prediction can be tested with ultracold atomic systems of ^{6}Li [194, 196], for example, by introducing dissipation using photoassociation processes [42, 92]. It is of interest to explore how the dimensionality or confinement by a trap potential affects the dynamics and associated collective modes [161–164].

3.7 Appendix for this chapter

Difficulties in the time-dependent Ginzburg-Landau theory

The time-evolution equation of the phase [Eq. (3.54)] can be understood as a consequence of the gauge transformation ($\Delta_i(t) = \exp(-2i\int_0^t dt\mu_{i\mathrm{eff}}(t))|\Delta_i(t)|$), which reflects the conjugate nature of the particle number and the phase. From a more phenomenological point of view, Eq. (3.51) can be understood using the time-dependent GL theory. Here we note that, strictly speaking, the GL theory cannot be applied to zero-temperature superfluids considered in our study, since the Taylor expansion of the free energy requires that the system should be close to the transition temperature. In nonequilibrium situations, the time-dependent GL theory cannot be applied to gapped superfluids and nonadiabatic regimes, since the time scale of the order-parameter dynamics becomes shorter than the lifetime of quasiparticles and quasiparticle contributions cannot be neglected [154, 178]. Moreover, for the application of the time-dependent GL theory, it is required that the deviation from equilibrium is sufficiently small, which cannot be satisfied in our dissipative superfluids which are driven far from equilibrium. However, we assume below that the GL theory could be phenomenologically used to investigate the dynamics of the dissipative superfluids. We start from the phenomenological GL equation of the superfluid condensate, which is expanded in a series of the order parameter

$$-\Gamma\left(\frac{\partial\Delta}{\partial t} + \frac{2ie\varphi}{\hbar}\Delta\right) = a\Delta + b|\Delta|^2\Delta, \tag{3.66}$$

where Γ is a positive constant, φ is the scalar potential, e is the charge, and we have assumed that the order parameter is spatially uniform. Here, we have introduced complex-valued coefficients a and b, which might describe the effect of the atom loss. However, we remark on the validity of this treatment below. In our study, the scalar potential does not exist. Instead, we introduce an effective chemical potential μ_{eff} that is determined from the total particle number of the system as follows:

$$-\Gamma\left(\frac{\partial\Delta}{\partial t} + 2i\mu_{\mathrm{eff}}\Delta\right) = a\Delta + b|\Delta|^2\Delta. \tag{3.67}$$

By rewriting the equation in terms of the phase θ and the amplitude $|\Delta|$ of the order parameter (the latter is proportional to the square root of the superfluid density), we obtain the equation of motion for the phase as

$$\frac{\partial\theta}{\partial t} = -2\mu_{\mathrm{eff}} - \frac{\mathrm{Im}(a) + \mathrm{Im}(b)|\Delta|^2}{\Gamma}. \tag{3.68}$$

For two superfluids connected via a Josephson junction, we similarly obtain

$$\frac{\partial(\theta_2-\theta_1)}{\partial t}=-2(\mu_{2\mathrm{eff}}-\mu_{1\mathrm{eff}})-\frac{\mathrm{Im}(a_2)+\mathrm{Im}(b_2)|\Delta_2|^2}{\Gamma_2}, \tag{3.69}$$

where the subscript 1 and 2 label the two superfluids, and we have introduced the effect of loss to superfluid 2. If the coefficients a and b are real, we arrive at Eq. (3.54): $\partial\Delta\theta/\partial t=-2\Delta\mu_{\mathrm{eff}}$. We note, however, that Eqs. (3.52) and (3.53) cannot be obtained from the GL theory, since N_1 and N_2 are the total particle numbers of the two superfluids, which are not directly related to the amplitude of the order parameter for dissipative superfluids. In the case of complex coefficients a and b, one might at first sight think that the effect of loss can be described by regarding the second term in Eq. (3.69) as an effective change in the chemical potential, which reads $\Delta\mu\simeq W(N-N_0)/N_0\propto|\Delta|^2-|\Delta_0|^2$. However, this result of the phenomenological treatment of the time-dependent GL theory has a serious problem. To see this, let us differentiate this equation with respect to time as $dN/dt\propto|\Delta|d|\Delta|/dt$. As the amplitude of the order parameter oscillates as shown in Fig. 3.2(a), the equation $dN/dt\propto|\Delta|d|\Delta|/dt$ indicates that the total particle number of the system can increase since the oscillating part $d|\Delta|/dt$ can take a positive value. Such an increase of the particle number is unphysical since our system has no particle gain. As the correct equation obtained from the microscopic theory is $dN/dt\propto-|\Delta|^2$ [see Eq. (3.27)], which indicates that the total particle number of the system monotonically decreases, Eq. (3.69) does not correctly describe the dynamics associated with the loss in the total particle number. Thus, it is highly nontrivial to consistently describe the dynamic evolution of the order parameter, collective excitations, and the dynamical phase transition caused by the particle loss in dissipative fermionic superfluids on the basis of the phenomenological GL theory.

If we wish to derive the time-dependent GL equation from the formalism based on CTC path integrals, we should start from a generating functional like Eq. (3.3), and introduce the order parameter by performing the Hubbard-Stratonovich transformation. Then, by integrating out the fermionic degrees of freedom, we arrive at the action with respect to the order parameter. By expanding the exact action $S(\Delta,\Delta^*)$ around its extremal value $S(\Delta_0,\Delta_0^*)$, where Δ_0 is usually the equilibrium value that satisfies the BCS gap equation, the time-dependent GL equation is obtained from a saddle-point equation $\partial S(\Delta,\Delta^*)/\partial\Delta^*(r,t)=0$ [204]. However, we have to pay careful attention to the condition that is assumed in the standard derivation: the deviation of the order parameter Δ around its extremal value Δ_0 should be small enough for the Taylor expansion to be justified. We also note that the standard derivation assumes that the total particle number of the system does not change. In contrast, as the particle number significantly changes in our system, the phase of the order parameter rotates and largely deviates from the stationary value as shown in Fig. 3.2(b). Thus, a time-dependent GL theory that fully incorporates the change in particle number needs highly nontrivial consideration, which deserves further study.

Chapter 4

Rectification in open quantum systems

4.1 Introduction

Nonreciprocal phenomena, which have been a long-standing problem in condensed matter physics and nonequilibrium statistical mechanics, play a vital role in a variety of areas, including solid-state physics [205–211], photonics [212–216], acoustics [217–222], and active matter [223–226]. While p-n junctions are nonreciprocal devices of commercial success, there is significant interest in exploring alternative mechanisms, and recent discoveries have shed light on generating nonreciprocal flows without any temperature biases [226–231]. While dissipation has been recognized as a key ingredient to control transport properties, Onsager's reciprocal theorem [232, 233] prohibits rectification by equilibrium baths and thus it is of central importance to introduce *nonequilibrium* baths.

In open quantum systems, one common way to introduce rectification is to couple a system with two different baths at boundaries and use temperature gradients as exemplified by thermal diodes [234–240]. Indeed, many of the previous studies have focused on inhomogeneous setups such as by introducing boundary driving [241–253]. On the other hand, experimental advances in controlling dissipation have allowed one to study nonequilibrium and NH phenomena in trapped ions [254, 255], photonics [256, 257], ultracold atoms [31, 32, 36, 37, 42, 43, 92], and exciton-polariton systems [258–263]. These remarkable developments have offered new opportunities for exploring intriguing phenomena unique to open quantum systems in *homogeneous* setups in contrast to boundary-driven systems [264]. Despite these experimental advances, rectification induced by *homogeneous* dissipation of nonequilibrium baths has scarcely been explored. To our knowledge, there are so far only a few studies in this direction, where nonreciprocal photon transmissions [265–267] and rectified heat currents in spin chains [97] are discussed. Thus, it is still unclear how translationally invariant homogeneous dissipation of nonequilibrium baths can be harnessed to realize unidirectional fermionic transports.

In this chapter, we propose minimal setups to obtain a unidirectional particle transport in NESSs of 1D open fermionic systems, where a nonequilibrium bath is uniformly coupled to the system and gives rise to homogeneous dissipation (see Fig. 4.1) [268]. We first consider a nonreciprocal Lindblad operator, which is translationally invariant and conserves the particle number of the system, and elucidate a general condition to acquire a nonreciprocal particle transport in NESSs. We numerically calculate the current by considering a specific dissipator that can be realized in ultracold atoms [5, 94]. Then, we demonstrate that a reciprocal Lindblad operator can also induce unidirectional particle transport in NESSs provided that the inversion symmetry and the time-reversal symmetry of the Hamiltonian are broken. We consider spin-dependent dephasing as a reciprocal Lindblad operator and evaluate the current by analytical and numerical methods in the presence of the Rashba spin-orbit coupling and the Zeeman magnetic field [269]. Our results should be tested by using ultracold atoms or semiconductor quantum dots, where the master-equation description can be used [270].

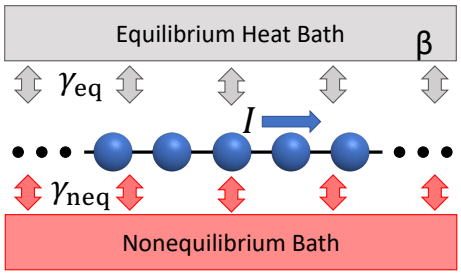

Figure 4.1: Schematic illustration of our setup. Fermions are trapped in a 1D lattice and uniformly coupled to a nonequilibrium bath, which gives rise to translationally invariant dissipation. An equilibrium heat bath with the inverse temperature β is also coupled to the system to ensure that the system reaches to the Gibbs state in the absence of nonequilibrium driving. The coupling strength to each bath is given by $\gamma_{\rm eq}$ and $\gamma_{\rm neq} = 1 - \gamma_{\rm eq}$, respectively. Unidirectional current I can arise in NESSs only when the system is driven out of equilibrium.

4.2 Setup

We consider a 1D lattice model coupled to both an equilibrium heat bath and a nonequilibrium Markovian bath. Such a situation is described by the Lindblad master equation

$$\partial_t \rho = -i[H_0, \rho] + \mathcal{L}_1 \rho, \tag{4.1}$$

$$\mathcal{L}_1 \rho = \epsilon(\gamma_{\rm eq}\mathcal{D}^{\rm eq}(\rho) + \gamma_{\rm neq}\mathcal{D}^{\rm neq}(\rho)), \tag{4.2}$$

with dissipators

$$\mathcal{D}^{(i)}(\rho) = \sum_m \left(L_m^{(i)} \rho L_m^{(i)\dagger} - \frac{1}{2}\left\{ L_m^{(i)\dagger} L_m^{(i)}, \rho \right\} \right), \tag{4.3}$$

where H_0 is a noninteracting Hamiltonian governing the internal dynamics, L_m is a so-called Lindblad operator, $\gamma_{\rm eq}$ and $\gamma_{\rm neq} = 1 - \gamma_{\rm eq}$ denote the relative coupling strengths between two baths, $\gamma_{\rm eq} \in [0, 1]$. We assume that the baths are weakly coupled to the system with a small dimensionless parameter ϵ. Here and henceforth, we set $\hbar = 1$. In AMO systems, the approximations involved in deriving the Lindblad master equation are typically well-satisfied to many orders of magnitudes, and a lot of experimental studies have revealed that these approximations are indeed applicable to various situations [2]. The Lindblad equation can be derived from a fully microscopic Hamiltonian of the system, the system-bath coupling, and the bath after tracing out the bath degrees of freedom with the Born approximation, Markov approximation, and rotating-wave approximation. We remark that the present model is an intrinsically interacting many-body problem because the dissipator cannot in general be expressed in terms of quadratic annihilation/creation operators as detailed below.

When the integrability of the translationally invariant internal system is weakly broken due to the coupling with the reservoir, the time evolution of the system can be described by a tGGE [96–98, 271] (see Sec. 1.3.2), which is justified for times t of the order of $1/\epsilon$ and larger,

$$\rho_{\rm GGE}(t) = \frac{e^{-\sum_q \lambda_q(t) I_q}}{{\rm Tr}[e^{-\sum_q \lambda_q(t) I_q}]}, \tag{4.4}$$

where I_q is an approximately conserved quantity as a consequence of weak driving. Previous studies [96–98] have shown that, by applying a linear-order perturbation theory to the Lindblad equation, one can obtain a differential equation that determines the dynamics of Lagrange parameters

$$\dot{\lambda}_q = -\sum_p (\chi(t)^{-1})_{qp} {\rm tr}\left[I_p \mathcal{L}_1 \rho_{\rm GGE}(t) \right], \tag{4.5}$$

$$\chi_{qp}(t) = \langle I_q I_p \rangle_{\rm GGE} - \langle I_q \rangle_{\rm GGE} \langle I_p \rangle_{\rm GGE}, \tag{4.6}$$

where $\langle \cdots \rangle_{\rm GGE} = {\rm tr}[\cdots \rho_{\rm GGE}(t)]$.

We note that λ_q and $\langle I_q \rangle_{\rm GGE}$ are of the order of ϵ^0 in NESSs, and this fact causes large current responses at arbitrarily weak system-bath coupling as shown below. The validity of these equations has been shown in Ref. [97] by comparing the results obtained from tGGE with those from the exact diagonalization, as also seen from Fig. 4.2 below.

4.3 Rectification in nonequilibrium steady states

In the following, we evaluate the current in NESSs by using tGGE approach with Eqs. (4.4)–(4.6) at arbitrarily weak system-bath coupling. We propose two minimal setups for rectifying the current in NESSs both for nonreciprocal dissipator and reciprocal dissipator.

4.3.1 Rectification by nonreciprocal dissipator

We first consider the 1D tight-binding model

$$H_0 = -J\sum_{j=0}^{L-1}(c_{j+1}^\dagger c_j + \text{H.c.}) = \sum_{-\pi\le k<\pi}\epsilon_k c_k^\dagger c_k, \tag{4.7}$$

where J is the hopping amplitude and $\epsilon_k = -2J\cos(k)$ is the eigenspectrum. We focus on the homogeneous couplings with nonequilibrium baths of infinite system sizes and assume that the system is subject to periodic boundary conditions and periodic dissipation of length L. Here, we note that a realistic system is sometimes affected by a particle source and sink at the edges, but we ignore such effects for simplicity. Then, I_q in Eq. (4.4) is given by the local number operator in the momentum space $I_q = c_q^\dagger c_q$.

The Lindblad operators corresponding to the equilibrium heat bath satisfy $[L_m, H_0] = \zeta_m L_m$ with $\zeta_m = \epsilon_k - \epsilon_l$, $m = (k,l) \in \{-\pi, -\pi + 2\pi/N, ..., \pi - 2\pi/N\}$ to ensure the detailed balance condition $L_{kl}^\dagger = L_{lk}e^{-\beta(\epsilon_k-\epsilon_l)/2}$ [95, 272, 273] in such a way that, without nonequilibrium driving, the system goes to the Gibbs state $\rho_{\rm can} = e^{-\beta H_0}/{\rm tr}(e^{-\beta H_0})$ irrespective of the initial state [see Figs. 4.2 and 4.3(a)]. For the sake of simplicity, we here employ the following Lindblad operator corresponding to the equilibrium heat bath

$$L_{lk}^{\rm eq} = \sqrt{\frac{J}{L}}c_l^\dagger c_k e^{\beta(\epsilon_k-\epsilon_l)/4}. \tag{4.8}$$

To realize current rectification in NESSs, we consider a nonreciprocal Lindblad operator corresponding to the nonequilibrium bath and assume that it is translationally invariant and conserves the particle number of the system. In this case, the Lindblad operator can in general be labeled by a wave number with coefficients Δ_{kq} as

$$L_q^{\rm neq} = \sqrt{\frac{J}{L}}\sum_{-\pi\le k<\pi}\Delta_{kq}c_{k-q}^\dagger c_k. \tag{4.9}$$

Using Eq. (4.5) and Lindblad operators (4.8) and (4.9), we obtain the rate equation that governs the dynamics of the system (see Appendix 4.5 for detailed derivations)

$$\dot\lambda_q = -\frac{\epsilon J}{L}\frac{1+e^{-\lambda_q}}{e^{-\lambda_q}}(\gamma_{\rm eq}F_q^{\rm eq} + \gamma_{\rm neq}F_q^{\rm neq}), \tag{4.10}$$

where

$$F_q^{\rm eq} = \sum_{-\pi\le k<\pi}\frac{e^{\beta(\epsilon_k-\epsilon_q)/2-\lambda_k} - e^{\beta(\epsilon_q-\epsilon_k)/2-\lambda_q}}{1+e^{-\lambda_k}}, \tag{4.11}$$

$$F_q^{\rm neq} = \sum_{-\pi\le k<\pi}\frac{|\Delta_{k,k-q}|^2e^{-\lambda_k} - |\Delta_{q,q-k}|^2e^{-\lambda_q}}{1+e^{-\lambda_k}}. \tag{4.12}$$

We numerically solve the rate equation (4.10) to obtain the dynamics of Lagrange parameters and their steady-state values. We first verify that Lagrange parameters go to the Gibbs state

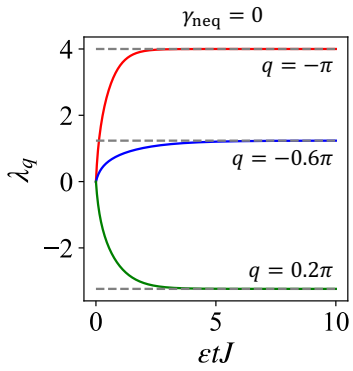

Figure 4.2: Dynamics of Langrange parameters λ_q without nonequilibrium driving obtained from Eq. (4.10), which satisfies the detailed balance condition Eq. (4.8) with $\gamma_{\rm eq} = 1$. The system goes to the Gibbs state (dashed lines) after sufficiently long-time evolution of the order of $1/\epsilon$. The initial state is set to infinite temperature. The parameters are set to $\beta = 2/J$ and $\epsilon = 0.05$.

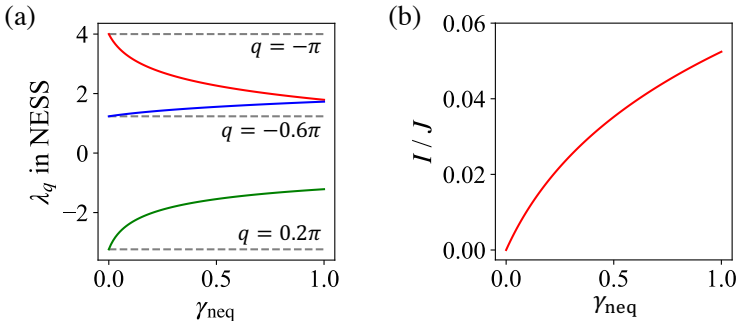

Figure 4.3: (a) Lagrange parameters in NESSs that are driven out of equilibrium as the nonequilibrium dissipation rate $\gamma_{\rm neq}$ is increased. The grey dashed line denotes the Gibbs state. (b) Current I in NESSs as a function of $\gamma_{\rm neq}$ with Lindblad operators (4.8) and (4.15). The parameters are set to $\beta = 2/J$, $\epsilon = 0.05$, $\delta = 1 + i$, and $\delta' = 1 + 0.5i$.

in NESSs if there is no nonequilibrium driving. Figure 4.2 shows the relaxation dynamics of Lagrange parameters, which obey Eq. (4.10) with $\gamma_{\rm eq} = 1$ satisfying the detailed balance condition Eq. (4.8). We see that the system goes to the Gibbs state (grey dashed lines) after sufficiently long time evolution. Then, we calculate steady-state values of Lagrange parameters following the rate equation (4.10). We see that Lagrange parameters depart from the Gibbs state when the system is driven out of equilibrium as the nonequilibrium dissipation rate $\gamma_{\rm neq}$ is increased [see Fig. 4.3(a)].

We now derive a general condition to realize a nonzero nonreciprocal current in NESSs. The current I generally consists of two terms including Hamiltonian current and dissipative current of order ϵ. For such a small ϵ that justifies the tGGE approach, the dissipative current can be ignored, which is consistent with a general description of the current in open quantum systems [274, 275]. We obtain the current from the continuity equation for the density matrix as $I = 2/L \sum_j {\rm Im}\langle c_j^\dagger c_{j-1} (H_0)_{j,j-1} \rangle_{\rm GGE}$ [276, 277], where $(H_0)_{j,j-1}$ denotes the coefficient of $c_j^\dagger c_{j-1}$ in H_0. In the present model, the current, which is the order of ϵ^0, is given by

$$\begin{aligned} I &= \frac{iJ}{L} \sum_{j=0}^{L-1} \langle c_{j+1}^\dagger c_j - {\rm H.c.} \rangle_{\rm GGE} \\ &= \frac{2J}{L} \sum_{-\pi \le q < \pi} \sin(q) \frac{e^{-\lambda_q}}{1 + e^{-\lambda_q}}. \end{aligned} \tag{4.13}$$

Thus, to obtain a nonreciprocal current, the Lagrange parameter λ_q must not be an even function of q. More specifically, as inferred from Eq. (4.12), this condition requires a set of $(k, q) \in [-\pi, \pi)$

to satisfy (at least) one of the following conditions:

$$|\Delta_{q,k+q}| \neq |\Delta_{-q,k-q}|, \quad |\Delta_{k,k-q}| \neq |\Delta_{k,k+q}|. \tag{4.14}$$

We note that the time-reversal symmetry of the internal Hamiltonian is not broken, and an even function λ_q prohibits the rectification of the current even when the dissipative current of order ϵ is included.

Let us apply the condition (4.14) for obtaining the nonreciprocal current to a specific example. We introduce a phenomenological dissipator which is proposed in ultracold atoms in an optical lattice illuminated by Raman laser [5, 94],

$$L_j^{\rm neq} = \sqrt{J}(c_j^\dagger + \delta c_{j+1}^\dagger)(c_j - \delta' c_{j+1}), \tag{4.15}$$

where the subscript j denotes the lattice site. This type of Lindblad operator causes the enhancement or suppression of the atomic phases in two adjacent lattice sites and it is not obvious how such type of superposition of the atomic phases leads to the transport of atoms. We rewrite Eq. (4.15) as

$$L_q^{\rm neq} = \sqrt{\frac{J}{L}} \sum_k (1 + \delta e^{-i(k-q)})(1 - \delta' e^{ik}) c_{k-q}^\dagger c_k, \tag{4.16}$$

where we set the lattice constant $a = 1$. From Eq. (4.14), the Lindblad operator (4.16) should give rise to a nonreciprocal current when either δ or δ' has the imaginary part. This is demonstrated in Fig. 4.3(b), where the current in NESSs is plotted as a function of $\gamma_{\rm neq}$ for $\delta = 1 + i$, $\delta' = 1 + 0.5i$. We see that a large current is built up on a timescale of $1/\epsilon$ as it is driven out of equilibrium though it exactly vanishes in equilibrium ($\gamma_{\rm neq} = 0$).

4.3.2 Rectification by reciprocal dissipator

We next discuss how to realize a nonzero nonreciprocal current by a *reciprocal* Lindblad operator at the expense of the broken inversion and time-reversal symmetries of the internal Hamiltonian. To be concrete, we include the Rashba spin-orbit coupling and the Zeeman magnetic field into the 1D tight-binding model [269]

$$\begin{aligned} H_0 =& -J \sum_{j\sigma} (c_{j+1\sigma}^\dagger c_{j\sigma} + \text{H.c.}) + h \sum_{j=0}^{L-1} (n_{j\uparrow} - n_{j\downarrow}) \\ & - \alpha_z \sum_{j\sigma\sigma'} (c_{j+1\sigma}^\dagger (i\sigma_y)_{\sigma\sigma'} c_{j\sigma'} + \text{H.c.}) \\ & + \alpha_y \sum_{j\sigma\sigma'} (c_{j+1\sigma}^\dagger (i\sigma_z)_{\sigma\sigma'} c_{j\sigma'} + \text{H.c.}) \\ =& \sum_{-\pi \le k < \pi} \sum_{\nu=\pm} \epsilon_{k\nu} \eta_{k\nu}^\dagger \eta_{k\nu}, \end{aligned} \tag{4.17}$$

where h denotes the Zeeman splitting, $\sigma_{y,z}$ are the Pauli matrices, $\alpha_{y,z}$ denote the Rashba hopping with spin flips, $\sigma = \uparrow\downarrow$ and $\nu = \pm$ label spin and band indices, respectively, and the system is subject to periodic boundary conditions and periodic dissipation of length L. The Rashba spin-orbit coupling and the Zeeman magnetic field break the inversion symmetry and the time-reversal symmetry of the Hamiltonian, respectively (see Fig. 4.4). The Hamiltonian is diagonalized with eigenvalues $\epsilon_{k\pm} = -2J\cos(k) \pm \sqrt{(2\alpha_y \sin(k) + h)^2 + 4\alpha_z^2 \sin^2(k)}$ and quasiparticle operators $\eta_{k\pm}$, which are given by a unitary transformation as $c_{k\sigma} = \sum_\nu u_{\sigma\nu}(k)\eta_{k\nu}$ and obey the anticommutation relation $\{\eta_{k\mu}, \eta_{k'\nu}^\dagger\} = \delta_{kk'}\delta_{\mu\nu}$ (see Appendix 4.5 for details). In this case, local conservation laws of few-body observables are given by the number operators of quasiparticles $I_{q\nu} = \eta_{q\nu}^\dagger \eta_{q\nu}$ [cf. Eq. (4.4)].

To identify the Lindblad operators $L_m^{\rm eq}$ that satisfy the detailed balance condition, we consider $\mu(\nu)$ dependence for the energy bands of quasiparticles in addition to Eq. (4.8):

$$L_{l\mu,k\nu}^{\rm eq} = \sqrt{\frac{J}{L}} \eta_{l\mu}^\dagger \eta_{k\nu} e^{\beta(\epsilon_{k\nu} - \epsilon_{l\mu})/4}. \tag{4.18}$$

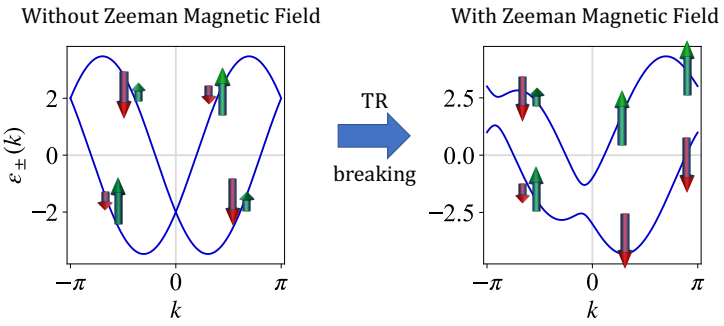

Figure 4.4: Schematic illustration of the energy spectrum of the tight-binding Hamiltonian with Rashba spin-orbit coupling Eq. (4.17). The time-reversal symmetry (TR) of the Hamiltonian is broken when the Zeeman magnetic field is applied to the system.

The relaxation dynamics of Lagrange parameters, which follow the detailed balance condition (4.18), is qualitatively the same as that in Fig. 4.2 except the fact that the degrees of freedom are doubled. As the reciprocal Lindblad operator of the nonequilibrium bath, we consider the spin-dependent dephasing given by

$$L_{j\sigma}^{\mathrm{neq}} = \sqrt{J\gamma_\sigma} c_{j\sigma}^\dagger c_{j\sigma}, \tag{4.19}$$

where j labels the lattice site and the dissipation rates of up and down spins satisfy $\gamma_\uparrow + \gamma_\downarrow = 1$. We calculate the rate equation for the Lagrange parameters (4.5) with Lindblad operators (4.18) and (4.19), which is given by (see Appendix 4.5 for detailed calculations)

$$\dot{\lambda}_{q\nu} = -\frac{\epsilon J}{L} \frac{1+e^{-\lambda_{q\nu}}}{e^{-\lambda_{q\nu}}} (\gamma_{\mathrm{eq}} F_{q\nu}^{\mathrm{eq}} + \gamma_{\mathrm{neq}} F_{q\nu}^{\mathrm{neq}}) \tag{4.20}$$

with the force

$$F_{q\nu}^{\mathrm{eq}} = \sum_{k\mu} \frac{e^{\beta(\epsilon_{k\mu}-\epsilon_{q\nu})/2-\lambda_{k\mu}} - e^{\beta(\epsilon_{q\nu}-\epsilon_{k\mu})/2-\lambda_{q\nu}}}{1+e^{-\lambda_{k\mu}}}, \tag{4.21}$$

$$F_{q\nu}^{\mathrm{neq}} = \sum_{k\mu\sigma} \gamma_\sigma |u_{\sigma\nu}(q)|^2 |u_{\sigma\mu}(k)|^2 \frac{e^{-\lambda_{k\mu}} - e^{-\lambda_{q\nu}}}{1+e^{-\lambda_{k\mu}}}. \tag{4.22}$$

We see from Eq. (4.22) that the system goes to the infinite temperature state, i.e., $\lambda_q = 0$ for all q, without equilibrium heat bath. Nevertheless, the current can rectify if the system couples to both equilibrium and nonequilibrium baths.

When the dynamics is determined from the rate equation (4.20), the current which is the order of ϵ^0 can be obtained from the continuity equation for the density matrix as

$$I = \sum_{\sigma=\uparrow\downarrow} I_\sigma, \tag{4.23}$$

where the spin-resolved current I_σ, is given by (see Appendix 4.5 for details)

$$\begin{aligned} I_\sigma = -\frac{i}{L}\Bigg[& -J\sum_j \langle c_{j+1\sigma}^\dagger c_{j\sigma} - \mathrm{H.c.}\rangle_{\mathrm{GGE}} \\ & - \alpha_z \sum_{j\sigma'} \langle c_{j+1\sigma}^\dagger (i\sigma_y)_{\sigma\sigma'} c_{j\sigma'} - \mathrm{H.c.}\rangle_{\mathrm{GGE}} \\ & + \alpha_y \sum_{j\sigma'} \langle c_{j+1\sigma}^\dagger (i\sigma_z)_{\sigma\sigma'} c_{j\sigma'} - \mathrm{H.c.}\rangle_{\mathrm{GGE}} \Bigg]. \end{aligned} \tag{4.24}$$

We have confirmed that, by numerical calculations using Eq. (4.23), the current I is nonzero only when both the Zeeman magnetic field and the Rashba spin-orbit coupling exist. This can

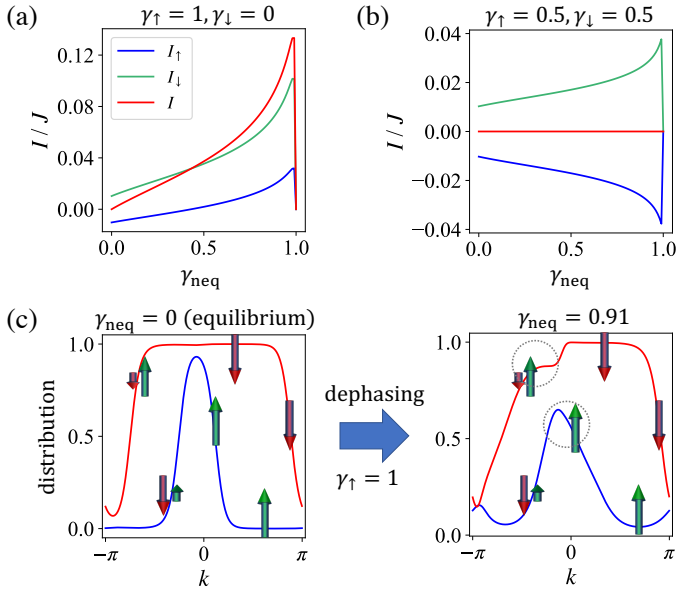

Figure 4.5: (a,b) NESSs current and its spin dependence as a function of $\gamma_{\rm neq}$ in the presence of the Zeeman magnetic field and the Rashba spin-orbit coupling. Dephasing is applied to up spins in (a), and to both up and down spins with equal rates in (b). (c) Distribution of the upper band (blue) and the lower band (red) in NESSs for the equilibrium Gibbs state (left) and the nonequilibrium state where dephasing is applied to up spins (right). Population changes are enhanced near the Fermi surface due to dephasing (marked by grey dotted circles). The parameters are set to $\beta = 2/J$, $\epsilon = 0.05$, $\alpha_y = 1.1J$, $\alpha_z = 0.9J$, and $h = J$. The initial state is at infinite temperature.

be understood as follows. Since dissipation by an equilibrium bath does not rectify the current, one must resort to a nonequilibrium bath for obtaining a nonzero nonreciprocal current. From Eq. (4.22), we see that nonreciprocity of the distribution of Lagrange parameters is determined from the property of the unitary transformation of quasiparticles, namely, the symmetry of the internal Hamiltonian H_0. In fact, due to the structure of the matrix component $u_{\sigma\nu}(k)$ (see Appendix 4.5), dephasing by the nonequilibrium bath in Eq. (4.22) contributes to the Lagrange parameters as an even function with respect to q if either one of the Zeeman magnetic field or the Rashba spin-orbit coupling is absent. Because of this inversion-symmetric distribution of Lagrange parameters, the current does not rectify even if dissipative correction of the order of ϵ is included.

Figures 4.5(a) and (b) show the currents in NESSs in the presence of the Rashba spin-orbit coupling and the Zeeman magnetic field. As shown in Fig. 4.5(a), the dephasing applied to up spins leads to a large nonreciprocal current I in NESSs after a time evolution set by $1/\epsilon$, and it becomes larger as the system is driven out of equilibrium. We recall that the system goes to the Gibbs state for $\gamma_{\rm neq} = 0$ and the infinite temperature state for $\gamma_{\rm neq} = 1$, both of which do not rectify the total current I. When the dephasing is applied to both up and down spins with equal rates [see Fig. 4.5(b)], the total current I vanishes irrespective of the dissipation rate $\gamma_{\rm neq}$, as up spins and down spins contribute to the current in the opposite directions and cancel out. Here, we note that the sharp peak of the current in Fig. 4.5(a) comes from the sudden heating up to the infinite temperature due to the nonequilibrium bath and the peak position can be controlled by the system parameters, e.g., the Zeeman magnetic field h.

Physically, rectification of the current in NESSs can be understood from the change of spin distribution near the Fermi surface. As shown in the left panel of Fig. 4.5(c), the spin distribution forms an effective Fermi surface in the steady state [see also the right panel in Fig. 4.4], reflecting the half-filled initial state. When dephasing is applied to up spins [see the right panel in Fig. 4.5(c)], they heat up and spins near the Fermi surface are most likely to move to the other eigenstates. As a result, the number of particles near the Fermi surface where up spins exist decreases, thereby contributing to the current in the positive direction [see also Eqs. (4.36) and (4.37) in Appendix 4.5]. However, as shown in Fig. 4, the main contribution to the current originates from down spins where dephasing is not applied, because up spins heated up by dephasing move to cancel out the

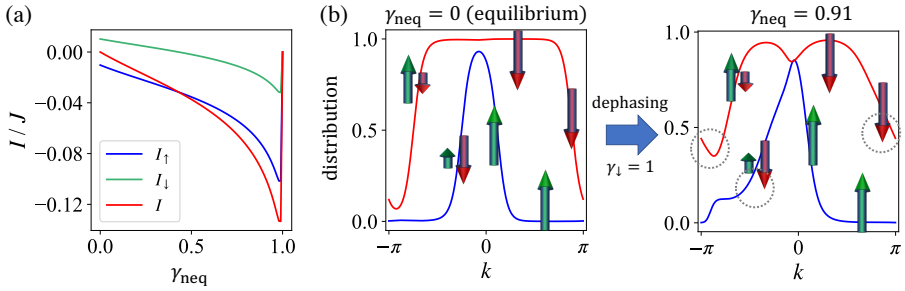

Figure 4.6: (a) Current in NESSs and its spin dependence as a function of $\gamma_{\rm neq}$ in the presence of the Zeeman magnetic field and the Rashba spin-orbit coupling, where dephasing is applied to down spins. (b) Distribution of the upper band (blue) and the lower band (red) in NESSs for the equilibrium Gibbs state (left) and the nonequilibrium state (right) corresponding to (a). Change of population near the Fermi surface where dephasing is applied becomes large (marked by grey dotted circles). The parameters are set to $\beta = 2/J$, $\alpha_y = 1.1J$, $\alpha_z = 0.9J$, and $h = J$ for the initial state at infinite temperature.

contribution to the current.

We also give the numerical results of the current in NESSs when dephasing is applied to down spins. From Fig. 4.6(a), we see that the current rectifies in the opposite direction and the total current I has the reversed value of that in Fig. 4.5(a). As shown in Fig. 4.6(b), the change of population near the Fermi surface where dephasing is applied becomes large (grey dotted circles) compared to the Gibbs state, which contributes to the current in the negative direction [see Eqs. (4.36) and (4.37)].

4.4 Summary of this chapter

We demonstrate arbitrarily weak translationally invariant system-bath coupling can induce large rectification in *homogeneous* open quantum systems, which arises from the interplay between nonequilibrium dissipator and internal Hamiltonian dynamics. This contrasts with conventional setups in, e.g., solids, where there are a less variety of nonreciprocal phenomena in linear response regimes than nonlinear ones due to the need of breaking the time-reversal symmetry. Our finding is distinct from most of the previous studies in open quantum systems that focused on inhomogeneous setups, where a system is coupled to different baths at its boundaries, thus relying on temperature biases or boundary driving. Our open-system formulation is not a response to external electric fields, but allows for featuring direct current generation. In particular, this provides a different framework, for instance, magnetochiral anisotropy, i.e., unidirectional nonlinear resistivity under the magnetic field and electric field for chiral conductors [278–280], or transmissions of an electron current in the presence of a potential barrier [269, 281]. From an experimental perspective, our results can be tested in ultracold atoms; the use of Raman-type spin-orbit coupling is also promissing to break the inversion symmetry. One can also consider semiconductor quantum dots in GaAs as possible experimental candidates [270, 282–284], where the spin relaxation time is very long; spin-resolved dephasing should be realized by using the Zeeman shift.

To summarize, we have proposed minimal setups to realize a nonreciprocal current in open many-body systems. In contrast to conventional approaches in open quantum systems, our finding provides a unique avenue for rectification, namely, the current is neither generated by temperature gradients nor boundary driving, but via the translationally invariant couplings to nonequilibrium baths. We have demonstrated that a nonreciprocal Lindblad operator in general rectifies the current in NESSs. We have also revealed that a reciprocal Lindblad operator can be used to rectify the current when the inversion symmetry and the time-reversal symmetry of the internal Hamiltonian are broken. The present analysis opens up various avenues of possible future research such as current rectification in higher dimensions or changes on transport properties by strong integrability breaking.

4.5 Appendix for this chapter

Detailed calculations of rate equations for Lagrange parameters

We here explain the detailed calculations to obtain the rate equations for Lagrange parameters. For the Hamiltonian in Eq. (4.7), the local conservation laws of few-body observables are given by $I_q = c_q^\dagger c_q$. Thus, χ_{qp} in Eq. (4.6) is nonzero only for the diagonal components, given by

$$\chi_{qq}(t) = \langle c_q^\dagger c_q c_q^\dagger c_q\rangle - \langle c_q^\dagger c_q\rangle^2 = \langle c_q^\dagger c_q\rangle\langle c_q c_q^\dagger\rangle = \frac{e^{-\lambda_q}}{(1+e^{-\lambda_q})^2}, \tag{4.25}$$

where we have omitted the subscript $\langle\cdots\rangle_{\rm GGE}$ and the same applies hereafter. Then, we calculate $\langle \dot{I}_q\rangle = {\rm tr}\,[I_q\mathcal{L}_1\rho_{\rm GGE}]$ on the right hand side of the rate equation (4.5) for the Lindblad operator (4.8) as

$$\begin{aligned}
\langle \dot{I}_q\rangle^{\rm eq} &= \frac{\epsilon\gamma_{\rm eq}}{L}{\rm tr}\left[I_q\sum_{kl}\left(L_{kl}^{\rm eq}\rho_{\rm GGE}L_{kl}^{\rm eq\dagger} - \frac{1}{2}\left\{L_{kl}^{\rm eq\dagger}L_{kl}^{\rm eq},\rho_{\rm GGE}\right\}\right)\right]\\
&= \frac{\epsilon\gamma_{\rm eq}J}{L}{\rm tr}\left[\sum_{kl}e^{\beta(\epsilon_l-\epsilon_k)/2}c_q^\dagger c_q\left(c_k^\dagger c_l\rho_{\rm GGE}c_l^\dagger c_k - \frac{1}{2}\left\{c_l^\dagger c_k c_k^\dagger c_l,\rho_{\rm GGE}\right\}\right)\right]\\
&= \frac{\epsilon\gamma_{\rm eq}J}{L}\sum_{kl}e^{\beta(\epsilon_l-\epsilon_k)/2}\left\langle c_l^\dagger c_k c_q^\dagger c_q c_k^\dagger c_l - \frac{1}{2}(c_q^\dagger c_q c_l^\dagger c_k c_k^\dagger c_l + c_l^\dagger c_k c_k^\dagger c_l c_q^\dagger c_q)\right\rangle\\
&= \frac{\epsilon\gamma_{\rm eq}J}{L}\sum_{k\neq q}\Big[e^{\beta(\epsilon_k-\epsilon_q)/2}\left(\langle c_k^\dagger c_k\rangle\langle c_q c_q^\dagger\rangle\langle c_q^\dagger c_q\rangle + \langle c_k^\dagger c_k\rangle\langle c_q c_q^\dagger\rangle^2\right)\\
&\qquad\qquad - e^{\beta(\epsilon_q-\epsilon_k)/2}\left(\langle c_q^\dagger c_q\rangle^2\langle c_k c_k^\dagger\rangle + \langle c_q^\dagger c_q\rangle\langle c_q c_q^\dagger\rangle\langle c_k c_k^\dagger\rangle\right)\Big]\\
&= \frac{\epsilon\gamma_{\rm eq}J}{L}\sum_k\frac{1}{(1+e^{-\lambda_k})(1+e^{-\lambda_q})}\left(e^{\beta(\epsilon_k-\epsilon_q)/2-\lambda_k} - e^{\beta(\epsilon_q-\epsilon_k)/2-\lambda_q}\right),
\end{aligned} \tag{4.26}$$

where we used Wick's theorem. Here, we note that the terms that do not include q in $\sum_{kl}$ becomes zero because such terms correspond to flows $k\to l$ or $l\to k$ ($k,l\neq q$) and do not contribute to the dynamics of I_q. In the same way, we calculate $\langle \dot{I}_q\rangle$ on the right hand side of the rate equation (4.5) for the Lindblad operator (4.9) as

$$\begin{aligned}
\langle \dot{I}_q\rangle^{\rm neq} &= \frac{\epsilon\gamma_{\rm neq}J}{L}\sum_{q'kk'}\Delta_{kq'}\Delta_{k'q'}^*\left\langle c_{k'}^\dagger c_{k'-q'}c_q^\dagger c_q c_{k-q'}^\dagger c_k - \frac{1}{2}(c_q^\dagger c_q c_{k'}^\dagger c_{k'-q'}c_{k-q'}^\dagger c_k + c_{k'}^\dagger c_{k'-q'}c_{k-q'}^\dagger c_k c_q^\dagger c_q)\right\rangle\\
&= \frac{\epsilon\gamma_{\rm neq}J}{L}\sum_k\left(-|\Delta_{qk}|^2\langle c_q^\dagger c_q\rangle\langle c_{q-k}c_{q-k}^\dagger\rangle + |\Delta_{q+k,k}|^2\langle c_{q+k}^\dagger c_{q+k}\rangle\langle c_q c_q^\dagger\rangle\right)\\
&= \frac{\epsilon\gamma_{\rm neq}J}{L}\sum_k\left[-|\Delta_{q,q-k}|^2\frac{e^{-\lambda_q}}{(1+e^{-\lambda_k})(1+e^{-\lambda_q})} + |\Delta_{k,k-q}|^2\frac{e^{-\lambda_k}}{(1+e^{-\lambda_k})(1+e^{-\lambda_q})}\right].
\end{aligned} \tag{4.27}$$

By using Eqs. (4.25)–(4.27), we obtain the rate equation (4.10) for the Hamiltonian in Eq. (4.5).

For the Hamiltonian in Eq. (4.17), we can calculate the rate equation almost in the same way as discussed above. As the local conservation law is given by $I_{q\nu} = \eta_{q\nu}^\dagger\eta_{q\nu}$ ($\nu=\pm$), $\chi_{q\nu,p\mu}$ in Eq. (4.6) is zero for the off-diagonal components and the diagonal component is calculated as

$$\chi_{q\nu,q\nu}(t) = \langle\eta_{q\nu}^\dagger\eta_{q\nu}\eta_{q\nu}^\dagger\eta_{q\nu}\rangle - \left[\langle\eta_{q\nu}^\dagger\eta_{q\nu}\rangle\right]^2 = \langle\eta_{q\nu}^\dagger\eta_{q\nu}\rangle\langle\eta_{q\nu}\eta_{q\nu}^\dagger\rangle = \frac{e^{-\lambda_{q\nu}}}{(1+e^{-\lambda_{q\nu}})^2}. \tag{4.28}$$

We see from Eq. (4.28) that the degrees of freedom in momentum space are doubled by upper and lower energy bands compared to Eq. (4.25). Then, $\langle \dot{I}_{q\nu}\rangle$ on the right hand side of the rate equation (4.5) for the Lindblad operator (4.18) is calculated by doubling the momentum space as [see also

Eq. (4.26)]

$$\langle \dot{I}_{q\nu}\rangle^{\rm eq} = \frac{\epsilon\gamma_{\rm eq}J}{L}\sum_{kl}\sum_{\mu,\kappa=\pm} e^{\beta(\epsilon_{l\kappa}-\epsilon_{k\mu})/2}\left\langle \eta^\dagger_{l\kappa}\eta_{k\mu}\eta^\dagger_{q\nu}\eta_{q\nu}\eta^\dagger_{k\mu}\eta_{l\kappa} - \frac{1}{2}(\eta^\dagger_{q\nu}\eta_{q\nu}\eta^\dagger_{l\kappa}\eta_{k\mu}\eta^\dagger_{k\mu}\eta_{l\kappa} + \eta^\dagger_{l\kappa}\eta_{k\mu}\eta^\dagger_{k\mu}\eta_{l\kappa}\eta^\dagger_{q\nu}\eta_{q\nu})\right\rangle$$
$$= \frac{\epsilon\gamma_{\rm eq}J}{L}\sum_{k\mu}\frac{1}{(1+e^{-\lambda_{k\mu}})(1+e^{-\lambda_{q\nu}})}\left(e^{\beta(\epsilon_{k\mu}-\epsilon_{q\nu})/2-\lambda_{k\mu}} - e^{\beta(\epsilon_{q\nu}-\epsilon_{k\mu})/2-\lambda_{q\nu}}\right). \tag{4.29}$$

The contribution from the nonequilibrium bath, denoted as $\langle \dot{I}_{q\nu}\rangle^{\rm neq}$, can also be simplified by using the expression of the Lindblad operator (4.19):

$$\langle \dot{I}_{q\nu}\rangle^{\rm neq} = \frac{\epsilon\gamma_{\rm neq}J}{L}\sum_{kk'q',\sigma=\uparrow\downarrow}\gamma_\sigma\Big\langle c^\dagger_{k\sigma}c_{k-q',\sigma}\eta^\dagger_{q\nu}\eta_{q\nu}c^\dagger_{k'-q',\sigma}c_{k'\sigma} - \frac{1}{2}\eta^\dagger_{q\nu}\eta_{q\nu}c^\dagger_{k\sigma}c_{k-q',\sigma}c^\dagger_{k'-q',\sigma}c_{k'\sigma}$$
$$- \frac{1}{2}c^\dagger_{k\sigma}c_{k-q',\sigma}c^\dagger_{k'-q',\sigma}c_{k'\sigma}\eta^\dagger_{q\nu}\eta_{q\nu}\Big\rangle. \tag{4.30}$$

To use Wick's theorem, we substitute the Bogoliubov transformation $c_{k\sigma} = u_{\sigma\nu}(k)\eta_{k\nu}$ in Eq. (4.30) (for the detailed form of $u_{\sigma\nu}(k)$, see the next subsection). We note that, though we have to calculate 2^4 times as many terms as Eq. (4.30) as a result of the substitution, many of which become zero since tGGE ensemble is defined by local conservation quantities. Then, we obtain

$$\langle \dot{I}_{q\nu}\rangle^{\rm neq} = \frac{\epsilon\gamma_{\rm neq}J}{L}\sum_{k}\sum_{\mu=\pm}\sum_{\sigma=\uparrow\downarrow}\gamma_\sigma|u_{\sigma\nu}(q)|^2|u_{\sigma\mu}(k)|^2\frac{e^{-\lambda_{k\mu}}-e^{-\lambda_{q\nu}}}{(1+e^{-\lambda_{k\mu}})(1+e^{-\lambda_{q\nu}})}. \tag{4.31}$$

Finally, Eq. (4.20) follows from Eqs. (4.28)–(4.31).

Detailed derivation of the quasiparticle operators

Here, we explain the detailed derivation of the quasiparticle operators for the Hamiltonian in Eq. (4.17). Equation (4.17) is diagonalized as

$$\begin{aligned} H_0 =& -J\sum_{j\sigma}(c^\dagger_{j+1\sigma}c_{j\sigma} + \text{H.c.}) + h\sum_j(n_{j\uparrow}-n_{j\downarrow}) \\ & - \alpha_z\sum_{j\sigma\sigma'}(c^\dagger_{j+1\sigma}(i\sigma_y)_{\sigma\sigma'}c_{j\sigma'} + \text{H.c.}) + \alpha_y\sum_{j\sigma\sigma'}(c^\dagger_{j+1\sigma}(i\sigma_z)_{\sigma\sigma'}c_{j\sigma'} + \text{H.c.}) \\ =& \sum_k\begin{pmatrix}c^\dagger_{k\uparrow} & c^\dagger_{k\downarrow}\end{pmatrix}\begin{pmatrix}-2J\cos k + 2\alpha_y\sin k + h & 2i\alpha_z\sin k \\ -2i\alpha_z\sin k & -2J\cos k - 2\alpha_y\sin k - h\end{pmatrix}\begin{pmatrix}c_{k\uparrow}\\ c_{k\downarrow}\end{pmatrix} \\ =& \sum_{k,\nu=\pm}\epsilon_{k\nu}\eta^\dagger_{k\nu}\eta_{k\nu}, \end{aligned} \tag{4.32}$$

with eigenvalues

$$\epsilon_{k\pm} = -2J\cos(k) \pm \sqrt{(2\alpha_y\sin(k)+h)^2 + 4\alpha_z^2\sin^2(k)}, \tag{4.33}$$

and quasiparticles, which are given by the unitary transformation,

$$\begin{pmatrix}c_{k\uparrow}\\ c_{k\downarrow}\end{pmatrix} = U(k)\begin{pmatrix}\eta_{k+}\\ \eta_{k-}\end{pmatrix}, \tag{4.34}$$

$$\begin{aligned} U(k) =& \begin{pmatrix}u_{\uparrow+}(k) & u_{\uparrow-}(k)\\ u_{\downarrow+}(k) & u_{\downarrow-}(k)\end{pmatrix} \\ =& \frac{1}{\sqrt{2}}\begin{pmatrix} -i\sqrt{\frac{2\alpha_y\sin k+h}{\sqrt{(2\alpha_y\sin k+h)^2+4\alpha_z^2\sin^2 k}}+1} & -i\sqrt{\frac{-2\alpha_y\sin k-h}{\sqrt{(2\alpha_y\sin k+h)^2+4\alpha_z^2\sin^2 k}}+1} \\ -\frac{\sin(k)}{|\sin(k)|}\sqrt{\frac{-2\alpha_y\sin k-h}{\sqrt{(2\alpha_y\sin k+h)^2+4\alpha_z^2\sin^2 k}}+1} & \frac{\sin(k)}{|\sin(k)|}\sqrt{\frac{2\alpha_y\sin k+h}{\sqrt{(2\alpha_y\sin k+h)^2+4\alpha_z^2\sin^2 k}}+1}\end{pmatrix}. \end{aligned} \tag{4.35}$$

We see from Eq. (4.22) and Eq. (4.35) that the contribution to Lagrange parameters from the nonequilibrium bath is inversion symmetric with respect to q if either one of the Zeeman magnetic field or the Rashba spin-orbit coupling is absent, which does not rectify the current. As a result, we need to break both the inversion symmetry and the time-reversal symmetry of the Hamiltonian to obtain the nonreciprocal current in NESSs. We can also calculate the current (4.24) in the main text by using these quasiparticle operators as

$$\begin{aligned}
I_\uparrow =&\frac{2J}{L}\sum_q \sin(q)\langle c^\dagger_{q\uparrow}c_{q\uparrow}\rangle + \frac{2\alpha_y}{L}\sum_q \cos(q)\langle c^\dagger_{q\uparrow}c_{q\uparrow}\rangle + \frac{2i\alpha_z}{L}\sum_q \cos(q)\langle c^\dagger_{q\uparrow}c_{q\downarrow}\rangle \\
=&\frac{1}{L}\sum_q \left(J\sin(q)+\alpha_y\cos(q)\right)\left\langle \left(\frac{2\alpha_y\sin(q)+h}{\sqrt{(2\alpha_y\sin q+h)^2+4\alpha_z^2\sin^2 q}}+1\right)\eta^\dagger_{q+}\eta_{q+}\right. \\
&\qquad\qquad \left. + \left(\frac{-2\alpha_y\sin(q)-h}{\sqrt{(2\alpha_y\sin q+h)^2+4\alpha_z^2\sin^2 q}}+1\right)\eta^\dagger_{q-}\eta_{q-}\right\rangle \\
&+\frac{2\alpha_z^2}{L}\sum_q \cos(q)\sin(q)\left\langle \frac{\eta^\dagger_{q+}\eta_{q+}-\eta^\dagger_{q-}\eta_{q-}}{\sqrt{(2\alpha_y\sin q+h)^2+4\alpha_z^2\sin^2 q}}\right\rangle
\end{aligned} \tag{4.36}$$

$$\begin{aligned}
I_\downarrow =&\frac{2J}{L}\sum_q \sin(q)\langle c^\dagger_{q\downarrow}c_{q\downarrow}\rangle - \frac{2\alpha_y}{L}\sum_q \cos(q)\langle c^\dagger_{q\downarrow}c_{q\downarrow}\rangle - \frac{2i\alpha_z}{L}\sum_q \cos(q)\langle c^\dagger_{q\downarrow}c_{q\uparrow} \\
=&\frac{1}{L}\sum_q \left(J\sin(q)-\alpha_y\cos(q)\right)\left\langle \left(\frac{-2\alpha_y\sin(q)-h}{\sqrt{(2\alpha_y\sin k+h)^2+4\alpha_z^2\sin^2 k}}+1\right)\eta^\dagger_{k+}\eta_{k+}\right. \\
&\qquad\qquad \left. + \left(\frac{2\alpha_y\sin(q)+h}{\sqrt{(2\alpha_y\sin q+h)^2+4\alpha_z^2\sin^2 q}}+1\right)\eta^\dagger_{q-}\eta_{q-}\right\rangle \\
&+\frac{2\alpha_z^2}{L}\sum_q \cos(q)\sin(q)\left\langle \frac{\eta^\dagger_{q+}\eta_{q+}-\eta^\dagger_{q-}\eta_{q-}}{\sqrt{(2\alpha_y\sin q+h)^2+4\alpha_z^2\sin^2 q}}\right\rangle.
\end{aligned} \tag{4.37}$$

Chapter 5

Universal properties of dissipative Tomonaga-Luttinger liquids

5.1 Introduction

In 1D NH quantum many-body systems, one of the most intriguing phenomena is the dissipation-induced quantum criticality [285–287]. For example, the emergence of exceptional points accompanied by the divergence of the correlation length is reported [15], a quantum critical point in an interacting Bose gas is shifted by measurement backaction [63], and anomalous enhancement of the superfluid correlation occurs as a result of a semicircular renormalization-group flow [64]. These studies have demonstrated that dissipation fundamentally alters the critical properties which have been studied in Hermitian quantum systems. Thus, a natural question arises about the universality of the unusual quantum critical phenomena. However, the universal properties of 1D NH quantum many-body systems are still elusive [288–290].

One-dimensional quantum systems in equilibrium have widely been explored in condensed matter physics. Examples include various spin chains [291] and the Hubbard model [292–295]. They show rich critical phenomena and universality emerging from quantum fluctuations in low-dimensional systems [296–299]. Importantly, 1D strongly correlated systems realize the TL liquid, where the low-energy physics is described by massless collective modes [296–303]. A unified description of 1D quantum critical systems is given by the conformal field theory (CFT) [304–309], where the TL liquid is characterized by the massless boson theory with the central charge $c = 1$. For identifying the universality class of 1D critical systems, a useful fact is that the conformal dimensions are obtained from the energy gap due to a finite-size effect in the spectrum of the critical Hamiltonian. The efficient method to evaluate the conformal dimensions is finite-size scaling [310–319]. However, it is highly nontrivial how to identify the unconventional universality class of NH quantum many-body systems from the finite-size scaling [289].

In this chapter, we demonstrate the universal properties of dissipative TL liquids by calculating correlation functions and performing a finite-size scaling analysis of a NH XXZ spin chain [320]. We first employ an effective field theory with bosonization to elucidate the long-distance properties of dissipative TL liquids, calculating two types of correlation functions called right-state correlation functions and biorthogonal correlation functions according to whether the right or left eigenstate is assigned to the bra vector in the expectation value. We then determine the parameters of the field theory from the exact Bethe ansatz (BA) solution of the NH XXZ chain with the help of the finite-size scaling in CFT. We find that the NH XXZ spin chain belongs to the universality class characterized by the complex-valued TL parameter $\tilde{K}$, which is related to the complex generalization of the $c = 1$ CFT. Finally, we give strong numerical evidence of the universal scaling with $\tilde{K}$ by calculating the energy spectrum and the correlation functions with the DMRG analysis generalized to NH systems. The results show that the model is described by the nonunitary massless Gaussian theory for weak dissipation. On the other hand, when dissipation is increased, both the TL parameter and the velocity of excitations obtained by NH-DMRG start to deviate from those obtained by the BA solution. This deviation indicates a significant finite-size effect and that the ground state can be gapped for strong dissipation. Our results can be tested

with the two-component Bose-Hubbard system of ultracold atoms subject to two-body loss [42].

5.2 Setup

In this section, we first derive the NH XXZ model as an effective model of a two-component Bose-Hubbard system subject to two-body loss. Then, we bosonize the Hamiltonian to analyze the TL-liquid properties, and obtain an effective TL Hamiltonian.

5.2.1 Non-Hermitian XXZ model

Non-Hermitian spin models in the presence of dissipation have been proposed as prototypical dissipative quantum systems relevant to experiments in ultracold atoms [10, 81, 82, 321]. However, NH many-body phenomena in dissipative spin systems are less explored [10, 82, 321], compared with the other dissipative spin models that can be mapped to noninteracting NH systems or to those in the master equation frameworks [81, 322–324]. Here we follow Ref. [82] to derive a NH XXZ spin chain from a dissipative two-component Bose-Hubbard model of ultracold atoms. The unitary dynamics of the system without loss is governed by the two-component Bose-Hubbard model

$$\begin{aligned} H =& -t_h \sum_{j,\sigma=\uparrow,\downarrow} (b^\dagger_{j+1\sigma} b_{j\sigma} + \text{H.c.}) + \sum_j U_{\uparrow\downarrow} n_{j\uparrow} n_{j\downarrow} \\ &+ \sum_{j,\sigma} \frac{U_{\sigma\sigma}}{2} n_{j\sigma}(n_{j\sigma} - 1), \end{aligned} \tag{5.1}$$

where $b_{j\sigma}$ is the annihilation operator of a boson with spin σ at site j, $n_{j\sigma} = b^\dagger_{j\sigma} b_{j\sigma}$, and $t_h > 0$ is the hopping amplitude, which we assume to be the same for every site and spin state. We assume that the on-site interaction is repulsive: $U_{\sigma\sigma'} > 0$. When the system is subject to two-body particle loss, the dynamics is described by the Lindblad master equation [53]

$$\begin{aligned} \frac{d\rho}{dt} &= -i[H, \rho] - \frac{1}{2} \sum_{j\sigma\sigma'} (\{L^\dagger_{j\sigma\sigma'} L_{j\sigma\sigma'}, \rho\} - 2 L_{j\sigma\sigma'} \rho L^\dagger_{j\sigma\sigma'}) \\ &= -i(H_{\text{eff}} \rho - \rho H^\dagger_{\text{eff}}) + \sum_{j\sigma\sigma'} L_{j\sigma\sigma'} \rho L^\dagger_{j\sigma\sigma'}, \end{aligned} \tag{5.2}$$

where ρ is the density matrix of the system, $L_{j\sigma\sigma'} = \sqrt{\gamma_{\sigma\sigma'}} b_{j\sigma} b_{j\sigma'}$ is the Lindblad operator that describes two-body loss with rate $\gamma_{\sigma\sigma'} > 0$ [11, 12, 14, 15, 37, 40–43, 82, 128, 185, 325–327]. In this case, the effective Hamiltonian H_{eff} is given by

$$\begin{aligned} H_{\text{eff}} =& -t_h \sum_{j\sigma} (b^\dagger_{j+1\sigma} b_{j\sigma} + \text{H.c.}) + \sum_j (U_{\uparrow\downarrow} - i\gamma_{\uparrow\downarrow}) n_{j\uparrow} n_{j\downarrow} \\ &+ \sum_{j\sigma} \frac{U_{\sigma\sigma} - i\gamma_{\sigma\sigma}}{2} n_{j\sigma}(n_{j\sigma} - 1), \end{aligned} \tag{5.3}$$

where we have used $H_{\text{eff}} = H - \frac{i}{2} \sum_{j\sigma\sigma'} L^\dagger_{j\sigma\sigma'} L_{j\sigma\sigma'}$ [2] and $\gamma_{\uparrow\downarrow} = \gamma_{\downarrow\uparrow}$. In ultracold atoms, the approximations involved in deriving the Lindblad master equation are typically satisfied to sufficient precision [2]. We note that Eq. (5.3) gives a negative imaginary part of the energy and its eigenstates decay due to atom loss. As discussed below, we consider the longest-surviving state which is given by the largest imaginary part of the energy (smallest absolute value of the negative imaginary part of the energy) in Eq. (5.3).

We invoke unraveling of the dynamics of the density matrix into quantum trajectories [2], each of which obeys the Schrödinger evolution with the effective Hamiltonian H_{eff} interrupted by quantum jumps described by the jump operators $L_{j\sigma\sigma'}$. We consider a strongly correlated regime $U_{\sigma\sigma'} \gg t_h$ and assume that each site is occupied on average by one particle so that a Mott insulating state is realized as an initial state. For simplicity, we assume $U_{\uparrow\uparrow} = U_{\downarrow\downarrow} \equiv U$ and $\gamma_{\uparrow\uparrow} = \gamma_{\downarrow\downarrow} \equiv \gamma$. Then, the

second-order perturbation theory with respect to t_h reduces the effective NH Hamiltonian (5.3) to the NH XXZ model [82, 328]

$$\begin{aligned} H_{\rm eff} =&(J_{\rm eff}^{\perp}+i\Gamma^{\perp})\sum_j (S_{j+1}^x S_j^x + S_{j+1}^y S_j^y) \\ &+ (J_{\rm eff}^{z}+i\Gamma^{z})\sum_j S_{j+1}^z S_j^z \\ =&(J_{\rm eff}^{\perp}+i\Gamma^{\perp})\sum_j (S_{j+1}^x S_j^x + S_{j+1}^y S_j^y + \Delta_\gamma S_{j+1}^z S_j^z), \end{aligned} \tag{5.4}$$

where S_j^α ($\alpha = x, y, z$) are the spin-1/2 operators, $J_{\rm eff}^{\perp} = -4t_h^2 U_{\uparrow\downarrow}/(U_{\uparrow\downarrow}^2+\gamma_{\uparrow\downarrow}^2)$, $\Gamma^{\perp} = -4t_h^2\gamma_{\uparrow\downarrow}/(U_{\uparrow\downarrow}^2+\gamma_{\uparrow\downarrow}^2)$, $J_{\rm eff}^{z} = -J_{\rm eff}^{\perp} - 8t_h^2 U/(U^2+\gamma^2)$, $\Gamma^z = -\Gamma^{\perp} - 8t_h^2\gamma/(U^2+\gamma^2)$, and we have ignored a constant term. We note that, since the energy spectrum of the original effective Hamiltonian (5.3) always has a negative imaginary part, the imaginary part of the energy of the NH XXZ model (5.4) should be negative if we include the ignored constant term. As the constant term does not change the structure of the energy spectrum, the eigenstate with the smallest decay rate of the effective Hamiltonian (5.4) is given by the one with the energy having the largest imaginary part, which corresponds to the smallest absolute value of the negative imaginary part of the energy in the original effective Hamiltonian (5.3). Here, the anisotropy parameter

$$\begin{aligned} \Delta_\gamma \equiv& \frac{J_{\rm eff}^{z}+i\Gamma^{z}}{J_{\rm eff}^{\perp}+i\Gamma^{\perp}} \\ =& 2\frac{U_{\uparrow\downarrow}U+\gamma_{\uparrow\downarrow}\gamma}{U^2+\gamma^2} - 1 + 2i\frac{U_{\uparrow\downarrow}\gamma - U\gamma_{\uparrow\downarrow}}{U^2+\gamma^2}, \end{aligned} \tag{5.5}$$

becomes complex in general, and its imaginary part can be either positive or negative. However, in the case where $U = \gamma \equiv G$ and $U_{\uparrow\downarrow} = \gamma_{\uparrow\downarrow} \equiv G_{\uparrow\downarrow}$, the anisotropy parameter becomes $\Delta_\gamma = 2G_{\uparrow\downarrow}/G - 1 \in \mathbb{R}$. Thus, we have to pay attention to the fact that the anisotropy parameter Δ_γ can be real even in the presence of dissipation.

In the case of $\Delta_\gamma \in \mathbb{R}$, the complex coefficients only appear as an overall constant and the eigenstates are the same as those of the Hermitian XXZ model [82]. As $J_{\rm eff}^{\perp}$ and $\Gamma^{\perp}$ have the same sign ($J_{\rm eff}^{\perp}, \Gamma^{\perp} < 0$), higher energy states (i.e., states with a larger real part of the energy) have smaller decay rates. Thus, after a sufficiently long time, only the high-energy spin states can survive in the Schrödinger evolution under $H_{\rm eff}$. In particular, the system approaches the ground state of the following XXZ model in the long-time limit:

$$H_{\rm eff}^{\rm XXZ} = \frac{J}{2}\sum_j (S_{j+1}^+ S_j^- + S_{j+1}^- S_j^+) + J\Delta_\gamma \sum_j S_{j+1}^z S_j^z, \tag{5.6}$$

where $S_j^{\pm} = S_j^x \pm iS_j^y$ and $J > 0$. Note that $\mathrm{sgn}[J] = -\mathrm{sgn}[J_{\rm eff}^{\perp}]$.

When $\Delta_\gamma \in \mathbb{C}$, the eigenstates of the effective NH Hamiltonian (5.4) are not equivalent to those of the Hermitian Hamiltonian and therefore unusual quantum critical phenomena may take place due to non-Hermiticity. In this case, the longest-surviving state with the largest imaginary part of the eigenenergy of the effective NH Hamiltonian (5.4) is given by the ground state with the lowest real part of the eigenenergy in the NH XXZ model (5.6), if the imaginary part of Δ_γ is sufficiently small so that no level crossing occurs. Therefore, for convenience of calculations, we hereafter focus on the ground state of the NH XXZ model (5.6).

The dynamics under the NH effective Hamiltonian (5.4) is realized when we measure the particle number with quantum-gas microscopy and postselect measurement outcomes in which the particle number is equal to that of the initial state. In Ref. [82], it was shown that the highest energy state in Eq. (5.4) is obtained even in quantum trajectories which involve quantum jumps, if the spin correlation is measured only at the sites that are occupied by single particles. This is a consequence of the spin-charge separation in 1D systems [122], where the spin degrees of freedom are decoupled from holes created by quantum jumps. Thus, by postselecting the occupied sites with quantum-gas microscopy, the spin correlations after a sufficiently long time are expected to be described by those of the ground state of Eq. (5.6). Here, we note that the steady state of the Lindblad master equation (5.2) is the vacuum. However, as the dynamics under the NH effective

Hamiltonian (5.4) is obtained by postselecting special measurement outcomes in which there are no loss events, it realizes a nontrivial steady state, which is different from the state obtained under the Lindblad master equation (5.2) [82]. In this chapter, we analyze the NH XXZ model (5.6) and elucidate how unconventional universal properties of TL liquids emerge in NH spin chains.

5.2.2 Non-Hermitian Tomonaga-Luttinger model

In order to elucidate the long-distance behavior of dissipative TL liquids, we bosonize the NH XXZ Hamiltonian (5.6). We use the standard boson mapping as detailed in Sec. 1.4.2 [122], and take the continuum limit by introducing $S^+(x) = S_j^+/\sqrt{a}$, $S^z(x) = S_j^z/a$, where a is the lattice spacing. After the bosonization procedure, the spin operators in the continuum limit are written as

$$S^z(x) = -\frac{1}{\pi}\nabla\phi(x) + \frac{(-1)^x}{\pi\alpha}\cos(2\phi(x)), \tag{5.7}$$

$$S^+(x) = \frac{e^{-i\theta(x)}}{\sqrt{2\pi\alpha}}\left((-1)^x + \cos(2\phi(x))\right), \tag{5.8}$$

where x is related to the lattice coordinate as $x = aj$ with $a = 1$, α is a cutoff, and the bosonic fields $\phi(x)$ and $\theta(x)$ satisfy the commutation relation $[\phi(x_1), \nabla\theta(x_2)] = i\pi\delta(x_2 - x_1)$. Then, we obtain the NH sine-Gordon Hamiltonian

$$H_{\rm eff}^{\rm sG} = H_{\rm eff}^{\rm TL} - \frac{2\tilde{g}_3}{(2\pi\alpha)^2}\int dx\cos(4\phi(x)), \tag{5.9}$$

where $\tilde{g}_3$ is a complex-valued coefficient that depends on Δ_γ, and

$$H_{\rm eff}^{\rm TL} = \frac{1}{2\pi}\int dx\Big[\tilde{u}\tilde{K}(\nabla\theta(x))^2 + \frac{\tilde{u}}{\tilde{K}}(\nabla\phi(x))^2\Big]. \tag{5.10}$$

Here, $\tilde{K}$ is the complex-valued TL parameter and $\tilde{u}$ is the complex-valued velocity of excitations. We obtain the exact solutions of $\tilde{K}$ and $\tilde{u}$ by using the BA method generalized to NH systems in Sec. 5.4. Here and henceforth, we use the symbol $\tilde{A}$ with a tilde to emphasize that a quantity $\tilde{A}$ is complex. In Sec. 5.3, we consider the situation where the model is in the massless regime, and we analyze the NH TL model $H_{\rm eff}^{\rm TL}$.

5.3 Correlation functions

In NH systems, a right eigenstate, which is defined by $H_{\rm eff}^{\rm TL}|\Psi^R\rangle = E|\Psi^R\rangle$, and a left eigenstate, which is defined by $H_{\rm eff}^{\rm TL\dagger}|\Psi^L\rangle = E^*|\Psi^L\rangle$, are different from each other. Therefore, two types of correlation functions can emerge according to whether the right or left eigenstate is assigned to the bra vector in the expectation value. The first type is defined by ${}_L\langle\cdots\rangle_R \equiv \langle\Psi_0^L|\cdots|\Psi_0^R\rangle/\langle\Psi_0^L|\Psi_0^R\rangle$, where $|\Psi_0^L\rangle$ and $|\Psi_0^R\rangle$ are the left and right ground states (in the sense of the real part of the energy) of $H_{\rm eff}^{\rm TL}$, respectively. This type of correlation functions is calculated through path integrals [128]. The second type is defined by ${}_R\langle\cdots\rangle_R \equiv \langle\Psi_0^R|\cdots|\Psi_0^R\rangle/\langle\Psi_0^R|\Psi_0^R\rangle$, which is calculated by the wave functional approach [63, 329]. Here, we note that the subscripts L and R for the bra and ket vectors stand for the left and right eigenstates of the NH Hamiltonian (5.10), and they are not related to the left and right branches of the TL model. We call the correlation functions ${}_L\langle\cdots\rangle_R$ and ${}_R\langle\cdots\rangle_R$ the biorthogonal correlation function and the right-state correlation function, respectively.

In the postselected sector with no loss events, the dynamics of the system is described by the Schrödinger equation $i\partial_t|\psi\rangle = H_{\rm eff}|\psi\rangle$, which gives the right ground state of the NH XXZ Hamiltonian (6) in the long-time limit. Then, the right-state correlation function is obtained as a standard quantum-mechanical expectation value for the state $|\psi(t\to\infty)\rangle = |\Psi_0^R\rangle$ and corresponds to an experimentally measured physical quantity. On the other hand, the biorthogonal correlation function gives a natural extension of the correlation function that can be calculated with a field-theoretical method in NH systems. We also emphasize that the biorthogonal correlation functions are directly related to the complex extension of the $c = 1$ CFT as detailed in Sec. 5.4. We calculate both correlation functions in this section.

5.3.1 Biorthogonal correlation functions

In this subsection, we discuss the biorthogonal correlation functions. We first calculate the correlation functions of the fields ϕ and θ, and use them to obtain the correlation functions of the spin operators. An important point is that a convergence problem of the Gaussian integration occurs due to the complex nature of $\tilde{u}$ and $\tilde{K}$. Our calculation is based on the path integral formalism [128].

Path-integral formalism and correlation functions of ϕ and θ

We start with the partition function defined by

$$Z = \mathrm{Tr}[e^{-\beta H_{\mathrm{eff}}^{\mathrm{TL}}}] = \int \mathcal{D}\phi\mathcal{D}\Pi e^{-S}, \tag{5.11}$$

$$S = -\int_0^\beta d\tau \int_{-\infty}^{\infty} dx[i\Pi\partial_\tau\phi - H_{\mathrm{eff}}^{\mathrm{TL}}(\phi,\Pi)], \tag{5.12}$$

where $\Pi(x,\tau) = \nabla\theta(x,\tau)/\pi$. We note that, as temperature is not well defined in generic open quantum systems, we only consider the limit of infinite β to elucidate the physics of the ground state, which is defined by the eigenstate that has the lowest real part of the eigenspectrum [63, 128]. Thus, β is a parameter used to formulate a path integral and should not be regarded as the temperature of the system. In the following, we calculate the equal-time correlation function ${}_L\langle[\phi(x_1,0)-\phi(x_2,0)]^2\rangle_R$. It is rewritten by using the Fourier transformation $\phi(x,\tau) = \frac{1}{\beta L}\sum_{\boldsymbol{q}} e^{i(xq-\omega_n\tau)}\phi(\boldsymbol{q})$ as

$$\begin{aligned}{}_L\langle[\phi(x_1,0)-\phi(x_2,0)]^2\rangle_R = &\frac{1}{(\beta L)^2}\sum_{\boldsymbol{q}_1,\boldsymbol{q}_2} \\ &\times\left[{}_L\langle\phi(\boldsymbol{q}_1)\phi(\boldsymbol{q}_2)\rangle_R(e^{ik_1x_1}-e^{ik_1x_2})(e^{ik_2x_1}-e^{ik_2x_2})\right],\end{aligned} \tag{5.13}$$

where $\boldsymbol{q} = (k,\omega_n/\tilde{u})$, $\omega_n = 2\pi n/\beta$ is the Matsubara frequency of bosons, and L is the length of the lattice. The action is calculated as

$$\begin{aligned}S =& \int_0^\beta d\tau\int_{-\infty}^{\infty} dx\Bigg[-i\frac{1}{\pi}\nabla\theta(x,\tau)\partial_\tau\phi(x,\tau) \\ &+\frac{1}{2\pi}\left(\tilde{u}\tilde{K}(\nabla\theta(x,\tau))^2+\frac{\tilde{u}}{\tilde{K}}(\nabla\phi(x,\tau))^2\right)\Bigg] \\ =&\frac{1}{2\beta L}\sum_{\boldsymbol{q}}(\theta^*(\boldsymbol{q}),\phi^*(\boldsymbol{q}))M\begin{pmatrix}\theta(\boldsymbol{q})\\ \phi(\boldsymbol{q})\end{pmatrix},\end{aligned} \tag{5.14}$$

where the matrix M is given by

$$M = \begin{pmatrix}k^2\frac{\tilde{u}\tilde{K}}{\pi} & \frac{ik\omega_n}{\pi}\\ \frac{ik\omega_n}{\pi} & k^2\frac{\tilde{u}}{\tilde{K}\pi}\end{pmatrix}. \tag{5.15}$$

In the Hermitian case, the Gaussian integration with the action (5.14) always converges. However, in the NH case, the Gaussian integration can be divergent because the velocity $\tilde{u}$ of excitations and the TL parameter $\tilde{K}$ become complex. To ensure the convergence of the Gaussian integration, the Hermitian part of the matrix M should be positive definite, i.e., $\mathrm{Re}(\tilde{u}\tilde{K}) > 0$ and $\mathrm{Re}(\tilde{u}/\tilde{K}) > 0$. These conditions are equivalent to those that ensure the energy spectrum of the NH TL liquids to be bounded from below (see Sec. 5.4.3). Thus, if these conditions are not satisfied, the NH TL liquids become unstable. With these conditions, we can conduct further calculations and obtain

$$\begin{aligned}{}_L\langle\phi(\boldsymbol{q}_1)\phi(\boldsymbol{q}_2)\rangle_R &= \frac{1}{Z_\phi}\int\mathcal{D}\phi e^{-S_\phi}\phi(\boldsymbol{q}_1)\phi(\boldsymbol{q}_2) \\ &= \frac{\pi\tilde{K}\delta_{\boldsymbol{q}_1,-\boldsymbol{q}_2}L\beta}{\frac{\omega_n^2}{\tilde{u}}+\tilde{u}k_1^2},\end{aligned} \tag{5.16}$$

where

$$Z_\phi = \int \mathcal{D}\phi e^{-S_\phi}, \tag{5.17}$$

$$S_\phi = \frac{1}{\beta L}\sum_{\boldsymbol{q}} \frac{1}{2\pi\tilde{K}}\left(\frac{\omega_n^2}{\tilde{u}} + \tilde{u}k^2\right)\phi^*(\boldsymbol{q})\phi(\boldsymbol{q}). \tag{5.18}$$

Then, we arrive at

$$\begin{aligned} {}_L\langle[\phi(x,0)-\phi(0,0)]^2\rangle_R &= \frac{1}{\beta L}\sum_{\boldsymbol{q}} \frac{\pi\tilde{K}}{\frac{\omega_n^2}{\tilde{u}}+\tilde{u}k^2}(2-2\cos kx) \\ &= \frac{\tilde{K}}{2}\log\left(\frac{x^2+\alpha^2}{\alpha^2}\right), \end{aligned} \tag{5.19}$$

where we have introduced a cutoff α and taken the limit $\beta\to\infty$. We note that the limit $\beta\to\infty$ is safely taken under the condition $\mathrm{Re}(\tilde{u}\tilde{K})>0$ and $\mathrm{Re}(\tilde{u}/\tilde{K})>0$. We can apply a similar procedure to ${}_L\langle[\theta(x,0)-\theta(0,0)]^2\rangle_R$ by replacing $\tilde{K}$ with $1/\tilde{K}$, and obtain

$${}_L\langle[\theta(x,0)-\theta(0,0)]^2\rangle_R = \frac{1}{2\tilde{K}}\log\left(\frac{x^2+\alpha^2}{\alpha^2}\right). \tag{5.20}$$

Finally, by using the formula

$$\begin{aligned} &{}_L\Big\langle \exp[i\sum_j (A_j\phi(x_j,0)+B_j\theta(x_j,0))]\Big\rangle_R \\ &= \exp\Big[-\frac{1}{2}{}_L\langle[\sum_j (A_j\phi(x_j,0)+B_j\theta(x_j,0))]^2\rangle_R\Big], \end{aligned} \tag{5.21}$$

and Eqs. (5.19) and (5.20), we arrive at

$${}_L\langle e^{i(2\phi(x,0)-2\phi(0,0))}\rangle_R = \left(\frac{\alpha}{x}\right)^{2\tilde{K}}, \tag{5.22}$$

$${}_L\langle e^{i(2\theta(x,0)-2\theta(0,0))}\rangle_R = \left(\frac{\alpha}{x}\right)^{\frac{2}{\tilde{K}}}. \tag{5.23}$$

We see that the correlation functions of the fields ϕ and θ are characterized by the complex-valued TL parameter $\tilde{K}$. This fact is related to the complex generalization of the $c=1$ CFT, which is discussed in Sec. 5.4.

Correlation function of the spin operators

We here calculate the correlation functions of the spin operators defined in Eqs. (5.7) and (5.8). For the correlation function of S^z, we obtain the free-fermion-like correlation $1/x^2$ and the power law characterized by $\tilde{K}$ by performing the Gaussian integration with Eq. (5.22) as

$$\begin{aligned} {}_L\langle S^z(x,0)S^z(0,0)\rangle_R =& \frac{1}{\pi^2}{}_L\langle\nabla\phi(x,0)\nabla\phi(0,0)\rangle_R \\ &+\frac{(-1)^x}{(2\pi\alpha)^2}{}_L\langle e^{i2(\phi(x,0)-\phi(0,0))}+\text{H.c.}\rangle_R \\ =& -\frac{\tilde{K}}{2\pi^2}\frac{1}{x^2}+\tilde{C}_2(-1)^x\left(\frac{1}{x}\right)^{2\tilde{K}}, \end{aligned} \tag{5.24}$$

where $\tilde{C}_2$ is a complex-valued nonuniversal amplitude. Here, we note that x is defined on the lattice $x=aj$, where we set $a=1$. For the x-y component of the correlation function, we obtain the power law characterized by $1/\tilde{K}$ and the linear combination of $\tilde{K}$ and $1/\tilde{K}$ by using Eqs. (5.22)

and (5.23) as

$$\begin{aligned} {}_L\langle S^+(x,0)S^-(0,0)\rangle_R =& \frac{1}{2\pi\alpha}{}_L\langle e^{-i(\theta(x,0)-\theta(0,0))}[(-1)^x \\ &+ \frac{1}{4}(e^{2i(\phi(x,0)-\phi(0,0))}+\text{H.c.})]\rangle_R \\ =& \tilde{C}_3\left(\frac{1}{x}\right)^{2\tilde{K}+\frac{1}{2\tilde{K}}} + \tilde{C}_4(-1)^x\left(\frac{1}{x}\right)^{\frac{1}{2\tilde{K}}}, \end{aligned} \tag{5.25}$$

where the off-diagonal terms with respect to the fields ϕ and θ such as ${}_L\langle\theta(x,0)\phi(0,0)\rangle_R$ only contribute to the sign, and we have used the fact that ${}_L\langle\exp[i\sum_j(A_j\phi(x_j,0)+B_j\theta(x_j,0))]\rangle_R = 0$ when $\sum_i A_i \neq 0$ or $\sum_i B_i \neq 0$. Here, $\tilde{C}_3$ and $\tilde{C}_4$ are nonuniversal complex-valued amplitudes, which satisfy $\tilde{C}_3 < 0$ in the Hermitian limit. Thus, we see that the power law decay of the biorthogonal correlation functions of the spin operators is universally characterized by the complex-valued TL parameter $\tilde{K}$.

5.3.2 Right-state correlation functions

In this subsection, we study the right-state correlation functions. We first calculate the correlation functions of the fields ϕ and θ, and then obtain the correlation functions of the spin operators by using them. Our calculation is based on the generalization of the harmonic oscillator to NH systems [63, 329].

Ground-state wave function and correlation functions of ϕ and θ

We start with the NH TL Hamiltonian (5.10), which is rewritten as

$$H_{\text{eff}}^{\text{TL}} = \frac{1}{2\pi}\int dx\left[v_J e^{-i\delta_J}(\nabla\theta(x))^2 + v_N e^{-i\delta_N}(\nabla\phi(x))^2\right], \tag{5.26}$$

where $v_J > 0$, $v_N > 0$, and $\delta_J, \delta_N \in \mathbb{R}$.

The case with $\delta_J = 0$ was analyzed in Ref. [63]. Since $e^{i\delta_J}H_{\text{eff}}^{\text{TL}}$ reduces to this case, the energy eigenspectrum and the ground state in the present case can be obtained by a straightforward extension of the results in Ref. [63]. The wave function of the ground state is given by

$$\langle\{\phi_k\}|\Psi_0^R\rangle = \frac{1}{\sqrt{\mathcal{N}}}\exp\left(-\frac{e^{-i(\delta_N-\delta_J)/2}}{K'}\sum_{k>0}k|\phi_k|^2\right), \tag{5.27}$$

where $\mathcal{N}$ is a normalization constant, $K' = \sqrt{v_J/v_N} \in \mathbb{R}$, and $|\{\phi_k\}\rangle$ is an eigenstate of $\phi(x)$ defined by

$$\phi(x)|\{\phi_k\}\rangle = \sqrt{\frac{\pi}{L}}\sum_{k>0}(\phi_k e^{ikx} + \phi_k^* e^{-ikx})|\{\phi_k\}\rangle. \tag{5.28}$$

The field $\theta(x)$ induces the shift of the eigenstate $|\{\phi_k\}\rangle$ as follows:

$$e^{2i\theta(x)}|\{\phi_k\}\rangle = \left|\left\{\phi_k - \frac{2i}{k}\sqrt{\frac{\pi}{L}}e^{-ikx}\right\}\right\rangle. \tag{5.29}$$

The eigenenergies are given by

$$E = v' e^{-i(\delta_N+\delta_J)/2}\sum_{k>0}k(n_k^+ + n_k^- + 1), \tag{5.30}$$

where $v' = \sqrt{v_J v_N}$, and n_k^+ and n_k^- are nonnegative integers. By using the ground-state wave function (5.27), the correlation functions of the fields ϕ and θ are calculated as [63]

$${}_R\langle e^{2i\phi(x)}e^{-2i\phi(0)}\rangle_R = \left(\frac{\alpha}{x}\right)^{2K_\phi}, \tag{5.31}$$

$${}_R\langle e^{2i\theta(x)}e^{-2i\theta(0)}\rangle_R = \left(\frac{\alpha}{x}\right)^{\frac{2}{K_\theta}}, \tag{5.32}$$

where a cutoff α is introduced, and the critical exponents are defined by $K_\phi = K'/\cos((\delta_N-\delta_J)/2)$ and $K_\theta = K'\cos((\delta_N-\delta_J)/2)$.

Here, we have to pay attention to the fact that the wave function (5.27) should be normalizable and the real part of the eigenvalues (5.30) should be bounded from below. For the model in Ref. [63], these conditions are equivalent to each other. However, in our model, these two conditions are inequivalent due to the phase factor $e^{-i\delta_J}$ in the eigenspectrum (5.30). In order that the wave function (5.27) and that of the zero mode can be normalized, δ_N and δ_J should satisfy $-\pi/2 < \delta_N-\delta_J < \pi/2$. For the eigenenergies, in order for the real part of the eigenspectrum including the zero-mode contribution to be bounded from below, δ_N and δ_J should satisfy $-\pi/2 < \delta_N < \pi/2$ and $-\pi/2 < \delta_J < \pi/2$. Further discussions on the condition for realizing NH TL liquids are given in Sec. 5.4.

Importantly, the right-state correlation functions of the NH TL liquid are characterized by the two critical exponents K_ϕ and K_θ, though they coincide in the Hermitian limit [63]. Since we can rewrite the complex-valued TL parameter as $\tilde{K} = K'e^{i(\delta_N-\delta_J)/2}$ by comparing Eqs. (5.10) and (5.26), the two critical exponents $K_\phi = K'/\cos((\delta_N-\delta_J)/2)$ and $K_\theta = K'\cos((\delta_N-\delta_J)/2)$ can be compactly written down as

$$\frac{1}{K_\phi} = \mathrm{Re}\frac{1}{\tilde{K}}, \tag{5.33}$$

$$K_\theta = \mathrm{Re}\tilde{K}. \tag{5.34}$$

We see that the critical exponents for the fields ϕ and θ are related to each other through Eqs. (5.33) and (5.34), and both are defined by the complex-valued TL parameter $\tilde{K}$. Thus, we conclude that all the universal properties of the biorthogonal and right-state correlation functions are encoded in the complex-valued TL parameter $\tilde{K}$, which is related to the NH generalization of the $c = 1$ CFT as discussed in Sec. 5.4.

Correlation functions of the spin operators

We now calculate the correlation functions of the spin operators (5.7) and (5.8). By performing the Gaussian integration and using Eq. (5.31), we obtain the correlation function of S^z as

$$\begin{aligned} {}_R\langle S^z(x)S^z(0)\rangle_R &= \frac{1}{\pi^2}{}_R\langle\nabla\phi(x)\nabla\phi(0)\rangle_R \\ &\quad + \frac{(-1)^x}{(2\pi\alpha)^2}{}_R\langle e^{i2\phi(x)-i2\phi(0)} + \mathrm{H.c.}\rangle_R \\ &= -\frac{K_\phi}{2\pi^2}\frac{1}{x^2} + C_2(-1)^x\left(\frac{1}{x}\right)^{2K_\phi}, \end{aligned} \tag{5.35}$$

where C_2 is a nonuniversal real correlation amplitude. We note that $x = aj$ is defined on the lattice and that we set $a = 1$. We see that the correlation function of S^z has the free-fermion-like correlation $1/x^2$ and anomalous power-law decay characterized by K_ϕ. Next, we go on to calculate the x-y component of the correlation function. The x-y component of the correlation function is rewritten as

$$\begin{aligned} {}_R\langle S^+(x)S^-(0)\rangle_R =& \frac{1}{2\pi\alpha}{}_R\langle e^{-i(\theta(x)-\theta(0))}[(-1)^x \\ &+ \frac{1}{4}(e^{2i(\phi(x)-\phi(0))} + \mathrm{H.c.})]\rangle_R. \end{aligned} \tag{5.36}$$

To proceed further with calculations, we consider the condition in which a general expectation value,

$${}_R\langle e^{-i(\theta(x)-\theta(0))}e^{i(A\phi(x)+B\phi(0))}\rangle_R, \tag{5.37}$$

becomes nonzero. By inserting the completeness condition for $|\{\phi_k\}\rangle$, Eq. (5.37) reads

$$
\begin{aligned}
&{}_R\langle e^{-i(\theta(x)-\theta(0))}e^{i(A\phi(x)+B\phi(0))}\rangle_R \\
=&\frac{1}{\mathcal{N}}\int \mathcal{D}\phi\mathcal{D}\phi^* \exp\Big\{\sum_{k>0}\Big[-\frac{k}{K'}\Big(e^{\frac{i(\delta_N-\delta_J)}{2}}\Big|\phi_k+\frac{i}{k}\sqrt{\frac{\pi}{L}}e^{-ikx}\Big|^2+e^{-\frac{i(\delta_N-\delta_J)}{2}}\Big|\phi_k+\frac{i}{k}\sqrt{\frac{\pi}{L}}\Big|^2\Big) \\
&+i\sqrt{\frac{\pi}{L}}\left(A(\phi'_k e^{ikx}+\phi'^*_k e^{-ikx})+B(\phi'_k+\phi'^*_k)\right)\Big]\Big\} \\
=&\exp\left\{\sum_{k>0}\left[-\frac{1}{K'\cos((\delta_N-\delta_J)/2)}\frac{\pi}{2kL}(2-e^{ikx}-e^{-ikx})-\frac{K'}{\cos((\delta_N-\delta_J)/2)}\frac{\pi}{2kL}((A+B)^2+2AB(\cos(kx)-1))\right.\right. \\
&\left.\left.+\frac{\pi(e^{ikx}-e^{-ikx})}{kL}\left(\frac{Ae^{-i(\delta_N-\delta_J)/2}-Be^{i(\delta_N-\delta_J)/2}}{2\cos((\delta_N-\delta_J)/2)}-A\right)\right]\right\},
\end{aligned}
\tag{5.38}
$$

where $\phi'_k=\phi_k+\frac{i}{k}\sqrt{\frac{\pi}{L}}$. The second term in the exponent in Eq. (5.38) diverges to the negative infinity if $A+B\neq 0$. Thus, the expectation value (5.37) is nonzero only when $A+B=0$. By substituting $(A,\,B)=(\pm 2,\,\mp 2)$ in Eq. (5.37), we obtain

$$
{}_R\langle e^{-i(\theta(x)-\theta(0))}e^{i(\pm 2\phi(x)\mp 2\phi(0))}\rangle_R=\left(\frac{\alpha}{x}\right)^{2K_\phi+\frac{1}{2K_\theta}}. \tag{5.39}
$$

Finally, by using Eqs. (5.32) and (5.39), we arrive at

$$
{}_R\langle S^+(x)S^-(0)\rangle_R=C_3\left(\frac{1}{x}\right)^{2K_\phi+\frac{1}{2K_\theta}}+C_4(-1)^x\left(\frac{1}{x}\right)^{\frac{1}{2K_\theta}}, \tag{5.40}
$$

where $C_3<0$ and C_4 are nonuniversal real correlation amplitudes. We see that the correlation function (5.40) is characterized by the anomalous power-law decay with two critical exponents K_ϕ and K_θ. Here, we emphasize that as the critical exponents K_ϕ and K_θ are written in terms of the real part of $1/\tilde{K}$ and that of $\tilde{K}$, respectively [see Eqs. (5.33) and (5.34)], the universal properties of the right-state spin correlation functions as well as the biorthogonal correlation functions are characterized by the complex-valued TL parameter $\tilde{K}$.

5.4 Exact results

The parameters $\tilde{u}$ and $\tilde{K}$ of the NH TL liquid theory (5.10) can be read off from the low-energy spectrum (in the sense of the real part of the energy) of the original lattice Hamiltonian. In this section, we exactly solve the NH XXZ model (5.6) by using the Bethe ansatz method and obtain the finite-size energy spectrum of the NH XXZ model (5.6), demonstrating that the model is described by the complex generalization of the $c=1$ CFT. We also calculate the complex-valued TL parameter from the exchange coupling J and the anisotropy parameter Δ_γ. Finally, we discuss the stability conditions to realize the NH TL liquids.

5.4.1 Bethe-ansatz solution

We consider the NH XXZ model (5.6) with length L. Here we employ the twisted boundary condition $S^+_{L+1}=e^{i\Phi}S^+_1$ for later convenience. Thanks to the U(1) symmetry of the Hamiltonian, energy eigenstates can be labeled by the number M of down spins. Then, the Bethe equations of the XXZ model are given by [330–332]

$$
e^{ik_jL-i\Phi}=(-1)^{M-1}\prod_{l\neq j}\frac{1+e^{i(k_j+k_l)}+2\Delta_\gamma e^{ik_j}}{1+e^{i(k_j+k_l)}+2\Delta_\gamma e^{ik_l}}, \tag{5.41}
$$

where k_j $(j=1,\cdots,M)$ are quasimomenta and $\Delta_\gamma\in\mathbb{C}$. An energy eigenvalue E_L is calculated from the solution of the Bethe equations as

$$
E_L(\Phi)=-J\sum_{j=1}^{M}(\cos k_j+\Delta_\gamma)+\frac{J\Delta_\gamma}{4}L. \tag{5.42}
$$

We note that the derivation of the Bethe equations (5.41) still holds for complex Δ_γ and therefore the NH XXZ model (5.6) is exactly solvable.

The Bethe equations (5.41) are rewritten as

$$\left(\frac{\sinh\frac{\mu}{2}(\lambda_j+i)}{\sinh\frac{\mu}{2}(\lambda_j-i)}\right)^L = e^{i\Phi}\prod_{l\neq j}\frac{\sinh\frac{\mu}{2}(\lambda_j-\lambda_l+2i)}{\sinh\frac{\mu}{2}(\lambda_j-\lambda_l-2i)}, \tag{5.43}$$

where

$$e^{ik_j} = -\frac{\sinh\frac{\mu}{2}(\lambda_j+i)}{\sinh\frac{\mu}{2}(\lambda_j-i)}, \tag{5.44}$$

and $\mu = \arccos\Delta_\gamma$. By taking the logarithm of Eq. (5.43), we have

$$\begin{aligned} &2L\arctan\left[\frac{\tanh(\mu\lambda_j/2)}{\tan(\mu/2)}\right] \\ =&2\pi I_j + \Phi + \sum_{l=1}^{M} 2\arctan\left[\frac{\tanh\frac{\mu}{2}(\lambda_j-\lambda_l)}{\tan\mu}\right], \end{aligned} \tag{5.45}$$

where we set the quantum numbers

$$I_j = -\frac{M+1}{2} + j \quad (j = 1, \cdots, M) \tag{5.46}$$

to obtain the ground state.

In the infinite-size limit with M/L being fixed, the spin rapidities λ_j $(j = 1, \cdots, M)$ are densely distributed along a path $\mathcal{C}$ in the complex plane (see also other cases of NH integrable models [15, 66, 321, 333]). In this limit, the Bethe equations (5.45) reduce to the following integral equation for the distribution function $\sigma_\infty(\lambda) = \lim_{L\to\infty}\sigma_L(\lambda, 0)$ of spin rapidities [see Eq. (5.77) in Appendix 5.7 for its precise definition]:

$$\sigma_\infty(\lambda) = a_1(\lambda) - \int_{\mathcal{C}} d\lambda' a_2(\lambda-\lambda')\sigma_\infty(\lambda'), \tag{5.47}$$

where

$$a_n(\lambda) \equiv \frac{1}{2\pi}\frac{\mu\sin(n\mu)}{\cosh(\mu\lambda)-\cos(n\mu)}. \tag{5.48}$$

In Fig. 5.1, we show the distribution of spin rapidities obtained from a numerical solution of the Bethe equations (5.45). In the Hermitian limit ($\Delta_\gamma \in \mathbb{R}$) with $M/L = 1/2$, the spin rapidities are distributed from $-\infty$ to $+\infty$ along the real axis. Here, we consider the case in which the path $\mathcal{C}$ can continuously be deformed onto the real axis without crossing the poles of the integrand of Eq. (5.47). Hence, by using the Fourier transformation, we obtain the solution of the integral equation (5.47) for $M/L = 1/2$ and $\Phi = 0$ in the same form of that for the ground state in the Hermitian limit as [332]

$$\sigma_\infty(\lambda) = \frac{1}{4\cosh(\pi\lambda/2)}, \tag{5.49}$$

and the energy density $e_L(\Phi) \equiv E_L(\Phi)/L$ of the ground state is given by

$$\begin{aligned} e_\infty(0) =&\frac{J\Delta_\gamma}{4} - \frac{2\pi J\sin\mu}{\mu}\int_{\mathcal{C}} d\lambda a_1(\lambda)\sigma_\infty(\lambda) \\ =&\frac{J\Delta_\gamma}{4} - \frac{J\sin\mu}{\mu}\int_{-\infty}^{\infty} d\omega \frac{\sinh\left(\frac{\pi}{\mu}-1\right)\omega}{2\cosh\omega\sinh(\pi\omega/\mu)}. \end{aligned} \tag{5.50}$$

The low-energy excitation spectrum is calculated in a similar way. Here we consider a solution with $\Phi = 0$ in the $M = L/2-1$ sector and set the quantum numbers as

$$\begin{aligned} I_j =&\frac{L}{4}, \frac{L}{4}-1, \cdots, \frac{L}{4}-r+1, \frac{L}{4}-r-1, \\ &\cdots, \frac{L}{4}-s+1, \frac{L}{4}-s-1, \cdots, -\frac{L}{4}, \end{aligned} \tag{5.51}$$

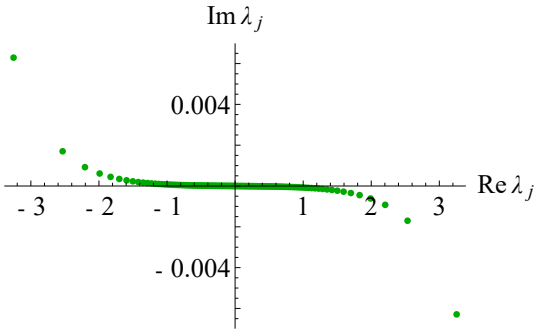

Figure 5.1: Numerical solution of the Bethe equations [Eq. (5.45)] for the ground state of the NH XXZ model with $L = 2M = 250$ and $\Phi = 0$. The model parameter is set to $\Delta_\gamma = 0.8 - 0.3i$. Green dots show spin rapidities λ_j $(j = 1, \cdots, M)$.

where $0 \le r < s \le L/4$. Then, the excitation energy ΔE from the ground state with $M = L/2$ is given by

$$\Delta E = \frac{J\pi \sin\mu}{2\mu}(\sin q_r + \sin q_s), \tag{5.52}$$

where $q_r = 2\pi r/L$ and $q_s = 2\pi s/L$ are the momenta of spinon excitations.

To calculate the finite-size energy spectrum of the NH XXZ model, we generalize the Wiener-Hopf method [332] to the NH model. As detailed in Appendix 5.7, the leading part of the energy spectrum is given by

$$e_L(\Phi) - e_\infty(0) = -\frac{\pi\tilde{u}}{6L^2} + \frac{2S^2}{\tilde{\chi}L^2} + \frac{\tilde{D}_s\Phi^2}{2L^2} + o(1/L^2), \tag{5.53}$$

where $S = L/2 - M$ is the magnetization,

$$\begin{aligned}\tilde{u} =& \frac{J\pi \sin\mu}{2\mu} \\ =& \frac{J\pi}{2\arccos\Delta_\gamma}\sin(\arccos\Delta_\gamma)\end{aligned} \tag{5.54}$$

is the complex-valued velocity of excitations,

$$\tilde{\chi} = \frac{4\mu}{J\pi(\pi-\mu)\sin\mu} \tag{5.55}$$

is the generalized susceptibility, and

$$\tilde{D}_s = \frac{\pi}{4}\frac{J\sin\mu}{\mu(\pi-\mu)} \tag{5.56}$$

is the generalized spin stiffness. Equations (5.53)-(5.56) provide a NH counterpart of the energy spectrum of the XXZ model [316–318, 332, 334–337].

The first term in the right-hand side of Eq. (5.53) gives the finite-size correction to the ground-state energy, which is related to the central charge $c = 1$ of the CFT [314, 315, 319]. This result suggests that a finite-size scaling based on the formula

$$E_L(0) = Le_\infty(0) - \frac{\pi\tilde{u}c}{6L} \tag{5.57}$$

is still valid for the NH model, while the algebraic characterization of the central charge c is nontrivial in the complex extension of the CFT.

5.4.2 Finite-size spectrum and the Tomonaga-Luttinger parameter

The finite-size spectrum of the excitation energies in TL liquids was obtained in Refs. [297, 299]. We generalize it to NH TL liquids [320, 338]. We first employ the mode expansion with the

bosonization procedure. By rescaling the fields ϕ and θ [see Eqs. (1.60) and (1.61) for their precise definitions] with $K' = \sqrt{v_J/v_N} \in \mathbb{R}$ and substituting them into the NH TL Hamiltonian (5.10), it is rewritten as

$$\begin{aligned} H_{\rm eff}^{\rm TL} =& \frac{v' e^{-i\delta_J}}{4} \sum_{k\neq 0} |k| \Big\{ (e^{-i(\delta_N-\delta_J)}+1)(b_k^\dagger b_k + b_{-k} b_{-k}^\dagger) \\ &+ (e^{-i(\delta_N-\delta_J)}-1)(b_k^\dagger b_{-k}^\dagger + b_{-k} b_k) \Big\} \\ &+ \frac{\pi}{2L}(\tilde{v}_N (N-N_0)^2 + \tilde{v}_J J_{\rm curt}^2), \end{aligned} \tag{5.58}$$

where the zero mode is explicitly written, $v' = \sqrt{v_J v_N}$, $\tilde{v}_N = v_N e^{-i\delta_N}$, $\tilde{v}_J = v_J e^{-i\delta_J}$, $N_0 = L/2$ at half-filling, $N - N_0$ is the change in particle number, and $J_{\rm curt}$ is the number of particles that are transferred from the left Fermi point to the right one. Then, we diagonalize Eq. (5.58) as follows:

$$H_{\rm eff}^{\rm TL} = \tilde{u} \sum_{k\neq 0} |k| \bar{a}_k a_k + \frac{\pi}{2L}(\tilde{v}_N (N-N_0)^2 + \tilde{v}_J J_{\rm curt}^2). \tag{5.59}$$

Importantly, the quasiparticle operators $a_k = b_k \cos((\delta_N - \delta_J)/4) - i b_{-k}^\dagger \sin((\delta_N - \delta_J)/4)$ and $\bar{a}_k = b_k^\dagger \cos((\delta_N - \delta_J)/4) - i b_{-k} \sin((\delta_N - \delta_J)/4)$ satisfy the commutation relation $[a_k, \bar{a}_{k'}] = \delta_{k,k'}$ though $\bar{a}_k \neq a_k^\dagger$ [128]. As this transformation is given by the similarity transformation as $a_k = S(\eta) b_k S(-\eta)$, $\bar{a}_k = S(\eta) b_k^\dagger S(-\eta)$ with $S(\eta) = \exp(\frac{i\eta}{2} \sum_{k\neq 0} (b_k^\dagger b_{-k}^\dagger - b_{-k} b_k))$ and $\eta = (\delta_N - \delta_J)/4$, it does not change the conformal-tower structure from the Hermitian limit with the central charge $c = 1$. Here, we note that the complex-valued velocities $\tilde{u}$, $\tilde{v}_N$, and $\tilde{v}_J$ are not independent but related by $\tilde{u} = \sqrt{\tilde{v}_N \tilde{v}_J}$, and the first term in Eq. (5.59) gives the eigenenergy in Eq. (5.30). Hence, we obtain the excitation energy in a finite system under the periodic boundary condition as

$$\Delta E_{\rm PBC} = \frac{2\pi \tilde{u}}{L} \left[\frac{1}{4\tilde{K}} (\Delta N)^2 + \tilde{K} (\Delta D)^2 + n^+ + n^- \right], \tag{5.60}$$

where $\Delta N = N - N_0 \in \mathbb{Z}$, $\Delta D = J_{\rm curt}/2 \in \mathbb{Z}$, n^+ and n^- are nonnegative integers characterizing particle-hole excitations, and $+(-)$ corresponds to the holomorphic (antiholomorphic) part in CFT. In Eq. (5.60), the complex-valued nature of $\tilde{K}$ and $\tilde{u}$ gives the complex energy spectrum and leads to dissipation of the system. We see that Eq. (5.60) is an extension of the finite-size scaling formula in $c = 1$ CFT of the Hermitian TL liquids to the NH TL liquids. Equation (5.60) is to be compared with the BA results [Eq. (5.53)] below. From Eq. (5.60), we obtain the conformal dimensions as follows:

$$\Delta_{\rm CFT}^{\pm} = \frac{1}{2} \left(\frac{\Delta N}{2\sqrt{\tilde{K}}} \pm \Delta D \sqrt{\tilde{K}} \right)^2 + n^{\pm}, \tag{5.61}$$

which gives the critical exponents of the correlation functions in the infinite system. For NH TL liquids with open boundary conditions (chiral NH TL liquids) [339, 340], they do not convey the current, and the excitation energy in a finite system reads

$$\Delta E_{\rm OBC} = \frac{\pi \tilde{u}}{L} \left(\frac{1}{2\tilde{K}} (\Delta N)^2 + n \right), \tag{5.62}$$

where n is a nonnegative integer. Equation (5.62) is relevant to the NH-DMRG calculation in Sec. 5.5. The corresponding conformal dimension reads

$$\Delta_{\rm CFT} = \frac{1}{2\tilde{K}} (\Delta N)^2 + n. \tag{5.63}$$

Thus, the conformal dimensions belong to the universality class characterized by the complex-valued TL parameter $\tilde{K}$.

We now obtain the TL parameter $\tilde{K}$. The quantum numbers of the particle number and the current in Eq. (5.60) are identified as $\Delta N = S$ and $\Delta D = \Phi/(2\pi)$. By comparing Eqs. (5.53) and (5.60), the TL parameter reads

$$\tilde{K} = \frac{\pi}{2(\pi - \arccos \Delta_\gamma)}. \tag{5.64}$$

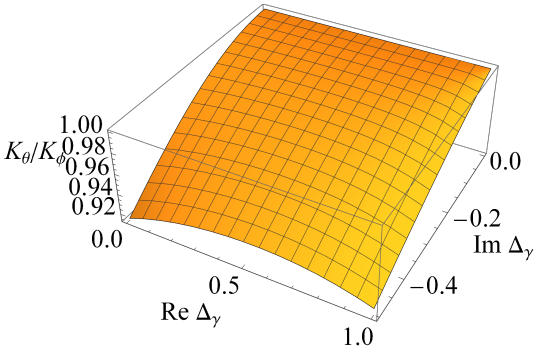

Figure 5.2: Ratio between the critical exponents K_ϕ and K_θ calculated from the exact result (5.64) on the NH XXZ model.

We note that, since the quantum numbers $n^\pm$ of particle-hole excitations in Eq. (5.60) characterize the spinon excitations in Eq. (5.52), we obtain $\tilde{u}$ in Eq. (5.54). In Fig. 5.2, we plot the ratio between the two critical exponents K_ϕ and K_θ [see Eqs. (5.33) and (5.34)] calculated from the exact result (5.64). Since the two critical exponents coincide in the Hermitian case, the deviation of the ratio from unity quantifies how the universality class of the NH XXZ model deviates from the standard Hermitian TL liquid theory.

Next, we discuss how the complex-valued TL parameter $\tilde{K}$ and the velocity $\tilde{u}$ of excitations are obtained from numerical calculations of the finite-size spectrum of the excitation energy. As we consider open boundary conditions in the NH-DMRG calculation in Sec. 5.5, we here assume the excitation energy with open boundary conditions given by Eq. (5.62). The parameters $\tilde{K}$ and $\tilde{u}$ are calculated through the following two types of energy gaps in a finite system

$$\Delta E_{\rm spectral} = \Delta E_{\rm OBC}(\Delta N = 0, n = 1) = \frac{\pi \tilde{u}}{L}, \tag{5.65}$$

$$\Delta E_{\rm spin} = \Delta E_{\rm OBC}(\Delta N = 1, n = 0) = \frac{\pi \tilde{u}}{L}\frac{1}{2\tilde{K}}, \tag{5.66}$$

which we call the spectral gap and the spin gap, respectively. In the Hermitian case, the spectral gap and the spin gap coalesce in the Heisenberg limit. From Eqs. (5.65) and (5.66), we obtain

$$\tilde{K} = \frac{\Delta E_{\rm spectral}}{2\Delta E_{\rm spin}}, \tag{5.67}$$

$$\tilde{u} = \frac{L\Delta E_{\rm spectral}}{\pi}. \tag{5.68}$$

We use Eqs. (5.67) and (5.68) in the NH-DMRG analysis in Sec. 5.5.

5.4.3 Stability conditions for realizing the non-Hermitian Tomonaga-Luttinger liquids

In contrast to Hermitian TL liquids, the velocity $\tilde{u}$ of excitations and the TL parameter $\tilde{K}$ become complex in NH TL liquids. In order for the NH TL liquids to be stable, the real part of the energy spectrum should be bounded from below and the ground state should be normalizable. From Eq. (5.60), the energy spectrum is bounded from below when the coefficients satisfy the conditions

$$\mathrm{Re}\left[\frac{\tilde{u}}{\tilde{K}}\right] > 0, \tag{5.69}$$

$$\mathrm{Re}\left[\tilde{u}\tilde{K}\right] > 0. \tag{5.70}$$

We note that the stability condition $\mathrm{Re}[\tilde{u}] > 0$ for the energy spectrum corresponding to the particle-hole excitations is satisfied if the conditions (5.69) and (5.70) hold. The conditions (5.69) and (5.70) are equivalent to those for ensuring the convergence of the Gaussian integration in the path integrals discussed in Sec. 5.3. Moreover, as discussed in Sec. 5.3, the condition $-\pi/2 < \delta_N -$

$\delta_J < \pi/2$ should be satisfied in order for the ground-state wave function (5.27) to be normalizable. This is equivalent to the following condition:

$$\mathrm{Re}\big[\tilde{K}^2\big] > 0. \tag{5.71}$$

As we have obtained the exact solutions for $\tilde{u}$ and $\tilde{K}$ in Eqs. (5.54) and (5.64), we have to choose appropriate Δ_γ so that the three conditions (5.69), (5.70), and (5.71) are satisfied in order to realize the NH TL liquids. If one of Eqs. (5.69), (5.70), and (5.71) is not satisfied, the dissipation causes the instability of the NH TL liquids. The nature of the ground state after the instability is an interesting problem but is left for future studies.

Finally, we explain the physical meaning of the critical exponents in the correlation functions obtained in Sec. 5.3. As the operator $e^{i\theta}$ makes a kink in ϕ, it results in a change in the particle number, thus causing an excitation in the second term in Eq. (5.10) or equivalently in the first term in Eq. (5.60). Such an excitation leads to the correlation functions for the field θ in Eqs. (5.23) and (5.32). Similarly, as the operator $e^{i\phi}$ creates a current, it causes an excitation in the first term in Eq. (5.10) or equivalently in the second term in Eq. (5.60). Such an excitation leads to the correlation functions for the field ϕ in Eqs. (5.22) and (5.31).

5.5 Non-Hermitian density-matrix renormalization group analysis

We conduct numerical calculations based on the DMRG generalized to NH systems [100–105]. We compare the NH-DMRG results for the lattice Hamiltonian $H_{\mathrm{eff}}^{\mathrm{XXZ}}$ [Eq. (5.6)] and the analytical results obtained by the effective field theory and the Bethe ansatz discussed in Secs. 5.3 and 5.4, thereby demonstrating that the quantum critical phenomena of the model are well described by the NH TL liquid theory.

The algorithm for NH-DMRG is summarized in Sec. 1.3.3. The main idea of NH-DMRG is to use the following form of the density matrix for truncation of eigenstates [106]:

$$\rho_i = \frac{1}{2}\widehat{\mathrm{Tr}}\left\{|\psi_i\rangle_{LL}\langle\psi_i| + |\psi_i\rangle_{RR}\langle\psi_i|\right\}, \tag{5.72}$$

where $\widehat{\mathrm{Tr}}$ describes the partial trace on the system block in the DMRG sweep, and $|\psi_i\rangle_{R(L)}$ denotes the right (left) eigenvector corresponding to the ith eigenvalue of the NH XXZ Hamiltonian (5.6). This type of density matrix was used in Refs. [99, 107–109], and its validity was confirmed numerically by comparing the NH-DMRG results with exact results and analytical calculations. We emphasize that, in NH-DMRG, we do not use the traditional variational ansatz to minimize the energy, but we use the numerically accurate density matrix to truncate the eigenstates. In particular, in Ref. [99], Eq. (5.72) was shown to be superior to the other choices of the density matrix such as $\rho_i = \widehat{\mathrm{Tr}}\{|\psi_i\rangle_{RR}\langle\psi_i|\}$. By using Eq. (5.72), we can avoid all problems related to the possibility of complex eigenvalues. To test the accuracy of the NH-DMRG algorithms, we have compared the ground-state energy obtained from NH-DMRG with that obtained from the exact diagonalization for the number of kept states $m = 40$ and the system size $L = 14$. We find the numerical error between them is small enough (the maximum numerical error is of the order of 10^{-9}) so that it does not affect the results obtained below for NH TL liquids. We note that we use the double-precision floating-point numbers for NH-DMRG and the exact diagonalization. We have also calculated the ground-state energy by using the exact diagonalization with quadruple-precision numbers for system sizes $L = 10$, 12, and 14, and the numerical error between the double precision and the quadruple precision is small enough (the maximum numerical error is of the order of 10^{-9}).

Below, we assume open boundary conditions, where the numerical accuracy is in general guaranteed to be better than the case with periodic boundary conditions. We assume $\mathrm{Im}\Delta_\gamma < 0$ without loss of generality, because the spectrum for $\mathrm{Im}\Delta_\gamma > 0$ is obtained by taking complex conjugation to that for $\mathrm{Im}\Delta_\gamma < 0$, and the right-state correlation functions discussed below are not affected by the sign of $\mathrm{Im}\Delta_\gamma$. In the following calculations, we have confirmed that all parameters satisfy the stability conditions (5.69), (5.70), and (5.71).

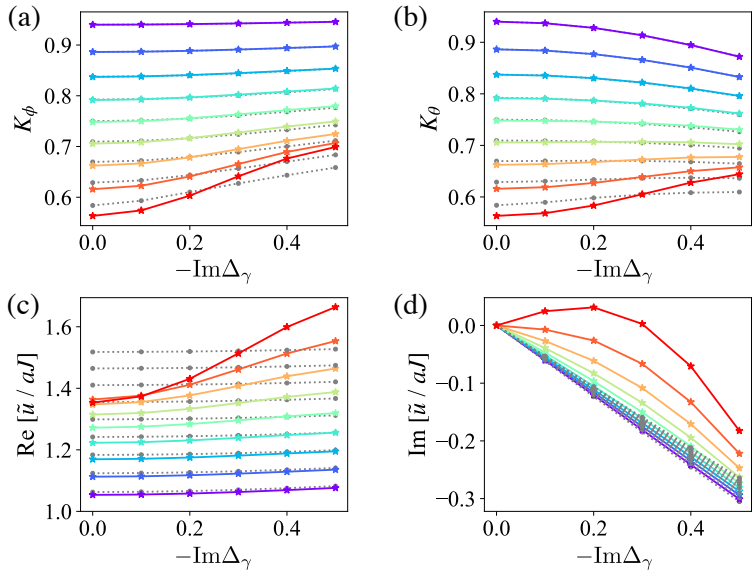

Figure 5.3: Numerical results (solid lines) obtained by the NH-DMRG and exact results (dotted lines) by the BA solution. (a), (b) Critical exponents K_ϕ and K_θ. (c), (d) Velocity of excitations as a function of dissipation $-\mathrm{Im}\Delta_\gamma$. Color plots show the data for $\mathrm{Re}\Delta_\gamma = 0.1, 0.2, 0.3, \cdots, 0.9$ from top to bottom in (a) and (b), and from bottom to top in (c) and (d). The system size is set to $L = 130$ and up to 200 states are kept during the NH-DMRG sweep.

By calculating the energy gaps in a finite system (see Appendix 5.7 for detailed results), we perform a finite-size scaling analysis to extract the critical exponents and the velocity of excitations with Eqs. (5.33), (5.34), (5.67) and (5.68). The results are shown in Fig. 5.3, where the exact solutions obtained by Eqs. (5.33), (5.34), (5.54) and (5.64) are also shown for comparison. In Fig. 5.3(a) and (b), we see that the critical exponents K_ϕ and K_θ obtained by NH-DMRG (solid lines) agree quite well with those obtained from the exact solutions (dotted lines) for small $|\Delta_\gamma|$. Though their difference increases for large $|\Delta_\gamma|$, we have conducted further calculations by changing the system size L and conclude that this is a finite-size effect, which may vanish in the thermodynamic limit. For the velocity $\tilde{u}$ of excitations shown in Figs. 5.3(c) and (d), the results obtained by NH-DMRG (solid lines) agree well with the exact solutions (dotted lines) for small $|\Delta_\gamma|$. Though their discrepancy becomes singnificant for large $|\Delta_\gamma|$, these features have also been reported in Hermitian cases [341, 342]. This is because the finite-size effect becomes significant as the model approaches the transition point, at which the cosine term of the NH sine-Gordon model (5.9) becomes relevant.

We note that these results are consistent with the renormalization group calculation of the NH sine-Gordon model [26]. In Ref. [26], measurement-induced phase transitions of Dirac fermions were studied in the framework of the replica Keldysh field theory, which gives the NH sine-Gordon Hamiltonian with complex-valued coefficients similar to Eq. (5.9). In Ref. [26], by studying the renormalization group flow of the NH sine-Gordon model, it is pointed out that the model for large $|\tilde{g}_3|$ is governed by the strong-coupling fixed point, where the cosine term in the NH sine-Gordon model becomes relevant. As the finite-size effect is known to become significant when the system approaches the transition point [341, 342], the renormalization group analysis is consistent with our NH-DMRG calculation.

It is worth noting that the dependence of K_ϕ and K_θ on dissipation in the NH XXZ model shows interesting behaviors qualitatively different from a model studied before [63]. In Ref. [63], the effect of dissipation on the critical exponents was studied in the NH Lieb-Liniger model [55, 343], where the translational invariance ensures that the phase stiffness [$\tilde{u}\tilde{K}$ in our model (5.10)] does not change due to dissipation. In the NH Lieb-Liniger model, both critical exponents K_ϕ and K_θ are suppressed by dissipation due to QZE. Thus, the enhancement of K_ϕ and K_θ in our model [see Fig. 5.3(a) and (b)] is qualitatively different from the behavior studied in Ref. [63]. As this difference is seen in the regime where $|\Delta_\gamma|$ is large and the system approaches the transition point,

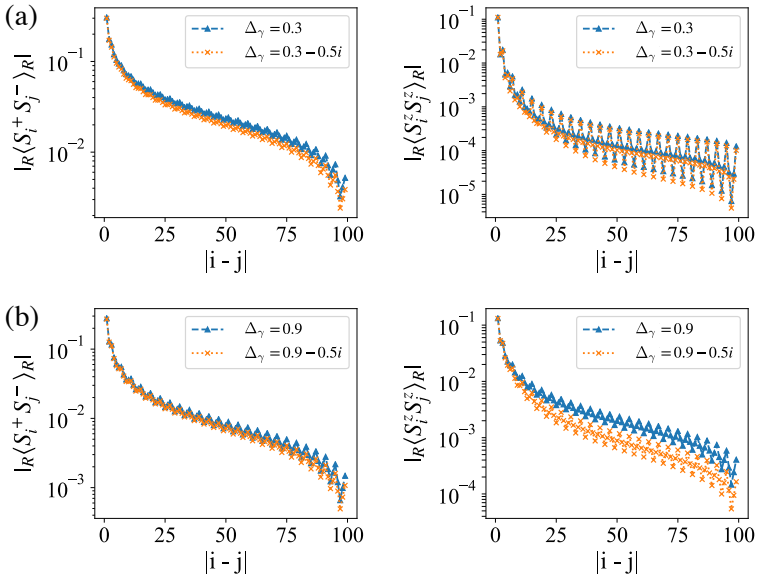

Figure 5.4: Numerical results of correlation functions versus $|i-j|$ for (a) $\mathrm{Re}\Delta_\gamma = 0.3$ and (b) $\mathrm{Re}\Delta_\gamma = 0.9$ obtained by NH-DMRG. The correlation functions are calculated with $i = (L-r+1)/2$ and $j = (L+r+1)/2$ for odd r and $i = (L-r+2)/2$ and $j = (L+r+2)/2$ for even r. The system size is set to $L = 100$ and up to 170 states are kept during the NH-DMRG sweep.

the Umklapp scattering due to the absence of the continuous translational symmetry in the lattice model affects the behavior of the critical exponents.

Next, by using NH-DMRG, we calculate the experimentally observable correlation functions, that is, the right-state correlation functions (5.35) and (5.40). The results are shown in Fig. 5.4. We estimate the maximum numerical error due to truncation to be of the order of 10^{-6} for ${}_R\langle S_i^z S_j^z \rangle_R$ and of the order of 10^{-5} for ${}_R\langle S_i^+ S_j^- \rangle_R$. These numerical errors are of the same orders as those in the Hermitian XXZ model [344], but a much more number of states need to be kept during the NH-DMRG sweep because the convergence problem is severe in the NH case (the number m of kept states is $m = 170$ for $L = 100$ in the NH case compared with $m = 80$ for $L = 200$ in the Hermitian case [344]). We have also confirmed that the numerical error in the imaginary part of the right-state correlation functions is very small and can be ignored.

In Fig. 5.4(a), the x-y and z components of the correlation functions with $\mathrm{Re}\Delta_\gamma = 0.3$ are plotted. We see that dissipation suppresses the correlation at long distances compared with that of the Hermitian limit for both ${}_R\langle S_i^z S_j^z \rangle_R$ and ${}_R\langle S_i^+ S_j^- \rangle_R$. For $\mathrm{Re}\Delta_\gamma = 0.3$, Fig. 5.3(a) and (b) show that K_ϕ increases with increasing dissipation, and that K_θ decreases with increasing dissipation. From Eqs. (5.35) and (5.40), these changes in the critical exponents indicate that both correlation functions are suppressed at long distances by dissipation. This is consistent with the NH-DMRG results shown in Fig. 5.4(a). In Fig. 5.4(b), the correlation functions for $\mathrm{Re}\Delta_\gamma = 0.9$ obtained by NH-DMRG are displayed. We see that both correlation functions ${}_R\langle S_i^z S_j^z \rangle_R$ and ${}_R\langle S_i^+ S_j^- \rangle_R$ are suppressed by dissipation at long distances, and the difference between the NH ($\Delta_\gamma = 0.9 - 0.5i$) and the Hermitian ($\Delta_\gamma = 0.9$) cases is smaller for ${}_R\langle S_i^+ S_j^- \rangle_R$ and larger for ${}_R\langle S_i^z S_j^z \rangle_R$ than the results for $\mathrm{Re}\Delta_\gamma = 0.3$. For $\mathrm{Re}\Delta_\gamma = 0.9$, the exact solutions shown in Fig. 5.3(a) and (b) indicate that both K_ϕ and K_θ increase with increasing dissipation. From the results obtained by the field theory in Eqs. (5.35) and (5.40), the exact solution states that ${}_R\langle S_i^z S_j^z \rangle_R$ is suppressed, but ${}_R\langle S_i^+ S_j^- \rangle_R$ is enhanced at long distances by dissipation. For ${}_R\langle S_i^z S_j^z \rangle_R$, this result is consistent with the NH-DMRG results shown in Fig. 5.4(b), but the behavior of ${}_R\langle S_i^+ S_j^- \rangle_R$ seems to be inconsistent. We attribute this inconsistency to the finite-size effect as the model becomes massive for large $|\Delta_\gamma|$. We also note that the behavior of ${}_R\langle S_i^+ S_j^- \rangle_R$ with $\Delta_\gamma = 0.9 - 0.5i$ obtained by NH-DMRG seems to be affected by the exponential decay of the correlation functions in the gapped regime, where the model becomes massive.

To further explore the behavior of the correlation functions obtained by NH-DMRG, we perform a two-parameter fitting for C_2 and K_ϕ in ${}_R\langle S_i^z S_j^z \rangle_R$ [see Eq. (5.35)]. In NH cases, it has not been

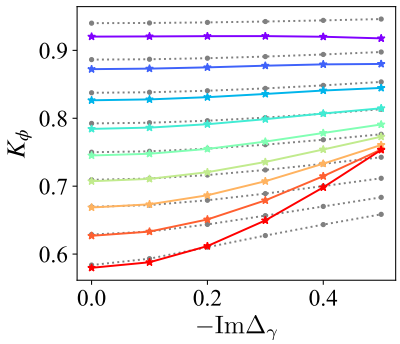

Figure 5.5: Numerical results (solid lines) obtained by the fitting of correlation functions with NH-DMRG and exact results (dotted lines) obtained by the BA solution of the critical exponent K_ϕ as a function of dissipation $-\mathrm{Im}\Delta_\gamma$. Color plots show the data for $\mathrm{Re}\Delta_\gamma = 0.1, 0.2, 0.3, \cdots, 0.9$ from top to bottom. The system size is set to $L = 100$ and up to 170 states are kept during the NH-DMRG sweep.

explored how the correlation amplitudes and the critical exponents behave in a finite system, and we deal with both the correlation amplitudes and the critical exponents as variables. The details of the fitting procedure are as follows. Since we deal with open boundary conditions, we have removed 11 sites from both ends of the spin chain (that is, $i = 1, 2, \cdots, 11$ and $i = 90, 91, \cdots, 100$ for $L = 100$) to exclude the effect of the edges as much as possible. We have also removed correlation functions at distances less than 10 sites (that is, $|i - j| = 1, 2, \cdots, 9$) to avoid the higher-order contributions in the correlation functions. We have performed the fitting for the correlation functions at an odd distance and an even distance separately, and confirmed that the parameters obtained by the correlation functions at an odd distance converge faster to those in an infinite system. While we have also performed a fitting for ${}_R\langle S_i^+ S_j^- \rangle_R$, there are too many fitting parameters in Eq. (5.40) and therefore the results do not converge with sufficient accuracy. We note that, as the biorthogonal correlation functions and the fitting parameters become complex, it is difficult to perform a fitting for the biorthogonal correlation functions with sufficient accuracy. The critical exponent K_ϕ obtained by the fitting of ${}_R\langle S_i^z S_j^z \rangle_R$ at an odd distance is shown in Fig. 5.5. We see that the fitting results show the behavior qualitatively consistent with that of the exact solutions for small $|\Delta_\gamma|$. We have also confirmed that the fitting results for C_2 agree qualitatively well with the exact results of an infinite system in the Hermitian limit [344] (exact results of C_2 for the NH cases are not known). Large difference between the fitting results and the exact results for large $|\Delta_\gamma|$ is due to a finite-size effect as the model approaches the transition point, where the cosine term in the NH sine-Gordon model (5.9) becomes relevant. Though the fitting accuracy is low compared to the results obtained by the finite-size scaling analysis in Fig. 5.3(a) due to the effect of the edges, the results shown in Fig. 5.5 give qualitatively the same behavior as those in Fig. 5.3(a). The NH-DMRG results obtained in this section strongly support the analytical results obtained in Secs. 5.3 and 5.4.

5.6 Summary of this chapter

We have demonstrated the universal properties of dissipative TL liquids by taking the NH XXZ spin chain as a prototypical model in 1D open quantum many-body systems. First, using the field theory with bosonization, we have calculated two types of correlation functions. Then, we have employed a finite-size scaling approach in CFT and the Bethe ansatz, and obtained exact solutions for the complex-valued TL parameter $\tilde{K}$ and the velocity $\tilde{u}$ of excitations. Importantly, we have demonstrated that the model belongs to the universality class characterized by $\tilde{K}$, which is related to the complex generalization of the $c = 1$ CFT. Moreover, we have confirmed that these analytical results are consistent with the numerical results obtained by NH-DMRG for the lattice Hamiltonian in the massless regime with weak dissipation. On the other hand, the NH-DMRG results and the exact solutions start to deviate from each other as the dissipation strength increases. This deviation indicates that the model can be massive for strong dissipation, and this

fact is consistent with the renormalization group analysis obtained in Ref. [26]. The NH XXZ spin chain can be derived from the two-component Bose-Hubbard model with two-body loss, which can be realized with long-lived excited states of ytterbium atoms [37, 43]. As a useful tool for controlling dissipation, artificial two-body loss processes with photoassociation techniques [42] can be utilized to observe the NH TL liquids.

The Bethe ansatz solution of the NH XXZ model for a general complex parameter Δ_γ merits further study. As the integrability of the NH XXZ model holds for arbitrary $\Delta_\gamma \in \mathbb{C}$, it is worthwhile to investigate the possible instability of the NH TL liquid on the basis of exact solutions. Moreover, if the integration path $\mathcal{C}$ in Eq. (5.47) touches a pole of the integrand, the analytic continuation of the solution from the Hermitian limit breaks down and novel criticality may arise at an exceptional point [15]. The exploration of the entire phase diagram of the NH XXZ model remains an interesting research subject.

It is of interest to explore applications of CFT to NH quantum many-body systems. While we have found that the NH TL liquids are successfully described by a complex extension of the $c = 1$ CFT, detailed investigation of the Virasoro algebra behind them remains for future studies. Another important question arises concerning a finite-size scaling of entanglement entropy in nonunitary conformal field theories [345–350]. As a generalization of their frameworks to the biorthogonal bases unique to NH systems has been actively investigated in recent years [290, 351, 352], it is an interesting problem to apply our formalism to the finite-size scaling of entanglement entropy. In view of the fact that CFT in measurement-induced dynamics is investigated in recent years [353–356], it is interesting to investigate how the CFT in NH quantum many-body systems is related to the one in the measurement-induced dynamics.

Dissipation breaks the unitarity of the theory and the entire spectrum of the NH XXZ model can be complicated. However, low-energy physics shows universal properties, which lead to unconventional quantum critical phenomena characterized by the complex extension of the $c = 1$ CFT. It is our hope that the our study facilitates further investigations on dissipative TL liquids in open quantum systems [285–287, 357–361].

5.7 Appendix for this chapter

Wiener-Hopf method for a NH integrable model

In this Appendix, we generalize the Wiener-Hopf method [318, 332, 334] to calculate the finite-size correction to the ground-state energy of the NH XXZ model. A major difference from the Hermitian case is that spin rapidities are not aligned on the real axis but distributed on the complex plane (see Fig. 5.1).

We consider the Bethe equations (5.45) for a large but finite L. We define the counting function by

$$z_L(\lambda,\Phi) \equiv -\frac{\Phi}{L} + 2\arctan\left[\frac{\tanh(\mu\lambda/2)}{\tan(\mu/2)}\right] - \frac{1}{L}\sum_{l=1}^{M} 2\arctan\left[\frac{\tanh\frac{\mu}{2}(\lambda-\lambda_l(\Phi))}{\tan\mu}\right]. \tag{5.73}$$

The spin rapidities $\lambda_j(\Phi)$ $(j = 1, \cdots, M)$ are determined from the condition

$$z_L(\lambda_j(\Phi),\Phi) = \frac{2\pi I_j}{L} = \frac{2\pi}{L}\left(-\frac{M+1}{2}+j\right). \tag{5.74}$$

Since $z_L(\lambda,-\Phi) = -z_L(-\lambda,\Phi)$ and $I_{M+1-j} = -I_j$, the spin rapidities satisfy

$$\lambda_j(-\Phi) = -\lambda_{M+1-j}(\Phi), \tag{5.75}$$

and thus the energy eigenvalue

$$E_L(\Phi) = \frac{J\Delta_\gamma}{4} - J\sum_{j=1}^{M}\frac{\sin^2\mu}{\cosh(\mu\lambda_j(\Phi))-\cos\mu} \tag{5.76}$$

satisfies $E_L(-\Phi) = E_L(\Phi)$.

The distribution function is defined by

$$\sigma_L(\lambda, \Phi) \equiv \frac{1}{2\pi} \frac{dz_L(\lambda, \Phi)}{d\lambda}, \tag{5.77}$$

and satisfies

$$\begin{aligned}\sigma_L(\lambda, \Phi) =& a_1(\lambda) - \frac{1}{L} \sum_{j=1}^{M} a_2(\lambda - \lambda_j(\Phi)) \\ =& a_1(\lambda) - \int_{\mathcal{C}'(\Phi)} d\lambda' a_2(\lambda - \lambda') \sigma_L(\lambda', \Phi) \\ & - \int_{\mathcal{C}'(\Phi)} d\lambda' a_2(\lambda - \lambda') S_L(\lambda', \Phi),\end{aligned} \tag{5.78}$$

where

$$a_n(\lambda) \equiv \frac{1}{2\pi} \frac{\mu \sin(n\mu)}{\cosh(\mu\lambda) - \cos(n\mu)}, \tag{5.79}$$

and

$$S_L(\lambda, \Phi) \equiv \frac{1}{L} \sum_{j=1}^{M} \delta_{\mathcal{C}'}(\lambda - \lambda_j(\Phi)) - \sigma_L(\lambda, \Phi). \tag{5.80}$$

Here, we have introduced a path $\mathcal{C}'(\Phi) = \mathcal{C}_+(\Phi) \cup \mathcal{C}(\Phi) \cup \mathcal{C}_-(\Phi)$. The path $\mathcal{C}(\Phi)$ smoothly connects the spin rapidities $\{\lambda_j(\Phi)\}_{j=1}^{M}$ from $Q_-(\Phi) \equiv \lambda_1(\Phi)$ to $Q_+(\Phi) \equiv \lambda_M(\Phi)$. The endpoints $Q_\pm(\Phi)$ are not located on the real axis in the case of the NH XXZ model. The other two paths $\mathcal{C}_+(\Phi) \equiv \{Q_+(\Phi) + x; x \in [0, \infty)\}$ and $\mathcal{C}_-(\Phi) \equiv \{Q_-(\Phi) + x; x \in (-\infty, 0]\}$ are half lines parallel to the real axis. The delta function $\delta_{\mathcal{C}'}(\lambda - \lambda_j(\Phi))$ is defined by

$$\int_{\mathcal{C}'(\Phi)} d\lambda F(\lambda) \delta_{\mathcal{C}'}(\lambda - \lambda_j(\Phi)) = F(\lambda_j(\Phi)) \tag{5.81}$$

for an arbitrary function $F(\lambda)$ defined on $\mathcal{C}'(\Phi)$.

Since the path $\mathcal{C}'(\Phi)$ in the second term on the right-hand side of Eq. (5.78) can be deformed onto the real axis, we have

$$\begin{aligned}& (1 + \hat{a}_2(\omega)) \hat{\sigma}_L(\omega, \Phi) \\ =& \hat{a}_1(\omega) - \int_{\mathcal{C}'(\Phi)} d\lambda' e^{i\omega\lambda'} \hat{a}_2(\omega) S_L(\lambda', \Phi),\end{aligned} \tag{5.82}$$

where the Fourier transformation of a function $f(\lambda)$ is denoted by

$$\hat{f}(\omega) \equiv \int_{-\infty}^{\infty} d\lambda f(\lambda) e^{i\omega\lambda}. \tag{5.83}$$

From Eq. (5.82), we have

$$\sigma_L(\lambda, \Phi) = \sigma_\infty(\lambda) - \int_{\mathcal{C}'(\Phi)} d\lambda' R(\lambda - \lambda') S_L(\lambda', \Phi), \tag{5.84}$$

where $\sigma_\infty(\lambda)$ is the distribution function in the infinite system-size limit with $\Phi = 0$ [see Eqs. (5.47) and (5.49)], and

$$\begin{aligned}R(\lambda) \equiv& \frac{1}{2\pi} \int_{-\infty}^{\infty} d\omega e^{-i\omega\lambda} \frac{\hat{a}_2(\omega)}{1 + \hat{a}_2(\omega)} \\ =& \frac{1}{2\pi} \int_{-\infty}^{\infty} d\omega e^{-i\omega\lambda} \frac{\sinh\left(\frac{\pi}{\mu} - 2\right)\omega}{2\sinh\left(\frac{\pi}{\mu} - 1\right)\omega \cosh\omega}.\end{aligned} \tag{5.85}$$

Using the Euler-Maclaurin formula

$$\begin{aligned}&\frac{1}{L}\sum_{j=1}^{M}F(\lambda_j(\Phi))\\ \simeq&\int_{\mathcal{C}(\Phi)}F(\lambda)\sigma_L(\lambda,\Phi)d\lambda+\frac{F(Q_+(\Phi))+F(Q_-(\Phi))}{2L}\\ &+\frac{1}{12L^2}\left[\frac{F'(Q_+(\Phi))}{\sigma_L(Q_+(\Phi),\Phi)}-\frac{F'(Q_-(\Phi))}{\sigma_L(Q_-(\Phi),\Phi)}\right],\end{aligned}\tag{5.86}$$

we evaluate the integral in Eq. (5.84) and obtain

$$\begin{aligned}\sigma_L(\lambda,\Phi)=&\sigma_\infty(\lambda)+\int_{\mathcal{C}_+(\Phi)\cup\mathcal{C}_-(\Phi)}d\lambda' R(\lambda-\lambda')\sigma_L(\lambda',\Phi)\\ &-\frac{R(\lambda-Q_+(\Phi))+R(\lambda-Q_-(\Phi))}{2L}\\ &+\frac{1}{12L^2}\left[\frac{R'(\lambda-Q_+(\Phi))}{\sigma_L(Q_+(\Phi),\Phi)}-\frac{R'(\lambda-Q_-(\Phi))}{\sigma_L(Q_-(\Phi),\Phi)}\right].\end{aligned}\tag{5.87}$$

To apply the Wiener-Hopf method, we introduce the functions

$$\begin{aligned}g(x,\Phi)\equiv&\sigma_L(x+Q_+(\Phi),\Phi)\\ =&g_+(x,\Phi)+g_-(x,\Phi),\end{aligned}\tag{5.88}$$

and

$$g_\pm(x,\Phi)\equiv\Theta(\pm x)\sigma_L(x+Q_+(\Phi),\Phi),\tag{5.89}$$

for $x\in\mathbb{R}$, where $\Theta(x)$ is the Heaviside unit-step function. Then, using $\sigma_L(\lambda,-\Phi)=\sigma_L(-\lambda,\Phi)$ and $Q_+(-\Phi)=-Q_-(\Phi)$, we rewrite Eq. (5.87) as

$$\begin{aligned}&g(x,\Phi)+\frac{R(x)+R(x+Q_+(\Phi)-Q_-(\Phi))}{2L}-\frac{1}{12L^2}\left[\frac{R'(x)}{\sigma_L(Q_+(\Phi),\Phi)}-\frac{R'(x+Q_+(\Phi)-Q_-(\Phi))}{\sigma_L(Q_-(\Phi),\Phi)}\right]\\ =&\sigma_\infty(x+Q_+(\Phi))+\int_{\mathcal{C}_+(\Phi)\cup\mathcal{C}_-(\Phi)}d\lambda' R(x+Q_+(\Phi)-\lambda')\sigma_L(\lambda',\Phi)\\ =&\sigma_\infty(x+Q_+(\Phi))+\int_0^\infty dx' R(x-x')g(x',\Phi)+\int_0^\infty dx' R(x+x'+Q_+(\Phi)-Q_-(\Phi))\sigma_L(-x'+Q_-(\Phi),\Phi)\\ =&\sigma_\infty(x+Q_+(\Phi))+\int_{-\infty}^\infty dx' R(x-x')g_+(x',\Phi)+\int_{-\infty}^\infty dx' R(x+x'+Q_+(\Phi)-Q_-(\Phi))g_+(x',-\Phi).\end{aligned}\tag{5.90}$$

Since $R(x+Q)\simeq -i\mathrm{Res}(\hat{R};-i\pi/2)\exp[-\frac{\pi}{2}(x+Q)]$ for large $\mathrm{Re}[Q]$ ($\mathrm{Res}(f;z_0)$ denotes the residue of a function $f(z)$ at $z=z_0$), the leading part of Eq. (5.90) is

$$\begin{aligned}g(x,\Phi)\simeq&\sigma_\infty(x+Q_+(\Phi))+\int_{-\infty}^\infty dx' R(x-x')g_+(x',\Phi)\\ &-\frac{1}{2L}R(x)+\frac{1}{12L^2}\frac{R'(x)}{\sigma_L(Q_+(\Phi),\Phi)},\end{aligned}\tag{5.91}$$

and its Fourier transformation reads

$$\begin{aligned}\hat{g}_+(\omega,\Phi)+\hat{g}_-(\omega,\Phi)=&\hat{\sigma}_\infty(\omega)e^{-i\omega Q_+(\Phi)}+\hat{R}(\omega)\hat{g}_+(\omega,\Phi)\\ &-\frac{1}{2L}\hat{R}(\omega)-\frac{1}{12L^2}\frac{i\omega\hat{R}(\omega)}{\sigma_L(Q_+(\Phi),\Phi)}.\end{aligned}\tag{5.92}$$

Here we use the decomposition

$$1-\hat{R}(\omega)=\frac{1}{G_+(\omega)G_-(\omega)},\tag{5.93}$$

where

$$G_+(\omega) \equiv \frac{\sqrt{2(\pi-\mu)}\Gamma\left(1-\frac{i\omega}{\mu}\right)}{\Gamma\left(\frac{1}{2}-\frac{i\omega}{\pi}\right)\Gamma\left(1-i\omega\frac{\pi-\mu}{\pi\mu}\right)}\left(\frac{\left(\frac{\pi}{\mu}-1\right)^{\frac{\pi}{\mu}-1}}{\left(\frac{\pi}{\mu}\right)^{\frac{\pi}{\mu}}}\right)^{-\frac{i\omega}{\pi}} \tag{5.94}$$

$[G_-(\omega) \equiv G_+(-\omega)]$ is analytic in the upper (lower) half plane [332, 337]. Then, we have

$$\begin{aligned}
&\frac{\hat{g}_+(\omega,\Phi)-C(\omega,\Phi)}{G_+(\omega)} - [G_-(\omega)\hat{\sigma}_\infty(\omega)e^{-i\omega Q_+(\Phi)}]_+ \\
=&-G_-(\omega)\hat{g}_-(\omega) + [G_-(\omega)\hat{\sigma}_\infty(\omega)e^{-i\omega Q_+(\Phi)}]_- \\
&-G_-(\omega)C(\omega,\Phi) \\
=&P(\omega,\Phi),
\end{aligned} \tag{5.95}$$

where

$$C(\omega,\Phi) \equiv \frac{1}{2L} + \frac{1}{12L^2}\frac{i\omega}{\sigma_L(Q_+(\Phi),\Phi)}, \tag{5.96}$$

$P(\omega,\Phi)$ is an entire function of ω, and

$$F(\omega) = [F(\omega)]_+ + [F(\omega)]_-, \tag{5.97}$$

$$[F(\omega)]_\pm \equiv \frac{\pm i}{2\pi}\int_{-\infty}^{\infty} d\omega' \frac{F(\omega')}{\omega-\omega'\pm i0} \tag{5.98}$$

is the decomposition of $F(\omega)$ into $[F(\omega)]_+$ and $[F(\omega)]_-$ which are analytic in the upper and lower complex planes, respectively [334]. Thus, the solution of Eq. (5.92) is given by

$$\begin{aligned}
\hat{g}_+(\omega,\Phi) =&C(\omega,\Phi) + G_+(\omega)P(\omega,\Phi) \\
&+ G_+(\omega)[G_-(\omega)\hat{\sigma}_\infty(\omega)e^{-i\omega Q_+(\Phi)}]_+ \\
\simeq&C(\omega,\Phi) + G_+(\omega)P(\omega,\Phi) \\
&+ \frac{i}{2}\frac{G_+(\omega)G_-(-i\pi/2)}{\omega+i\pi/2}e^{-\frac{\pi}{2}Q_+(\Phi)},
\end{aligned} \tag{5.99}$$

where we have evaluated the lowest-order contribution to $[G_-(\omega)\hat{\sigma}_\infty(\omega)e^{-i\omega Q_+(\Phi)}]_+$ using the pole $\omega = -i\pi/2$ of $\hat{\sigma}_\infty(\omega)$.

The entire function $P(\omega,\Phi)$ is determined from its asymptotic behavior [334]. From $\lim_{\omega\to\infty}\hat{g}_+(\omega,\Phi) = 0$, $\lim_{\omega\to\infty}\hat{\sigma}_\infty(\omega) = 0$, and

$$G_+(\omega) = 1 + \frac{g_1}{\omega} + \frac{g_1^2}{2\omega^2} + \mathcal{O}\left(\frac{1}{\omega^3}\right), \tag{5.100}$$

we get

$$P(\omega,\Phi) = -C(\omega,\Phi) + \frac{1}{12L^2}\frac{ig_1}{\sigma_L(Q_+(\Phi),\Phi)}. \tag{5.101}$$

From Eqs. (5.99), (5.100), and (5.101), the distribution function at the endpoint satisfies

$$\begin{aligned}
\sigma_L(Q_+(\Phi),\Phi) =&g(0,\Phi) \\
=&-\lim_{\omega\to\infty} i\omega\hat{g}_+(\omega,\Phi) \\
=&\frac{ig_1}{2L} + \frac{g_1^2}{24L^2\sigma_L(Q_+(\Phi),\Phi)} \\
&+ \frac{1}{2}G_-\left(-\frac{i\pi}{2}\right)e^{-\frac{\pi}{2}Q_+(\Phi)}.
\end{aligned} \tag{5.102}$$

From Eq. (5.84) and

$$\begin{aligned}\int_{-\infty}^{\infty} d\lambda a_1(\lambda)R(\lambda-\lambda') =& \int_{-\infty}^{\infty} d\lambda a_1(\lambda)R(\lambda'-\lambda)\\ =&\frac{1}{2\pi}\int_{-\infty}^{\infty} d\omega e^{-i\omega\lambda'}\frac{\hat{a}_1(\omega)\hat{a}_2(\omega)}{1+\hat{a}_2(\omega)}\\ =&\int_{-\infty}^{\infty} d\lambda a_2(\lambda'-\lambda)\sigma_\infty(\lambda)\\ =&a_1(\lambda')-\sigma_\infty(\lambda'),\end{aligned} \tag{5.103}$$

the difference of the energy density $e_L(\Phi)=E_L(\Phi)/L$ is given by

$$\begin{aligned}\frac{e_L(\Phi)-e_\infty(0)}{A} =& -\int_{\mathcal{C}'(\Phi)} d\lambda a_1(\lambda)\\ &\times[S_L(\lambda,\Phi)+\sigma_L(\lambda,\Phi)-\sigma_\infty(\lambda)]\\ =& -\int_{\mathcal{C}'(\Phi)} d\lambda a_1(\lambda)\Big[S_L(\lambda,\Phi)\\ &-\int_{\mathcal{C}'(\Phi)} d\lambda' R(\lambda-\lambda')S_L(\lambda',\Phi)\Big]\\ =& -\int_{\mathcal{C}'(\Phi)} d\lambda\sigma_\infty(\lambda)S_L(\lambda,\Phi),\end{aligned} \tag{5.104}$$

where $A=2\pi J\sin\mu/\mu$. Using the Euler-Maclaurin formula (5.86) and $\sigma_\infty(\lambda+Q)\simeq\frac{1}{2}\exp[-\frac{\pi}{2}(\lambda+Q)]$ for large $\mathrm{Re}[Q]$, we evaluate the energy difference as

$$\begin{aligned}\frac{e_L(\Phi)-e_\infty(0)}{A} \simeq& \int_{-\infty}^{\infty} dx\sigma_\infty(x+Q_+(\Phi))g_+(x,\Phi)+\int_{-\infty}^{\infty} dx\sigma_\infty(x+Q_+(-\Phi))g_+(x,-\Phi)\\ &-\frac{\sigma_\infty(Q_+(\Phi))+\sigma_\infty(Q_-(\Phi))}{2L}-\frac{1}{12L^2}\left[\frac{\sigma'_\infty(Q_+(\Phi))}{\sigma_L(Q_+(\Phi),\Phi)}-\frac{\sigma'_\infty(Q_-(\Phi))}{\sigma_L(Q_-(\Phi),\Phi)}\right]\\ \simeq&\frac{1}{2}e^{-\frac{\pi}{2}Q_+(\Phi)}\hat{g}_+\left(\frac{i\pi}{2},\Phi\right)+\frac{1}{2}e^{-\frac{\pi}{2}Q_+(-\Phi)}\hat{g}_+\left(\frac{i\pi}{2},-\Phi\right)\\ &-\frac{1}{4L}(e^{-\frac{\pi}{2}Q_+(\Phi)}+e^{-\frac{\pi}{2}Q_+(-\Phi)})+\frac{\pi}{48L^2}\left[\frac{e^{-\frac{\pi}{2}Q_+(\Phi)}}{\sigma_L(Q_+(\Phi),\Phi)}+\frac{e^{-\frac{\pi}{2}Q_+(-\Phi)}}{\sigma_L(Q_+(-\Phi),-\Phi)}\right]\\ \simeq&\frac{1}{2}P\left(\frac{i\pi}{2},\Phi\right)G_+\left(\frac{i\pi}{2}\right)e^{-\frac{\pi}{2}Q_+(\Phi)}+\frac{1}{4\pi}\left[G_+\left(\frac{i\pi}{2}\right)e^{-\frac{\pi}{2}Q_+(\Phi)}\right]^2\\ &+\frac{1}{2}P\left(\frac{i\pi}{2},-\Phi\right)G_+\left(\frac{i\pi}{2}\right)e^{-\frac{\pi}{2}Q_+(-\Phi)}+\frac{1}{4\pi}\left[G_+\left(\frac{i\pi}{2}\right)e^{-\frac{\pi}{2}Q_+(-\Phi)}\right]^2.\end{aligned} \tag{5.105}$$

On the other hand, since $\mathrm{Re}[\mu]>0$, we have

$$\begin{aligned}\hat{g}_+(0,\Phi) =& \int_{-\infty}^{\infty} dx g_+(x,\Phi)\\ =&\int_{\mathcal{C}_+(\Phi)} d\lambda\sigma_L(\lambda,\Phi)\\ =&\frac{1}{2\pi}\left[\lim_{x\to\infty} z_L(Q_+(\Phi)+x,\Phi)-z_L(\lambda_M,\Phi)\right]\\ =&\frac{(\pi-\mu)S}{\pi L}+\frac{1}{2L}-\frac{\Phi}{2\pi L},\end{aligned} \tag{5.106}$$

where $S=L/2-M$ is the magnetization. From Eqs. (5.99) and (5.106), we obtain

$$\frac{1}{\pi}G_+\left(\frac{i\pi}{2}\right)e^{-\frac{\pi}{2}Q_+(\Phi)} = -P(0,\Phi)+\frac{B(\Phi)}{G_+(0)}, \tag{5.107}$$

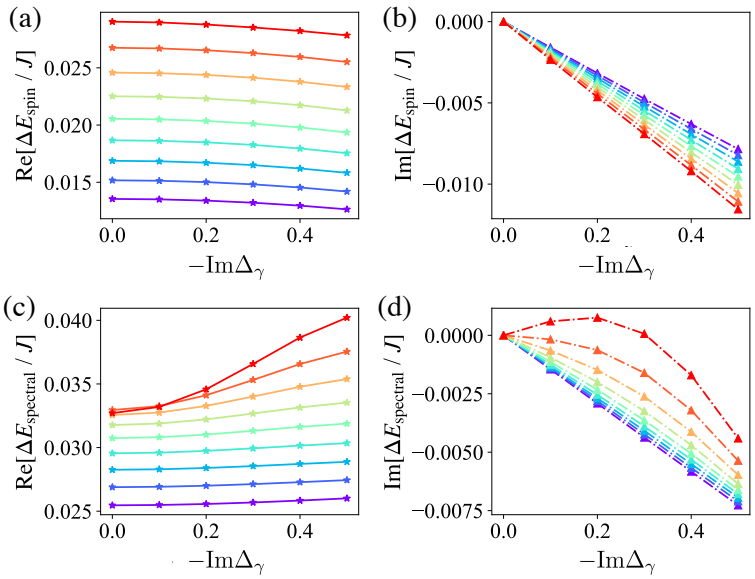

Figure 5.6: NH-DMRG results of energy gaps in a finite system as a function of dissipation $-\mathrm{Im}\Delta_\gamma$. Color plots show the data for $\mathrm{Re}\Delta_\gamma = 0.1, 0.2, 0.3, \cdots, 0.9$ from bottom to top in (a), (c), and (d), and from top to bottom in (b). The system size is set to $L = 130$, and up to 200 states are kept during the NH-DMRG sweep.

where $B(\Phi) = \frac{(\pi-\mu)S}{\pi L} - \frac{\Phi}{2\pi L}$. Substituting Eq. (5.107) into Eq. (5.102), we have

$$\begin{aligned}\sigma_L(Q_+(\Phi),\Phi) =& \frac{2ig_1+\pi}{4L} + \frac{g_1^2 - i\pi g_1}{24L^2\sigma_L(Q_+(\Phi),\Phi)} \\ &+ \frac{\pi B(\Phi)}{2G_+(0)}.\end{aligned} \tag{5.108}$$

Finally, by substituting Eq. (5.107) into Eq. (5.105) and using Eq. (5.108), we arrive at

$$\begin{aligned}&\frac{e_L(\Phi) - e_\infty(0)}{A} \\ \simeq& -\frac{\pi}{24L^2} + \frac{(\pi-\mu)^2S^2}{2\pi[G_+(0)]^2L^2} + \frac{\Phi^2}{8\pi[G_+(0)]^2L^2} \\ =& -\frac{\pi}{24L^2} + \frac{(\pi-\mu)S^2}{4L^2} + \frac{\Phi^2}{16(\pi-\mu)L^2},\end{aligned} \tag{5.109}$$

which is equivalent to Eq. (5.53).

Detailed results for the energy gaps in a finite system

We show the details of the NH-DMRG results for the energy gap in a finite system of the NH XXZ spin chain. The results are shown in Fig. 5.6. We estimate the maximum numerical error due to truncation to be of the order of 10^{-8} for the ground-state energy. When dissipation is increased, the real part of the spin gap shown in Fig. 5.6(a) gradually decreases, while the real part of the spectral gap shown in Fig. 5.6(c) gradually increases. This result shows that the real part of the spectral gap is always larger than that of the spin gap in the weak dissipation regime shown in Fig. 5.6. As for the imaginary part, the spin gap shown in Fig. 5.6(b) gradually decreases as dissipation increases, while the imaginary part of the spectral gap shown in Fig. 5.6(d) seems to increase with increasing dissipation for large $\mathrm{Re}\Delta_\gamma$. To check whether this behavior persists or not in the thermodynamic limit, we have conducted further calculations by changing the system size L (not shown). According to them, we conclude that the increase of $\mathrm{Im}[\Delta E_{\mathrm{spectral}}/J]$ shown in Fig. 5.6(d) is a finite-size effect as a result of the higher-order correction to Eqs. (5.65) and (5.66) with respect to $1/L$. We observe that the finite-size effect becomes significant for large $|\Delta_\gamma|$.

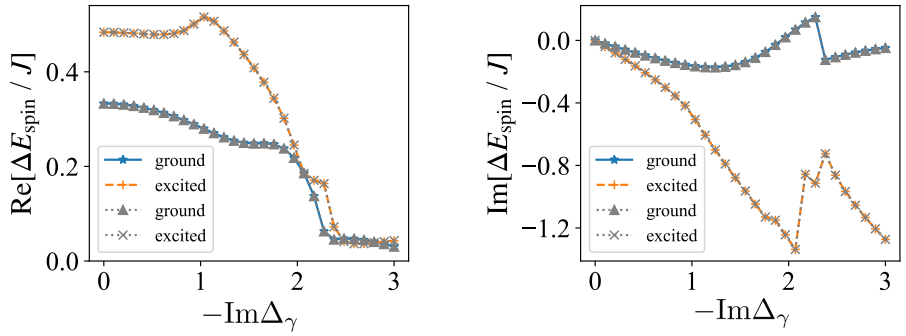

Figure 5.7: Comparison of the energy gaps obtained by NH-DMRG (solid lines and broken lines) and the exact diagonalization (dotted lines). As the ground states for $\mathrm{Re}\Delta_\gamma > 1$ are doubly degenerate in an infinite system, spin gaps for the two lowest states are plotted. The system size is set to $L = 14$, $\mathrm{Re}\Delta_\gamma = 1.5$, and up to 40 states are kept during the NH-DMRG sweep. We use the double-precision data for both NH-DMRG and the exact diagonalization (see text).

NH-DMRG results for the gapped regime in the NH XXZ spin chain

We have also conducted a NH-DMRG calculation for the gapped regime, that is, for $\mathrm{Re}\Delta_\gamma > 1$. However, we have encountered the energy-level crossing problem [362] which leads to the breakdown of the NH-DMRG algorithm. We here explain the problem of NH-DMRG in the gapped regime $\mathrm{Re}\Delta_\gamma > 1$ in the NH XXZ spin chain. We note that, in this appendix, the gapped regime stands for the regime where the system shows an Ising order with double degeneracy. In the NH-DMRG calculation for the massless regime, the energy levels do not merge with each other as dissipation increases (at least for sufficiently weak dissipation considered in our study). In this regime, we have not encountered the energy-level crossing problem as we increase the system size during the infinite-system algorithm of NH-DMRG, and the NH-DMRG algorithm works well. However, in the gapped regime, the energy levels are nearly degenerate and cross with each other in the complex plane as dissipation increases [362]. One of these points corresponds to exceptional points at which the Hamiltonian cannot be diagonalized. Around such dissipation-induced (exceptional) critical points unique to NH systems, we have found an energy-level crossing problem as we increase the size of the system block during the infinite- and finite-system algorithm of NH-DMRG. In this case, the NH-DMRG algorithm usually breaks down. This is explained as follows. The main procedure in the NH-DMRG algorithm is discarding all but the largest m eigenvalues and associated eigenvectors. In this process, m states sufficient to describe the ground state are kept during NH-DMRG. However, when the energy levels cross and the ground state is changed as we increase the size of the system block, the m kept states no longer describe the ground state of the superblock Hamiltonian in the next iteration. Thus, the m kept states do not describe the ground state with sufficient accuracy and the NH-DMRG algorithm breaks down.

In spite of the above problems, we have systematically conducted the NH-DMRG calculation and compared the results with the exact diagonalization by using the double-precision numbers as shown in Fig. 5.7. We see that the results obtained by NH-DMRG and the exact diagonalization agree quite well. However, we find that the results are very sensitive to the number of kept states, and in general, the NH-DMRG results are not trustworthy without comparison with those obtained by the exact diagonalization. Moreover, we have performed the exact diagonalization by using quadruple precision for system sizes $L = 10$, 12, and 14. By comparing the quadruple-precision data and the double-precision data of the ground-state energy obtained from the exact diagonalization, we have found that the numerical error between them increases for large $-\mathrm{Im}\Delta_\gamma$. Thus, we have to pay attention to the precision of the data for large dissipation in the gapped regime. It seems of interest to generalize the NH-DMRG algorithm to gapped regimes in order to explore the ground-state properties. For example, it may be useful to keep all states that are related to the energy-level crossing. This problem is left for future studies.

Chapter 6

Conclusion

In this thesis, we have focused on nonequilibrium quantum many-body phenomena with dissipation, motivated by recent experimental and theoretical progress of open quantum systems. In Chap. 1, we have reviewed several important properties of open quantum systems, by focusing on Markovian environments, which produce Lindblad master equations and NH Hamiltonians. We have also explained the basics of quantum many-body phenomena taking fermionic superfluidity and 1D spin chains as examples.

In Chap. 2, we have investigated NH BCS superfluidity by introducing inelastic collisions between atoms as dissipation. We have elucidated that exotic Bogoliubov quasiparticles which belong to neither fermions nor bosons emerge, and found unconventional reentrant superfluidity induced by non-Hermiticity. Remarkably, this phase transition is accompanied by distinctive features of the non-Hermiticity, i.e. the emergence of exceptional manifolds. We have also discussed possible experimental setups by using QZE, which will play a decisive role in detecting NH phase transitions in experiments. While we have focused on a conventional s-wave superfluid, there seem to be a lot of NH generalizations of other exotic superfluids that have been proposed in condensed matter physics, and this issue merits future investigation.

In Chap. 3, we have investigated the loss-quench dynamics of fermionic superfluids, which is a dissipative counterpart of conventional interaction-quench dynamics of BCS superconductivity. We have demonstrated that the dynamics exhibits both amplitude and phase modes with chirped oscillations, the latter of which is a salient feature of a dissipative superfluid. To observe the characteristic phase mode in dissipative fermionic superfluids, we have proposed a Josephson junction comprised of dissipative and nondissipative superfluids. We have shown that the relative-phase Leggett mode can be detected from the Josephson current for weak dissipation. Importantly, we have elucidated that superfluids exhibit unique nonequilibrium phase transitions triggered by particle loss in Josephson junctions. Our prediction can be tested with ultracold atomic systems of degenerate fermionic gases, and introducing dissipation by using photoassociation laser can be a useful candidate. It is of interest to explore how the dimensionality affects the dynamics and associated collective modes.

In Chap. 4, we have proposed minimal setups to realize a nonreciprocal current in open many-body systems in NESSs. In contrast to conventional approaches in open quantum systems, our finding provides a unique avenue for rectification, namely, the current is neither generated by temperature gradients nor boundary driving, but via homogeneous dissipation by nonequilibrium baths. We have demonstrated that a nonreciprocal Lindblad operator in general rectifies the current in NESSs. We have also revealed that a reciprocal Lindblad operator can be used to rectify the current when the internal symmetry of the Hamiltonian is broken. Though our current model mainly focuses on ultracold atoms, it is of interest to study the regime in solid state systems where Lindblad master equations are relevant.

In Chap. 5, we have demonstrated the universal properties of dissipative TL liquids by taking the NH XXZ spin chain, which is experimentally realized by introducing two-body loss into the two-component Bose-Hubbard model. First, using bosonization techniques with path integrals, we have calculated two types of correlation functions, which in general occur in NH quantum systems. Then, we have employed the finite-size scaling analysis in CFT, and obtained exact solutions for the complex-valued TL parameter $\tilde{K}$ by using the Bethe ansatz. Importantly, we

have demonstrated that the model belongs to the universality class characterized by $\tilde{K}$, which is related to the complex generalization of the $c = 1$ CFT. Moreover, we have confirmed these analytical results by employing NH-DMRG for the lattice Hamiltonian in the massless regime with weak dissipation. On the other hand, the NH-DMRG results and the exact solutions start to deviate from each other as the dissipation strength increases. This deviation indicates that the model can be massive for strong dissipation. The current study offers the opportunity to investigate strongly-correlated NH phenomena by using various analytical and numerical methods, in particular, NH-DMRG and CFT can be strong theoretical tools in open quantum systems.

Bibliography

[1] Markus Müller, Sebastian Diehl, Guido Pupillo, and Peter Zoller. Engineered open systems and quantum simulations with atoms and ions. *Adv. Atom. Mol. Opt. Phys.*, 61:1–80, 2012.

[2] Andrew J. Daley. Quantum trajectories and open many-body quantum systems. *Adv. Phys.*, 63(2):77–149, 2014. doi: 10.1080/00018732.2014.933502. URL https://doi.org/10.1080/00018732.2014.933502.

[3] Lukas M Sieberer, Michael Buchhold, and Sebastian Diehl. Keldysh field theory for driven open quantum systems. *Rep. Prog. Phys.*, 79(9):096001, 2016.

[4] Sebastian Diehl, A Micheli, A Kantian, B Kraus, HP Büchler, and P Zoller. Quantum states and phases in driven open quantum systems with cold atoms. *Nat. Phys.*, 4(11):878, 2008.

[5] B. Kraus, H. P. Büchler, S. Diehl, A. Kantian, A. Micheli, and P. Zoller. Preparation of entangled states by quantum Markov processes. *Phys. Rev. A*, 78:042307, Oct 2008. doi: 10.1103/PhysRevA.78.042307. URL https://link.aps.org/doi/10.1103/PhysRevA.78.042307.

[6] D. Witthaut, F. Trimborn, and S. Wimberger. Dissipation Induced Coherence of a Two-Mode Bose-Einstein Condensate. *Phys. Rev. Lett.*, 101:200402, Nov 2008. doi: 10.1103/PhysRevLett.101.200402. URL https://link.aps.org/doi/10.1103/PhysRevLett.101.200402.

[7] Andrea Tomadin, Sebastian Diehl, and Peter Zoller. Nonequilibrium phase diagram of a driven and dissipative many-body system. *Phys. Rev. A*, 83:013611, Jan 2011. doi: 10.1103/PhysRevA.83.013611. URL https://link.aps.org/doi/10.1103/PhysRevA.83.013611.

[8] Alexandre Le Boité, Giuliano Orso, and Cristiano Ciuti. Steady-State Phases and Tunneling-Induced Instabilities in the Driven Dissipative Bose-Hubbard Model. *Phys. Rev. Lett.*, 110:233601, Jun 2013. doi: 10.1103/PhysRevLett.110.233601. URL https://link.aps.org/doi/10.1103/PhysRevLett.110.233601.

[9] Birger Horstmann, J. Ignacio Cirac, and Géza Giedke. Noise-driven dynamics and phase transitions in fermionic systems. *Phys. Rev. A*, 87:012108, Jan 2013. doi: 10.1103/PhysRevA.87.012108. URL https://link.aps.org/doi/10.1103/PhysRevA.87.012108.

[10] Berislav Buča, Cameron Booker, Marko Medenjak, and Dieter Jaksch. Bethe ansatz approach for dissipation: exact solutions of quantum many-body dynamics under loss. *New J. Phys.*, 22(12):123040, 2020.

[11] Juan José García-Ripoll, Stephan Dürr, Niels Syassen, Dominik M Bauer, Matthias Lettner, Gerhard Rempe, and J Ignacio Cirac. Dissipation-induced hard-core boson gas in an optical lattice. *New J. Phys.*, 11(1):013053, 2009.

[12] S. Dürr, J. J. García-Ripoll, N. Syassen, D. M. Bauer, M. Lettner, J. I. Cirac, and G. Rempe. Lieb-Liniger model of a dissipation-induced Tonks-Girardeau gas. *Phys. Rev. A*, 79:023614, Feb 2009. doi: 10.1103/PhysRevA.79.023614. URL https://link.aps.org/doi/10.1103/PhysRevA.79.023614.

[13] A. J. Daley, J. M. Taylor, S. Diehl, M. Baranov, and P. Zoller. Atomic Three-Body Loss as a Dynamical Three-Body Interaction. *Phys. Rev. Lett.*, 102:040402, Jan 2009. doi: 10.1103/PhysRevLett.102.040402. URL https://link.aps.org/doi/10.1103/PhysRevLett.102.040402.

[14] B. Zhu, B. Gadway, M. Foss-Feig, J. Schachenmayer, M. L. Wall, K. R. A. Hazzard, B. Yan, S. A. Moses, J. P. Covey, D. S. Jin, J. Ye, M. Holland, and A. M. Rey. Suppressing the Loss of Ultracold Molecules Via the Continuous Quantum Zeno Effect. *Phys. Rev. Lett.*, 112:070404, Feb 2014. doi: 10.1103/PhysRevLett.112.070404. URL https://link.aps.org/doi/10.1103/PhysRevLett.112.070404.

[15] Masaya Nakagawa, Norio Kawakami, and Masahito Ueda. Exact Liouvillian Spectrum of a One-Dimensional Dissipative Hubbard Model. *Phys. Rev. Lett.*, 126:110404, Mar 2021. doi: 10.1103/PhysRevLett.126.110404. URL https://link.aps.org/doi/10.1103/PhysRevLett.126.110404.

[16] Sebastian Diehl, Andrea Tomadin, Andrea Micheli, Rosario Fazio, and Peter Zoller. Dynamical Phase Transitions and Instabilities in Open Atomic Many-Body Systems. *Phys. Rev. Lett.*, 105:015702, Jul 2010. doi: 10.1103/PhysRevLett.105.015702. URL https://link.aps.org/doi/10.1103/PhysRevLett.105.015702.

[17] M. Höning, M. Moos, and M. Fleischhauer. Critical exponents of steady-state phase transitions in fermionic lattice models. *Phys. Rev. A*, 86:013606, Jul 2012. doi: 10.1103/PhysRevA.86.013606. URL https://link.aps.org/doi/10.1103/PhysRevA.86.013606.

[18] L. M. Sieberer, S. D. Huber, E. Altman, and S. Diehl. Dynamical Critical Phenomena in Driven-Dissipative Systems. *Phys. Rev. Lett.*, 110:195301, May 2013. doi: 10.1103/PhysRevLett.110.195301. URL https://link.aps.org/doi/10.1103/PhysRevLett.110.195301.

[19] Yaodong Li, Xiao Chen, and Matthew P. A. Fisher. Quantum Zeno effect and the many-body entanglement transition. *Phys. Rev. B*, 98:205136, Nov 2018. doi: 10.1103/PhysRevB.98.205136. URL https://link.aps.org/doi/10.1103/PhysRevB.98.205136.

[20] Amos Chan, Rahul M. Nandkishore, Michael Pretko, and Graeme Smith. Unitary-projective entanglement dynamics. *Phys. Rev. B*, 99:224307, Jun 2019. doi: 10.1103/PhysRevB.99.224307. URL https://link.aps.org/doi/10.1103/PhysRevB.99.224307.

[21] Brian Skinner, Jonathan Ruhman, and Adam Nahum. Measurement-Induced Phase Transitions in the Dynamics of Entanglement. *Phys. Rev. X*, 9:031009, Jul 2019. doi: 10.1103/PhysRevX.9.031009. URL https://link.aps.org/doi/10.1103/PhysRevX.9.031009.

[22] Oliver Lunt and Arijeet Pal. Measurement-induced entanglement transitions in many-body localized systems. *Phys. Rev. Research*, 2:043072, Oct 2020. doi: 10.1103/PhysRevResearch.2.043072. URL https://link.aps.org/doi/10.1103/PhysRevResearch.2.043072.

[23] Yohei Fuji and Yuto Ashida. Measurement-induced quantum criticality under continuous monitoring. *Phys. Rev. B*, 102:054302, Aug 2020. doi: 10.1103/PhysRevB.102.054302. URL https://link.aps.org/doi/10.1103/PhysRevB.102.054302.

[24] Shimpei Goto and Ippei Danshita. Measurement-induced transitions of the entanglement scaling law in ultracold gases with controllable dissipation. *Phys. Rev. A*, 102:033316, Sep 2020. doi: 10.1103/PhysRevA.102.033316. URL https://link.aps.org/doi/10.1103/PhysRevA.102.033316.

[25] Qicheng Tang and W. Zhu. Measurement-induced phase transition: A case study in the nonintegrable model by density-matrix renormalization group calculations. *Phys. Rev. Research*, 2:013022, Jan 2020. doi: 10.1103/PhysRevResearch.2.013022. URL https://link.aps.org/doi/10.1103/PhysRevResearch.2.013022.

[26] M. Buchhold, Y. Minoguchi, A. Altland, and S. Diehl. Effective Theory for the Measurement-Induced Phase Transition of Dirac Fermions. *Phys. Rev. X*, 11:041004, Oct 2021. doi: 10.1103/PhysRevX.11.041004. URL `https://link.aps.org/doi/10.1103/PhysRevX.11.041004`.

[27] T. Müller, S. Diehl, and M. Buchhold. Measurement-Induced Dark State Phase Transitions in Long-Ranged Fermion Systems. *Phys. Rev. Lett.*, 128:010605, Jan 2022. doi: 10.1103/PhysRevLett.128.010605. URL `https://link.aps.org/doi/10.1103/PhysRevLett.128.010605`.

[28] Maxwell Block, Yimu Bao, Soonwon Choi, Ehud Altman, and Norman Y. Yao. Measurement-Induced Transition in Long-Range Interacting Quantum Circuits. *Phys. Rev. Lett.*, 128:010604, Jan 2022. doi: 10.1103/PhysRevLett.128.010604. URL `https://link.aps.org/doi/10.1103/PhysRevLett.128.010604`.

[29] Takaaki Minato, Koudai Sugimoto, Tomotaka Kuwahara, and Keiji Saito. Fate of Measurement-Induced Phase Transition in Long-Range Interactions. *Phys. Rev. Lett.*, 128:010603, Jan 2022. doi: 10.1103/PhysRevLett.128.010603. URL `https://link.aps.org/doi/10.1103/PhysRevLett.128.010603`.

[30] Kazuki Yamamoto and Ryusuke Hamazaki. Localization properties in disordered quantum many-body dynamics under continuous measurement. *arXiv: 2301.07290*, 2023. URL `https://arxiv.org/abs/2301.07290`.

[31] G. Barontini, R. Labouvie, F. Stubenrauch, A. Vogler, V. Guarrera, and H. Ott. Controlling the Dynamics of an Open Many-Body Quantum System with Localized Dissipation. *Phys. Rev. Lett.*, 110:035302, Jan 2013. doi: 10.1103/PhysRevLett.110.035302. URL `https://link.aps.org/doi/10.1103/PhysRevLett.110.035302`.

[32] Ralf Labouvie, Bodhaditya Santra, Simon Heun, Sandro Wimberger, and Herwig Ott. Negative Differential Conductivity in an Interacting Quantum Gas. *Phys. Rev. Lett.*, 115:050601, Jul 2015. doi: 10.1103/PhysRevLett.115.050601. URL `https://link.aps.org/doi/10.1103/PhysRevLett.115.050601`.

[33] Ralf Labouvie, Bodhaditya Santra, Simon Heun, and Herwig Ott. Bistability in a Driven-Dissipative Superfluid. *Phys. Rev. Lett.*, 116:235302, Jun 2016. doi: 10.1103/PhysRevLett.116.235302. URL `https://link.aps.org/doi/10.1103/PhysRevLett.116.235302`.

[34] Y. S. Patil, S. Chakram, and M. Vengalattore. Measurement-Induced Localization of an Ultracold Lattice Gas. *Phys. Rev. Lett.*, 115:140402, Oct 2015. doi: 10.1103/PhysRevLett.115.140402. URL `https://link.aps.org/doi/10.1103/PhysRevLett.115.140402`.

[35] Henrik P. Lüschen, Pranjal Bordia, Sean S. Hodgman, Michael Schreiber, Saubhik Sarkar, Andrew J. Daley, Mark H. Fischer, Ehud Altman, Immanuel Bloch, and Ulrich Schneider. Signatures of Many-Body Localization in a Controlled Open Quantum System. *Phys. Rev. X*, 7:011034, Mar 2017. doi: 10.1103/PhysRevX.7.011034. URL `https://link.aps.org/doi/10.1103/PhysRevX.7.011034`.

[36] Raphaël Bouganne, Manel Bosch Aguilera, Alexis Ghermaoui, Jérôme Beugnon, and Fabrice Gerbier. Anomalous decay of coherence in a dissipative many-body system. *Nat. Phys.*, 16:21–25, 2020.

[37] Takafumi Tomita, Shuta Nakajima, Yosuke Takasu, and Yoshiro Takahashi. Dissipative Bose-Hubbard system with intrinsic two-body loss. *Phys. Rev. A*, 99:031601(R), Mar 2019. doi: 10.1103/PhysRevA.99.031601. URL `https://link.aps.org/doi/10.1103/PhysRevA.99.031601`.

[38] Nishant Dogra, Manuele Landini, Katrin Kroeger, Lorenz Hruby, Tobias Donner, and Tilman Esslinger. Dissipation-induced structural instability and chiral dynamics in a quantum gas. *Science*, 366(6472):1496–1499, 2019.

[39] Hideki Konishi, Kevin Roux, Victor Helson, and Jean-Philippe Brantut. Universal pair polaritons in a strongly interacting Fermi gas. *Nature*, 596(7873):509–513, 2021.

[40] Niels Syassen, Dominik M Bauer, Matthias Lettner, Thomas Volz, Daniel Dietze, Juan J Garcia-Ripoll, J Ignacio Cirac, Gerhard Rempe, and Stephan Dürr. Strong dissipation inhibits losses and induces correlations in cold molecular gases. *Science*, 320(5881):1329–1331, 2008.

[41] Bo Yan, Steven A Moses, Bryce Gadway, Jacob P Covey, Kaden RA Hazzard, Ana Maria Rey, Deborah S Jin, and Jun Ye. Observation of dipolar spin-exchange interactions with lattice-confined polar molecules. *Nature (London)*, 501(7468):521, 2013.

[42] Takafumi Tomita, Shuta Nakajima, Ippei Danshita, Yosuke Takasu, and Yoshiro Takahashi. Observation of the Mott insulator to superfluid crossover of a driven-dissipative Bose-Hubbard system. *Sci. Adv.*, 3(12):e1701513, 2017. doi: 10.1126/sciadv.1701513. URL `http://advances.sciencemag.org/content/3/12/e1701513`.

[43] Koen Sponselee, Lukas Freystatzky, Benjamin Abeln, Marcel Diem, Bastian Hundt, André Kochanke, Thomas Ponath, Bodhaditya Santra, Ludwig Mathey, Klaus Sengstock, and C. Becker. Dynamics of ultracold quantum gases in the dissipative Fermi–Hubbard model. *Quantum Sci. Technol.*, 4(1):014002, 2018.

[44] Y-J Han, Y-H Chan, Wei Yi, Andrew J. Daley, Sebastian Diehl, Peter Zoller, and L-M Duan. Stabilization of the p-wave superfluid state in an optical lattice. *Phys. Rev. Lett.*, 103(7): 070404, 2009.

[45] Ren Zhang, Yanting Cheng, Hui Zhai, and Peng Zhang. Orbital Feshbach Resonance in Alkali-Earth Atoms. *Phys. Rev. Lett.*, 115:135301, Sep 2015. doi: 10.1103/PhysRevLett.115.135301. URL `https://link.aps.org/doi/10.1103/PhysRevLett.115.135301`.

[46] M. Iskin. Two-band superfluidity and intrinsic Josephson effect in alkaline-earth-metal Fermi gases across an orbital Feshbach resonance. *Phys. Rev. A*, 94:011604(R), Jul 2016. doi: 10.1103/PhysRevA.94.011604. URL `https://link.aps.org/doi/10.1103/PhysRevA.94.011604`.

[47] Junjun Xu, Ren Zhang, Yanting Cheng, Peng Zhang, Ran Qi, and Hui Zhai. Reaching a Fermi-superfluid state near an orbital Feshbach resonance. *Phys. Rev. A*, 94:033609, Sep 2016. doi: 10.1103/PhysRevA.94.033609. URL `https://link.aps.org/doi/10.1103/PhysRevA.94.033609`.

[48] Lianyi He, Jia Wang, Shi-Guo Peng, Xia-Ji Liu, and Hui Hu. Strongly correlated Fermi superfluid near an orbital Feshbach resonance: Stability, equation of state, and Leggett mode. *Phys. Rev. A*, 94:043624, Oct 2016. doi: 10.1103/PhysRevA.94.043624. URL `https://link.aps.org/doi/10.1103/PhysRevA.94.043624`.

[49] M. Höfer, L. Riegger, F. Scazza, C. Hofrichter, D. R. Fernandes, M. M. Parish, J. Levinsen, I. Bloch, and S. Fölling. Observation of an Orbital Interaction-Induced Feshbach Resonance in ^{173}Yb. *Phys. Rev. Lett.*, 115:265302, Dec 2015. doi: 10.1103/PhysRevLett.115.265302. URL `https://link.aps.org/doi/10.1103/PhysRevLett.115.265302`.

[50] G. Pagano, M. Mancini, G. Cappellini, L. Livi, C. Sias, J. Catani, M. Inguscio, and L. Fallani. Strongly Interacting Gas of Two-Electron Fermions at an Orbital Feshbach Resonance. *Phys. Rev. Lett.*, 115:265301, Dec 2015. doi: 10.1103/PhysRevLett.115.265301. URL `https://link.aps.org/doi/10.1103/PhysRevLett.115.265301`.

[51] G. Cappellini, L. F. Livi, L. Franchi, D. Tusi, D. Benedicto Orenes, M. Inguscio, J. Catani, and L. Fallani. Coherent Manipulation of Orbital Feshbach Molecules of Two-Electron Atoms. *Phys. Rev. X*, 9:011028, Feb 2019. doi: 10.1103/PhysRevX.9.011028. URL `https://link.aps.org/doi/10.1103/PhysRevX.9.011028`.

[52] N. Darkwah Oppong, L. Riegger, O. Bettermann, M. Höfer, J. Levinsen, M. M. Parish, I. Bloch, and S. Fölling. Observation of Coherent Multiorbital Polarons in a Two-Dimensional Fermi Gas. *Phys. Rev. Lett.*, 122:193604, May 2019. doi: 10.1103/PhysRevLett.122.193604. URL `https://link.aps.org/doi/10.1103/PhysRevLett.122.193604`.

[53] Goran Lindblad. On the generators of quantum dynamical semigroups. *Commun. Math. Phys.*, 48(2):119–130, 1976.

[54] Baidyanath Misra and EC George Sudarshan. The Zeno's paradox in quantum theory. *J. Math. Phys.*, 18(4):756–763, 1977.

[55] Elliott H. Lieb and Werner Liniger. Exact Analysis of an Interacting Bose Gas. I. The General Solution and the Ground State. *Phys. Rev.*, 130:1605–1616, May 1963. doi: 10.1103/PhysRev.130.1605. URL `https://link.aps.org/doi/10.1103/PhysRev.130.1605`.

[56] Yuto Ashida, Zongping Gong, and Masahito Ueda. Non-hermitian physics. *Adv. Phys.*, 69 (3):249–435, 2020.

[57] Jean Dalibard, Yvan Castin, and Klaus Mølmer. Wave-function approach to dissipative processes in quantum optics. *Phys. Rev. Lett.*, 68:580–583, Feb 1992. doi: 10.1103/PhysRevLett.68.580. URL `https://link.aps.org/doi/10.1103/PhysRevLett.68.580`.

[58] Carl M. Bender and Stefan Boettcher. Real Spectra in Non-Hermitian Hamiltonians Having PT Symmetry. *Phys. Rev. Lett.*, 80:5243–5246, Jun 1998. doi: 10.1103/PhysRevLett.80.5243. URL `https://link.aps.org/doi/10.1103/PhysRevLett.80.5243`.

[59] Carl M Bender. Making sense of non-Hermitian Hamiltonians. *Rep. Prog. Phys.*, 70(6):947, 2007. URL `http://stacks.iop.org/0034-4885/70/i=6/a=R03`.

[60] Ryusuke Hamazaki, Kohei Kawabata, and Masahito Ueda. Non-Hermitian Many-Body Localization. *Phys. Rev. Lett.*, 123:090603, Aug 2019. doi: 10.1103/PhysRevLett.123.090603. URL `https://link.aps.org/doi/10.1103/PhysRevLett.123.090603`.

[61] Ryo Hanai, Alexander Edelman, Yoji Ohashi, and Peter B. Littlewood. Non-Hermitian Phase Transition from a Polariton Bose-Einstein Condensate to a Photon Laser. *Phys. Rev. Lett.*, 122:185301, May 2019. doi: 10.1103/PhysRevLett.122.185301. URL `https://link.aps.org/doi/10.1103/PhysRevLett.122.185301`.

[62] Norifumi Matsumoto, Kohei Kawabata, Yuto Ashida, Shunsuke Furukawa, and Masahito Ueda. Continuous Phase Transition without Gap Closing in Non-Hermitian Quantum Many-Body Systems. *Phys. Rev. Lett.*, 125:260601, Dec 2020. doi: 10.1103/PhysRevLett.125.260601. URL `https://link.aps.org/doi/10.1103/PhysRevLett.125.260601`.

[63] Yuto Ashida, Shunsuke Furukawa, and Masahito Ueda. Quantum critical behavior influenced by measurement backaction in ultracold gases. *Phys. Rev. A*, 94:053615, Nov 2016. doi: 10.1103/PhysRevA.94.053615. URL `https://link.aps.org/doi/10.1103/PhysRevA.94.053615`.

[64] Yuto Ashida, Shunsuke Furukawa, and Masahito Ueda. Parity-time-symmetric quantum critical phenomena. *Nat. Commun.*, 8:15791, 2017. doi: 10.1038/ncomms15791. URL `https://www.nature.com/articles/ncomms15791`.

[65] Kohei Kawabata, Yuto Ashida, and Masahito Ueda. Information Retrieval and Criticality in Parity-Time-Symmetric Systems. *Phys. Rev. Lett.*, 119:190401, Nov 2017. doi: 10.1103/PhysRevLett.119.190401. URL `https://link.aps.org/doi/10.1103/PhysRevLett.119.190401`.

[66] Masaya Nakagawa, Norio Kawakami, and Masahito Ueda. Non-Hermitian Kondo Effect in Ultracold Alkaline-Earth Atoms. *Phys. Rev. Lett.*, 121:203001, Nov 2018. doi: 10.1103/PhysRevLett.121.203001. URL `https://link.aps.org/doi/10.1103/PhysRevLett.121.203001`.

[67] José A. S. Lourenço, Ronivon L. Eneias, and Rodrigo G. Pereira. Kondo effect in a $\mathcal{PT}$-symmetric non-Hermitian Hamiltonian. *Phys. Rev. B*, 98:085126, Aug 2018. doi: 10.1103/PhysRevB.98.085126. URL https://link.aps.org/doi/10.1103/PhysRevB.98.085126.

[68] Ryo Hanai and Peter B. Littlewood. Critical fluctuations at a many-body exceptional point. *Phys. Rev. Research*, 2:033018, Jul 2020. doi: 10.1103/PhysRevResearch.2.033018. URL https://link.aps.org/doi/10.1103/PhysRevResearch.2.033018.

[69] M. S. Rudner and L. S. Levitov. Topological Transition in a Non-Hermitian Quantum Walk. *Phys. Rev. Lett.*, 102:065703, Feb 2009. doi: 10.1103/PhysRevLett.102.065703. URL https://link.aps.org/doi/10.1103/PhysRevLett.102.065703.

[70] Tony E. Lee. Anomalous Edge State in a Non-Hermitian Lattice. *Phys. Rev. Lett.*, 116:133903, Apr 2016. doi: 10.1103/PhysRevLett.116.133903. URL https://link.aps.org/doi/10.1103/PhysRevLett.116.133903.

[71] Huitao Shen, Bo Zhen, and Liang Fu. Topological Band Theory for Non-Hermitian Hamiltonians. *Phys. Rev. Lett.*, 120:146402, Apr 2018. doi: 10.1103/PhysRevLett.120.146402. URL https://link.aps.org/doi/10.1103/PhysRevLett.120.146402.

[72] Shunyu Yao and Zhong Wang. Edge States and Topological Invariants of Non-Hermitian Systems. *Phys. Rev. Lett.*, 121:086803, Aug 2018. doi: 10.1103/PhysRevLett.121.086803. URL https://link.aps.org/doi/10.1103/PhysRevLett.121.086803.

[73] Flore K. Kunst, Elisabet Edvardsson, Jan Carl Budich, and Emil J. Bergholtz. Biorthogonal Bulk-Boundary Correspondence in Non-Hermitian Systems. *Phys. Rev. Lett.*, 121:026808, Jul 2018. doi: 10.1103/PhysRevLett.121.026808. URL https://link.aps.org/doi/10.1103/PhysRevLett.121.026808.

[74] Shunyu Yao, Fei Song, and Zhong Wang. Non-Hermitian Chern Bands. *Phys. Rev. Lett.*, 121:136802, Sep 2018. doi: 10.1103/PhysRevLett.121.136802. URL https://link.aps.org/doi/10.1103/PhysRevLett.121.136802.

[75] Kohei Kawabata, Ken Shiozaki, and Masahito Ueda. Anomalous helical edge states in a non-Hermitian Chern insulator. *Phys. Rev. B*, 98:165148, Oct 2018. doi: 10.1103/PhysRevB.98.165148. URL https://link.aps.org/doi/10.1103/PhysRevB.98.165148.

[76] Zongping Gong, Yuto Ashida, Kohei Kawabata, Kazuaki Takasan, Sho Higashikawa, and Masahito Ueda. Topological Phases of Non-Hermitian Systems. *Phys. Rev. X*, 8:031079, Sep 2018. doi: 10.1103/PhysRevX.8.031079. URL https://link.aps.org/doi/10.1103/PhysRevX.8.031079.

[77] Kohei Kawabata, Sho Higashikawa, Zongping Gong, Yuto Ashida, and Masahito Ueda. Topological unification of time-reversal and particle-hole symmetries in non-Hermitian physics. *Nat. Commun.*, 10(1):297, 2019.

[78] Kohei Kawabata, Ken Shiozaki, Masahito Ueda, and Masatoshi Sato. Symmetry and topology in non-hermitian physics. *Phys. Rev. X*, 9:041015, Oct 2019. doi: 10.1103/PhysRevX.9.041015. URL https://link.aps.org/doi/10.1103/PhysRevX.9.041015.

[79] Hengyun Zhou and Jong Yeon Lee. Periodic table for topological bands with non-Hermitian symmetries. *Phys. Rev. B*, 99:235112, Jun 2019. doi: 10.1103/PhysRevB.99.235112. URL https://link.aps.org/doi/10.1103/PhysRevB.99.235112.

[80] Linhu Li, Ching Hua Lee, and Jiangbin Gong. Topological Switch for Non-Hermitian Skin Effect in Cold-Atom Systems with Loss. *Phys. Rev. Lett.*, 124:250402, Jun 2020. doi: 10.1103/PhysRevLett.124.250402. URL https://link.aps.org/doi/10.1103/PhysRevLett.124.250402.

[81] Tony E. Lee and Ching-Kit Chan. Heralded Magnetism in Non-Hermitian Atomic Systems. *Phys. Rev. X*, 4:041001, Oct 2014. doi: 10.1103/PhysRevX.4.041001. URL https://link.aps.org/doi/10.1103/PhysRevX.4.041001.

[82] Masaya Nakagawa, Naoto Tsuji, Norio Kawakami, and Masahito Ueda. Dynamical Sign Reversal of Magnetic Correlations in Dissipative Hubbard Models. *Phys. Rev. Lett.*, 124: 147203, Apr 2020. doi: 10.1103/PhysRevLett.124.147203. URL `https://link.aps.org/doi/10.1103/PhysRevLett.124.147203`.

[83] A. Guo, G. J. Salamo, D. Duchesne, R. Morandotti, M. Volatier-Ravat, V. Aimez, G. A. Siviloglou, and D. N. Christodoulides. Observation of $\mathcal{PT}$-Symmetry Breaking in Complex Optical Potentials. *Phys. Rev. Lett.*, 103:093902, Aug 2009. doi: 10.1103/PhysRevLett.103.093902. URL `https://link.aps.org/doi/10.1103/PhysRevLett.103.093902`.

[84] Christian E. Rüter, Konstantinos G. Makris, Ramy El-Ganainy, Demetrios N. Christodoulides, Mordechai Segev, and Detlef Kip. Observation of parity–time symmetry in optics. *Nat. Phys.*, 6:192, Jan 2010. doi: 10.1038/nphys1515. URL `https://www.nature.com/articles/nphys1515`.

[85] Liang Feng, Maurice Ayache, Jingqing Huang, Ye-Long Xu, Ming-Hui Lu, Yan-Feng Chen, Yeshaiahu Fainman, and Axel Scherer. Nonreciprocal light propagation in a silicon photonic circuit. *Science*, 333(6043):729–733, 2011. ISSN 0036-8075. doi: 10.1126/science.1206038. URL `http://science.sciencemag.org/content/333/6043/729`.

[86] Alois Regensburger, Christoph Bersch, Mohammad-Ali Miri, Georgy Onishchukov, Demetrios N. Christodoulides, and Ulf Peschel. Parity–time synthetic photonic lattices. *Nature*, 488:167, Aug 2012. doi: 10.1038/nature11298. URL `https://www.nature.com/articles/nature11298`.

[87] Julia M. Zeuner, Mikael C. Rechtsman, Yonatan Plotnik, Yaakov Lumer, Stefan Nolte, Mark S. Rudner, Mordechai Segev, and Alexander Szameit. Observation of a Topological Transition in the Bulk of a Non-Hermitian System. *Phys. Rev. Lett.*, 115:040402, Jul 2015. doi: 10.1103/PhysRevLett.115.040402. URL `https://link.aps.org/doi/10.1103/PhysRevLett.115.040402`.

[88] Jiaming Li, Andrew K Harter, Ji Liu, Leonardo de Melo, Yogesh N Joglekar, and Le Luo. Observation of parity-time symmetry breaking transitions in a dissipative Floquet system of ultracold atoms. *Nat. Commun.*, 10(1):855, 2019.

[89] L. Xiao, X. Zhan, Z. H. Bian, K. K. Wang, X. Zhang, X. P. Wang, J. Li, K. Mochizuki, D. Kim, N. Kawakami, W. Yi, H. Obuse, B. C. Sanders, and P. Xue. Observation of topological edge states in parity–time-symmetric quantum walks. *Nat. Phys.*, 13:1117, 2017. doi: 10.1038/nphys4204. URL `https://www.nature.com/articles/nphys4204`.

[90] Hengyun Zhou, Chao Peng, Yoseob Yoon, Chia Wei Hsu, Keith A. Nelson, Liang Fu, John D. Joannopoulos, Marin Soljačić, and Bo Zhen. Observation of bulk Fermi arc and polarization half charge from paired exceptional points. *Science*, 359(6379):1009–1012, 2018. ISSN 0036-8075. doi: 10.1126/science.aap9859. URL `http://science.sciencemag.org/content/359/6379/1009`.

[91] Lei Xiao, Kunkun Wang, Xiang Zhan, Zhihao Bian, Kohei Kawabata, Masahito Ueda, Wei Yi, and Peng Xue. Observation of Critical Phenomena in Parity-Time-Symmetric Quantum Dynamics. *Phys. Rev. Lett.*, 123:230401, Dec 2019. doi: 10.1103/PhysRevLett.123.230401. URL `https://link.aps.org/doi/10.1103/PhysRevLett.123.230401`.

[92] Yosuke Takasu, Tomoya Yagami, Yuto Ashida, Ryusuke Hamazaki, Yoshihito Kuno, and Yoshiro Takahashi. PT-symmetric non-Hermitian quantum many-body system using ultracold atoms in an optical lattice with controlled dissipation. *Prog. Theor. Exp. Phys.*, 2020 (12):12A110, 2020.

[93] Herwig Ott. Single atom detection in ultracold quantum gases: a review of current progress. *Rep. Prog. Phys.*, 79(5):054401, 2016.

[94] Sebastian Diehl, A Micheli, A Kantian, B Kraus, HP Büchler, and P Zoller. Quantum states and phases in driven open quantum systems with cold atoms. *Nat. Phys.*, 4(11):878–883, 2008.

[95] Tatsuhiko N. Ikeda and Masahiro Sato. General description for nonequilibrium steady states in periodically driven dissipative quantum systems. *Sci. Adv.*, 6(27):eabb4019, 2020.

[96] Florian Lange, Zala Lenarčič, and Achim Rosch. Pumping approximately integrable systems. *Nat. Commun.*, 8:15767, 2017.

[97] Florian Lange, Zala Lenarčič, and Achim Rosch. Time-dependent generalized Gibbs ensembles in open quantum systems. *Phys. Rev. B*, 97:165138, Apr 2018. doi: 10.1103/PhysRevB.97.165138. URL https://link.aps.org/doi/10.1103/PhysRevB.97.165138.

[98] Zala Lenarčič, Florian Lange, and Achim Rosch. Perturbative approach to weakly driven many-particle systems in the presence of approximate conservation laws. *Phys. Rev. B*, 97:024302, Jan 2018. doi: 10.1103/PhysRevB.97.024302. URL https://link.aps.org/doi/10.1103/PhysRevB.97.024302.

[99] Enrico Carlon, Malte Henkel, and Ulrich Schollwöck. Density matrix renormalization group and reaction-diffusion processes. *Eur. Phys. J. B*, 12(1):99–114, 1999.

[100] Steven R. White. Density Matrix Formulation for Quantum Renormalization Groups. *Phys. Rev. Lett.*, 69:2863–2866, Nov 1992. doi: 10.1103/PhysRevLett.69.2863. URL https://link.aps.org/doi/10.1103/PhysRevLett.69.2863.

[101] Steven R. White. Density-matrix algorithms for quantum renormalization groups. *Phys. Rev. B*, 48:10345–10356, Oct 1993. doi: 10.1103/PhysRevB.48.10345. URL https://link.aps.org/doi/10.1103/PhysRevB.48.10345.

[102] Steven R. White. Spin Gaps in a Frustrated Heisenberg Model for CaV_4O_9. *Phys. Rev. Lett.*, 77:3633–3636, Oct 1996. doi: 10.1103/PhysRevLett.77.3633. URL https://link.aps.org/doi/10.1103/PhysRevLett.77.3633.

[103] U. Schollwöck. The density-matrix renormalization group. *Rev. Mod. Phys.*, 77:259–315, Apr 2005. doi: 10.1103/RevModPhys.77.259. URL https://link.aps.org/doi/10.1103/RevModPhys.77.259.

[104] Karen A Hallberg. New trends in density matrix renormalization. *Adv. Phys.*, 55(5-6):477–526, 2006.

[105] Ulrich Schollwöck. The density-matrix renormalization group in the age of matrix product states. *Annals of physics*, 326(1):96–192, 2011.

[106] Ingo Peschel, X. Wang, M. Kaulke, and Karen Hallberg, editors. *Density-Matrix Renormalization, A New Numerical Method in Physics*. Springer, Berlin, 1999.

[107] J Kondev and JB Marston. Supersymmetry and localization in the quantum Hall effect. *Nucl. Phys. B*, 497(3):639–657, 1997.

[108] Walter Hofstetter, Ian Affleck, D Nelson, and Ulrich Schollwöck. Non-Hermitian Luttinger liquids and vortex physics. *Europhys. Lett.*, 66(2):178, 2004.

[109] Ian Affleck, Walter Hofstetter, David R Nelson, and Ulrich Schollwöck. Non-Hermitian Luttinger liquids and flux line pinning in planar superconductors. *J. Stat. Mech.*, 2004(10):P10003, 2004.

[110] M Kaulke and Ingo Peschel. A DMRG study of the q-symmetric Heisenberg chain. *Eur. Phys. J. B*, 5(3):727–734, 1998.

[111] Yasuhiro Hieida. Application of the density matrix renormalization group method to a non-equilibrium problem. *J. Phys. Soc. Jpn.*, 67(2):369–372, 1998.

[112] Xiaoqun Wang and Tao Xiang. Transfer-matrix density-matrix renormalization-group theory for thermodynamics of one-dimensional quantum systems. *Phys. Rev. B*, 56:5061–5064, Sep 1997. doi: 10.1103/PhysRevB.56.5061. URL https://link.aps.org/doi/10.1103/PhysRevB.56.5061.

[113] Dan-Wei Zhang, Yu-Lian Chen, Guo-Qing Zhang, Li-Jun Lang, Zhi Li, and Shi-Liang Zhu. Skin superfluid, topological Mott insulators, and asymmetric dynamics in an interacting non-Hermitian Aubry-André-Harper model. *Phys. Rev. B*, 101:235150, Jun 2020. doi: 10.1103/PhysRevB.101.235150. URL https://link.aps.org/doi/10.1103/PhysRevB.101.235150.

[114] Selim Jochim, Markus Bartenstein, Alexander Altmeyer, Gerhard Hendl, Stefan Riedl, Cheng Chin, J Hecker Denschlag, and Rudolf Grimm. Bose-Einstein condensation of molecules. *Science*, 302(5653):2101–2103, 2003.

[115] Markus Greiner, Cindy A Regal, and Deborah S Jin. Emergence of a molecular Bose–Einstein condensate from a Fermi gas. *Nature*, 426(6966):537–540, 2003.

[116] M. W. Zwierlein, C. A. Stan, C. H. Schunck, S. M. F. Raupach, S. Gupta, Z. Hadzibabic, and W. Ketterle. Observation of Bose-Einstein Condensation of Molecules. *Phys. Rev. Lett.*, 91:250401, Dec 2003. doi: 10.1103/PhysRevLett.91.250401. URL https://link.aps.org/doi/10.1103/PhysRevLett.91.250401.

[117] C. A. Regal, M. Greiner, and D. S. Jin. Observation of Resonance Condensation of Fermionic Atom Pairs. *Phys. Rev. Lett.*, 92:040403, Jan 2004. doi: 10.1103/PhysRevLett.92.040403. URL https://link.aps.org/doi/10.1103/PhysRevLett.92.040403.

[118] M. W. Zwierlein, C. A. Stan, C. H. Schunck, S. M. F. Raupach, A. J. Kerman, and W. Ketterle. Condensation of Pairs of Fermionic Atoms near a Feshbach Resonance. *Phys. Rev. Lett.*, 92:120403, Mar 2004. doi: 10.1103/PhysRevLett.92.120403. URL https://link.aps.org/doi/10.1103/PhysRevLett.92.120403.

[119] C Chin, M Bartenstein, A Altmeyer, S Riedl, S Jochim, J Hecker Denschlag, and R Grimm. Observation of the pairing gap in a strongly interacting Fermi gas. *Science*, 305(5687): 1128–1130, 2004.

[120] JT Stewart, JP Gaebler, and DS Jin. Using photoemission spectroscopy to probe a strongly interacting Fermi gas. *Nature (London)*, 454(7205):744, 2008.

[121] Jit Kee Chin, DE Miller, Y Liu, Claudiu Stan, W Setiawan, C Sanner, K Xu, and W Ketterle. Evidence for superfluidity of ultracold fermions in an optical lattice. *Nature (London)*, 443 (7114):961, 2006.

[122] Thierry Giamarchi. *Quantum physics in one dimension*, volume 121. Clarendon press, Oxford, 2003.

[123] J. Bardeen, L. N. Cooper, and J. R. Schrieffer. Theory of superconductivity. *Phys. Rev.*, 108:1175–1204, Dec 1957. doi: 10.1103/PhysRev.108.1175. URL https://link.aps.org/doi/10.1103/PhysRev.108.1175.

[124] M. Bartenstein, A. Altmeyer, S. Riedl, S. Jochim, C. Chin, J. Hecker Denschlag, and R. Grimm. Crossover from a Molecular Bose-Einstein Condensate to a Degenerate Fermi Gas. *Phys. Rev. Lett.*, 92:120401, Mar 2004. doi: 10.1103/PhysRevLett.92.120401. URL https://link.aps.org/doi/10.1103/PhysRevLett.92.120401.

[125] Ananya Ghatak and Tanmoy Das. Theory of superconductivity with non-Hermitian and parity-time reversal symmetric Cooper pairing symmetry. *Phys. Rev. B*, 97:014512, Jan 2018. doi: 10.1103/PhysRevB.97.014512. URL https://link.aps.org/doi/10.1103/PhysRevB.97.014512.

[126] Lihong Zhou and Xiaoling Cui. Enhanced fermion pairing and superfluidity by an imaginary magnetic field. *iSience*, 14:257–263, 2019.

[127] N. M. Chtchelkatchev, A. A. Golubov, T. I. Baturina, and V. M. Vinokur. Stimulation of the Fluctuation Superconductivity by $\mathcal{PT}$ Symmetry. *Phys. Rev. Lett.*, 109:150405, Oct 2012. doi: 10.1103/PhysRevLett.109.150405. URL https://link.aps.org/doi/10.1103/PhysRevLett.109.150405.

[128] Kazuki Yamamoto, Masaya Nakagawa, Kyosuke Adachi, Kazuaki Takasan, Masahito Ueda, and Norio Kawakami. Theory of Non-Hermitian Fermionic Superfluidity with a Complex-Valued Interaction. *Phys. Rev. Lett.*, 123:123601, Sep 2019. doi: 10.1103/PhysRevLett.123.123601. URL https://link.aps.org/doi/10.1103/PhysRevLett.123.123601.

[129] W D Heiss. The physics of exceptional points. *J. Phys. A: Math. Theor.*, 45(44):444016, 2012. URL http://stacks.iop.org/1751-8121/45/i=44/a=444016.

[130] Michael V Berry. Physics of nonhermitian degeneracies. *Czechoslov. J. Phys.*, 54(10):1039–1047, 2004.

[131] Thilo Stöferle, Henning Moritz, Kenneth Günter, Michael Köhl, and Tilman Esslinger. Molecules of Fermionic Atoms in an Optical Lattice. *Phys. Rev. Lett.*, 96:030401, Jan 2006. doi: 10.1103/PhysRevLett.96.030401. URL https://link.aps.org/doi/10.1103/PhysRevLett.96.030401.

[132] Debayan Mitra, Peter T Brown, Elmer Guardado-Sanchez, Stanimir S Kondov, Trithep Devakul, David A Huse, Peter Schauss, and Waseem S Bakr. Quantum gas microscopy of an attractive Fermi–Hubbard system. *Nat. Phys.*, 14(2):173, 2018.

[133] Dorje C Brody. Biorthogonal quantum mechanics. *J. Phys. A: Math. Theor.*, 47(3):035305, 2013.

[134] Anthony J Leggett. Cooper pairing in spin-polarized fermi systems. *Le Journal de Physique Colloques*, 41(C7):C7–19, 1980.

[135] Anthony James Leggett. *Diatomic molecules and Cooper pairs*. Springer, 1980.

[136] Ph Nozieres and S Schmitt-Rink. Bose condensation in an attractive fermion gas: From weak to strong coupling superconductivity. *J. Low Temp. Phys.*, 59(3):195–211, 1985.

[137] Roberto B. Diener, Rajdeep Sensarma, and Mohit Randeria. Quantum fluctuations in the superfluid state of the BCS-BEC crossover. *Phys. Rev. A*, 77:023626, Feb 2008. doi: 10.1103/PhysRevA.77.023626. URL https://link.aps.org/doi/10.1103/PhysRevA.77.023626.

[138] M. J. Mark, E. Haller, K. Lauber, J. G. Danzl, A. Janisch, H. P. Büchler, A. J. Daley, and H.-C. Nägerl. Preparation and Spectroscopy of a Metastable Mott-Insulator State with Attractive Interactions. *Phys. Rev. Lett.*, 108:215302, May 2012. doi: 10.1103/PhysRevLett.108.215302. URL https://link.aps.org/doi/10.1103/PhysRevLett.108.215302.

[139] G. Barontini, R. Labouvie, F. Stubenrauch, A. Vogler, V. Guarrera, and H. Ott. Controlling the Dynamics of an Open Many-Body Quantum System with Localized Dissipation. *Phys. Rev. Lett.*, 110:035302, Jan 2013. doi: 10.1103/PhysRevLett.110.035302. URL https://link.aps.org/doi/10.1103/PhysRevLett.110.035302.

[140] B. Zhu, B. Gadway, M. Foss-Feig, J. Schachenmayer, M. L. Wall, K. R. A. Hazzard, B. Yan, S. A. Moses, J. P. Covey, D. S. Jin, J. Ye, M. Holland, and A. M. Rey. Suppressing the Loss of Ultracold Molecules Via the Continuous Quantum Zeno Effect. *Phys. Rev. Lett.*, 112:070404, Feb 2014. doi: 10.1103/PhysRevLett.112.070404. URL https://link.aps.org/doi/10.1103/PhysRevLett.112.070404.

[141] Ryo Okugawa and Takehito Yokoyama. Topological exceptional surfaces in non-Hermitian systems with parity-time and parity-particle-hole symmetries. *Phys. Rev. B*, 99:041202, Jan 2019. doi: 10.1103/PhysRevB.99.041202. URL https://link.aps.org/doi/10.1103/PhysRevB.99.041202.

[142] Tsuneya Yoshida, Robert Peters, Norio Kawakami, and Yasuhiro Hatsugai. Symmetry-protected exceptional rings in two-dimensional correlated systems with chiral symmetry. *Phys. Rev. B*, 99:121101, Mar 2019. doi: 10.1103/PhysRevB.99.121101. URL https://link.aps.org/doi/10.1103/PhysRevB.99.121101.

[143] Jan Carl Budich, Johan Carlström, Flore K. Kunst, and Emil J. Bergholtz. Symmetry-protected nodal phases in non-Hermitian systems. *Phys. Rev. B*, 99:041406, Jan 2019. doi: 10.1103/PhysRevB.99.041406. URL https://link.aps.org/doi/10.1103/PhysRevB.99.041406.

[144] Hengyun Zhou, Jong Yeon Lee, Shang Liu, and Bo Zhen. Exceptional surfaces in PT-symmetric non-Hermitian photonic systems. *Optica*, 6(2):190–193, Feb 2019. doi: 10.1364/OPTICA.6.000190. URL http://www.osapublishing.org/optica/abstract.cfm?URI=optica-6-2-190.

[145] Anthony J Leggett and Fernando Sols. On the concept of spontaneously broken gauge symmetry in condensed matter physics. *Found. Phys.*, 21(3):353–364, 1991.

[146] Anthony James Leggett. *Quantum liquids: Bose condensation and Cooper pairing in condensed-matter systems*. Oxford university press, 2006.

[147] P. W. Anderson. Random-Phase Approximation in the Theory of Superconductivity. *Phys. Rev.*, 112:1900–1916, Dec 1958. doi: 10.1103/PhysRev.112.1900. URL https://link.aps.org/doi/10.1103/PhysRev.112.1900.

[148] AJ Leggett. Number-phase fluctuations in two-band superconductors. *Prog. Theor. Phys.*, 36(5):901–930, 1966.

[149] AF Volkov and Sh M Kogan. Collisionless relaxation of the energy gap in superconductors. *Sov. Phys. JETP*, 38:1018, 1974.

[150] P. B. Littlewood and C. M. Varma. Gauge-Invariant Theory of the Dynamical Interaction of Charge Density Waves and Superconductivity. *Phys. Rev. Lett.*, 47:811–814, Sep 1981. doi: 10.1103/PhysRevLett.47.811. URL https://link.aps.org/doi/10.1103/PhysRevLett.47.811.

[151] P. B. Littlewood and C. M. Varma. Amplitude collective modes in superconductors and their coupling to charge-density waves. *Phys. Rev. B*, 26:4883–4893, Nov 1982. doi: 10.1103/PhysRevB.26.4883. URL https://link.aps.org/doi/10.1103/PhysRevB.26.4883.

[152] C. M. Varma. Higgs boson in superconductors. *J. Low Temp. Phys.*, 126(3):901–909, 2002.

[153] A. V. Andreev, V. Gurarie, and L. Radzihovsky. Nonequilibrium Dynamics and Thermodynamics of a Degenerate Fermi Gas Across a Feshbach Resonance. *Phys. Rev. Lett.*, 93:130402, Sep 2004. doi: 10.1103/PhysRevLett.93.130402. URL https://link.aps.org/doi/10.1103/PhysRevLett.93.130402.

[154] R. A. Barankov, L. S. Levitov, and B. Z. Spivak. Collective Rabi Oscillations and Solitons in a Time-Dependent BCS Pairing Problem. *Phys. Rev. Lett.*, 93:160401, Oct 2004. doi: 10.1103/PhysRevLett.93.160401. URL https://link.aps.org/doi/10.1103/PhysRevLett.93.160401.

[155] R. A. Barankov and L. S. Levitov. Dynamical selection in developing fermionic pairing. *Phys. Rev. A*, 73:033614, Mar 2006. doi: 10.1103/PhysRevA.73.033614. URL https://link.aps.org/doi/10.1103/PhysRevA.73.033614.

[156] Emil A. Yuzbashyan and Maxim Dzero. Dynamical Vanishing of the Order Parameter in a Fermionic Condensate. *Phys. Rev. Lett.*, 96:230404, Jun 2006. doi: 10.1103/PhysRevLett.96.230404. URL https://link.aps.org/doi/10.1103/PhysRevLett.96.230404.

[157] R. A. Barankov and L. S. Levitov. Synchronization in the BCS Pairing Dynamics as a Critical Phenomenon. *Phys. Rev. Lett.*, 96:230403, Jun 2006. doi: 10.1103/PhysRevLett.96.230403. URL https://link.aps.org/doi/10.1103/PhysRevLett.96.230403.

[158] Emil A. Yuzbashyan, Oleksandr Tsyplyatyev, and Boris L. Altshuler. Relaxation and Persistent Oscillations of the Order Parameter in Fermionic Condensates. *Phys. Rev. Lett.*, 96:097005, Mar 2006. doi: 10.1103/PhysRevLett.96.097005. URL https://link.aps.org/doi/10.1103/PhysRevLett.96.097005.

[159] V. Gurarie. Nonequilibrium Dynamics of Weakly and Strongly Paired Superconductors. *Phys. Rev. Lett.*, 103:075301, Aug 2009. doi: 10.1103/PhysRevLett.103.075301. URL https://link.aps.org/doi/10.1103/PhysRevLett.103.075301.

[160] E. A. Yuzbashyan, M. Dzero, V. Gurarie, and M. S. Foster. Quantum quench phase diagrams of an s-wave BCS-BEC condensate. *Phys. Rev. A*, 91:033628, Mar 2015. doi: 10.1103/PhysRevA.91.033628. URL https://link.aps.org/doi/10.1103/PhysRevA.91.033628.

[161] S. Hannibal, P. Kettmann, M. D. Croitoru, A. Vagov, V. M. Axt, and T. Kuhn. Quench dynamics of an ultracold Fermi gas in the BCS regime: Spectral properties and confinement-induced breakdown of the Higgs mode. *Phys. Rev. A*, 91:043630, Apr 2015. doi: 10.1103/PhysRevA.91.043630. URL https://link.aps.org/doi/10.1103/PhysRevA.91.043630.

[162] P. Kettmann, S. Hannibal, M. D. Croitoru, V. M. Axt, and T. Kuhn. Pure Goldstone mode in the quench dynamics of a confined ultracold Fermi gas in the BCS-BEC crossover regime. *Phys. Rev. A*, 96:033618, Sep 2017. doi: 10.1103/PhysRevA.96.033618. URL https://link.aps.org/doi/10.1103/PhysRevA.96.033618.

[163] S. Hannibal, P. Kettmann, M. D. Croitoru, V. M. Axt, and T. Kuhn. Dynamical vanishing of the order parameter in a confined Bardeen-Cooper-Schrieffer Fermi gas after an interaction quench. *Phys. Rev. A*, 97:013619, Jan 2018. doi: 10.1103/PhysRevA.97.013619. URL https://link.aps.org/doi/10.1103/PhysRevA.97.013619.

[164] S. Hannibal, P. Kettmann, M. D. Croitoru, V. M. Axt, and T. Kuhn. Persistent oscillations of the order parameter and interaction quench phase diagram for a confined Bardeen-Cooper-Schrieffer Fermi gas. *Phys. Rev. A*, 98:053605, Nov 2018. doi: 10.1103/PhysRevA.98.053605. URL https://link.aps.org/doi/10.1103/PhysRevA.98.053605.

[165] David Pekker and CM Varma. Amplitude/Higgs modes in condensed matter physics. *Annu. Rev. Condens. Matter Phys.*, 6(1):269–297, 2015.

[166] Ryo Shimano and Naoto Tsuji. Higgs Mode in Superconductors. *Annu. Rev. Condens. Matter Phys.*, 11:103, 2020.

[167] Ulf Bissbort, Sören Götze, Yongqiang Li, Jannes Heinze, Jasper S. Krauser, Malte Weinberg, Christoph Becker, Klaus Sengstock, and Walter Hofstetter. Detecting the Amplitude Mode of Strongly Interacting Lattice Bosons by Bragg Scattering. *Phys. Rev. Lett.*, 106:205303, May 2011. doi: 10.1103/PhysRevLett.106.205303. URL https://link.aps.org/doi/10.1103/PhysRevLett.106.205303.

[168] Manuel Endres, Takeshi Fukuhara, David Pekker, Marc Cheneau, Peter Schauβ, Christian Gross, Eugene Demler, Stefan Kuhr, and Immanuel Bloch. The 'Higgs' amplitude mode at the two-dimensional superfluid/Mott insulator transition. *Nature (London)*, 487(7408): 454–458, 2012.

[169] A Behrle, T Harrison, J Kombe, K Gao, M Link, J-S Bernier, C Kollath, and M Köhl. Higgs mode in a strongly interacting fermionic superfluid. *Nat. Phys.*, 14(8):781, 2018.

[170] Timothy Harrison, Martin Link, Alexandra Behrle, Kuiyi Gao, Andreas Kell, Johannes Kombe, Jean-Sébastien Bernier, Corinna Kollath, and Michael Köhl. Decay and revival of a transient trapped Fermi condensate. *Phys. Rev. Research*, 3:023205, Jun 2021. doi: 10.1103/PhysRevResearch.3.023205. URL https://link.aps.org/doi/10.1103/PhysRevResearch.3.023205.

[171] Ryusuke Matsunaga, Yuki I. Hamada, Kazumasa Makise, Yoshinori Uzawa, Hirotaka Terai, Zhen Wang, and Ryo Shimano. Higgs Amplitude Mode in the BCS Superconductors $Nb_{1-x}Ti_xN$ Induced by Terahertz Pulse Excitation. *Phys. Rev. Lett.*, 111:057002, Jul 2013. doi: 10.1103/PhysRevLett.111.057002. URL https://link.aps.org/doi/10.1103/PhysRevLett.111.057002.

[172] Ryusuke Matsunaga, Naoto Tsuji, Hiroyuki Fujita, Arata Sugioka, Kazumasa Makise, Yoshinori Uzawa, Hirotaka Terai, Zhen Wang, Hideo Aoki, and Ryo Shimano. Light-induced collective pseudospin precession resonating with Higgs mode in a superconductor. *Science*, 345 (6201):1145–1149, 2014.

[173] T. Papenkort, V. M. Axt, and T. Kuhn. Coherent dynamics and pump-probe spectra of BCS superconductors. *Phys. Rev. B*, 76:224522, Dec 2007. doi: 10.1103/PhysRevB.76.224522. URL `https://link.aps.org/doi/10.1103/PhysRevB.76.224522`.

[174] T. Papenkort, T. Kuhn, and V. M. Axt. Coherent control of the gap dynamics of BCS superconductors in the nonadiabatic regime. *Phys. Rev. B*, 78:132505, Oct 2008. doi: 10.1103/PhysRevB.78.132505. URL `https://link.aps.org/doi/10.1103/PhysRevB.78.132505`.

[175] Andreas P. Schnyder, Dirk Manske, and Adolfo Avella. Resonant generation of coherent phonons in a superconductor by ultrafast optical pump pulses. *Phys. Rev. B*, 84:214513, Dec 2011. doi: 10.1103/PhysRevB.84.214513. URL `https://link.aps.org/doi/10.1103/PhysRevB.84.214513`.

[176] Martin Zachmann, Mikhail D Croitoru, Alexei Vagov, Vollrath M Axt, Thomas Papenkort, and Tilmann Kuhn. Ultrafast terahertz-field-induced dynamics of superconducting bulk and quasi-1D samples. *New J. Phys.*, 15(5):055016, 2013.

[177] H. Krull, D. Manske, G. S. Uhrig, and A. P. Schnyder. Signatures of nonadiabatic BCS state dynamics in pump-probe conductivity. *Phys. Rev. B*, 90:014515, Jul 2014. doi: 10.1103/PhysRevB.90.014515. URL `https://link.aps.org/doi/10.1103/PhysRevB.90.014515`.

[178] Naoto Tsuji and Hideo Aoki. Theory of Anderson pseudospin resonance with Higgs mode in superconductors. *Phys. Rev. B*, 92:064508, Aug 2015. doi: 10.1103/PhysRevB.92.064508. URL `https://link.aps.org/doi/10.1103/PhysRevB.92.064508`.

[179] H Krull, N Bittner, GS Uhrig, D Manske, and AP Schnyder. Coupling of Higgs and Leggett modes in non-equilibrium superconductors. *Nat. Commun.*, 7:11921, 2016.

[180] SG Sharapov, VP Gusynin, and H Beck. Effective action approach to the Leggett's mode in two-band superconductors. *Eur. Phys. J. B*, 30(1):45–51, 2002.

[181] F. J. Burnell, Jiangping Hu, Meera M. Parish, and B. Andrei Bernevig. Leggett mode in a strong-coupling model of iron arsenide superconductors. *Phys. Rev. B*, 82:144506, Oct 2010. doi: 10.1103/PhysRevB.82.144506. URL `https://link.aps.org/doi/10.1103/PhysRevB.82.144506`.

[182] Nikolaj Bittner, Dietrich Einzel, Ludwig Klam, and Dirk Manske. Leggett Modes and the Anderson-Higgs Mechanism in Superconductors without Inversion Symmetry. *Phys. Rev. Lett.*, 115:227002, Nov 2015. doi: 10.1103/PhysRevLett.115.227002. URL `https://link.aps.org/doi/10.1103/PhysRevLett.115.227002`.

[183] T. Cea and L. Benfatto. Signature of the Leggett mode in the A_{1g} Raman response: From MgB_2 to iron-based superconductors. *Phys. Rev. B*, 94:064512, Aug 2016. doi: 10.1103/PhysRevB.94.064512. URL `https://link.aps.org/doi/10.1103/PhysRevB.94.064512`.

[184] Yuta Murotani, Naoto Tsuji, and Hideo Aoki. Theory of light-induced resonances with collective Higgs and Leggett modes in multiband superconductors. *Phys. Rev. B*, 95:104503, Mar 2017. doi: 10.1103/PhysRevB.95.104503. URL `https://link.aps.org/doi/10.1103/PhysRevB.95.104503`.

[185] Kazuki Yamamoto, Masaya Nakagawa, Naoto Tsuji, Masahito Ueda, and Norio Kawakami. Collective Excitations and Nonequilibrium Phase Transition in Dissipative Fermionic Superfluids. *Phys. Rev. Lett.*, 127:055301, Jul 2021. doi: 10.1103/PhysRevLett.127.055301. URL `https://link.aps.org/doi/10.1103/PhysRevLett.127.055301`.

[186] Scott Smale, Peiru He, Ben A Olsen, Kenneth G Jackson, Haille Sharum, Stefan Trotzky, Jamir Marino, Ana Maria Rey, and Joseph H Thywissen. Observation of a transition between dynamical phases in a quantum degenerate Fermi gas. *Sci. Adv.*, 5(8):eaax1568, 2019.

[187] Juan A Muniz, Diego Barberena, Robert J Lewis-Swan, Dylan J Young, Julia RK Cline, Ana Maria Rey, and James K Thompson. Exploring dynamical phase transitions with cold atoms in an optical cavity. *Nature (London)*, 580(7805):602–607, 2020.

[188] M. J. Mark, E. Haller, K. Lauber, J. G. Danzl, A. Janisch, H. P. Büchler, A. J. Daley, and H.-C. Nägerl. Preparation and Spectroscopy of a Metastable Mott-Insulator State with Attractive Interactions. *Phys. Rev. Lett.*, 108:215302, May 2012. doi: 10.1103/PhysRevLett.108.215302. URL https://link.aps.org/doi/10.1103/PhysRevLett.108.215302.

[189] Alex Kamenev. *Field theory of non-equilibrium systems*. Cambridge University Press, Cambridge, England, 2011.

[190] Berislav Buča and Tomaž Prosen. A note on symmetry reductions of the Lindblad equation: transport in constrained open spin chains. *New J. Phys.*, 14(7):073007, 2012.

[191] Victor V. Albert and Liang Jiang. Symmetries and conserved quantities in Lindblad master equations. *Phys. Rev. A*, 89:022118, Feb 2014. doi: 10.1103/PhysRevA.89.022118. URL https://link.aps.org/doi/10.1103/PhysRevA.89.022118.

[192] Naoyuki Shibata and Hosho Katsura. Dissipative spin chain as a non-Hermitian Kitaev ladder. *Phys. Rev. B*, 99:174303, May 2019. doi: 10.1103/PhysRevB.99.174303. URL https://link.aps.org/doi/10.1103/PhysRevB.99.174303.

[193] Naoyuki Shibata and Hosho Katsura. Dissipative quantum Ising chain as a non-Hermitian Ashkin-Teller model. *Phys. Rev. B*, 99:224432, Jun 2019. doi: 10.1103/PhysRevB.99.224432. URL https://link.aps.org/doi/10.1103/PhysRevB.99.224432.

[194] Giacomo Valtolina, Alessia Burchianti, Andrea Amico, Elettra Neri, Klejdja Xhani, Jorge Amin Seman, Andrea Trombettoni, Augusto Smerzi, Matteo Zaccanti, Massimo Inguscio, and Giacomo Roati. Josephson effect in fermionic superfluids across the BEC-BCS crossover. *Science*, 350(6267):1505–1508, 2015.

[195] A. Spuntarelli, P. Pieri, and G. C. Strinati. Josephson Effect throughout the BCS-BEC Crossover. *Phys. Rev. Lett.*, 99:040401, Jul 2007. doi: 10.1103/PhysRevLett.99.040401. URL https://link.aps.org/doi/10.1103/PhysRevLett.99.040401.

[196] A. Burchianti, F. Scazza, A. Amico, G. Valtolina, J. A. Seman, C. Fort, M. Zaccanti, M. Inguscio, and G. Roati. Connecting Dissipation and Phase Slips in a Josephson Junction between Fermionic Superfluids. *Phys. Rev. Lett.*, 120:025302, Jan 2018. doi: 10.1103/PhysRevLett.120.025302. URL https://link.aps.org/doi/10.1103/PhysRevLett.120.025302.

[197] Niclas Luick, Lennart Sobirey, Markus Bohlen, Vijay Pal Singh, Ludwig Mathey, Thomas Lompe, and Henning Moritz. An ideal Josephson junction in an ultracold two-dimensional Fermi gas. *Science*, 369(6499):89–91, 2020.

[198] WJ Kwon, G Del Pace, R Panza, M Inguscio, W Zwerger, M Zaccanti, F Scazza, and G Roati. Strongly correlated superfluid order parameters from dc Josephson supercurrents. *Science*, 369(6499):84–88, 2020.

[199] Michael Tinkham. *Introduction to superconductivity*. Courier Corporation, 2004.

[200] In Ref. [15], it is shown that exceptional points of a non-Hermitian Hamiltonian and a Liouvillian are the same when the system has either gain or loss. Thus, the Liouvillian under consideration exhibits the spectral singularity originating from the same exceptional points as those of the non-Hermitian BCS Hamiltonian [128].

[201] A. O. Caldeira and A. J. Leggett. Influence of Dissipation on Quantum Tunneling in Macroscopic Systems. *Phys. Rev. Lett.*, 46:211–214, Jan 1981. doi: 10.1103/PhysRevLett.46.211. URL https://link.aps.org/doi/10.1103/PhysRevLett.46.211.

[202] Albert Schmid. Diffusion and Localization in a Dissipative Quantum System. *Phys. Rev. Lett.*, 51:1506–1509, Oct 1983. doi: 10.1103/PhysRevLett.51.1506. URL `https://link.aps.org/doi/10.1103/PhysRevLett.51.1506`.

[203] F. Guinea, V. Hakim, and A. Muramatsu. Diffusion and Localization of a Particle in a Periodic Potential Coupled to a Dissipative Environment. *Phys. Rev. Lett.*, 54:263–266, Jan 1985. doi: 10.1103/PhysRevLett.54.263. URL `https://link.aps.org/doi/10.1103/PhysRevLett.54.263`.

[204] H. T. C. Stoof. Time-dependent Ginzburg-Landau theory for a weak-coupling superconductor. *Phys. Rev. B*, 47:7979–7985, Apr 1993. doi: 10.1103/PhysRevB.47.7979. URL `https://link.aps.org/doi/10.1103/PhysRevB.47.7979`.

[205] Yoshinori Tokura and Naoto Nagaosa. Nonreciprocal responses from non-centrosymmetric quantum materials. *Nat. Commun.*, 9:3740, 2018.

[206] GLJA Rikken and E Raupach. Observation of magneto-chiral dichroism. *Nature (London)*, 390(6659):493–494, 1997.

[207] H Linke, TE Humphrey, A Löfgren, AO Sushkov, R Newbury, RP Taylor, and P Omling. Experimental tunneling ratchets. *Science*, 286(5448):2314–2317, 1999.

[208] Takahiro Morimoto and Naoto Nagaosa. Topological nature of nonlinear optical effects in solids. *Sci. Adv.*, 2(5):e1501524, 2016.

[209] Sota Kitamura, Naoto Nagaosa, and Takahiro Morimoto. Nonreciprocal Landau–Zener tunneling. *Commun. Phys.*, 3:63, 2020.

[210] K Ono, DG Austing, Y Tokura, and S Tarucha. Current rectification by pauli exclusion in a weakly coupled double quantum dot system. *Science*, 297(5585):1313–1317, 2002.

[211] R Scheibner, M König, D Reuter, AD Wieck, C Gould, H Buhmann, and LW Molenkamp. Quantum dot as thermal rectifier. *New J. Phys.*, 10(8):083016, 2008.

[212] Hamidreza Ramezani, Tsampikos Kottos, Ramy El-Ganainy, and Demetrios N. Christodoulides. Unidirectional nonlinear $\mathcal{PT}$-symmetric optical structures. *Phys. Rev. A*, 82:043803, Oct 2010. doi: 10.1103/PhysRevA.82.043803. URL `https://link.aps.org/doi/10.1103/PhysRevA.82.043803`.

[213] Long Chang, Xiaoshun Jiang, Shiyue Hua, Chao Yang, Jianming Wen, Liang Jiang, Guanyu Li, Guanzhong Wang, and Min Xiao. Parity–time symmetry and variable optical isolation in active–passive-coupled microresonators. *Nat. Photon.*, 8(7):524–529, 2014.

[214] Bo Peng, Şahin Kaya Özdemir, Fuchuan Lei, Faraz Monifi, Mariagiovanna Gianfreda, Gui Lu Long, Shanhui Fan, Franco Nori, Carl M Bender, and Lan Yang. Parity–time-symmetric whispering-gallery microcavities. *Nat. Phys.*, 10(5):394–398, 2014.

[215] F Nazari, N Bender, H Ramezani, MK Moravvej-Farshi, DN Christodoulides, and Tsampikos Kottos. Optical isolation via $\mathcal{PT}$-symmetric nonlinear Fano resonances. *Opt. Express*, 22(8): 9574–9584, 2014.

[216] Sylvain Lannebère and Mário G Silveirinha. Optical meta-atom for localization of light with quantized energy. *Nat. Commun.*, 6:8766, 2015.

[217] Bin Liang, Bo Yuan, and Jian-chun Cheng. Acoustic Diode: Rectification of Acoustic Energy Flux in One-Dimensional Systems. *Phys. Rev. Lett.*, 103:104301, Sep 2009. doi: 10.1103/PhysRevLett.103.104301. URL `https://link.aps.org/doi/10.1103/PhysRevLett.103.104301`.

[218] Romain Fleury, Dimitrios L Sounas, Caleb F Sieck, Michael R Haberman, and Andrea Alù. Sound isolation and giant linear nonreciprocity in a compact acoustic circulator. *Science*, 343(6170):516–519, 2014.

[219] Feng Li, Paul Anzel, Jinkyu Yang, Panayotis G Kevrekidis, and Chiara Daraio. Granular acoustic switches and logic elements. *Nat. Commun.*, 5:5311, 2014.

[220] Qing Wang, Yang Yang, Xu Ni, Ye-Long Xu, Xiao-Chen Sun, Ze-Guo Chen, Liang Feng, Xiao-ping Liu, Ming-Hui Lu, and Yan-Feng Chen. Acoustic asymmetric transmission based on time-dependent dynamical scattering. *Sci. Rep.*, 5(10880):1–10, 2015.

[221] Yifan Wang, Behrooz Yousefzadeh, Hui Chen, Hussein Nassar, Guoliang Huang, and Chiara Daraio. Observation of Nonreciprocal Wave Propagation in a Dynamic Phononic Lattice. *Phys. Rev. Lett.*, 121:194301, Nov 2018. doi: 10.1103/PhysRevLett.121.194301. URL `https://link.aps.org/doi/10.1103/PhysRevLett.121.194301`.

[222] Giuseppe Trainiti, Yiwei Xia, Jacopo Marconi, Gabriele Cazzulani, Alper Erturk, and Massimo Ruzzene. Time-Periodic Stiffness Modulation in Elastic Metamaterials for Selective Wave Filtering: Theory and Experiment. *Phys. Rev. Lett.*, 122:124301, Mar 2019. doi: 10.1103/PhysRevLett.122.124301. URL `https://link.aps.org/doi/10.1103/PhysRevLett.122.124301`.

[223] Nicholas A Estep, Dimitrios L Sounas, Jason Soric, and Andrea Alù. Magnetic-free non-reciprocity and isolation based on parametrically modulated coupled-resonator loops. *Nat. Phys.*, 10(12):923–927, 2014.

[224] Corentin Coulais, Dimitrios Sounas, and Andrea Alù. Static non-reciprocity in mechanical metamaterials. *Nature (London)*, 542(7642):461–464, 2017.

[225] Martin Brandenbourger, Xander Locsin, Edan Lerner, and Corentin Coulais. Non-reciprocal robotic metamaterials. *Nat. Commun.*, 10:4608, 2019.

[226] Zhenghan Liao, William T. M. Irvine, and Suriyanarayanan Vaikuntanathan. Rectification in Nonequilibrium Parity Violating Metamaterials. *Phys. Rev. X*, 10:021036, May 2020. doi: 10.1103/PhysRevX.10.021036. URL `https://link.aps.org/doi/10.1103/PhysRevX.10.021036`.

[227] S. Flach, Y. Zolotaryuk, A. E. Miroshnichenko, and M. V. Fistul. Broken Symmetries and Directed Collective Energy Transport in Spatially Extended Systems. *Phys. Rev. Lett.*, 88:184101, Apr 2002. doi: 10.1103/PhysRevLett.88.184101. URL `https://link.aps.org/doi/10.1103/PhysRevLett.88.184101`.

[228] Souvik Das, Onuttom Narayan, and Sriram Ramaswamy. Ratchet for energy transport between identical reservoirs. *Phys. Rev. E*, 66:050103(R), Nov 2002. doi: 10.1103/PhysRevE.66.050103. URL `https://link.aps.org/doi/10.1103/PhysRevE.66.050103`.

[229] Jie Ren and Baowen Li. Emergence and control of heat current from strict zero thermal bias. *Phys. Rev. E*, 81:021111, Feb 2010. doi: 10.1103/PhysRevE.81.021111. URL `https://link.aps.org/doi/10.1103/PhysRevE.81.021111`.

[230] Linxiao Zhu and Shanhui Fan. Persistent Directional Current at Equilibrium in Nonreciprocal Many-Body Near Field Electromagnetic Heat Transfer. *Phys. Rev. Lett.*, 117:134303, Sep 2016. doi: 10.1103/PhysRevLett.117.134303. URL `https://link.aps.org/doi/10.1103/PhysRevLett.117.134303`.

[231] B. Sabass. Fluctuating, Lorentz-force-like coupling of Langevin equations and heat flux rectification. *Phys. Rev. E*, 96:022109, Aug 2017. doi: 10.1103/PhysRevE.96.022109. URL `https://link.aps.org/doi/10.1103/PhysRevE.96.022109`.

[232] Lars Onsager. Reciprocal Relations in Irreversible Processes. I. *Phys. Rev.*, 37:405–426, Feb 1931. doi: 10.1103/PhysRev.37.405. URL `https://link.aps.org/doi/10.1103/PhysRev.37.405`.

[233] Giuliano Benenti, Giulio Casati, Keiji Saito, and Robert S Whitney. Fundamental aspects of steady-state conversion of heat to work at the nanoscale. *Phys. Rep.*, 694:1–124, 2017.

[234] T. Werlang, M. A. Marchiori, M. F. Cornelio, and D. Valente. Optimal rectification in the ultrastrong coupling regime. *Phys. Rev. E*, 89:062109, Jun 2014. doi: 10.1103/PhysRevE.89.062109. URL https://link.aps.org/doi/10.1103/PhysRevE.89.062109.

[235] Emmanuel Pereira. Requisite ingredients for thermal rectification. *Phys. Rev. E*, 96:012114, Jul 2017. doi: 10.1103/PhysRevE.96.012114. URL https://link.aps.org/doi/10.1103/PhysRevE.96.012114.

[236] Thomas Motz, Michael Wiedmann, Jürgen T Stockburger, and Joachim Ankerhold. Rectification of heat currents across nonlinear quantum chains: a versatile approach beyond weak thermal contact. *New J. Phys.*, 20(11):113020, 2018.

[237] Emmanuel Pereira. Thermal rectification in classical and quantum systems: Searching for efficient thermal diodes. *Europhys. Lett.*, 126(1):14001, 2019.

[238] Emmanuel Pereira. Perfect thermal rectification in a many-body quantum ising model. *Phys. Rev. E*, 99:032116, Mar 2019. doi: 10.1103/PhysRevE.99.032116. URL https://link.aps.org/doi/10.1103/PhysRevE.99.032116.

[239] Andreu Riera-Campeny, Mohammad Mehboudi, Marisa Pons, and Anna Sanpera. Dynamically induced heat rectification in quantum systems. *Phys. Rev. E*, 99:032126, Mar 2019. doi: 10.1103/PhysRevE.99.032126. URL https://link.aps.org/doi/10.1103/PhysRevE.99.032126.

[240] Vinitha Balachandran, Giuliano Benenti, Emmanuel Pereira, Giulio Casati, and Dario Poletti. Heat current rectification in segmented XXZ chains. *Phys. Rev. E*, 99:032136, Mar 2019. doi: 10.1103/PhysRevE.99.032136. URL https://link.aps.org/doi/10.1103/PhysRevE.99.032136.

[241] Keiji Saito. Strong evidence of normal heat conduction in a one-dimensional quantum system. *Europhys. Lett.*, 61(1):34, 2003.

[242] Hannu Wichterich, Markus J. Henrich, Heinz-Peter Breuer, Jochen Gemmer, and Mathias Michel. Modeling heat transport through completely positive maps. *Phys. Rev. E*, 76:031115, Sep 2007. doi: 10.1103/PhysRevE.76.031115. URL https://link.aps.org/doi/10.1103/PhysRevE.76.031115.

[243] Tomaz Prosen. Open XXZ Spin Chain: Nonequilibrium Steady State and a Strict Bound on Ballistic Transport. *Phys. Rev. Lett.*, 106:217206, May 2011. doi: 10.1103/PhysRevLett.106.217206. URL https://link.aps.org/doi/10.1103/PhysRevLett.106.217206.

[244] Gabriel T. Landi, E. Novais, Mário J. de Oliveira, and Dragi Karevski. Flux rectification in the quantum XXZ chain. *Phys. Rev. E*, 90:042142, Oct 2014. doi: 10.1103/PhysRevE.90.042142. URL https://link.aps.org/doi/10.1103/PhysRevE.90.042142.

[245] Zala Lenarčič and Tomaz Prosen. Exact asymptotics of the current in boundary-driven dissipative quantum chains in large external fields. *Phys. Rev. E*, 91:030103(R), Mar 2015. doi: 10.1103/PhysRevE.91.030103. URL https://link.aps.org/doi/10.1103/PhysRevE.91.030103.

[246] Emmanuel Pereira. Rectification and one-way street for the energy current in boundary-driven asymmetric quantum spin chains. *Phys. Rev. E*, 95:030104(R), Mar 2017. doi: 10.1103/PhysRevE.95.030104. URL https://link.aps.org/doi/10.1103/PhysRevE.95.030104.

[247] Emmanuel Pereira. Heat, work, and energy currents in the boundary-driven XXZ spin chain. *Phys. Rev. E*, 97:022115, Feb 2018. doi: 10.1103/PhysRevE.97.022115. URL https://link.aps.org/doi/10.1103/PhysRevE.97.022115.

[248] Lucas Schuab, Emmanuel Pereira, and Gabriel T. Landi. Energy rectification in quantum graded spin chains: Analysis of the XXZ model. *Phys. Rev. E*, 94:042122, Oct 2016. doi: 10.1103/PhysRevE.94.042122. URL https://link.aps.org/doi/10.1103/PhysRevE.94.042122.

[249] Vinitha Balachandran, Giuliano Benenti, Emmanuel Pereira, Giulio Casati, and Dario Poletti. Perfect Diode in Quantum Spin Chains. *Phys. Rev. Lett.*, 120:200603, May 2018. doi: 10.1103/PhysRevLett.120.200603. URL https://link.aps.org/doi/10.1103/PhysRevLett.120.200603.

[250] Daniel Malz and Andreas Nunnenkamp. Current rectification in a double quantum dot through fermionic reservoir engineering. *Phys. Rev. B*, 97:165308, Apr 2018. doi: 10.1103/PhysRevB.97.165308. URL https://link.aps.org/doi/10.1103/PhysRevB.97.165308.

[251] Karen V Hovhannisyan and Alberto Imparato. Quantum current in dissipative systems. *New J. Phys.*, 21(5):052001, 2019.

[252] Eduardo Mascarenhas, François Damanet, Stuart Flannigan, Luca Tagliacozzo, Andrew J. Daley, John Goold, and Inés de Vega. Nonreciprocal quantum transport at junctions of structured leads. *Phys. Rev. B*, 99:245134, Jun 2019. doi: 10.1103/PhysRevB.99.245134. URL https://link.aps.org/doi/10.1103/PhysRevB.99.245134.

[253] F Damanet, Eduardo Mascarenhas, David Pekker, and Andrew J. Daley. Controlling Quantum Transport via Dissipation Engineering. *Phys. Rev. Lett.*, 123:180402, Oct 2019. doi: 10.1103/PhysRevLett.123.180402. URL https://link.aps.org/doi/10.1103/PhysRevLett.123.180402.

[254] Julio T Barreiro, Markus Müller, Philipp Schindler, Daniel Nigg, Thomas Monz, Michael Chwalla, Markus Hennrich, Christian F Roos, Peter Zoller, and Rainer Blatt. An open-system quantum simulator with trapped ions. *Nature (London)*, 470(7335):486–491, 2011.

[255] Philipp Schindler, Markus Müller, Daniel Nigg, Julio T Barreiro, Esteban A Martinez, Markus Hennrich, T Monz, Sebastian Diehl, Peter Zoller, and Rainer Blatt. Quantum simulation of dynamical maps with trapped ions. *Nat. Phys.*, 9(6):361–367, 2013.

[256] Bi-Heng Liu, Li Li, Yun-Feng Huang, Chuan-Feng Li, Guang-Can Guo, Elsi-Mari Laine, Heinz-Peter Breuer, and Jyrki Piilo. Experimental control of the transition from Markovian to non-Markovian dynamics of open quantum systems. *Nat. Phys.*, 7(12):931–934, 2011.

[257] Zhao-Di Liu, Henri Lyyra, Yong-Nan Sun, Bi-Heng Liu, Chuan-Feng Li, Guang-Can Guo, Sabrina Maniscalco, and Jyrki Piilo. Experimental implementation of fully controlled dephasing dynamics and synthetic spectral densities. *Nat. Commun.*, 9:3453, 2018.

[258] Jacek Kasprzak, M Richard, S Kundermann, A Baas, P Jeambrun, J. M. J Keeling, F. M Marchetti, M. H Szymańska, R André, J. L Staehli, V Savona, P. B Littlewood, B Deveaud, and Le Si Dang. Bose–Einstein condensation of exciton polaritons. *Nature (London)*, 443 (7110):409–414, 2006.

[259] Charles Leyder, Marco Romanelli, J Ph Karr, Elisabeth Giacobino, Tim CH Liew, Mikhail M Glazov, Alexey V Kavokin, Guillaume Malpuech, and Alberto Bramati. Observation of the optical spin Hall effect. *Nat. Phys.*, 3(9):628–631, 2007.

[260] Tim Byrnes, Na Young Kim, and Yoshihisa Yamamoto. Exciton–polariton condensates. *Nat. Phys.*, 10(11):803–813, 2014.

[261] Tiejun Gao, E Estrecho, K. Y Bliokh, T. C. H Liew, M. D Fraser, Sebastian Brodbeck, Martin Kamp, Christian Schneider, Sven Höfling, Y Yamamoto, F Nori, A. G Truscott, R. G Dall, and E. A Ostrovskaya. Observation of non-Hermitian degeneracies in a chaotic exciton-polariton billiard. *Nature (London)*, 526(7574):554–558, 2015.

[262] F. Baboux, L. Ge, T. Jacqmin, M. Biondi, E. Galopin, A. Lemaître, L. Le Gratiet, I. Sagnes, S. Schmidt, H. E. Türeci, A. Amo, and J. Bloch. Bosonic Condensation and Disorder-Induced Localization in a Flat Band. *Phys. Rev. Lett.*, 116:066402, Feb 2016. doi: 10.1103/PhysRevLett.116.066402. URL https://link.aps.org/doi/10.1103/PhysRevLett.116.066402.

[263] S Klembt, TH Harder, OA Egorov, K Winkler, R Ge, MA Bandres, M Emmerling, L Worschech, TCH Liew, M Segev, C Schneider, and S Höfling. Exciton-polariton topological insulator. *Nature (London)*, 562(7728):552–556, 2018.

[264] William R. Frensley. Boundary conditions for open quantum systems driven far from equilibrium. *Rev. Mod. Phys.*, 62:745–791, Jul 1990. doi: 10.1103/RevModPhys.62.745. URL `https://link.aps.org/doi/10.1103/RevModPhys.62.745`.

[265] A. Metelmann and A. A. Clerk. Nonreciprocal Photon Transmission and Amplification via Reservoir Engineering. *Phys. Rev. X*, 5:021025, Jun 2015. doi: 10.1103/PhysRevX.5.021025. URL `https://link.aps.org/doi/10.1103/PhysRevX.5.021025`.

[266] Peter Lodahl, Sahand Mahmoodian, Søren Stobbe, Arno Rauschenbeutel, Philipp Schneeweiss, Jürgen Volz, Hannes Pichler, and Peter Zoller. Chiral quantum optics. *Nature (London)*, 541(7638):473–480, 2017.

[267] Maximilian Keck, Davide Rossini, and Rosario Fazio. Persistent currents by reservoir engineering. *Phys. Rev. A*, 98:053812, Nov 2018. doi: 10.1103/PhysRevA.98.053812. URL `https://link.aps.org/doi/10.1103/PhysRevA.98.053812`.

[268] Kazuki Yamamoto, Yuto Ashida, and Norio Kawakami. Rectification in nonequilibrium steady states of open many-body systems. *Phys. Rev. Research*, 2:043343, Dec 2020. doi: 10.1103/PhysRevResearch.2.043343. URL `https://link.aps.org/doi/10.1103/PhysRevResearch.2.043343`.

[269] JE Birkholz and V Meden. Spin–orbit coupling effects in one-dimensional ballistic quantum wires. *J. Condens. Matter Phys.*, 20(8):085226, 2008.

[270] Takashi Nakajima, Matthieu R Delbecq, Tomohiro Otsuka, Shinichi Amaha, Jun Yoneda, Akito Noiri, Kenta Takeda, Giles Allison, Arne Ludwig, Andreas D Wieck, Xuedong Hu, Franco Nori, and Seigo Tarucha. Coherent transfer of electron spin correlations assisted by dephasing noise. *Nat. Commun.*, 9:2133, 2018.

[271] Lev Vidmar and Marcos Rigol. Generalized Gibbs ensemble in integrable lattice models. *J. Stat. Mech. (2016) 064007.*

[272] Fei Liu. Equivalence of two Bochkov-Kuzovlev equalities in quantum two-level systems. *Phys. Rev. E*, 89:042122, Apr 2014. doi: 10.1103/PhysRevE.89.042122. URL `https://link.aps.org/doi/10.1103/PhysRevE.89.042122`.

[273] Zongping Gong, Yuto Ashida, and Masahito Ueda. Quantum-trajectory thermodynamics with discrete feedback control. *Phys. Rev. A*, 94:012107, Jul 2016. doi: 10.1103/PhysRevA.94.012107. URL `https://link.aps.org/doi/10.1103/PhysRevA.94.012107`.

[274] Ralph Gebauer and Roberto Car. Current in Open Quantum Systems. *Phys. Rev. Lett.*, 93:160404, Oct 2004. doi: 10.1103/PhysRevLett.93.160404. URL `https://link.aps.org/doi/10.1103/PhysRevLett.93.160404`.

[275] András Bodor and Lajos Diósi. Conserved current in Markovian open-quantum systems. *Phys. Rev. A*, 73:064101, Jun 2006. doi: 10.1103/PhysRevA.73.064101. URL `https://link.aps.org/doi/10.1103/PhysRevA.73.064101`.

[276] Erasmo A de Andrada e Silva. Probability current in the tight-binding model. *Am. J. Phys.*, 60(8):753–754, 1992.

[277] Gerald D Mahan. *Many-particle physics*. Kluwer Academic / Plenum Publishers, New York, 2000.

[278] G. L. J. A. Rikken, J. Fölling, and P. Wyder. Electrical Magnetochiral Anisotropy. *Phys. Rev. Lett.*, 87:236602, Nov 2001. doi: 10.1103/PhysRevLett.87.236602. URL `https://link.aps.org/doi/10.1103/PhysRevLett.87.236602`.

[279] Takahiro Morimoto and Naoto Nagaosa. Chiral Anomaly and Giant Magnetochiral Anisotropy in Noncentrosymmetric Weyl Semimetals. *Phys. Rev. Lett.*, 117:146603, Sep 2016. doi: 10.1103/PhysRevLett.117.146603. URL https://link.aps.org/doi/10.1103/PhysRevLett.117.146603.

[280] T Ideue, K Hamamoto, S Koshikawa, M Ezawa, S Shimizu, Y Kaneko, Y Tokura, N Nagaosa, and Y Iwasa. Bulk rectification effect in a polar semiconductor. *Nat. Phys.*, 13(6):578–583, 2017.

[281] P. Středa and P. Šeba. Antisymmetric Spin Filtering in One-Dimensional Electron Systems with Uniform Spin-Orbit Coupling. *Phys. Rev. Lett.*, 90:256601, Jun 2003. doi: 10.1103/PhysRevLett.90.256601. URL https://link.aps.org/doi/10.1103/PhysRevLett.90.256601.

[282] Junsaku Nitta, Tatsushi Akazaki, Hideaki Takayanagi, and Takatomo Enoki. Gate Control of Spin-Orbit Interaction in an Inverted $In_{0.53}Ga_{0.47}As/In_{0.52}Al_{0.48}As$ Heterostructure. *Phys. Rev. Lett.*, 78:1335–1338, Feb 1997. doi: 10.1103/PhysRevLett.78.1335. URL https://link.aps.org/doi/10.1103/PhysRevLett.78.1335.

[283] Dirk Grundler. Large Rashba Splitting in InAs Quantum Wells due to Electron Wave Function Penetration into the Barrier Layers. *Phys. Rev. Lett.*, 84:6074–6077, Jun 2000. doi: 10.1103/PhysRevLett.84.6074. URL https://link.aps.org/doi/10.1103/PhysRevLett.84.6074.

[284] P. Scarlino, E. Kawakami, P. Stano, M. Shafiei, C. Reichl, W. Wegscheider, and L. M. K. Vandersypen. Spin-Relaxation Anisotropy in a GaAs Quantum Dot. *Phys. Rev. Lett.*, 113:256802, Dec 2014. doi: 10.1103/PhysRevLett.113.256802. URL https://link.aps.org/doi/10.1103/PhysRevLett.113.256802.

[285] Balázs Dóra and C. P. Moca. Quantum Quench in $\mathcal{PT}$-Symmetric Luttinger Liquid. *Phys. Rev. Lett.*, 124:136802, Mar 2020. doi: 10.1103/PhysRevLett.124.136802. URL https://link.aps.org/doi/10.1103/PhysRevLett.124.136802.

[286] Balázs Dóra, Doru Sticlet, and Catalin Pascu Moca. Correlations at PT-symmetric quantum critical point. *arXiv:2112.08294*, 2021.

[287] C. P. Moca and Balázs Dóra. Universal conductance of a $\mathcal{PT}$-symmetric luttinger liquid after a quantum quench. *Phys. Rev. B*, 104:125124, Sep 2021. doi: 10.1103/PhysRevB.104.125124. URL https://link.aps.org/doi/10.1103/PhysRevB.104.125124.

[288] Giuseppe Albertini, Silvio Renato Dahmen, and Birgit Wehefritz. Phase diagram of the non-Hermitian asymmetric XXZ spin chain. *J. Phys. A*, 29(15):L369, 1996.

[289] Ulrich Bilstein and Birgit Wehefritz. Spectra of non-Hermitian quantum spin chains describing boundary induced phase transitions. *J. Phys. A*, 30(14):4925, 1997.

[290] Romain Couvreur, Jesper Lykke Jacobsen, and Hubert Saleur. Entanglement in Nonunitary Quantum Critical Spin Chains. *Phys. Rev. Lett.*, 119:040601, Jul 2017. doi: 10.1103/PhysRevLett.119.040601. URL https://link.aps.org/doi/10.1103/PhysRevLett.119.040601.

[291] F Duncan M Haldane. Continuum dynamics of the 1-D Heisenberg antiferromagnet: Identification with the O(3) nonlinear sigma model. *Phys. Lett. A*, 93(9):464–468, 1983.

[292] Elliott H. Lieb and F. Y. Wu. Absence of Mott Transition in an Exact Solution of the Short-Range, One-Band Model in One Dimension. *Phys. Rev. Lett.*, 20:1445–1448, Jun 1968. doi: 10.1103/PhysRevLett.20.1445. URL https://link.aps.org/doi/10.1103/PhysRevLett.20.1445.

[293] Norio Kawakami and Sung-Kil Yang. Luttinger anomaly exponent of momentum distribution in the Hubbard chain. *Phys. Lett. A*, 148(6-7):359–362, 1990.

[294] H. J. Schulz. Correlation Exponents and the Metal-Insulator Transition in the One-Dimensional Hubbard Model. *Phys. Rev. Lett.*, 64:2831–2834, Jun 1990. doi: 10.1103/PhysRevLett.64.2831. URL https://link.aps.org/doi/10.1103/PhysRevLett.64.2831.

[295] Holger Frahm and V. E. Korepin. Critical exponents for the one-dimensional Hubbard model. *Phys. Rev. B*, 42:10553–10565, Dec 1990. doi: 10.1103/PhysRevB.42.10553. URL https://link.aps.org/doi/10.1103/PhysRevB.42.10553.

[296] F. D. M. Haldane. General Relation of Correlation Exponents and Spectral Properties of One-Dimensional Fermi Systems: Application to the Anisotropic $S = \frac{1}{2}$ Heisenberg Chain. *Phys. Rev. Lett.*, 45:1358–1362, Oct 1980. doi: 10.1103/PhysRevLett.45.1358. URL https://link.aps.org/doi/10.1103/PhysRevLett.45.1358.

[297] F. D. M. Haldane. 'Luttinger liquid theory' of one-dimensional quantum fluids. I. Properties of the Luttinger model and their extension to the general 1D interacting spinless Fermi gas. *J. Phys. C*, 14(19):2585, 1981.

[298] F Duncan M Haldane. Demonstration of the "Luttinger liquid" character of Bethe-ansatz-soluble models of 1-D quantum fluids. *Phys. Lett. A*, 81(12):153–155, 1981.

[299] F. D. M. Haldane. Effective Harmonic-Fluid Approach to Low-Energy Properties of One-Dimensional Quantum Fluids. *Phys. Rev. Lett.*, 47:1840–1843, Dec 1981. doi: 10.1103/PhysRevLett.47.1840. URL https://link.aps.org/doi/10.1103/PhysRevLett.47.1840.

[300] Norio Kawakami and Sung-Kil Yang. Correlation Functions in the One-Dimensional t-J Model. *Phys. Rev. Lett.*, 65:2309–2311, Oct 1990. doi: 10.1103/PhysRevLett.65.2309. URL https://link.aps.org/doi/10.1103/PhysRevLett.65.2309.

[301] Norio Kawakami and Sung-Kil Yang. Luttinger liquid properties of highly correlated electron systems in one dimension. *J. Phys.: Condens. Matter*, 3:5983, 1991.

[302] Norio Kawakami and Sung-Kil Yang. Finite-Size Scaling in One-Dimensional Quantum Liquid with Long-Range Interaction. *Phys. Rev. Lett.*, 67:2493–2496, Oct 1991. doi: 10.1103/PhysRevLett.67.2493. URL https://link.aps.org/doi/10.1103/PhysRevLett.67.2493.

[303] Norio Kawakami and Sung-Kil Yang. Conformal field theory approach to one-dimensional quantum liquids. *Prog. Theor. Phys. Suppl.*, 107:59–75, 1992.

[304] Alexander A Belavin, Alexander M Polyakov, and Alexander B Zamolodchikov. Infinite conformal symmetry in two-dimensional quantum field theory. *Nucl. Phys. B*, 241(2):333–380, 1984.

[305] Alexander A Belavin, Alexander M Polyakov, and Alexander B Zamolodchikov. Infinite conformal symmetry of critical fluctuations in two dimensions. *J. Stat. Phys.*, 34(5):763–774, 1984.

[306] Daniel Friedan, Zongan Qiu, and Stephen Shenker. Conformal Invariance, Unitarity, and Critical Exponents in Two Dimensions. *Phys. Rev. Lett.*, 52:1575–1578, Apr 1984. doi: 10.1103/PhysRevLett.52.1575. URL https://link.aps.org/doi/10.1103/PhysRevLett.52.1575.

[307] E. Brézin and J. Zinn-Justin, editors. *Fields, strings and critical phenomena*. North-Holland, Amsterdam, 1988.

[308] Pasquale Calabrese and John Cardy. Entanglement entropy and quantum field theory. *J. Stat. Mech.*, 2004(06):P06002, 2004. URL https://iopscience.iop.org/article/10.1088/1742-5468/2004/06/P06002.

[309] Philippe Francesco, Pierre Mathieu, and David Sénéchal. *Conformal field theory*. Springer, New York, 2012.

[310] John L Cardy. Conformal invariance and universality in finite-size scaling. *J. Phys. A*, 17 (7):L385, 1984.

[311] John L Cardy. Finite-size scaling in strips: antiperiodic boundary conditions. *J. Phys. A*, 17(18):L961, 1984. URL https://iopscience.iop.org/article/10.1088/0305-4470/17/18/005.

[312] John L Cardy. Operator content of two-dimensional conformally invariant theories. *Nucl. Phys. B*, 270:186–204, 1986.

[313] John L Cardy. Logarithmic corrections to finite-size scaling in strips. *J. Phys. A*, 19(17): L1093, 1986.

[314] H. W. J. Blöte, John L. Cardy, and M. P. Nightingale. Conformal Invariance, the Central Charge, and Universal Finite-Size Amplitudes at Criticality. *Phys. Rev. Lett.*, 56:742–745, Feb 1986. doi: 10.1103/PhysRevLett.56.742. URL https://link.aps.org/doi/10.1103/PhysRevLett.56.742.

[315] Ian Affleck. Universal Term in the Free Energy at a Critical Point and the Conformal Anomaly. *Phys. Rev. Lett.*, 56:746–748, Feb 1986. doi: 10.1103/PhysRevLett.56.746. URL https://link.aps.org/doi/10.1103/PhysRevLett.56.746.

[316] CJ Hamer. Finite-size corrections for ground states of the XXZ Heisenberg chain in the critical region. *J. Phys. A*, 18(18):L1133, 1985.

[317] CJ Hamer. Finite-size corrections for ground states of the XXZ Heisenberg chain. *J. Phys. A*, 19(16):3335, 1986.

[318] F Woynarovich and H-P Eckle. Finite-size corrections and numerical calculations for long spin 1/2 Heisenberg chains in the critical region. *J. Phys. A*, 20(2):L97, 1987.

[319] Francisco C. Alcaraz, Michael N. Barber, and Murray T. Batchelor. Conformal Invariance and the Spectrum of the XXZ Chain. *Phys. Rev. Lett.*, 58:771–774, Feb 1987. doi: 10.1103/PhysRevLett.58.771. URL https://link.aps.org/doi/10.1103/PhysRevLett.58.771.

[320] Kazuki Yamamoto, Masaya Nakagawa, Masaki Tezuka, Masahito Ueda, and Norio Kawakami. Universal properties of dissipative Tomonaga-Luttinger liquids: Case study of a non-Hermitian XXZ spin chain. *Phys. Rev. B*, 105:205125, May 2022. doi: 10.1103/PhysRevB.105.205125. URL https://link.aps.org/doi/10.1103/PhysRevB.105.205125.

[321] Naoyuki Shibata and Hosho Katsura. Dissipative quantum Ising chain as a non-Hermitian Ashkin-Teller model. *Phys. Rev. B*, 99:224432, Jun 2019. doi: 10.1103/PhysRevB.99.224432. URL https://link.aps.org/doi/10.1103/PhysRevB.99.224432.

[322] T. Prosen and Iztok Pižorn. Quantum Phase Transition in a Far-from-Equilibrium Steady State of an XY Spin Chain. *Phys. Rev. Lett.*, 101:105701, Sep 2008. doi: 10.1103/PhysRevLett.101.105701. URL https://link.aps.org/doi/10.1103/PhysRevLett.101.105701.

[323] Tony E. Lee, Sarang Gopalakrishnan, and Mikhail D. Lukin. Unconventional Magnetism via Optical Pumping of Interacting Spin Systems. *Phys. Rev. Lett.*, 110:257204, Jun 2013. doi: 10.1103/PhysRevLett.110.257204. URL https://link.aps.org/doi/10.1103/PhysRevLett.110.257204.

[324] Chaitanya Joshi, Felix Nissen, and Jonathan Keeling. Quantum correlations in the one-dimensional driven dissipative XY model. *Phys. Rev. A*, 88:063835, Dec 2013. doi: 10.1103/PhysRevA.88.063835. URL https://link.aps.org/doi/10.1103/PhysRevA.88.063835.

[325] Mingyuan He, Chenwei Lv, Hai-Qing Lin, and Qi Zhou. Universal relations for ultracold reactive molecules. *Sci. Adv.*, 6(51):eabd4699, 2020.

[326] Zhihao Xu and Shu Chen. Topological Bose-Mott insulators in one-dimensional non-Hermitian superlattices. *Phys. Rev. B*, 102:035153, Jul 2020. doi: 10.1103/PhysRevB.102.035153. URL https://link.aps.org/doi/10.1103/PhysRevB.102.035153.

[327] Tao Liu, James Jun He, Tsuneya Yoshida, Ze-Liang Xiang, and Franco Nori. Non-Hermitian topological Mott insulators in one-dimensional fermionic superlattices. *Phys. Rev. B*, 102: 235151, Dec 2020. doi: 10.1103/PhysRevB.102.235151. URL https://link.aps.org/doi/10.1103/PhysRevB.102.235151.

[328] L.-M. Duan, E. Demler, and M. D. Lukin. Controlling Spin Exchange Interactions of Ultracold Atoms in Optical Lattices. *Phys. Rev. Lett.*, 91:090402, Aug 2003. doi: 10.1103/PhysRevLett.91.090402. URL https://link.aps.org/doi/10.1103/PhysRevLett.91.090402.

[329] Shunsuke Furukawa and Yong Baek Kim. Entanglement entropy between two coupled Tomonaga-Luttinger liquids. *Phys. Rev. B*, 83:085112, Feb 2011. doi: 10.1103/PhysRevB.83.085112. URL https://link.aps.org/doi/10.1103/PhysRevB.83.085112.

[330] C. N. Yang and C. P. Yang. One-Dimensional Chain of Anisotropic Spin-Spin Interactions. I. Proof of Bethe's Hypothesis for Ground State in a Finite System. *Phys. Rev.*, 150:321–327, Oct 1966. doi: 10.1103/PhysRev.150.321. URL https://link.aps.org/doi/10.1103/PhysRev.150.321.

[331] C. N. Yang and C. P. Yang. One-Dimensional Chain of Anisotropic Spin-Spin Interactions. II. Properties of the Ground-State Energy Per Lattice Site for an Infinite System. *Phys. Rev.*, 150:327–339, Oct 1966. doi: 10.1103/PhysRev.150.327. URL https://link.aps.org/doi/10.1103/PhysRev.150.327.

[332] M. Takahashi. *Thermodynamics of One-Dimensional Solvable Models*. Cambridge University Press, Cambridge, 1993.

[333] Takahiro Fukui and Norio Kawakami. Breakdown of the Mott insulator: Exact solution of an asymmetric Hubbard model. *Phys. Rev. B*, 58:16051–16056, Dec 1998. doi: 10.1103/PhysRevB.58.16051. URL https://link.aps.org/doi/10.1103/PhysRevB.58.16051.

[334] C J Hamer, G R W Quispel, and M T Batchelor. Conformal anomaly and surface energy for Potts and Ashkin-Teller quantum chains. *J. Phys. A: Math. Gen.*, 20(16):5677–5693, nov 1987. doi: 10.1088/0305-4470/20/16/040. URL https://doi.org/10.1088/0305-4470/20/16/040.

[335] B. Sriram Shastry and Bill Sutherland. Twisted Boundary Conditions and Effective Mass in Heisenberg-Ising and Hubbard Rings. *Phys. Rev. Lett.*, 65:243–246, Jul 1990. doi: 10.1103/PhysRevLett.65.243. URL https://link.aps.org/doi/10.1103/PhysRevLett.65.243.

[336] Bill Sutherland and B. Sriram Shastry. Adiabatic Transport Properties of an Exactly Soluble One-Dimensional Quantum Many-Body Problem. *Phys. Rev. Lett.*, 65:1833–1837, Oct 1990. doi: 10.1103/PhysRevLett.65.1833. URL https://link.aps.org/doi/10.1103/PhysRevLett.65.1833.

[337] Yuhi Tanikawa, Kazuaki Takasan, and Hosho Katsura. Exact results for nonlinear Drude weights in the spin-$\frac{1}{2}$ XXZ chain. *Phys. Rev. B*, 103:L201120, May 2021. doi: 10.1103/PhysRevB.103.L201120. URL https://link.aps.org/doi/10.1103/PhysRevB.103.L201120.

[338] Kazuki Yamamoto and Norio Kawakami. Universal description of dissipative Tomonaga-Luttinger liquids with SU(N) spin symmetry: Exact spectrum and critical exponents. *Phys. Rev. B*, 107:045110, Jan 2023. doi: 10.1103/PhysRevB.107.045110. URL https://link.aps.org/doi/10.1103/PhysRevB.107.045110.

[339] X. G. Wen. Chiral Luttinger liquid and the edge excitations in the fractional quantum Hall states. *Phys. Rev. B*, 41:12838–12844, Jun 1990. doi: 10.1103/PhysRevB.41.12838. URL https://link.aps.org/doi/10.1103/PhysRevB.41.12838.

[340] Norio Kawakami. Novel Hierarchy of the SU(N) Electron Models and Edge States of Fractional Quantum Hall Effect. *Phys. Rev. Lett.*, 71:275–278, Jul 1993. doi: 10.1103/PhysRevLett.71.275. URL https://link.aps.org/doi/10.1103/PhysRevLett.71.275.

[341] Andreas M Läuchli. Operator content of real-space entanglement spectra at conformal critical points. *arXiv:1303.0741*, 2013.

[342] Pochung Chen, Zhi-long Xue, IP McCulloch, Ming-Chiang Chung, Miguel Cazalilla, and SK Yip. Entanglement entropy scaling of the XXZ chain. *J. Stat. Mech.*, 2013(10):P10007, 2013.

[343] Elliott H. Lieb. Exact Analysis of an Interacting Bose Gas. II. The Excitation Spectrum. *Phys. Rev.*, 130:1616–1624, May 1963. doi: 10.1103/PhysRev.130.1616. URL `https://link.aps.org/doi/10.1103/PhysRev.130.1616`.

[344] T. Hikihara and A. Furusaki. Correlation amplitude for the $S = \frac{1}{2}$ XXZ spin chain in the critical region: Numerical renormalization-group study of an open chain. *Phys. Rev. B*, 58: R583–R586, Jul 1998. doi: 10.1103/PhysRevB.58.R583. URL `https://link.aps.org/doi/10.1103/PhysRevB.58.R583`.

[345] Davide Bianchini, O Castro-Alvaredo, Benjamin Doyon, Emanuele Levi, and Francesco Ravanini. Entanglement entropy of non-unitary conformal field theory. *J. Phys. A*, 48(4): 04FT01, 2015.

[346] Davide Bianchini, Olalla A Castro-Alvaredo, and Benjamin Doyon. Entanglement entropy of non-unitary integrable quantum field theory. *Nucl. Phys. B*, 896:835–880, 2015.

[347] Davide Bianchini and Francesco Ravanini. Entanglement entropy from corner transfer matrix in Forrester–Baxter non-unitary RSOS models. *J. Phys. A*, 49(15):154005, 2016.

[348] K. Narayan. On dS_4 extremal surfaces and entanglement entropy in some ghost CFTs. *Phys. Rev. D*, 94:046001, Aug 2016. doi: 10.1103/PhysRevD.94.046001. URL `https://link.aps.org/doi/10.1103/PhysRevD.94.046001`.

[349] Dileep P. Jatkar and K. Narayan. Ghost-spin chains, entanglement, and *bc*-ghost CFTs. *Phys. Rev. D*, 96:106015, Nov 2017. doi: 10.1103/PhysRevD.96.106015. URL `https://link.aps.org/doi/10.1103/PhysRevD.96.106015`.

[350] Thomas Dupic, Benoit Estienne, and Yacine Ikhlef. Entanglement entropies of minimal models from null-vectors. *SciPost Phys.*, 4(6):031, 2018.

[351] Loïc Herviou, Nicolas Regnault, and Jens H Bardarson. Entanglement spectrum and symmetries in non-Hermitian fermionic non-interacting models. *SciPost Phys.*, 7(5):069, 2019.

[352] Po-Yao Chang, Jhih-Shih You, Xueda Wen, and Shinsei Ryu. Entanglement spectrum and entropy in topological non-Hermitian systems and nonunitary conformal field theory. *Phys. Rev. Research*, 2:033069, Jul 2020. doi: 10.1103/PhysRevResearch.2.033069. URL `https://link.aps.org/doi/10.1103/PhysRevResearch.2.033069`.

[353] Yaodong Li, Xiao Chen, and Matthew P. A. Fisher. Measurement-driven entanglement transition in hybrid quantum circuits. *Phys. Rev. B*, 100:134306, Oct 2019. doi: 10.1103/PhysRevB.100.134306. URL `https://link.aps.org/doi/10.1103/PhysRevB.100.134306`.

[354] Chao-Ming Jian, Yi-Zhuang You, Romain Vasseur, and Andreas W. W. Ludwig. Measurement-induced criticality in random quantum circuits. *Phys. Rev. B*, 101:104302, Mar 2020. doi: 10.1103/PhysRevB.101.104302. URL `https://link.aps.org/doi/10.1103/PhysRevB.101.104302`.

[355] Xiao Chen, Yaodong Li, Matthew P. A. Fisher, and Andrew Lucas. Emergent conformal symmetry in nonunitary random dynamics of free fermions. *Phys. Rev. Research*, 2:033017, Jul 2020. doi: 10.1103/PhysRevResearch.2.033017. URL `https://link.aps.org/doi/10.1103/PhysRevResearch.2.033017`.

[356] Yaodong Li, Xiao Chen, Andreas W. W. Ludwig, and Matthew P. A. Fisher. Conformal invariance and quantum nonlocality in critical hybrid circuits. *Phys. Rev. B*, 104:104305, Sep 2021. doi: 10.1103/PhysRevB.104.104305. URL `https://link.aps.org/doi/10.1103/PhysRevB.104.104305`.

[357] Michael Buchhold and Sebastian Diehl. Nonequilibrium universality in the heating dynamics of interacting Luttinger liquids. *Phys. Rev. A*, 92:013603, Jul 2015. doi: 10.1103/PhysRevA.92.013603. URL https://link.aps.org/doi/10.1103/PhysRevA.92.013603.

[358] Jean-Sébastien Bernier, Ryan Tan, Chu Guo, Corinna Kollath, and Dario Poletti. Melting of the critical behavior of a Tomonaga-Luttinger liquid under dephasing. *Phys. Rev. B*, 102: 115156, Sep 2020. doi: 10.1103/PhysRevB.102.115156. URL https://link.aps.org/doi/10.1103/PhysRevB.102.115156.

[359] Ádám Bácsi, C. P. Moca, and Balázs Dóra. Dissipation-Induced Luttinger Liquid Correlations in a One-Dimensional Fermi Gas. *Phys. Rev. Lett.*, 124:136401, Mar 2020. doi: 10.1103/PhysRevLett.124.136401. URL https://link.aps.org/doi/10.1103/PhysRevLett.124.136401.

[360] Ádám Bácsi, C. P. Moca, Gergely Zaránd, and Balázs Dóra. Vaporization Dynamics of a Dissipative Quantum Liquid. *Phys. Rev. Lett.*, 125:266803, Dec 2020. doi: 10.1103/PhysRevLett.125.266803. URL https://link.aps.org/doi/10.1103/PhysRevLett.125.266803.

[361] Á. Bácsi, C. P. Moca, G. Zaránd, and B. Dóra. Dissipative dynamics in the free massive boson limit of the sine-Gordon model. *SciPost Phys. Core*, 5:004, 2022. doi: 10.21468/SciPostPhysCore.5.1.004. URL https://scipost.org/10.21468/SciPostPhysCore.5.1.004.

[362] Yuichi Nakamura and Naomichi Hatano. A non-Hermitian critical point and the correlation length of strongly correlated quantum systems. *J. Phys. Soc. Jpn.*, 75(10):104001–104001, 2006.

Acknowledgments

First, I would like to express my gratitude to Prof. Norio Kawakami for his kind help during my graduate course. His supervision is essential for the completion of my work so far. Especially, discussion on CFT in strongly correlated systems has helped me a lot.

Second, I would like to thank Prof. Masahito Ueda for the collaboration in my studies on ultracold atoms in open quantum systems as well as discussions through the stay in his laboratory. His kind support has been a lot of help through my graduate course.

Third, I would like to thank Prof. Yoshiro Takahashi for a lot of discussions and his insightful comments on the experimental platform in ultracold atoms. His knowledge on experiments is essential for the understanding of current experimental progress in ultracold atoms.

I also thank Prof. Masaya Nakagawa for a lot of discussions and collaborations in the field of open quantum systems. I am also grateful to Prof. Kyosuke Adachi and Prof. Kazuaki Takasan for a lot of discussions in my master course, Prof. Naoto Tsuji for the collaboration on dissipative BCS superfluidity, Prof. Yuto Ashida for the collaboration on nonequilibrium statistical mechanics, and Prof. Masaki Tezuka for the discussion on DMRG. I also thank Prof. Tsuneya Yoshida, Prof. Shuntaro Sumita, Prof. Shunsuke Furukawa, Prof. Philipp Werner, Prof. Takahiro Morimoto, Prof. Sota Kitamura, Prof. Hosho Katsura, Dr. Naoyuki Shibata, and Prof. Yasuhiko Yamada, for fruitfull discussions.

In terms of my daily life in Condensed Matter Theory group in Kyoto University, I would like to thank the staffs, Prof. Youichi Yanase, Prof. Ryusuke Ikeda, Prof. Tsuneya Yoshida, Prof. Robert Peters, Prof. Masaki Tezuka, and Prof. Akito Daido for their support. I have enjoyed various discussions with all the other members in the condensed matter theory group. I acknowledge the financial supports from JSPS Research Fellowship for Young Scientists (JSPS KAKENHI Grant No. 20J21318) and WISE program, MEXT.

Last but not least, I would like to express my deepest gratitude to my family for their continuous support during my life from birth to the present.